

Global Drought in the 20th and 21st Centuries

Analysis of retrospective simulations and future
projections of soil moisture

Promotor:

Prof. dr. ir. P.A. Troch

Hoogleraar Hydrologie en
Kwantitatief Waterbeheer (1999-2005),
Wageningen Universiteit.
Professor of Hydrology and Water Resources,
Professor of Civil Engineering and Engineering
Mechanics,
University of Arizona, USA.

Copromotor:

Prof. dr. ir. E.F. Wood

Visiting Professor (2003-2004),
Wageningen Universiteit.
Department of Civil Engineering,
Princeton University, USA.

Promotiecommissie:

Prof. dr. B. van den Hurk

Koninklijk Nederlands Meteorologisch Insti-
tuut.

Prof. dr. ir. M.F.P. Bierkens

Universiteit Utrecht.

Prof. dr. ir. Z. Su

International Institute of Geo-information Sci-
ence and Earth Observation (ITC) and Twente
University.

Prof. dr. ir. P. Kabat

Wageningen Universiteit.

Global Drought in the 20th and 21st Centuries

Analysis of retrospective simulations and future
projections of soil moisture

Justin Sheffield

Proefschrift
ter verkrijging van de graad van doctor
op gezag van de rector magnificus
van Wageningen Universiteit,
Prof. dr. M.J. Kropff,
in het openbaar te verdedigen
op dinsdag 15 januari 2008
des namiddags te vier uur in de Aula.

Sheffield, J.

Global Drought in the 20th and 21st Centuries: Analysis of retrospective simulations and future projections of soil moisture. [Ph.D. thesis, Wageningen University, 2008, xii+206 pp.]

In Dutch: Mondiale droogte in de 20ste en 21ste eeuw: analyse van simulaties van het verleden en toekomstige projecties van bodemvocht. [proefschrift, Wageningen Universiteit, 2008, xii+206 pp.]

ISBN 978-90-8504-806-0

Abstract

We describe the analysis of global and regional drought over the second half of the 20th century from a retrospective model simulation of the terrestrial water cycle, and projected 21st century changes using multi-scenario data from multiple climate models. A global meteorological forcing dataset is developed for 1948-2000 to drive the retrospective simulation by combining observations with reanalysis. Biases in the reanalysis precipitation, temperature and radiation are corrected for systematic bias and spurious trends, which exert erroneous effects on the land water budgets. A monthly soil moisture based drought index is developed from the simulation and is used to investigate the occurrence, variability and trends in drought for 1950-2000. The frequencies of short-term droughts (6 months and less) are highest in humid regions. Medium term droughts (6-12 months) are more prevalent in mid- to high-latitudes, driven by persistent frozen soil moisture anomalies. Over the Sahel and parts of high northern latitudes, the frequency of long-term droughts is at a maximum. Severe drought events are systematically identified in terms of spatial coverage, including the 1988 USA, 1982/83 Australian, 1983/4 Sahel and 1965/66 Indian droughts. There is an overall increasing trend in global soil moisture, driven by precipitation, reflected especially in North America. Regional variation is nevertheless apparent and significant drying over West Africa, stands out. Trends in drought characteristics are mostly decreasing but statistically significant changes are limited in areal extent and generally less than 10% of continental areas. Concurrent decreases in global drought spatial extent are 0.04% yr⁻¹. Within the long-term trends we find interannual and decadal variations in soil moisture and drought characteristics driven mainly by ENSO variability, although the AMO plays an important role in many regions. Drought is driven primarily by variability in precipitation, but temperature has an effect that appears to be exaggerated in the late 20th century, especially in high northern latitudes. At global scales the soil moisture index and the PDSI are reasonably well correlated but this breaks down in cooler regions and seasons, and notably for recent years when the PDSI shows a larger drying trend, possibly due to its temperature-based evaporation estimate. To investigate future projected changes in drought, soil moisture data is analyzed for three future IPCC AR4 climate scenarios (B1, A1B, A2) from eight GCMs. A decrease in 21st century global soil moisture is accompanied by a doubling of the spatial extent and frequency of short-term droughts. Long-term droughts become three

times more common. Regionally, the Mediterranean, West African, Central Asian and Central American regions show large increases, as does mid-latitude North America but with larger inter-scenario variation. Changes under the B1 scenario are the least and the A1B and A2 results are similar. Although the changes are generally monotonic increasing, they are not statistically different from natural variability for multiple decades, in contrast to air temperature, and this depends on the drought variable, magnitude of change, natural variability and statistical confidence. In contrast, changes in the means of hydrologic variables, including soil moisture, are essentially undetectable within the 21st century, implying that changes in extremes may be more detectable than changes in mean quantities.

Foreword

This thesis was carried out while I was a researcher in the Department of Civil Engineering at Princeton University under the stewardship of Professor Eric F. Wood. The work sprung from research into the large scale hydrologic cycle and some initial work done on drought over the USA. Extending this to the global domain and future climate projections were logical next steps.

My path towards completing this thesis was a long and twisted one, and there are many people I would like to thank for trying to help keep it as straight as possible. A big thank you to my mum and dad for letting me do what I wanted academically and professionally. They watched me aimlessly wonder from undergraduate student to full time road-sweeper, to half-hearted masters student, to fully engaged researcher. My dad, who is sadly deceased, was happy for me to do what I wanted (except go into real estate, for some reason) and I thank him for that. To the rest of my family, I hope that I haven't bored you too much with the year-long response of "nearly" to the "have you finished yet" question.

My interest in the hydrological sciences began many years ago when I had grandiose ideas of solving the water crises in Africa by digging wells by hand, only to be disappointed to find out that you had to be a certified engineer to hold a shovel. So I went from undergraduate mathematics (with oceanography to keep the subject from becoming too dry), via engineering mathematics and some interesting minor courses in dam failure, latrine design and sewerage reuse, to water resources and the hydrological sciences. Thanks to my masters supervisor for letting me take courses that were essentially extra-curricula. I would also give thanks to Enda O'Connell and James Bathurst at the University of Newcastle, in the UK, for giving me my first research position, especially after a dismal job interview and having excessively long hair and facial jewelry.

Thanks go to Eric Wood for providing the means and inspiration for this work, and hosting me as a visiting researcher who is still visiting 7 years later. Although a 10 minute telephone interview across the Atlantic was little to go on, he was brave enough to take me on. I thank him for introducing me to the broader issues in hydrology and for teaching me how to write proper English, which is a hard thing for an Englishman to take from a Canadian. If only we could all have "creative thoughts everyday". The motivation for this thesis began in the Annex Bar in Princeton after a discussion with Eric about how I could translate some of the research we were doing into a doctorate degree. For

me, a doctoral thesis is perhaps 15 years overdue, so I thank him for finding a way for an old timer to pursue this.

I must also thank Peter Troch, formerly at Wageningen University (now at University of Arizona, USA) for encouraging me to begin the doctorate program and giving me periodic reminders to pull my finger out and finish the thesis. At Wageningen, thanks to Remko Uijlenhoet for taking care of everything there and to Hidde Leijnse for keeping me on track logistically and for providing the thesis template that prompted me to learn Latex in three days.

I should also thank my current and former colleagues at Princeton who have helped so much and in many ways. Alan Ziegler for getting me to understand that the laid-back approach to hydrology was often the most productive (“let the hydrology come to you, not the other way around”), and for doing great impressions of our boss at the time. Also thanks to Rob Bruant who never talked about work but had great stories of his PhD experiences, and to Matt McCabe, former officemate at Princeton, for Australian style encouragement (“I didn’t know they lowered the PhD standards, mate.”). Thanks to Fenghua Wen and Gopi Goteti for initial work on the drought index and the forcing dataset, respectively.

My wife, Catherine, has probably earned a degree in patience as she tolerated me toiling over the laptop every evening and many weekends for a year or so, trying to analyze gigabytes of soil moisture data over a dial-up internet link. Thanks to you Catherine for your patience and encouragement. I should also mention my children, Talle (4) and Medi (2), who have no idea what a thesis is but enjoyed looking at time series of soil moisture (“look Daddy, wiggly worms!”) being drawn on the computer screen. This is the best kind of encouragement you can find. They do now know that drought is a serious problem although this does not affect their consumption of water at the sink, in the bath or with the garden hosepipe.

Justin Sheffield
Princeton, New Jersey, USA
October, 2007

Contents

1	Introduction	1
1.1	Background	1
1.2	Motivation and Research Objectives	2
1.3	Thesis Overview	4
2	Correction of the rain day statistics in the NCEP/NCAR re-analysis	7
2.1	Introduction	8
2.2	Precipitation Datasets	10
2.2.1	NCEP/NCAR reanalysis	10
2.2.2	UW daily dataset	10
2.2.3	Climatic Research Unit monthly dataset	10
2.2.4	GPCP daily dataset	11
2.2.5	Spatial resolution and temporal coverage	11
2.3	The NCEP/NCAR high-latitude anomaly	11
2.4	Correction of the NCEP reanalysis high-latitude anomaly . . .	15
2.4.1	Correction method	15
2.4.2	Consistency of related variables	16
2.5	Correction results	17
2.5.1	Grid cells corrected	17
2.5.2	Corrected datasets	17
2.6	Discussion	19
2.6.1	Choice of correcting dataset	19
2.6.2	Loss of spatial coherence and storm tracking	19
2.6.3	Temporal persistence in related variables	23
2.6.4	Effects on the land surface water budget	24
2.7	Summary and conclusions	29
3	Development of a global meteorological forcing dataset, 1950-2000	31
3.1	Introduction	32
3.2	Datasets	35
3.2.1	NCEP/NCAR reanalysis	36
3.2.2	CRU monthly climate variables	36

3.2.3	GPCP daily precipitation	38
3.2.4	TRMM 3-hourly precipitation	38
3.2.5	NASA Langley monthly surface radiation budget (SRB)	38
3.3	Development of the forcing dataset	39
3.3.1	Correction of the reanalysis rain day anomaly	39
3.3.2	Spatial downscaling	40
3.3.3	Temporal downscaling	45
3.3.4	Monthly bias corrections	48
3.4	Discussion and Conclusions	58
3.4.1	Comparison with GSWP-2 forcing dataset	59
3.4.2	Future improvements	62
3.4.3	Dataset availability	63
3.4.4	Concluding remarks	63
4	Development of a global dataset of soil moisture and drought, 1950-2000	65
4.1	Introduction	66
4.2	Datasets and methods	68
4.2.1	Off-line land surface simulation	69
4.2.2	Analysis of soil moisture and derivation of drought index	70
4.2.3	Temporal and spatial drought statistics	73
4.2.4	Some caveats and uncertainties	75
4.3	Results	76
4.3.1	Global variation of soil moisture	76
4.3.2	Spatial extent of drought	77
4.3.3	Run frequency and duration	80
4.3.4	Run intensity and severity	81
4.3.5	Relationship between run duration and intensity	83
4.4	Discussion	84
4.4.1	Comparison with the PDSI	84
4.4.2	Identification of severe drought events	85
4.4.3	Analysis of selected major drought events	89
4.5	Summary and conclusions	94
5	Trends and variability in 20th century global drought	97
5.1	Introduction	98
5.2	Datasets and methods	100
5.2.1	Land surface hydrological simulation	100
5.2.2	Relationship with previous studies of drought using the VIC model	101
5.2.3	Soil moisture based drought index	102
5.3	Trends in soil moisture and drought	103
5.3.1	Trends in soil moisture	103
5.3.2	Global trends in drought characteristics	108
5.3.3	Regional trends in drought spatial extent	112
5.3.4	Epochal changes in drought frequency	112

5.4	Temporal variability of soil moisture and drought	114
5.4.1	Regional temporal variability	114
5.4.2	Variation and robustness of trends	121
5.5	Relationships with meteorological forcings	124
5.5.1	Relationship with precipitation and temperature variability	124
5.5.2	Sensitivity of drought to temperature trends	125
5.6	Discussion and conclusions	128
5.6.1	Uncertainties in the meteorological forcings and hydro- logic modeling	128
5.6.2	Summary and conclusions	131
6	Projected changes in 21st century drought	133
6.1	Introduction	134
6.2	Datasets and methods	138
6.2.1	Climate model simulations	138
6.2.2	Drought estimation	138
6.2.3	Statistical methods	140
6.2.4	Data preparation	140
6.3	Results	141
6.3.1	Natural variability of drought from GCM control simu- lations	141
6.3.2	20 th century drought and comparison with off-line modeling	143
6.3.3	Global and regional drought under future climate scenarios	145
6.3.4	Statistical significance of changes	145
6.3.5	Drivers of changes in drought occurrence	155
6.4	Detectability of changes in drought	158
6.4.1	Examples of regional detectability	158
6.4.2	Detectability under different scenarios	159
6.4.3	Detectability as a function of risk	159
6.4.4	Detectability relative to the 20 th Century	162
6.4.5	Multi-Model ensemble versus single model detectability	162
6.4.6	Comparison with detection times of primary climate vari- ables	164
6.5	Discussion and conclusions	165
7	Synthesis	171
7.1	Summary	171
7.2	Conclusions and Future Directions	176
	Bibliography	181
	Samenvatting	201
	Curriculum Vitae	203

Chapter 1

Introduction

1.1 Background

Drought is a pervasive climate phenomenon that is considered to be one of the most damaging natural hazards in terms of economic cost (Wilhite, 2000). In the US, it is the costliest natural hazard, averaging \$6-8 billion in damages annually, with the 1988 central U.S. drought impact estimated to be over \$60 billion. Drought can cover extensive areas and last from months to multiple years and may have major impacts on agriculture, water supply and the environment. Historically drought has persistently affected human activity (e.g. Hodell et al., 1995, Stine, 1994) and impacts in every part of the globe in which habitation is possible.

Drought occurs as a result of extremes in climate that are driven by natural variability but may be exacerbated or dampened by anthropogenic influences. The climate varies naturally in response to external forcings, such as solar radiation (Christensen and Lassen, 1991) and atmospheric aerosols (Robock and Mao, 1995), and because of internal interactions between components of the climate system (Trenberth and Hurrell, 1994). This internal variability is driven in the main by the El Nino Southern Oscillation (ENSO), which impacts the Tropics and many regions in mid-latitudes (Ropelewski and Halpert, 1987). Other climate oscillations and modes of large-scale variability, such as the North Atlantic Oscillation (NAO), the Pacific Decadal Oscillation (PDO), and the Atlantic Multi-Decadal Oscillation (AMO), act on generally longer time scales and interact with ENSO or are the primary climate drivers elsewhere and more regional in their impacts.

The extremes of climate variations have consequences on the terrestrial water cycle in general, and when coupled with potential climate change, which may impact regionally and exaggerate the influence of natural variability, the extremes of climate may become more pronounced (Easterling et al., 2000; Palmer and Räisänen, 2002). As temperatures rise, the capacity of the atmosphere to hold moisture would increase as governed by the Clausius-Clapeyron equation (Held and Soden, 2000), with potential for an intensification of the

water cycle in terms of increased evaporation and/or precipitation (Trenberth, 1999), although these may be limited by other factors such as available energy and aerosol concentration. Climate model studies have shown that variability is likely to increase under plausible future climate scenarios (Wetherald and Manabe, 2002), dependent upon climate sensitivity, with large regional changes in the water cycle. The potential for more droughts and of greater drought severity is a worrisome possibility (Wetherald and Manabe, 1999; Wang 2005).

Huntington (2006) reviews the observational evidence so far for water cycle intensification to date and concludes that despite some contradictions the overall picture points towards intensification. For drought specifically, trends have been analyzed over the past 50 to 100 years at regional (e.g. Lloyd-Hughes and Saunders, 2002; Rouault and Richard, 2005; Andreadis and Lettenmaier, 2006) and global scales (Dai et al., 2004). When analyzing the Palmer Drought Severity Index (PDSI) and the Standardized Precipitation Index (SPI) over Europe, Lloyd-Hughes and Saunders (2002) found insignificant change in the proportion of land experiencing medium to extreme drought during the 20th century. A drought analysis of South African SPI by Rouault and Richard (2005) found a substantial increase in 2-year droughts since the 1970s. They also found inter-decadal variability in the spatial extent of drought since the beginning of the century, most of the severest of which are associated with ENSO. Andreadis and Lettenmaier (2006) analyzed a long-term (1915-2003) hydrological simulation over the USA and found a general increasing trend in soil moisture, with concurrent decrease in drought duration and extent, except for the Southwest and parts of the West. Globally, Dai et al., (2004) showed the global pattern of trends in annual PDSI and found that generally drier conditions have prevailed since the 1970s.

1.2 Motivation and Research Objectives

The reduction of the impacts of drought has obvious benefits economically and environmentally. Progress towards this involves making improvements to operational monitoring and seasonal forecasting which in turn requires greater understanding of the occurrence of drought and the mechanisms that drive its initiation, persistence and recovery. There is also a need to understand the potential changes in drought under future climate warming.

Despite its omnipresent nature, our knowledge of the onset, development and recession of drought is deficient. This hampers not only our ability to monitor drought but also to predict its occurrence at seasonal time scales, and evaluate climate model projections of future changes. Part of the reason for this is the lack of detailed data about its spatial and temporal variability across large scales. We also have an insufficient understanding of the hydrologic and weather conditions and mechanisms that lead to drought initiation, persistence and recovery. The generally poor predictive ability of seasonal climate models to forecast drought reflects this lack of understanding.

Given the pervasive nature of drought and the magnitude of its impacts,

there is a general need for greater understanding of its occurrence and the potential changes in the future. This thesis is therefore motivated by the following underlying research question:

What has been the occurrence of global and regional drought over recent decades and how is this likely to change in the future?

More specifically, this can be broken down into a series of questions that guide the research presented. “Can we describe the variability of the terrestrial water cycle and drought through existing data sources and models?”, “What has been the occurrence of global and regional drought over the 20th century?”, “How will the occurrence of drought change in the future?”.

At a more general level, quantifying the variability in the terrestrial water budget is central to understanding the interaction of the hydrologic cycle with human activities and identifying the signals of climate change. Improved estimates of seasonal to inter-annual variability are vital for determining the requirements of water resources operations, quantifying the risks of flooding and droughts, and for understanding the effect of climate change on water resources and environmental well-being (Oki and Kanae, 2006). These estimates can also provide the necessary basis for a multitude of hydro-climatological research activities including the assessment of hydrological extremes (Sheffield and Wood, 2007) and studies of the predictability of future hydrologic states as seasonal scales, through the characterization of persistence and teleconnections (Maurer et al., 2004). Furthermore, the detection of climate and anthropogenic induced changes requires accurate estimates of natural variability to be able to discern the forced signal from the background noise, and confidence in future climate projections, especially on regional scales, is dependent on the ability of climate models to replicate this variability (Giorgi, 2002).

To understand how drought varies (and other characteristics of the large scale hydrologic cycle), long-term observations of relevant variables, such as precipitation, streamflow and soil moisture, are required. Global datasets of these variables are lacking at high spatial resolution or are available only for limited time periods. Alternatively, models can provide spatially and temporally consistent fields of these variables at large scales when forced with observed boundary conditions. Therefore, to address the above research questions, we have focused on model output and particularly soil moisture to characterize drought and its variability. We carry out analyses of historic and future projected soil moisture using data from off-line simulations of the global terrestrial water cycle and projections from global climate models. It is argued that retrospective simulation provides our best estimate of the variation of the terrestrial water cycle and its extremes over the last 50 years. Similarly, projections of future changes can only be derived from models and climate model output is our best resource for this. We focus on soil moisture anomalies as an indicator of drought given that it captures the aggregate balance of all hydrologic processes and represents available water.

1.3 Thesis Overview

This thesis describes the analysis of global and regional drought over the second half of the 20th century from a retrospective simulation of the terrestrial water cycle, and projected changes for the 21st century using multi-scenario data from multiple climate models. A meteorological forcing dataset is developed to drive the retrospective simulation and this is described in the first two chapters. Given that the forcing data for off-line land surface modeling are usually the first order source of errors in the subsequent modeled states, this dataset was carefully constructed to reduce these as far as possible. The third paper introduces the retrospective simulation, as driven by this forcing dataset, and the development of the soil moisture based drought index. A detailed evaluation of this simulation in terms of its setup, comparisons with available observations of the water cycle, and analysis of variability is reported elsewhere (Sheffield et al., 2007c). However, an overview of the main features of the simulation are given in chapter 3, as well as an evaluation of the representation of historic drought events over past 50 years. Chapters 4 and 5 then analyze trends and variability in drought occurrence, historically and for several future scenario projections. Each chapter of the thesis was originally written as a separate paper and as such there is some overlap between chapters in the description of background material, motivation and datasets.

The forcing dataset is developed by combining near surface meteorological fields from reanalysis with observation based datasets to provide the best estimate at the highest supportable spatial and temporal resolution. Chapter 1 describes the initial development of the forcing dataset, specifically the correction of the precipitation statistics of the reanalysis which are found to exhibit a spurious wavelike pattern in high latitudes and are generally biased elsewhere. The impact of these features on the terrestrial water cycle are analyzed and are then corrected so that they match the statistics of observations.

In chapter 2 the development of the full, 50-yr (1950-2000), global, meteorological forcing dataset is described. This extends the work described in chapter 1, to provide bias corrected fields of precipitation, air temperature, radiation and other near surface meteorological fields suitable for retrospective land surface modeling at regional to global scales. Evaluations are made of the biases in the reanalysis against available observations and comparisons are made between the corrected dataset and a similar product.

The retrospective drought dataset is developed in chapter 3 using output fields from a 50-yr simulation of the global terrestrial water cycle as driven by the forcing dataset. Drought is defined as a period of deficit soil moisture below a threshold. Soil moisture and drought characteristics are analyzed in terms of their spatial variability to develop climatological estimates of drought frequency, duration and severity globally. The dataset is systematically scanned to identify historic regional drought events and some of the major events are analyzed further to see how well the dataset represents drought globally over the past 50 years.

Chapter 4 analyzes this dataset in terms of the variability and trends in soil

moisture and drought characteristics on global and regional scales. Evaluations are made on changes in soil moisture over the last 50 years as well as changes in drought duration, intensity and severity. The variability of soil moisture is investigated at large scales by relating the major modes of variability to large scale climate oscillations and at local scales through relationships with precipitation and temperature. These relationships are further investigated in the context of global warming by analyzing a second simulation driven by climatological air temperature to see the impact of temperature trends on changes in soil moisture.

In chapter 5, projected changes in soil moisture and drought are evaluated through analysis of data from the recent Intergovernmental Panel on Climate Change (IPCC) Fourth Assessment Report (AR4) simulations. To take into account the uncertainty derived from representation of physical processes, data are taken from multiple models. Uncertainty in how greenhouse gas emissions will change in the future are also taken into account by assessing changes under three scenarios that represent a range of plausible futures. Assessments are also made of the detectability of changes, given that the magnitude of the signal of change relative to the noise of natural variability is likely to increase with time.

The final summary describes the major findings of the work and puts this into context of other ongoing work and future directions.

Chapter 2

Correction of the rain day statistics in the NCEP/NCAR reanalysis

This chapter is a slightly modified version of: Sheffield, J., A. D. Ziegler, E. F. Wood, and Y. Chen, 2004: Correction of the high-latitude rain day anomaly in the NCEP/NCAR reanalysis for land surface hydrological modeling, *J. Climate*, 17(19), 3814-3828.

Abstract

A spurious wavelike pattern in the monthly rain day statistics exists within the National Centers for Environmental Prediction and National Center for Atmospheric Research (NCEP/NCAR) Reanalysis precipitation product. The anomaly, which is an artifact of the parameterization of moisture diffusion, occurs during the winter months in the northern and southern hemisphere high latitudes. We correct the anomaly using monthly statistics from three different global precipitation products from (1) the University of Washington (UW), (2) the Global Precipitation Climate Project (GPCP) and (3) the Climatic Research Unit (CRU), resulting in three slightly different corrected precipitation products. The correction methodology, however, compromises spatial consistency (e.g., storm tracking) on a daily time scale. We investigate the effect the precipitation correction has on the reanalysis-derived global land-surface water budgets by forcing the Variable Infiltration Capacity (VIC) land-surface model with all four datasets (i.e., the original reanalysis product and the three corrected datasets). The main components of the land-surface water budget cycle are not affected substantially; however, the increased spatial variability in precipitation is reflected in the evaporation and runoff components but reduced in the case of soil moisture. Furthermore, the partitioning of precipitation into canopy evaporation and throughfall is sensitive to the rain day statistics of the correcting dataset, especially in the tropics, and this has implications for the required accuracy of the correcting dataset. The output fields from these long-term, land-surface simulations provide a global, consistent dataset of water and energy states and fluxes that can be used for model inter-comparisons, studies of annual and seasonal climate variability, and comparisons with current versions of numerical weather prediction models.

2.1 Introduction

Off-line computer simulations of continental- and global-scale water balances are valuable for studying climate variability/change and the hydrological implications thereof. The lack of consistent, long-term observations of land surface water states and fluxes over large spatial scales means that the use of such simulations for determining variability in the major components of the hydrological cycle is an attractive alternative. Conversely, the relative wealth of observations of the atmosphere and sea surface means that a number of global, long-term, near surface atmospheric analyses exist: e.g. the NCEP/NCAR reanalysis (Kalnay et al., 1996; Kistler et al., 2001), the NCEP/DOE reanalysis (Kanamitsu et al., 2002) and the ECMWF reanalysis (Gibson et al, 1997). These analyses assimilate observed atmospheric and sea surface states into an atmospheric forecast model to obtain global coverage of surface meteorology which can then be used to force land surface models to generate global, sub-daily, datasets of land surface water and energy fluxes and states. Although these model derived forcing fields may not be perfect, they are self-consistent

and are used by many to model the land surface water and energy balances.

The NCEP/NCAR Reanalysis provides long-term, near surface meteorological data (e.g., precipitation, temperature, wind speed, vapor pressure, radiation) at the high temporal resolution (daily and higher) required by land surface models. However, the structure of the atmospheric model used in the reanalysis assimilation system introduces systematic errors into some reanalysis fields, particularly at high latitudes and other regions where observations are scarce. Some analysis variables, such as precipitation, are generated entirely by the model without assimilation of observational data and are therefore dependent on the model parameterizations. As such, the precipitation data are acknowledged to be somewhat unreliable at regional and sub-seasonal scales (Kalnay et al., 1996), although comparisons with independent observations and with several climatologies show that the data contain useful information at seasonal to annual scales (Kalnay et al., 1996; Janowiak et al., 1998; Kistler et al., 2001).

Figure 2.1 shows, the seasonal average number of rain days of the NCEP/NCAR reanalysis for the period 1948-1998. At the global scale the spatial patterns of rain days and precipitation seem reasonable with high values in the tropics that follow the seasonal undulation of the Inter-Tropical Convergence Zone (ITCZ), lower values in the mid- and high-latitudes and the distinctive desert regions in Africa, the Middle East and Australia, amongst others. However, a noticeable wave-like pattern (alternating zones of high and low) exists in the high northern latitudes for both the number of wet days and to a lesser extent for the precipitation totals (not shown). This pattern, also reported by Cullather et al. (2000), is most apparent in the winter months of the northern hemisphere, reduces somewhat in the spring and autumn, and disappears in the summer months. A similar anomaly, not shown (over ocean), exists in high southern latitudes during the southern hemisphere winter.

In this paper the uncertainty in the daily variability of the reanalysis precipitation is assessed by comparison with three other global precipitation datasets: (4.1) the 15-year dataset developed by the surface water modeling group at the University of Washington, (4.2) the 1997-1999, Global Precipitation Climatology Project product and (3) the Climatic Research Unit 98-year dataset. A methodology for correcting the anomaly in the NCEP dataset using the monthly statistics from another precipitation dataset is presented. The correction method is applied to the NCEP dataset using monthly statistics from each of the three comparison datasets. Motivation for this study is the creation of a global, multi-decade, terrestrial, meteorological forcing dataset to drive land surface model simulations of the global water and energy balance. Therefore, the effect of the correction is discussed in terms of the land surface water budget by analyzing long-term simulations using the VIC land surface model.

2.2 Precipitation Datasets

2.2.1 NCEP/NCAR reanalysis

The NCEP/NCAR Reanalysis (referred to hereafter as the NCEP reanalysis) is a retrospective global analysis of atmospheric and surface fields extending from 1948 to the near present (Kalnay et al., 1996, Kistler et al., 2001). Available observations are assimilated into a global atmospheric spectral model implemented at a horizontal resolution of T62 (approximately 210-km) and with 28 sigma vertical levels. The reanalysis is created using a “frozen” version of the data assimilation system, although assimilated observations are subject to changing observing systems. Consistent gridded output fields are generated continuously in space and time and are classified according to how they are determined and their reliability. Class “A” variables are strongly influenced by assimilated observations and are therefore regarded as being the most reliable fields. These fields include upper air temperatures, rotational wind and geopotential height. Less reliable are class “B” variables, such as moisture, divergent wind and surface parameters, which are influenced by observations and the model. Class “C” variables, such as surface fluxes and heating rates, are completely determined by the model and as such are the least reliable. Precipitation is classified as a class “C” variable.

2.2.2 UW daily dataset

The University of Washington (UW) surface water modeling group precipitation data set (Nijssen et al., 2001a) covers a 15-year (1979–1993) time period at 2-degree resolution. Daily observations from 7800 stations from the Climate Prediction Center (CPC) global dataset are used to downscale the monthly precipitation datasets of Hulme (1995) and the Global Precipitation Climatology Project (GPCP) (Huffman et al., 1997). Aggregation from station data to 2-degree resolution is carried out using inverse distance square weights based on the distance from each station to the center of each of the 16 0.5-degree subcells. The final 2-degree value is the mean of the 16 subcells. In areas where station data are sparse, daily series were generated using a stochastic model consisting of a two-state (wet/dry) first-order Markov chain for precipitation occurrences and a two-parameter gamma distribution for intensities. The parameters are initially estimated from the data derived where station data are available and then interpolated to the data sparse regions.

2.2.3 Climatic Research Unit monthly dataset

The Climatic Research Unit (CRU) product is a 0.5-degree gridded dataset of monthly terrestrial surface climate variables for the period of 1901–1998 (New et al., 1999, 2000). The spatial coverage extends over all land areas, including oceanic islands but excluding Antarctica. Fields of monthly climate anomalies, relative to a 1961–1990 climatology, were interpolated using thin-plate splines

from surface climate data. The anomaly grids are then combined with the 1961–1990 climatology resulting in grids of monthly climate over the 98-year period. Primary variables (precipitation, mean temperature, and diurnal temperature range) are interpolated directly from station observations. The remaining secondary climatic elements (including rain day frequency) are interpolated from merged datasets comprising station observations and, in regions without station data, synthetic data estimated using predictive relationships with the primary variables.

2.2.4 GPCP daily dataset

The Global Precipitation Climatology Project (GPCP) is a central element of the World Climate Research Program (WCRP, 1990; Huffman et al., 1997), providing a daily precipitation product for the period 1997-1999 at 1° resolution (Huffman et al., 2001). The data are based on a combination of precipitation estimates from a merged satellite IR dataset over 40°N - 40°S and a rescaling of the Susskind et al. (1997) TIROS Operational Vertical Sounder (TOVS) satellite estimates at higher latitudes. Both contributing estimates are scaled to match the GPCP version 2 monthly satellite-gauge dataset totals (Huffman et al., 1997). Rain day frequencies of the IR based estimate are adjusted to match data from the Special Sensor Microwave Imager (SSM/I) retrieval. The TOVS based rain day frequencies are adjusted to the IR based estimate at 40°N and 40°S separately.

2.2.5 Spatial resolution and temporal coverage

To carry out inter-comparisons, all datasets were interpolated to a spatial resolution of 2° using bilinear interpolation over their common spatial coverage of terrestrial areas excluding Greenland and Antarctica. Although previous studies have reported that the high-latitude anomaly in precipitation can be smoothed through interpolation (Cullather et al., 2000; Serreze and Hurst, 2000), Figure 2.1 shows that the anomaly is still evident in the rain day frequencies after interpolation. There is no single common time period amongst the four precipitation datasets and so comparison of any two datasets is carried out over their common overlap period. The final corrected precipitation datasets were generated at 2° resolution for 1948-1998, this being the common time period of the NCEP and CRU datasets and the CRU dataset being used to scale the corrected precipitation monthly totals as described in section 4.

2.3 The NCEP/NCAR high-latitude anomaly

The anomaly results from the formulation used for the moisture diffusion in the atmospheric model of the NCEP/NCAR Reanalysis system (Kistler et al., 2001; NCEP/NCAR Reanalysis web page <http://wesley.wvb.noaa.gov/reanalysis.html>). The resulting spurious moisture sink/source creates unrealistically large or

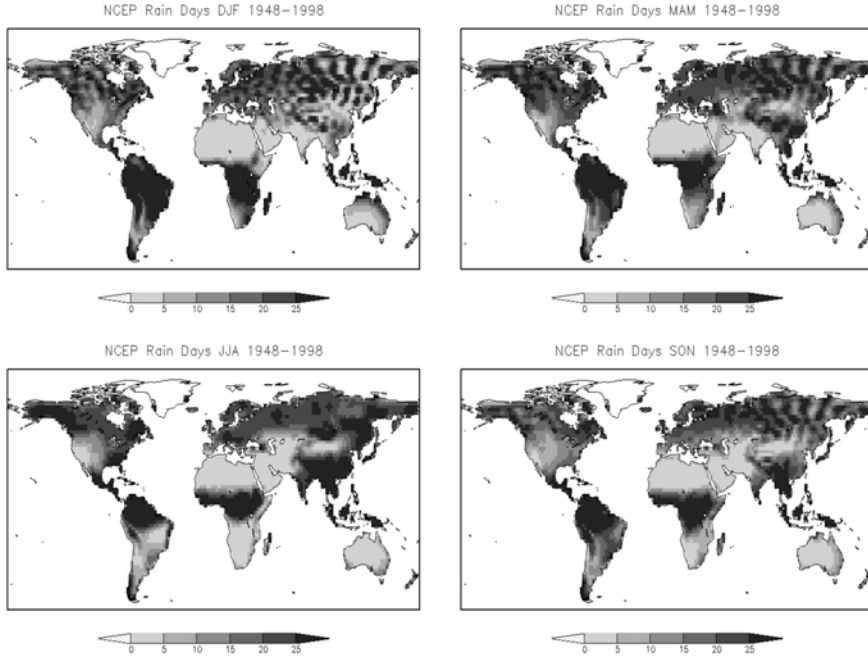


Figure 2.1: Seasonally averaged monthly rain days over the period 1948-1998 for the NCEP/NCAR Reanalysis showing the spurious pattern in the high-latitudes of the northern hemisphere in the non-summer months.

small amounts of precipitation, and is sensitive to elevation and high-latitudes where the specific humidity is low in comparison with the global average specific humidity. A more accurate approximation of moisture diffusion has been introduced in the next version of the NCEP Reanalysis (Kanamitsu et al., 2002), which has corrected the problem. Regardless, the methodology presented in this paper can be applied to this new reanalysis, or any other dataset, to correct any other biases that are revealed.

A comparison of the mean monthly number of rain days of the NCEP reanalysis with the UW, CRU and GPCP datasets is shown in Figure 2.2 for the northern hemisphere winter months (DJF). The values are determined for a period of time corresponding to the overlap of the NCEP dataset with the comparison dataset (CRU: 1948-1998, UW: 1979-1993, GPCP: 1997-1998). From a global perspective, the four datasets are largely similar; however, some important regional differences exist. Most prominent is the high-latitude wave-like anomaly in the NCEP reanalysis. Furthermore, the NCEP reanalysis has more wet days in the tropics than any of the other datasets, although the GPCP dataset is somewhat similar. The sub-tropical dry areas compare well between the NCEP reanalysis and each of the other datasets. The high latitudes in the northern hemisphere have more wet days in the NCEP reanalysis, most

notably in northeast Asia and the northwest and northeast of North America. Similar biases are also evident in all other seasons (not shown), although the high-latitude wave-like anomaly is not apparent in the northern hemisphere summer months.

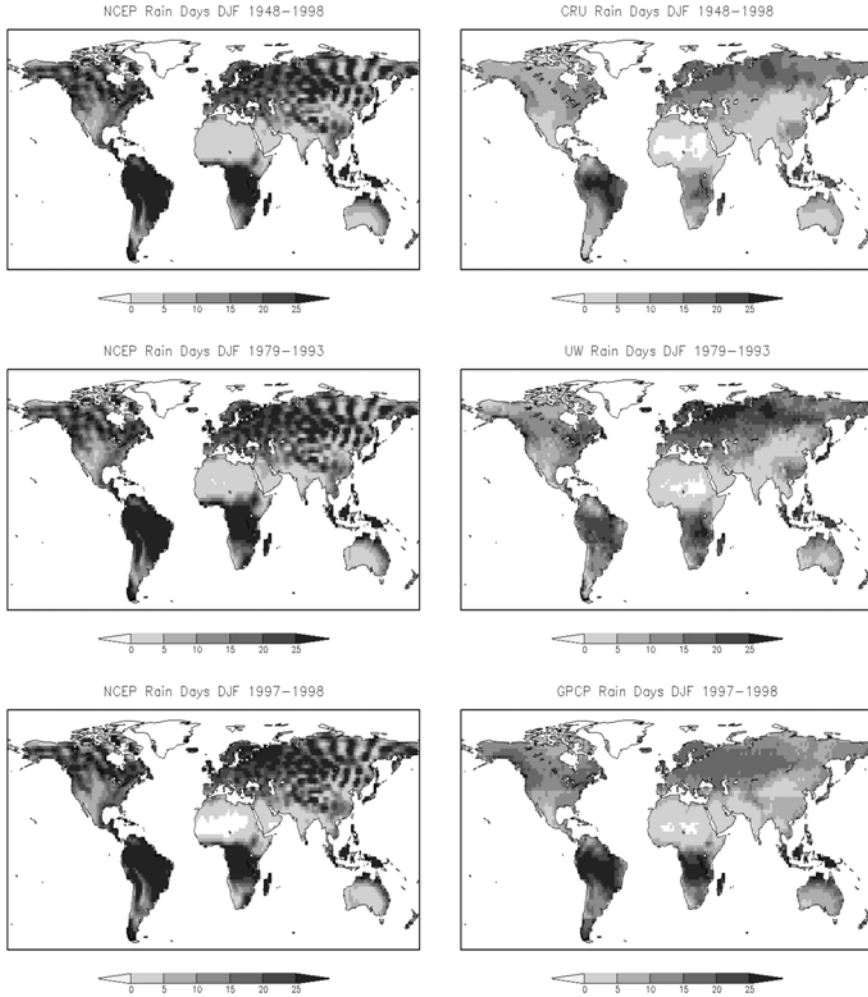


Figure 2.2: Seasonally averaged monthly rain days for DJF for a) the NCEP and CRU datasets for the period 1948-1998, b) the NCEP and the UW datasets for the period 1979-1993 and c) the NCEP and the GPCP datasets for the period 1997-1998.

Figure 2.3 shows the time series of the mean monthly number of rain days for each continent for the common period of all datasets (1979-1993), except for the GPCP dataset, which is not shown as it only overlaps the period 1997-

1998. In general, the NCEP rain day means are higher than those of the UW dataset, which are in turn higher than the CRU dataset. The exceptions to this are Oceania, for which the NCEP and UW values are similar except for the early part of the year, and South America, where the UW and CRU values match well.

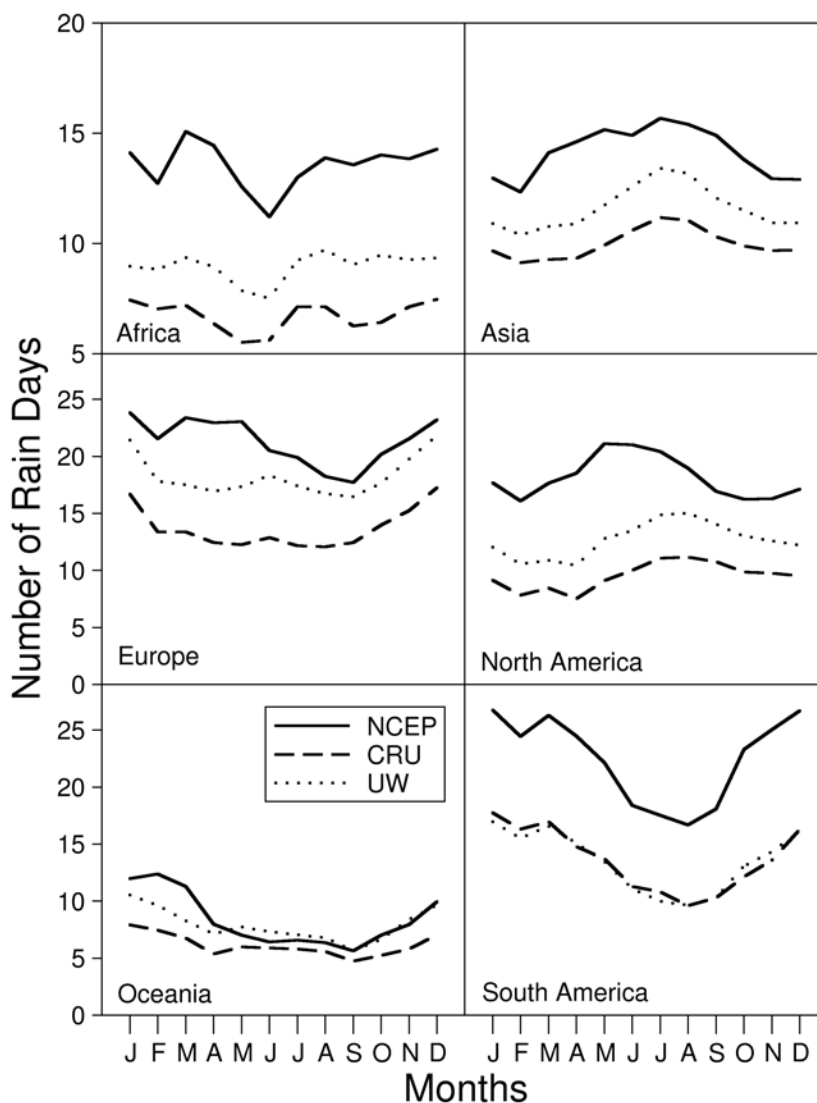


Figure 2.3: Time series of average monthly rain days over the period 1979-1993 for the continents for the NCEP, CRU and UW datasets.

2.4 Correction of the NCEP reanalysis high-latitude anomaly

2.4.1 Correction method

The correction of the anomaly in the NCEP precipitation may be divided into a number of steps: 1) the systematic identification of the grid cells to be corrected, 2) the correction of the NCEP precipitation values for each of these grid cells using the monthly statistics of one of the other precipitation datasets and 3) scaling of the monthly precipitation totals to match those of the CRU dataset.

i) Step 1: Identify the grid cells to be corrected

To decide which grid cells are to be corrected, a statistical test is carried out to determine whether the NCEP dataset is statistically similar to the comparison dataset or not. A Z statistic (based on proportion) is computed for each cell, and this is used to test the null hypothesis that the number of rain days in the NCEP dataset and the comparison dataset are equal. This is repeated for each of the three comparison datasets (CRU, UW and GPCP). The statistic is calculated based on the total number of rain days for any given month:

$$z = \frac{p_1 - p_2}{\sqrt{p(1-p)(1/n_1 + 1/n_2)}} \quad (2.1)$$

where p_1 is the number of rain days in the NCEP dataset; p_2 is the number of rain days in the comparison dataset; n_1 is the total number of days in the NCEP dataset; n_2 is the total number of days in the comparison dataset; and p is the pooled estimate for the common population proportion:

$$p = \frac{n_1 p_1 + n_2 p_2}{n_1 + n_2} \quad (2.2)$$

ii) Step 2: Correct the daily precipitation for inconsistent grid cells

The aim of the correction is to force the rain day statistics of the NCEP data to match those of the comparison dataset by using the monthly wet-wet and dry-dry conditional probabilities of the comparison dataset. These probabilities are used within a first-order Markov-type process (Wilks and Wilby, 1999) to make decisions on whether the NCEP precipitation on a certain day is of the correct type (wet or dry) in relation to the previous day. The correction algorithm is applied separately for each grid cell and is as follows. To begin, the first day of the NCEP precipitation time series is accepted as being correct. The type of the next day is generated at random using the conditional probabilities of the correcting dataset for the current month and grid cell. If the type of the original NCEP day matches the type of the randomly generated day, then the NCEP precipitation value is accepted. If it does not match, then a day of the appropriate type (wet or dry) is selected at random from the total population of all days of this type in the NCEP dataset for the current month and grid cell. This is repeated for every day in the time series.

The conditional probabilities cannot be calculated for the CRU product, as it is a monthly dataset. Therefore, these are generated by sampling from the archive of UW conditional probabilities for months which have the same rain day frequency as the CRU dataset. For some months, a matching rain day frequency may not exist in the UW archive and so a month-long time series of wet and dry days was repeatedly generated at random until it matched the CRU rain day frequency and the conditional probabilities were then calculated from this.

iii) Step 3: Scale the monthly totals

Although the correction method described in the previous section ensures that the number of rain days in the NCEP dataset is consistent with the correcting dataset, it ignores the consistency of the precipitation totals. Inconsistent dry days are corrected by replacement with a rain day chosen at random without regard to the precipitation total for the chosen day. This is likely to introduce errors in the monthly precipitation totals that are in addition to the biases that are seen in the precipitation totals of the original NCEP dataset (Trenberth and Guillemot, 1998; Kistler et al., 2001). Therefore, in step 3 of the correction method, the NCEP corrected daily totals are scaled by the ratio of the monthly totals of the CRU and the NCEP corrected datasets, so that the NCEP corrected monthly totals match those of the CRU dataset. This simple scaling method can potentially produce unreasonably high daily precipitation values when the un-scaled daily value is an outlier and the CRU monthly precipitation is much higher than the NCEP precipitation. Such situations are localized and generally occur at the limits of desert regions and at the edge of large-scale climate phenomena with strong seasonal cycles such as the Inter-Tropical Convergence Zone. In these regions, relatively small differences between the NCEP and CRU datasets in the location and seasonal variation of these large-scale features can lead to large monthly precipitation ratios at the grid scale. Although the occurrence of unreasonably high daily values is rare and localized, a more robust method of scaling the data to match observed monthly totals would have to be employed in any final version of the corrected dataset.

2.4.2 Consistency of related variables

Correcting the precipitation field may result in the related near surface meteorological variables in the NCEP reanalysis being inconsistent with the corrected precipitation. For example, if a dry day is changed to a wet day then the original solar radiation for this day may be for a clear day. Therefore, as part of the correction method, the related variables were changed for the same days for which the precipitation was corrected, including wet days that are changed to dry days, ensuring that the dataset is self-consistent.

2.5 Correction results

The NCEP daily precipitation is corrected with the above methodology using the statistics from each of the three datasets (CRU, UW and GPCP), resulting in three slightly different corrected precipitation datasets. As the UW and GPCP datasets do not overlap the 1948-1998 period completely, the mean monthly conditional probabilities for these datasets are applied repeatedly for all years. This assumes that the mean monthly statistics for the overlap period are representative of the whole 49 years.

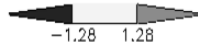
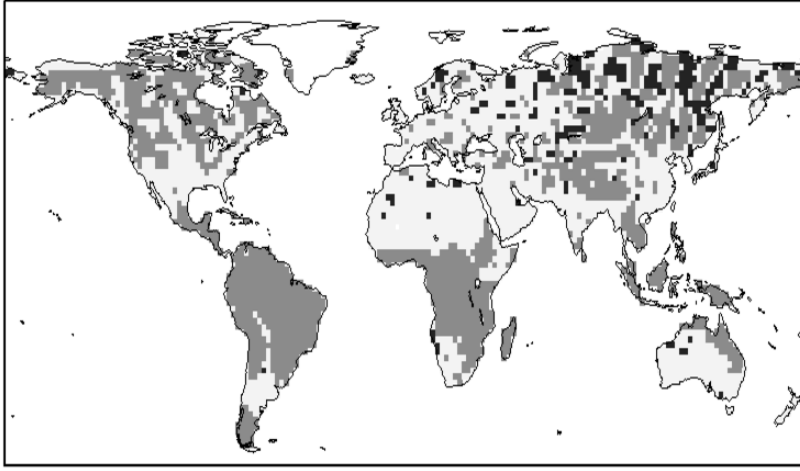
2.5.1 Grid cells corrected

The Z statistic was calculated with Equation 2.1 for the NCEP dataset and the three comparison datasets over the time periods common to each pair of datasets and an example of the results using the UW statistics are shown in Figure 2.4. The unshaded areas indicate where the NCEP data are statistically similar to the comparison dataset. The shaded areas indicate where the NCEP dataset has significantly more (dark gray shading) or less (light gray shading) rain days, based on a 75% confidence level (equivalent to a p value of ± 1.28). It is the data values from these shaded areas that are corrected. The maps highlight the before-mentioned differences in rain day frequencies, including the spurious wave-like pattern in the NCEP dataset in the winter months and the significantly higher number of wet days in the NCEP than the UW (and CRU) datasets over much of the globe. The comparison with the GPCP dataset (not shown) shows a closer match in general which may be due to the GPCP rain days being based on satellite grid values as opposed to gauge data which may tend to underestimate the frequency of rain. However, the short time period (3 years) of the GPCP dataset results in a weak statistical test and therefore the worth of the comparison is unknown.

2.5.2 Corrected datasets

An example of the results of the correction is shown in Figure 2.5. This is the seasonally averaged number of rain days for the northern hemisphere winter (DJF) for the UW dataset and the corresponding corrected dataset. The corrected precipitation dataset resembles the corresponding correcting dataset, which is desirable and to be expected as the correction method is designed to force the statistics of the two datasets to match. The results for the other seasons and correcting datasets (CRU and GPCP) show similarly good matches. In addition to correcting the high-latitude rain day anomaly, differences that occur elsewhere are also removed. For example, in the tropics the high numbers of rain days in the NCEP dataset are reduced to the levels found in the CRU and UW datasets. This is illustrated more clearly in Figure 2.6, which shows a scatter plot of the NCEP average monthly number of rain days versus that for the CRU, UW and GPCP datasets and their respective corrected versions for the six continents. The corrected datasets are similar to the corresponding

Z-statistic NCEP vs UW 1979–1993 January



Z-statistic NCEP vs UW 1979–1993 July

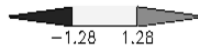
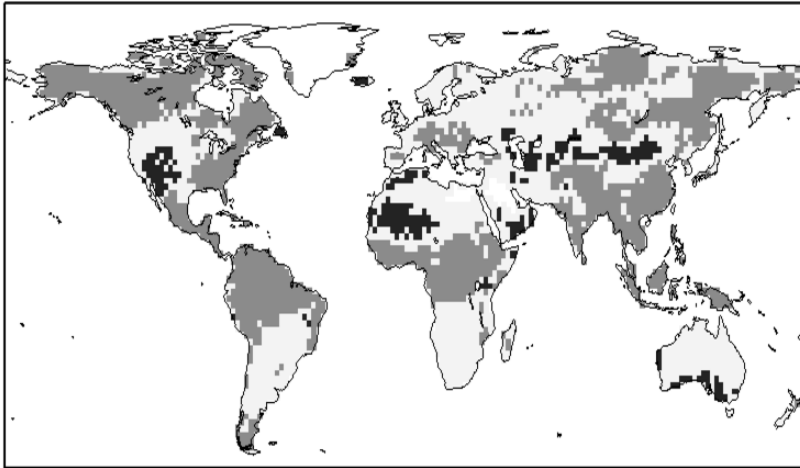


Figure 2.4: Z statistic (Equation 2.1) indicating the statistical similarity between the mean monthly number of rain days of the NCEP dataset and UW dataset for January and July. The values of ± 1.28 are the critical levels of the Z statistic in a two-tailed test at a 75% confidence level.

correcting dataset for both the CRU and UW with some slight differences most evident for the UW dataset over Europe and Oceania. In the case of the GPCP dataset, the corrected data are generally closer to the GPCP dataset than the NCEP, yet there are still large differences for most continents. In any case, the monthly statistics of the corrected dataset will never be identical to those of the correcting dataset because of the stochastic nature of the correction method. How well they match depends also on the difference between the NCEP and correcting dataset and the threshold (or confidence level) of the statistical test for determining if a grid cell requires correction.

2.6 Discussion

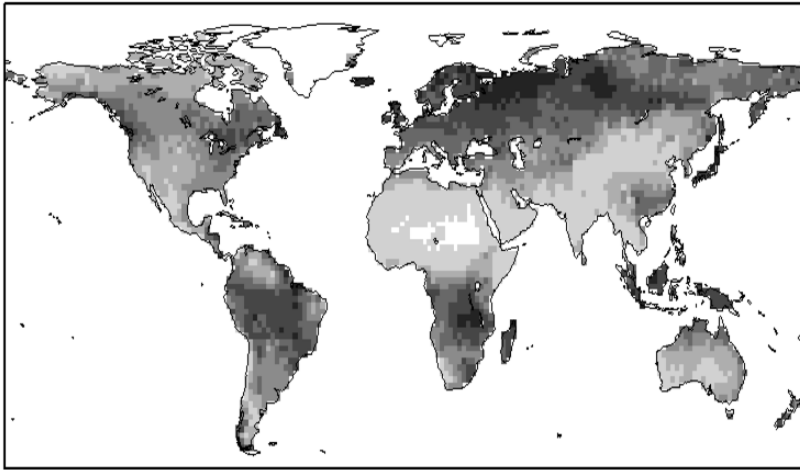
2.6.1 Choice of correcting dataset

The correction method may be applied using the statistics from any dataset and each of the datasets used here (CRU, GPCP and UW) may be equally valid for correcting the high-latitude anomaly. However, the methods used to construct each dataset results in differences in the rain day statistics that are regionally and seasonally variable. Deciding on which dataset to use for correcting the NCEP precipitation may be somewhat subjective, but certain factors may influence the decision. The accuracy of the dataset is perhaps of greatest importance and this is highly dependent on the methods and observations used to construct the datasets. The accuracy of the UW and CRU datasets is highly dependent on the density of stations and methods used to interpolate to the grid scale. Low station density will tend to give an underestimation of precipitation occurrence in a grid, especially when convective precipitation dominates as in humid regions in summer months (New et al., 2000). The GPCP dataset relies on satellite data sources, which have much more uniform and consistent spatial coverage and may give better estimates at grid scales. The temporal extent of the dataset is also an important factor. A dataset with long temporal overlap with the NCEP dataset would likely provide a better representation of inter-annual variability and any trends over the 50-year period than a mean monthly climatology based on fewer years. For the GPCP dataset (1997-1999), the level to which the average monthly statistics are representative of the full time period (1948-1998) is unknown. The CRU dataset may be more representative, by providing rain day frequencies and monthly totals for the whole time period, but it is of concern that monthly conditional probability statistics had to be generated from the UW dataset. In the end, it may be that a hybrid of these datasets would provide the best estimate.

2.6.2 Loss of spatial coherence and storm tracking

Because the correction method is carried out individually for each grid cell, spatial coherence between neighboring cells may be lost. For example, during correction, the precipitation at one grid cell may be replaced with precipitation from a day chosen at random from the population of appropriate days (wet or

UW Rain Days DJF 1979–1993



UW Corrected Rain Days DJF 1979–1993

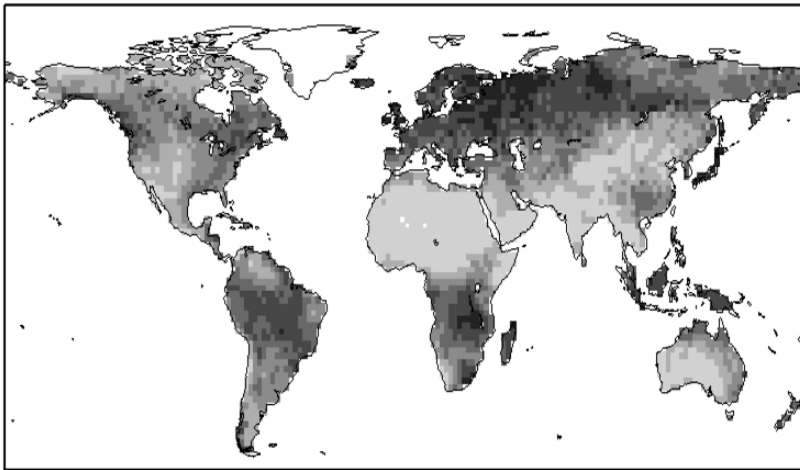


Figure 2.5: Seasonally averaged monthly rain days for DJF over the period 1948–1998 for the UW dataset and the NCEP dataset corrected with the UW monthly statistics.

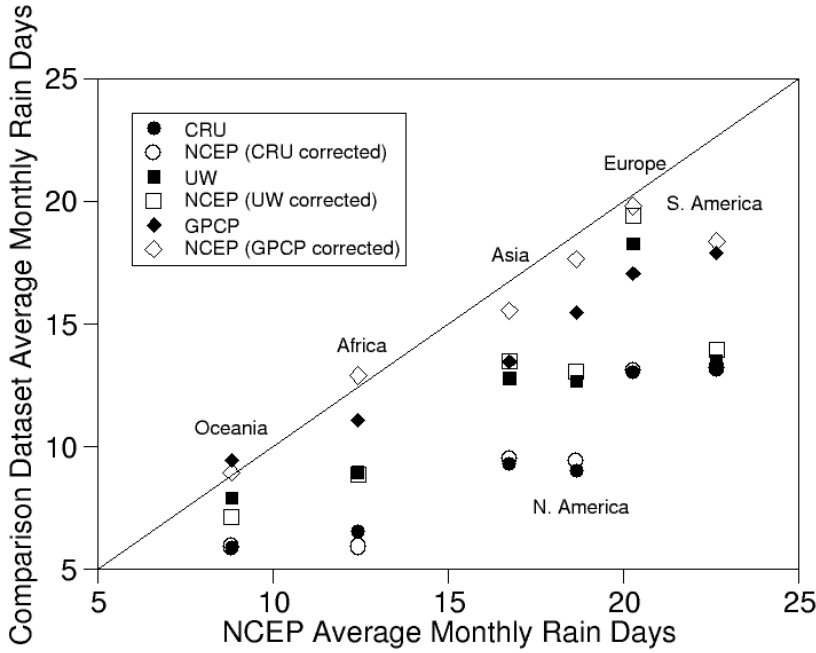


Figure 2.6: Scatter plot of the NCEP average monthly number of rain days versus that for the comparison datasets (CRU, UW and GPCP) (closed symbols) and the NCEP dataset corrected with each of the comparison datasets (open symbols) for the six continents.

dry). However, the precipitation in an adjacent cell may not to be replaced with data from the same day, if it is replaced at all, thereby losing spatial coherence between the two cells. For storm systems that span multiple grid cells, there may be a loss of spatial structure. Although this may not have major consequences on the mean precipitation over time and space scales larger than that of the storm, the effects at smaller spatial scales may be more profound. The passing of the storm over an area may be interrupted by the insertion of dry days into the continuous sequence of rain days. If the corrected dataset is to be used to force simulations of the land surface hydrology, this has potential effects on the dynamics of soil moisture and the occurrence of droughts and floods at the small scale. Figure 2.7 shows an example of the loss of storm tracking and spatial consistency for a sequence of four daily snapshots over North America. As large scale weather systems move from west to east, their general features are retained in the corrected dataset but noise has been introduced. At the scale of an individual grid, the continuous sequence of rain days as a storm system passes over is disrupted by days of no precipitation. The opposite effect can occur over areas experiencing a period of dry weather.

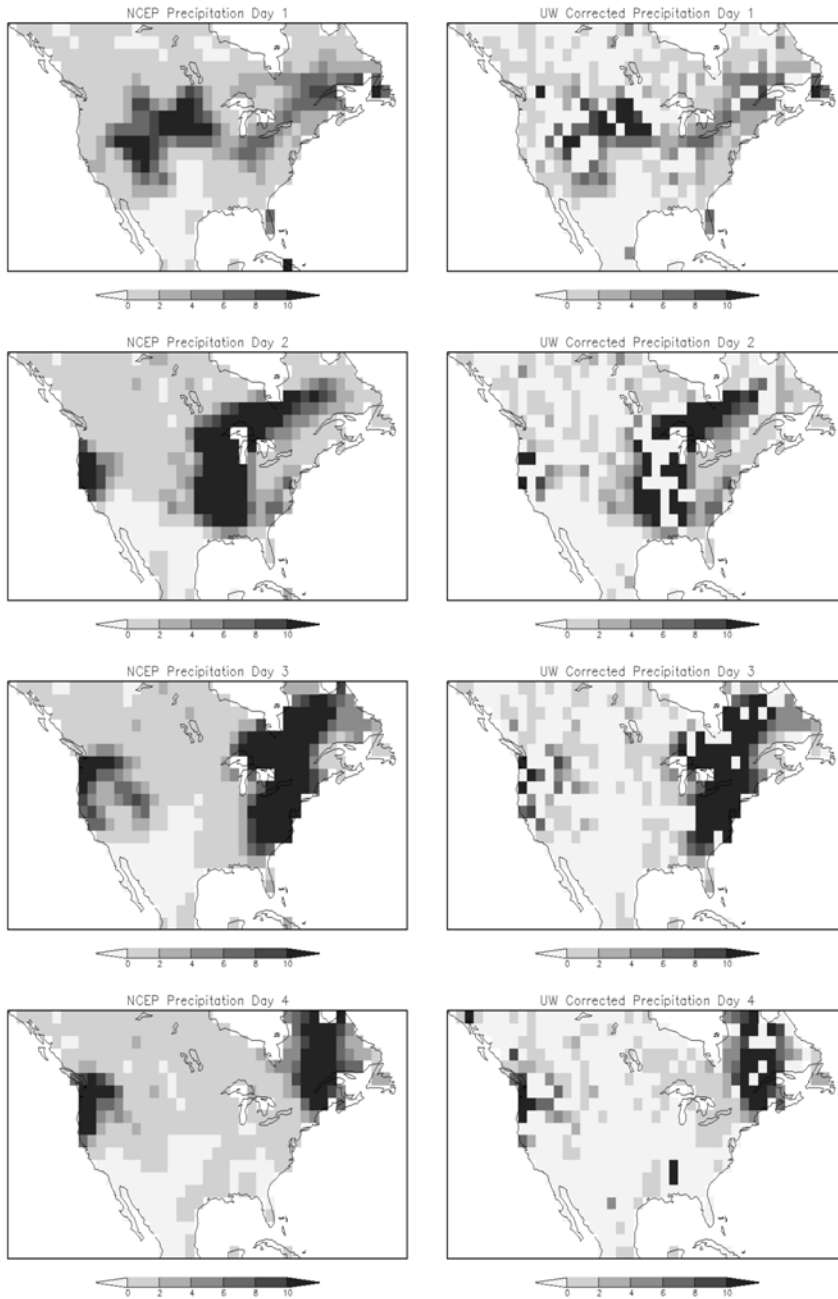


Figure 2.7: A sequence of 4 daily precipitation (mm day^{-1}) maps for a) the NCEP dataset and b) the NCEP dataset corrected with the UW inter-monthly statistics. Note the introduction of noise and the loss of storm tracking in the corrected dataset.

2.6.3 Temporal persistence in related variables

The related meteorological variables are resampled for the same days as the precipitation to ensure consistency (Section 4.b.). However, this may lead to a potential loss in the temporal persistence (lag-1 autocorrelation) in these variables because days are replaced at random without regard for the weather on preceding or following days. As an example, Table 2.1 shows the daily lag-1 autocorrelations averaged over 30-degree latitude bands for Asia for the NCEP dataset and the corrected dataset (using the CRU wet day frequencies). For both datasets, autocorrelations are lowest for precipitation and wind speed, which is to be expected given the intermittent nature of storms and changes in wind speed at daily time scales. Values are high for most other variables, especially temperature, as they are dominated by the seasonal solar cycle, which tends to increase autocorrelation.

Latitude Band	Dataset	P	T	SW	LW	SH	Ps	W
60° - 90°	NCEP	0.42	0.97	0.97	0.90	0.96	0.83	0.44
	Corrected	0.16	0.89	0.94	0.80	0.86	0.41	0.22
30° - 60°	NCEP	0.45	0.97	0.91	0.91	0.93	0.84	0.45
	Corrected	0.16	0.91	0.88	0.83	0.82	0.60	0.26
0° - 30°	NCEP	0.66	0.94	0.82	0.92	0.92	0.94	0.66
	Corrected	0.23	0.84	0.65	0.79	0.76	0.81	0.44

Table 2.1: Lag-1 autocorrelations for the NCEP dataset and the corrected dataset (using the CRU wet day frequencies). Autocorrelations are averaged over three latitude bands over Asia. Variables are precipitation (P), air temperature (T), downward shortwave radiation (SW), downward longwave radiation (LW), specific humidity (SH), surface pressure (Ps) and wind speed (W).

The reduced autocorrelation for precipitation in the corrected dataset is a result of the random sampling of wet days, which tends to break up multi-day storms. As a result, the autocorrelation values for the other variables are also reduced in the corrected dataset but the extent to which this happens varies by type of variable and latitude band. Some of the largest differences occur in the tropics for nearly all variables, and smaller differences are seen in higher latitudes. The exceptions to this are wind speed, which has significantly reduced autocorrelation in all regions, and surface pressure, which exhibits small differences in the tropics due to the dominance of the Asian Monsoon, and larger differences at higher latitudes where autocorrelations are less affected by the smaller seasonal variations.

Although it is apparent that there is a general loss in temporal persistence in all variables due to the correction, it is not clear whether the original NCEP lag-1 autocorrelations are realistic. As the NCEP dataset has incorrect auto-

correlations because of the rain day problem, these will spill over into the other variables because of the correlation between them. Therefore, it can be argued that the correction method may reduce any autocorrelation bias in these variables whilst maintaining physical consistency amongst variables.

2.6.4 Effects on the land surface water budget

The motivation for correcting the NCEP precipitation is to generate long-term global fields of water and energy states and fluxes which entails forcing state of the art land surface schemes with the best estimate of precipitation and surface meteorology available. The methods presented in this study combine observation based global datasets with reanalysis datasets in order to obtain the best forcing dataset at the highest spatial and temporal scales possible. However, it is important to understand how the choice of dataset and methods used to construct such forcings affect the simulated land surface water budget. If the water budget is sensitive to the differences in these forcing datasets and the methods used to combine the data, then such simulations will only add to the uncertainty in our understanding of the land surface water cycle.

To examine this, a number of experiments were conducted by forcing the Variable Infiltration Capacity (VIC) land surface model (Nijssen et al., 2001a, 2001b; Wood et al., 1997; Maurer et al., 2001) with each of the three corrected precipitation datasets, the NCEP dataset and the NCEP dataset scaled to match the CRU monthly totals. These simulations are denoted as VIC_{CRU} , VIC_{UW} , VIC_{GPCP} , VIC_{NCEP} and VIC_{NCEP_SCALED} . In addition to precipitation, the VIC model also requires, at the least, the daily maximum and minimum surface air temperature and the wind speed, which were derived from the NCEP dataset and made consistent with the corrected precipitation as described in section 4(c).

i) Effect of the NCEP high-latitude anomaly

Without correction of the biases and anomalies seen in the NCEP precipitation, the validity of using the NCEP dataset for land surface modeling in its native form is questionable. To illustrate this, an example of the effect of the high-latitude precipitation anomaly on the land surface hydrology is given in Figure 2.8. This shows the average DJF snow water equivalent (SWE) for the VIC_{NCEP} simulation. This simulation was forced with the NCEP dataset in its raw form. The spurious pattern can clearly be seen in the SWE field in the high northern latitudes. Results for other land surface variables, such as evaporation, soil moisture content and runoff (not shown), show little at these seasonal scales. This can be attributed to the fact that, at high latitudes in winter, the evaporation is very low and significant runoff and changes in soil moisture will not occur until the onset of spring melt, by which time the effects of the anomalous precipitation have begun to dissipate. The spurious pattern is of course not seen in the simulations forced with the corrected precipitation datasets.

ii) Effect of different rain day statistics

The previous section showed that the land surface reflects the anomalies in

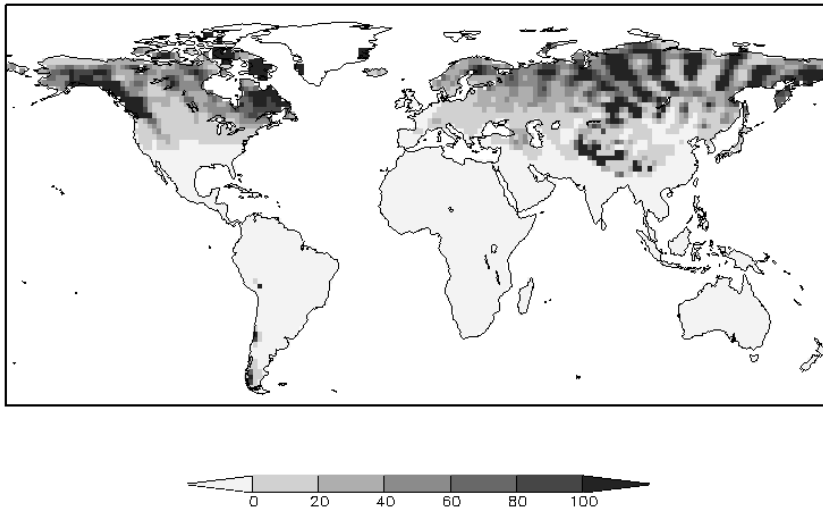


Figure 2.8: Average DJF snow water equivalent (mm) for the VIC simulation forced by the NCEP precipitation.

the NCEP precipitation in its raw form and indicates that the correction to the rain day statistics is required to remove the effects of these biases. Therefore, it is important to determine the sensitivity of the land surface to the rain day statistics, and to know the effect of the correction using rain day statistics from different datasets. In the context of large-scale modeling, the effects on the land surface budget at continental and global scales are of particular interest.

Table 2.2 shows the global and continental mean annual water budget for the VIC simulations. Also shown are the percentage changes in each of the budget components between each simulation and the VIC_{NCEP_SCALED} simulation. All simulations, except the VIC_{NCEP} simulation, are forced with precipitation scaled to match the monthly totals of the CRU dataset and this is reflected in the equal monthly precipitation totals in Table 2.2. The differences between the simulations show the effect of the choice of correcting dataset and are consistent with the comparison of rain day statistics shown previously in which, in general, the CRU dataset showed the largest differences with the NCEP dataset and the GPCP dataset showed the least.

The most notable effect on the land surface water budget is the way in which the precipitation is partitioned into evaporation and runoff. For all simulations forced with corrected precipitation, the evaporation is reduced and the excess water appears as a matching increase in runoff. The decrease in

	VIC _{NCEP_SC.}		VIC _{CRU}		VIC _{UW}		VIC _{GPCP}	
	annual mean	% change	annual mean	% change	annual mean	% change	annual mean	% change
P								
World	771	0.0	771	0.0	771	0.0	771	0.0
Africa	666	0.0	666	0.0	666	0.0	666	0.0
Asia	618	0.0	618	0.0	618	0.0	618	0.0
Europe	632	0.0	632	0.0	632	0.0	632	0.0
N. America	668	0.0	668	0.0	668	0.0	668	0.0
Oceania	712	0.0	712	0.0	712	0.0	712	0.0
S. America	1538	0.0	1538	0.0	1538	0.0	1538	0.0
E								
World	519	0.0	472	-9.1	484	-6.7	506	-2.5
Africa	562	0.0	523	-6.9	543	-3.4	555	-1.2
Asia	389	0.0	356	-8.5	375	-3.6	380	-2.3
Europe	494	0.0	479	-3.0	492	-0.4	492	-0.4
N. America	447	0.0	419	-6.3	434	-2.9	444	-0.7
Oceania	483	0.0	460	-4.8	470	-2.7	480	-0.6
S. America	870	0.0	726	-16.6	711	-18.3	813	-6.6
Q								
World	252	0.0	299	18.7	287	13.9	265	5.2
Africa	104	0.0	143	37.5	123	18.3	111	6.7
Asia	229	0.0	262	14.4	243	6.1	238	3.9
Europe	138	0.0	153	10.9	140	1.4	140	1.4
N. America	221	0.0	249	12.7	234	5.9	224	1.4
Oceania	229	0.0	252	10.0	242	5.7	232	1.3
S. America	668	0.0	812	21.6	827	23.8	725	8.5
S								
World	486	0.0	493	1.4	489	0.7	487	0.3
Africa	716	0.0	721	0.7	717	0.1	715	-0.1
Asia	391	0.0	397	1.5	394	0.7	394	0.6
Europe	659	0.0	664	0.8	662	0.5	661	0.3
N. America	358	0.0	364	1.5	361	0.7	359	0.2
Oceania	347	0.0	356	2.5	351	1.1	348	0.3
S. America	439	0.0	452	2.9	450	2.5	443	0.9
SWE								
World	20	0.0	17	-16.2	17	-14.3	19	-4.4
Africa	0	0.0	0	-11.6	0	-9.4	0	-5.3
Asia	22	0.0	18	-15.1	19	-12.2	21	-4.5
Europe	26	0.0	24	-6.4	25	-4.1	26	-0.3
N. America	55	0.0	43	-20.7	45	-18.0	51	-6.3
Oceania	0	0.0	0	-8.3	0	-17.6	0	18.6
S. America	4	0.0	5	10.5	4	-3.0	4	0.4

Table 2.2: Global and continental mean annual hydrological budget for the VIC simulations forced with the NCEP dataset with scaled precipitation (VIC_{NCEP_SCALED}) and the three corrected datasets (VIC_{CRU}, VIC_{UW} and VIC_{GPCP}). Water budget components are precipitation (P), evaporation (E), runoff (Q), soil moisture content (S) and snow water equivalent (SWE).

evaporation is mainly due to a decrease in canopy evaporation. For example, in North America, the evaporation for the VIC_{CRU} simulation is 28 mm lower than the VIC_{NCEP_SCALED} simulation and is matched by an increase of 28 mm in the runoff. Canopy evaporation is lower by 101 mm and this is balanced by increases in transpiration (79 mm), soil evaporation (4 mm), soil moisture content (6 mm) and SWE (4 mm). The changes in snow sublimation and canopy storage are negligible.

Despite the monthly precipitation totals being equal for these simulations, the differences in the individual water budget components are quite large, and especially in the partitioning of evaporation between canopy evaporation and transpiration. These differences can be explained by the differences in the monthly number of rain days and precipitation intensities. The NCEP data has less low intensity precipitation and more high intensity precipitation than the CRU and UW corrected datasets. The fixed capacity of the vegetation canopy in the VIC model is exceeded by the more intense precipitation of the corrected datasets more often than for the NCEP dataset. The excess water is routed as throughfall to the soil surface, which reduces the amount of water available for canopy evaporation and increases the potential for surface and subsurface runoff and transpiration.

iii) Effect of loss of spatial coherence

To determine the sensitivity of the land surface to the potential loss of spatial coherence in the corrected precipitation, spatial statistics were calculated over the Amazon river basin for the VIC_{NCEP_SCALED} and VIC_{CRU} simulations (see Figure 2.9). This illustrates the effect of not only the differences in the rain day statistics but also how the loss of spatial coherence of precipitation occurrence affects the spatial variability of the land surface water budget. From Figure 2.9, the basin average precipitation is approximately the same for both simulations, which is to be expected, as the monthly precipitation totals are the same. Differences in the distribution of the daily basin averaged values are due to changes made at the grid scale by the correction method. The CV values for precipitation for the two simulations show large differences. The mean CV values for the VIC_{CRU} simulation are higher than those for the VIC_{NCEP_SCALED} simulation, as are, in general, the maximum and minimum values and the 25 and 75 percentiles. This is due to the breaking up of storm systems and the introduction of “noise” into the corrected precipitation dataset, which increases both the mean and the spread of the distribution of spatial variability.

Differences in basin averaged evaporation are notable, with the mean VIC_{CRU} evaporation values being on average 21-42% lower than for the VIC_{NCEP_SCALED} simulation. This is a result of the differential partitioning of precipitation into canopy evaporation and throughfall between the two simulations as was seen in the continental scale analysis. Evaporation and runoff CV values tend to mimic the variability in the precipitation forcing, although the differences for runoff are small. Soil moisture CV values are high relative to the other components, which is to be expected at these spatial scales. However, any changes in variability resulting from changes in the spatial variability of

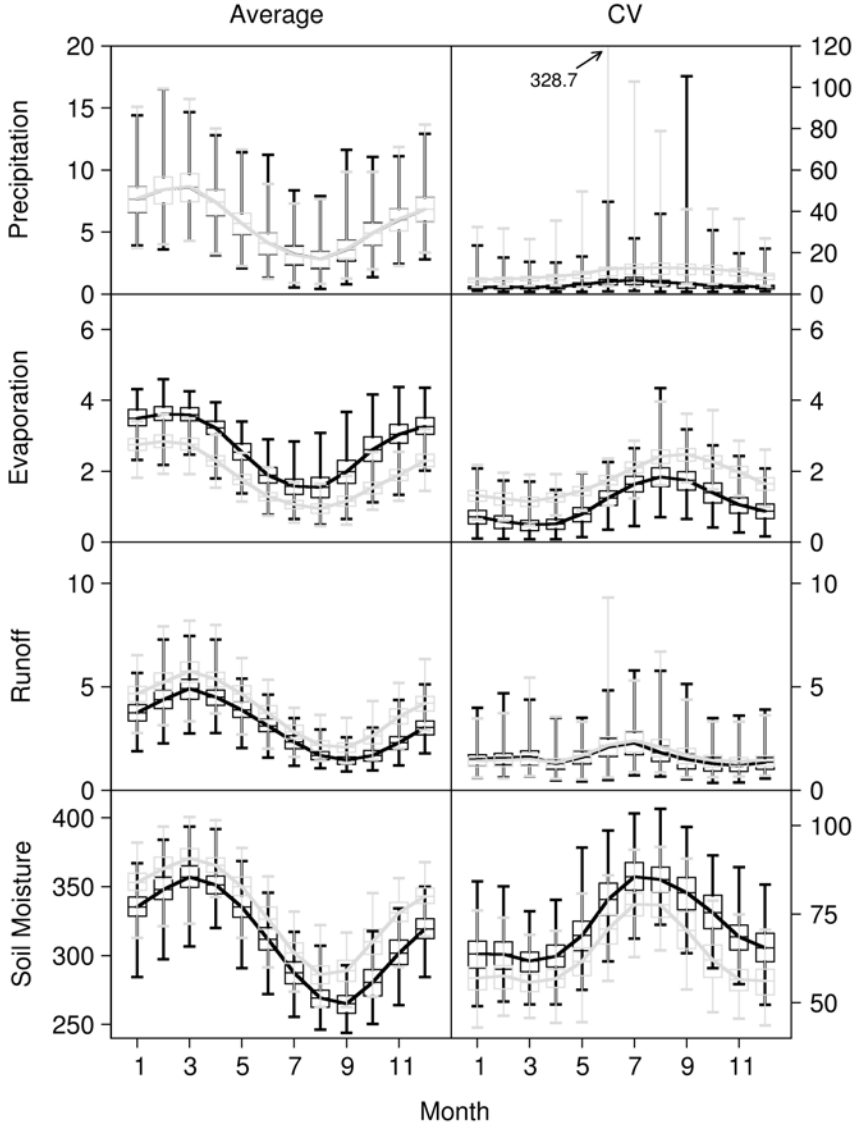


Figure 2.9: Mean monthly time series of the distribution of the spatial average and CV of the main components of the land surface water budget over the Amazon basin for the VIC_{NCEP_SCALED} (black line) and VIC_{CRU} simulations (gray line). The solid line represents the mean daily value. The upper and lower bars represent the maximum and minimum values whilst the upper and lower limits of the boxes are the 75% and 25% quartiles. Units are mm day^{-1} for the fluxes and mm for the soil moisture. Note the different scales for the basin average and basin CV for precipitation and soil moisture.

precipitation are likely to be dampened because the soil moisture values are for the total active soil column which includes deep moisture stores. Although the spatial variability in the VIC_{CRU} simulation precipitation is higher than for the VIC_{NCEP_SCALED} simulation, the corresponding variability in soil moisture is actually lower. This may be because the increased spatial variability in precipitation tends to produce a higher proportion of saturated or near saturated soil moisture conditions across the basin and thus will reduce the spatial variability. This is more likely in a humid environment such as the Amazon basin. The same analysis was carried out for the Mississippi and Mackenzie basins to investigate the effect for different climates and the results showed similar but smaller effects.

2.7 Summary and conclusions

A spurious wave-like pattern exists in the mean monthly precipitation and number of rain days of the NCEP dataset over terrestrial areas in high latitudes in winter. Comparison with the CRU, GPCP and UW precipitation datasets verified the anomaly and other regional biases in the NCEP precipitation field. The rain day anomaly was corrected using the monthly precipitation statistics from each of the three comparison datasets and the resulting daily precipitation values were then scaled so that their monthly totals matched those of the CRU dataset. The monthly statistics of the resulting corrected datasets match well the statistics of the respective dataset used for the correction but the degree to which it does this depends on the statistical similarity of the NCEP and correcting dataset.

In the context of land surface modeling, the need for the correction is clear, as the high latitude anomalous pattern is reflected in the land surface states. A number of experiments were carried out to investigate the effect of the correction on the land surface by forcing the VIC land surface model with the original and corrected NCEP datasets. The results show that the land surface water budget is sensitive to the sub-monthly distribution of precipitation. Simulations forced with identical monthly precipitation totals but different rain day statistics can differ significantly in the partitioning of precipitation into canopy evaporation and throughfall with implications for the level of accuracy required of the correcting dataset. Ultimately, the choice of the correcting dataset would be based on the level of confidence in the data and the accuracy of the rain day statistics at the grid scale. However, attention must also be paid to the temporal extent of the data and whether it is representative of the long-term variability over the multiple decades of the NCEP dataset period. In the absence of a single dataset that fulfills these criteria it may be that a hybrid dataset would have to be used.

A side effect of the correction method is that it introduces a degree of spatial inconsistency in the resultant precipitation fields because it is carried out independently for each grid cell. This results in the introduction of “noise” in the spatial pattern of precipitation and the potential loss of storm tracking at

the regional scale. The spatial variability of water budget components appears to be sensitive to the increased spatial variability in the corrected precipitation field, at least over the scale of a large river basin such as the Amazon. The results for other basins indicate that there is less of an effect in cooler and drier climates. An important implication of this is for the simulation of the occurrence and magnitude of floods and droughts as the soil moisture field may develop very differently when forced with the corrected precipitation, not only because of the change in rain day statistics but also because the spatial structure of storms may be broken down. One potential solution to the problem of spatial incoherence is to use the method of correlated random numbers (Wilks, 1998) although this is beyond the scope of this study. Nevertheless, for large-scale modeling, the side effects of the correction at continental and seasonal scales are small.

This work forms part of an effort to create a global, multi-decade, daily, sub-2°, terrestrial, meteorological forcing dataset to drive land surface model simulations of the global water and energy balance. These simulations will provide a long-term, globally consistent and validated set of land surface water and energy fluxes and states at a high spatio-temporal resolution. The dataset will facilitate the study of seasonal and inter-annual variability studies to an extent not possible with currently available datasets. Furthermore, the dataset will be suitable for evaluating the ability of coupled models and other land surface prediction schemes to reproduce observed variability of surface fluxes and state variables in space, and temporally for time scales up to decadal. In addition, this long-term dataset will be useful for diagnostic studies related to terrestrial hydrology, and for intercomparison studies with numerical weather prediction (NWP) reanalysis datasets.

Acknowledgments

This work was funded by NASA grant NAG5-9414. The GPCP data were provided by the Global Precipitation Climatology Center (GPCC), from their web site at <http://www.dwd.de/research/gpcc> (downloaded November 2000). NCEP/NCAR Reanalysis data were provided by the NOAA-CIRES Climate Diagnostics Center, Boulder, Colorado, USA, from their web site at <http://www.cdc.noaa.gov/> (downloaded November 2000). The CRU data were created and supplied by Dr. Mike Hulme at the Climatic Research Unit, University of East Anglia (UK) (provided January 2001). The UW data were provided by the Surface Water Modeling group at the University of Washington.

Chapter 3

Development of a global meteorological forcing dataset, 1950-2000

This chapter is a slightly modified version of: Sheffield, J., G. Goteti, and E. F. Wood, 2006: Development of a 50-yr high-resolution global dataset of meteorological forcings for land surface modeling, *J. Climate*, 19(13), 3088-3111.

Abstract

Understanding the variability of the terrestrial hydrologic cycle is central to determining the potential for extreme events and susceptibility to future change. In the absence of long-term, large-scale observations of the components of the hydrologic cycle, modeling can provide consistent fields of land surface fluxes and states. This paper describes the creation of a global, 50-year, 3-hourly, 1.0 degree, dataset of meteorological forcings that can be used to drive models of land surface hydrology. The dataset is constructed by combining a suite of global observation-based datasets with the NCEP/NCAR reanalysis. Known biases in the reanalysis precipitation and near-surface meteorology have been shown to exert an erroneous effect on modeled land surface water and energy budgets and are thus corrected using observation-based datasets of precipitation, air temperature and radiation. Corrections are also made to the rain day statistics of the reanalysis precipitation which have been found to exhibit a spurious wave-like pattern in high-latitude wintertime. Wind-induced undercatch of solid precipitation is removed using the results from the World Meteorological Organization (WMO) Solid Precipitation Measurement Inter-comparison. Precipitation is disaggregated in space to 1.0 degree by statistical downscaling using relationships developed with the Global Precipitation Climatology Project (GPCP) daily product. Disaggregation in time from daily to 3-hourly is accomplished similarly, using the Tropical Rainfall Measuring Mission (TRMM) 3-hourly real-time dataset. Other meteorological variables (downward short- and longwave, specific humidity, surface air pressure and wind speed) are downscaled in space with account for changes in elevation. The dataset is evaluated against the bias-corrected forcing dataset of the second Global Soil Wetness Project (GSWP-2). The final product provides a long-term, globally-consistent dataset of near-surface meteorological variables that can be used to drive models of the terrestrial hydrologic and ecological processes for the study of seasonal and inter-annual variability and for the evaluation of coupled models and other land surface prediction schemes.

3.1 Introduction

The availability of large-scale, long-term datasets of the land surface water and energy budgets is essential for understanding the global environmental system and interactions with human activity, especially in the face of potential climatic change. However, consistent observations of components of the land surface water and energy budgets are routinely not available over large-scales. While some terms of the surface water balance are reasonably well observed, at least over some parts of the globe (precipitation and runoff in particular), other terms, including evapotranspiration, soil moisture, and surface water are virtually absent of direct observations at large scales. Many of these variables are difficult to measure because of technical, monetary and political limitations. In the case of soil moisture, which forms a key element for drought assessment and medium

and long-range prediction, global (or even regional, with only a few exceptions) in situ measurement networks are grossly inadequate for hydrologic prediction purposes, and land surface hydrology models have generally evolved without the use of direct observations of this key state variable. In terms of surface energy fluxes and evaporation, these are inherently difficult to measure and are thus essentially non-existent over large scales. The use of remote sensing has provided great potential for large scale measurement of some variables (notably albedo, radiative surface temperature and soil moisture) but is restricted to indirect quantities and, in the case of soil moisture, to low-vegetated regions and the top few centimeters.

It has been suggested that an alternative to estimating large-scale water cycle terms directly from observations is to use land surface models (LSM), in either off-line (forced with surface meteorological observations) or coupled (with an atmospheric GCM) mode (e.g. Lau et al., 1994; Liang et al., 1994; Levis et al., 1996; Werth and Avissar, 2002). LSMs close the water budget by construct, so if the meteorological forcing data are accurate, and model biases are small, these constructed water balance terms might be used in lieu of observations and provide a consistent picture of the water and energy budgets. Budget closure is not achievable from observations even at small scales. In fact, analyses of water and energy cycle variables estimated through observations (in-situ and/or remote sensing) will not provide water cycle closure (Roads et al., 2003; Pan and Wood 2004) due to sampling and retrieval errors. However, through research activities like the North American Land Data Assimilation System (N-LDAS; Mitchell et al, 2004a), and Global LDAS (G-LDAS; Rodell et al, 2004), the capability of land surface models to produce meaningful estimates of land surface hydrologic conditions over large areas has been demonstrated. Therefore, the contention is that observation-forced, off-line simulations using state-of-the-art land surface model provides the best estimate of global water cycle variables.

Nevertheless, while estimates of water cycle variables obtained through land surface modeling are consistent, these estimates can be subject to large errors due to errors in model inputs and meteorological forcings. The importance of accurate forcings for large-sale land surface modeling efforts has been demonstrated previously (Berg et al., 2003; Fekete et al., 2004; Nijssen and Lettenmaier, 2004). Results from the NLDAS project (Mitchell et al., 2004a) indicated that first order errors in the land surface simulations were due to inaccurate specification of the forcings and especially in precipitation (Robock et al., 2003; Pan et al., 2003). Other studies have shown the sensitivity of the land surface to the atmospheric forcings and especially precipitation (Berg et al., 2003; Fekete et al., 2004; Sheffield et al., 2004). The conclusion is that accurate forcings are necessary to provide accurate land surface simulations when compared to observations. The implication is that the use of sufficiently accurate forcings for land surface modeling in regions of sparse land surface observations will provide a suitable surrogate.

The availability of near-surface meteorological observations is not pervasive across all global areas and certainly not at the spatial and temporal resolu-

tions that are required by land surface hydrologic models for most hydrologic applications. Coupled with the lack of temporal extent and consistency in the majority of observations, the development of forcing datasets using observations alone is unsatisfactory. With the increasing availability of remote sensing products the prospect for the future is more promising, although this does not help in the development of long-term retrospective datasets that are required for extracting information about climate variability. In the global context, the use of atmospheric reanalysis products may be the only alternative for providing near surface meteorological forcings at high temporal resolution. In contrast to the lack of terrestrial observations, the relative wealth of observations of the atmosphere and sea surface has allowed the emergence of a number of global, long-term, reanalysis datasets such as the NCEP/NCAR (Kalnay et al., 1996; Kistler et al., 2001), ECMWF ERA-40 and ERA-15 (Gibson et al., 1997), NCEP-DOE (Kanamitsu et al., 2002), and NASA-DAO (Schubert et al., 1993) reanalyses. These products are constructed using “frozen” versions of numerical weather prediction and assimilation systems that ingest a variety of atmospheric and sea surface observations to provide long-term, continuous fields in time and space, of atmospheric (and land surface) variables. Although these model derived fields may not be perfect, they are self-consistent and are used by many to force models of the land surface water and energy balances.

The power of reanalyses is their consistent and coherent framework for ingesting in situ and remote sensing data into a time- and space-discretized representation of the global land, oceans, and atmosphere, in a way that is essentially impossible to achieve directly from observations. Reanalysis has been suggested as an alternate approach to the problem of estimating the surface water balance, yet the reanalysis land surface products have many problems, including: (i) The data that are assimilated are primarily atmospheric profiles of moisture, temperature, and other variables and few, if any, land surface data are assimilated, resulting in the fact that they represent better variables like atmospheric moisture and large scale circulation than the representation of land surface variables, like soil moisture and snow water content; (ii) the land surface is forced by precipitation that is essentially a model output product so that errors in model representation of precipitation (Janowiak et al., 1998; Trenberth and Guillemot, 1998; Serreze and Hurst, 2000), which can be quite large, are translated into errors in land surface fields like evapotranspiration, runoff and soil moisture (e.g. Lenters et al., 2000; Maurer et al., 2001); and (iii) the effects of “nudging” of the land surface to avoid drift have the effect of creating unrealistic soil moisture, and biasing (by large amounts in many cases) water budget flux terms (Betts et al., 1998; Maurer et al., 2001; Betts et al., 2003a, b; Roads et al. 2002a, b).

The effect that these biases have on land surface processes has to be addressed for these products to be of use as forcings in modeling studies. The results of Berg et al. (2003), who tested bias correction of ECWMF reanalysis over North America, suggest that modelers using reanalysis products for forcing LSMs should consider a bias reduction strategy for their input forcings. Also, Sheffield et al. (2004) showed that systematic biases in reanalysis filter down

into the modeled land surface fluxes and states. Ngo-Duc et al. (2005) found that precipitation biases in the NCEP/NCAR reanalysis were responsible for significant errors in modeled streamflow for continental scale basins. Nevertheless, the results of such studies have shown that there is great potential for using hybrid datasets which combine reanalysis with observation based datasets to remove biases. This approach retains the consistency and continuity of the reanalysis but constrains it to the best available observation datasets, which are generally available at coarser resolutions and reduced spatial and temporal extents.

This paper describes the development of a long-term, global dataset of near-surface meteorology that can be used to force models of the land surface water and energy budgets. Reanalysis products are combined with a suite of observation-based, global datasets that are used to correct for biases in the monthly mean values and intra-monthly statistics of the reanalysis and for downscaling in time and space to scales relevant for hydrologic applications. The dataset has global coverage over the extra-polar land surface (i.e. excluding Antarctica) at 1.0 degree spatial resolution and a 3-hourly time step, for 1948-2000.

Previously, a number of studies have developed large-scale, long-term datasets of a similar nature. However, these have been limited to smaller domains (e.g. Maurer et al., 2002) and/or shorter time periods (e.g. Levis et al., 1996; Nijssen et al., 2001a; (International Satellite Land-Surface Climatology Project (ISLSCP) I, Meeson et al., 1995; ISLSCP II, Hall et al., 2005; Global Soil Wetness Project (GSWP) 2, Dirmeyer et al., 2005) or have been implemented globally, but at coarser spatial and temporal resolutions (e.g. Levis et al., 1996; Nijssen et al., 2001a; Ngo-Duc et al., 2005). This dataset represents an improvement over these products in terms of higher spatial and temporal resolution and global coverage and through the implementation of a number of enhancements in addition to correcting for monthly biases and accounting for topographic effects. These enhancements include: 1) adjustments to precipitation for gauge undercatch; 2) temporal and spatial disaggregation of precipitation and downward solar radiation with account for observed sub-grid and diurnal variability statistics; 3) adjustment to rain day frequencies to match observed statistics; and 4) trend correction and probability weighted scaling for biases in downward short and long-wave radiation.

3.2 Datasets

The forcing dataset is based on the NCEP/NCAR reanalysis, which includes near-surface meteorological variables from 1948 to the present. This time period provides the length of data necessary to infer the variability of the land surface water and energy budgets at timescales up to multi-decadal. Alternative sources of reanalysis data are available, including the NCEP-DOE and ERA-40 products that have been shown to be more accurate, in general, than the NCEP-NCAR reanalysis. However, the NCEP-NCAR reanalysis offers the

benefits of a long time period and ongoing production that may offset any potential deficiencies that the bias correction methodology cannot address. Even if the ERA-40 or NCEP-DOE reanalysis has been used, the comparisons would reveal any biases that exist in these products and the correction methods could easily be applied.

The reanalysis data are combined with a suite of global, observation based datasets of precipitation, temperature and radiation. Table 3.1 summarizes the contributing datasets that are used in the development of the forcing dataset and these are described in more detail in the following sections. These observation based datasets are generally available at coarser temporal resolutions, e.g. monthly. The reanalysis is essentially used to downscale these observation datasets to the sub-daily temporal scale necessary for land surface modeling. In contrast, the observation-based datasets are generally available at higher spatial resolutions and are used to downscale the reanalysis in space. Thus a hybrid forcing dataset is formed by using the sub-monthly variability in the reanalysis, with bias corrections made at a monthly scale.

3.2.1 NCEP/NCAR reanalysis

The NCEP/NCAR reanalysis (referred to hereafter as the NCEP reanalysis) is a retrospective global analysis of atmospheric and surface fields extending from 1948 to the near present (Kalnay et al., 1996, Kistler et al., 2001). Available observations are assimilated into a global atmospheric spectral model implemented at a horizontal resolution of T62 (approximately 2.0 degree) and with 28 sigma vertical levels. The reanalysis is created using a “frozen” version of the data assimilation system, although assimilated observations are subject to changing observing systems. Consistent gridded output fields are generated continuously in time and are classified according to how they are determined and their reliability. Class “A” variables are strongly influenced by assimilated observations and are therefore regarded as being the most reliable fields (e.g. upper air temperatures and geopotential height). Less reliable are class “B” variables (moisture, divergent wind and surface parameters), which are influenced by observations and the model. Class “C” variables (surface fluxes and heating rates), are completely determined by the model and as such are the least reliable. Precipitation is classified as a class “C” variable.

3.2.2 CRU monthly climate variables

The Climatic Research Unit (CRU) product is a 0.5 degree gridded dataset of monthly terrestrial surface climate variables for the period of 1901–1998 (New et al., 1999, 2000) and updated to 2000 by Mitchell et al. (2004b). The spatial coverage extends over all land areas, including oceanic islands but excluding Antarctica. Fields of monthly climate anomalies, relative to a 1961–90 climatology, were interpolated using thin-plate splines from surface climate data. The anomaly grids were then combined with the 1961–1990 climatology resulting in grids of monthly climate the full period. Primary variables (pre-

Dataset	Variables	Temporal Coverage	Spatial Coverage	Source
NCEP/NCAR reanalysis	P, T, SW, LW, q, Ps, w	1948-present, 6-hourly	Global, $\sim 2.0^\circ \times 2.0^\circ$	Kalnay et al. (1996)
CRU TS2.0	P, T, Cld	1901-2000, monthly	Global land excluding Antarctica, $0.5^\circ \times 0.5^\circ$	Mitchell et al. (2004b)
GPCP	P	1997-present, daily	Global, $1.0^\circ \times 1.0^\circ$	Huffman et al. (2001)
TRMM	P	Feb 2002 – present, 3- hourly	50S-50N, $0.25^\circ \times 0.25^\circ$	Huffman et al. (2003)
NASA-Langley SRB	LW, SW	1983-1995, monthly	Global, 1.0° lat. \times 1.0° 120° long.	Stackhouse et al. (2004)

Table 3.1: Summary of datasets used in the construction of the forcing dataset. The temporal resolutions given here are those used in this study but original data may be available at finer temporal resolutions. Variables are precipitation (P), surface air temperature (T), downward shortwave radiation (SW), downward longwave radiation (LW), surface air pressure (Ps), specific humidity (q), windspeed (w) and cloud cover (Cld).

precipitation, mean temperature, and diurnal temperature range) are interpolated directly from station observations. The secondary variables (including rain day frequency and cloud cover) are interpolated from merged datasets comprising station observations and, in regions without station data, synthetic data estimated using predictive relationships with the primary variables.

3.2.3 GPCP daily precipitation

The Global Precipitation Climatology Project (GPCP) daily, 1997-present, 1.0 degree precipitation product (Huffman et al., 2001) is based on a combination of estimates from a merged satellite IR dataset over 40°N-40°S and a rescaling of the Susskind et al. (1997) TIROS Operational Vertical Sounder (TOVS) satellite estimates at higher latitudes. Both contributing estimates are scaled to match the GPCP version 2 monthly satellite-gauge dataset totals (Huffman et al., 1997). Rain day frequencies of the IR based estimate are adjusted to match data from the Special Sensor Microwave Imager (SSM/I) retrieval. The TOVS based rain day frequencies are adjusted to the IR based estimate at 40°N and 40°S separately.

3.2.4 TRMM 3-hourly precipitation

The Tropical Rainfall Measuring Mission (TRMM) is a joint mission between the National Aeronautics and Space Administration (NASA) of the United States and the Japan Aerospace Exploration Agency (JAXA). The TRMM satellite was launched in November of 1997 and covers the tropics between approximately 40S to 40N latitude. A number of experimental, real-time datasets, based on the TRMM products and other satellite sources are currently available (Huffman et al., 2003), including the 3B42RT product which is a merger of the 3B40RT and 3B41RT products. The 3B40RT product is a merger of all available SSM/I and TRMM microwave imager (TMI) precipitation estimates. The SSM/I are calibrated to the TMI using separate global land and ocean matched histograms. The 3B41RT product consists of precipitation estimates from geostationary infrared (IR) observations using spatially and temporally varying calibration by the 3B40RT product.

3.2.5 NASA Langley monthly surface radiation budget (SRB)

The NASA/Langley Research Center product is available from 1983-1995 (Gupta et al., 1999) with an extension to 2001 being planned (Stackhouse et al., 2004). The primary data sources are satellite data from the International Satellite Cloud Climatology Project (ISCCP) C1 data product (Rossow and Schiffer 1991) and from the Earth Radiation Budget Experiment (ERBE; Barkstrom et al. 1989). The C1 data provide cloud parameters derived from a network of geostationary satellites and NOAA's polar orbiters, along with temperature and humidity profiles from TOVS, on a 2.5

degree equal-area global grid and a 3-hourly time resolution. Monthly average clear-sky planetary albedos used for deriving surface albedos over snow/ice-free land areas were obtained from ERBE data. Two versions are available for short and longwave radiation. Firstly, the SRB-SW and SRB-LW products are derived using the algorithms of Pinker and Laszlo (1992) and Fu et al. (1997) respectively. Secondly, the SRB-QCSW and SRB-QCLW products are derived using the algorithms of Darnell et al. (1992) and Gupta et al. (1992), respectively. Comparison of these products with surface measurements has indicated that no one product is superior globally. For example, the SW product underestimates shortwave radiation over the higher elevations of the Tibetan Plateau and western China but the QCSW product does not, although comparisons undertaken for the GSWP2 over North America showed that the SW product performed better (GSWP2 forcing data webpage at <http://www.jamstec.go.jp/frcgc/research/p2/masuda/gswp/b1alpha.html>). Given these preliminary analyses, the SRB-QCSW and SRB-LW products are used in this study.

3.3 Development of the forcing dataset

The development of the forcing dataset has progressed through a number of stages in terms of the spatial and temporal resolution and the sophistication of the correction methods. This has resulted in a number of intermediate products at coarser spatial and temporal resolutions. To perform calculations of the land surface water and energy cycles, land surface models, in general, require sub-daily time series of the following near-surface atmospheric variables: precipitation, air temperature, downward short- and longwave radiation, surface pressure, specific humidity and windspeed. Initially the reanalysis variables were bilinearly interpolated from their native resolution of 1.875 degree longitude by approximately 1.9 degree latitude to a 2.0 degree regular grid with consideration for changes in elevation (see section 3b). This grid is commensurate with the observation based datasets. Next corrections are made to the daily precipitation statistics. All variables are then downscaled in space to 1.0 degree resolution (again with corrections for changes in elevation) and down-scaled in time to a 3-hourly timestep. Finally, biases at the monthly scale are removed. The following sections describe in detail the various stages in the development of the forcing dataset.

3.3.1 Correction of the reanalysis rain day anomaly

A high-latitude anomaly in the rain day statistics exists in the NCEP reanalysis in the winter months of the northern hemisphere (Cullather et al., 2000; Serreze and Hurst, 2000; Sheffield et al., 2004). The anomaly results from the use of a simplified approximation to moisture divergence in the atmospheric forecast model used in the reanalysis. This results in a spurious wave-like pattern in the monthly rain day statistics that is most noticeable in the northern hemisphere

winter at high latitudes (Figure 1). The anomaly filters down into land surface states when the precipitation is used to force a land surface model (Sheffield et al., 2004). This study also showed the sensitivity of the land surface to the monthly rain day statistics. Using various estimates of rain day statistics, but the same monthly totals, to force a land surface model, resulted in large differences in estimated water balance components (up to 9% error in global average evaporation and 17% in runoff, with higher values at the continental and regional scale). The conclusion is that it is vital to use not only the best estimates of monthly total precipitation but also of monthly rain day statistics to achieve accurate simulations of the land surface water budget. A correction to the rain day statistics is described in detail in Sheffield et al. (2004) and a brief description is given here. The correction involves resampling the daily precipitation data to match the statistics of observation based terrestrial daily precipitation datasets (CRU, GPCP and a 15-year gauge-based dataset developed by Nijssen et al. (2001a)). To ensure consistency in the related meteorological variables, these are also resampled for the same days that the precipitation was resampled for. Figure 1 shows the correction of the NCEP precipitation using the CRU dataset. In addition to correcting the high-latitude rain day anomaly, differences that occur elsewhere are also removed. For example, in the tropics the high numbers of rain days in the NCEP dataset are reduced to the levels found in the CRU dataset. One side effect of this correction method is that spatial consistency at the daily time scale is not maintained because the correction is carried out independently on each grid cell. Sheffield et al. (2004) found that the effect of this on the large scale terrestrial water balance was small compared to that resulting from the correction of the precipitation frequencies.

3.3.2 Spatial downscaling

Precipitation

Daily precipitation (corrected for monthly rain day biases) was downscaled from 2.0 to 1.0 degree resolution using a probabilistic approach based on relationships between precipitation intensity and grid cell fractional precipitation coverage. Precipitation varies considerably in space, especially at daily time scales and it has been recognized that the land surface is sensitive to this variability (Johnson et al. 1993; Eltahir and Bras 1993) and the effects on the atmosphere through enhanced feedback can be significant (Hahmann, 2003). In general, low intensity, large area precipitation will tend to increase evaporation and infiltration compared to high intensity, localized precipitation that will result in increased runoff production through infiltration excess.

For downscaling the precipitation data to 1.0 degree resolution, it is of interest to know the fractional wetted area within the 2.0 degree grid cell and the distribution of precipitation intensities among the 1.0 degree grid cells within. Fractional area is seasonally and geographically variable (Gong et al., 1994), and depends, among other factors, on storm type, grid resolution and temporal scale (Eltahir and Bras, 1993). Figure 2 shows an example of the

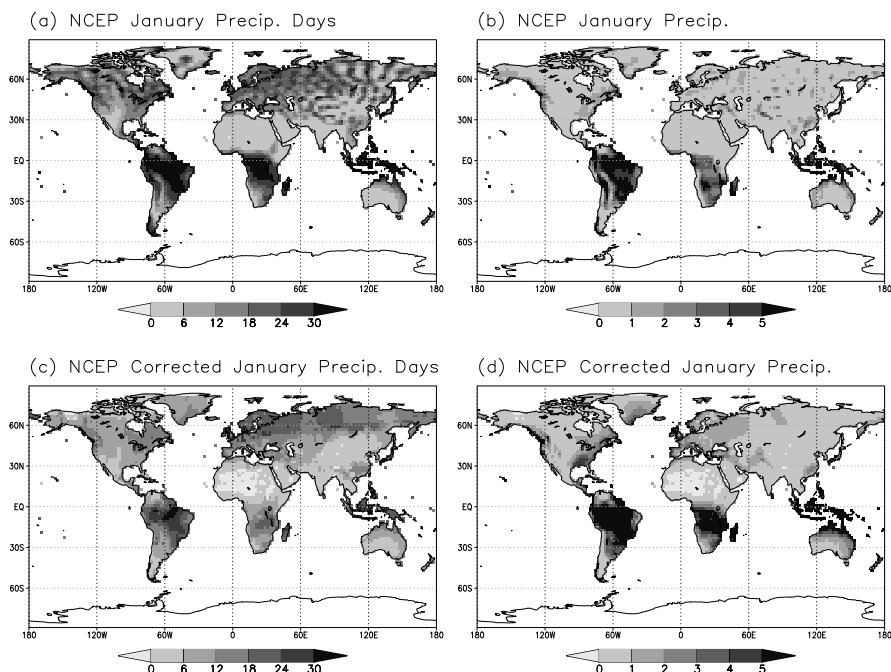


Figure 3.1: Figure 1. Average January precipitation statistics for the NCEP and corrected data sets. a) Number of precipitation days and b) total precipitation (mm/day) from the NCEP dataset, showing the spurious wave-like pattern in northern hemisphere high-latitudes. c) Number of precipitation days and d) total precipitation (mm/day) as corrected by Sheffield et al. (2004) using data from the CRU TS2.0 global 1901-2000 climate data set of Mitchell et al. (2004b).

scaling behavior of precipitation fractional area for the 0.25 degree TRMM and 1.0 degree GPCP datasets. Values for a range of spatial resolutions are shown such that the scale is relative to the dataset resolution. Fractional area of the TRMM data drops off rapidly with increasing scale but tends towards a threshold value at larger scales that appears to be seasonal. At the scale of the forcing dataset (1.0 degree) the fractional coverage of the TRMM data is on average much less than 1 (full coverage). This implies that downscaling by simply applying the 2.0 degree grid cell average precipitation to the four 1.0 degree cells may be inappropriate in terms of representing the spatial variability of wet and dry areas, with subsequent effects on the land surface hydrology. The GPCP data show similar relative scaling behavior (window sizes larger than 4.0 degrees had a limited number of land cells and so were not included) that may indicate some form of self-similarity. Because of this and their multi-year, global coverage, the GPCP data were considered suitable for downscaling the NCEP data.

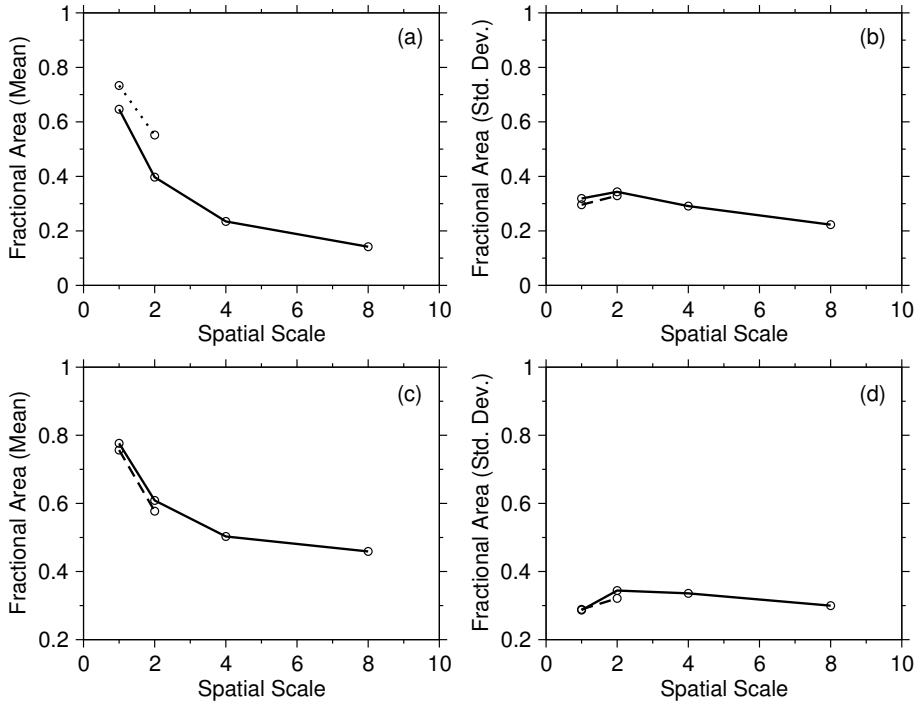


Figure 3.2: Fractional area of precipitation as a function of spatial scale for mild, mid-latitude climate regions. a) Mean and b) standard deviation for January. c) Mean and d) standard deviation for July. Solid lines are the TRMM data, dashed lines are the GPCP data. The spatial scale is relative to the resolution of the precipitation datasets (TRMM = 0.25 degree, GPCP = 1.0 degree).

The 2.0 degree daily data are downscaled using a probabilistic approach that relates the fractional area of precipitation with the precipitation intensity at 2.0 degree. From Bayesian theory, the probability of occurrence of precipitation within a 2.0 degree grid cell with fractional coverage (A) for a given grid cell average precipitation intensity (I) can be written as

$$p(A|I) = \frac{p(I|A)p(A)}{p(I)}, \quad (3.1)$$

where $p(I|A)$ is the conditional probability of an intensity I given a fractional area A . Probabilities for each term on the right hand side of equation 3.1 are generated for each month and grid cell using data from the GPCP daily data set which has global and multiple year coverage. The NCEP daily data are then downscaled to 1.0 degree by sampling at random from the resultant conditional probability distribution $p(A|I)$ to determine the spatial coverage of precipitation in terms of the number of 1.0 degree grid cells.

This disaggregation method was validated by reconstructing the 1.0 degree GPCP data set from a 2.0 degree aggregated version using the probability distributions from equation 3.1. Figure 3.3 shows an example of the spatial statistics for the GPCP data set and three different reconstructed versions over the North American continent. These three versions were created, respectively, by 1) distributing the 2.0 degree precipitation value uniformly over all 1.0 degree cells within; 2) using the probabilistic approach to determine the fractional area of precipitation (number of 1.0 degree cells) within a 2.0 degree cell and distributing the 2.0 degree grid cell precipitation uniformly within these cells; and 3) as for (4.2) but weighting the precipitation among the wet 1.0 degree grid cells based on the precipitation in neighboring 2.0 degree cells. This final method assumes that precipitation occurrence has some spatial coherence and the wet cells are deemed to have some simple connectivity with neighboring regions of precipitation. Figure 3 indicates that the distributed method does little better than using a uniform approach, although the effect on land surface states may be quite different. However, weighting the distribution of the precipitation gives values of spatial variability that are consistent with the original GPCP data, although slightly higher. Similar results apply for other regions across the globe. The local autocorrelation of the original and reconstructed datasets was also calculated at various lag times to see whether the correction methods preserved the temporal characteristics of precipitation at each grid cell (Figure 4). In general, the errors reduce with increasing lag time for all three methods. Again, the weighted method shows the least error, except for Europe and North America where all methods perform essentially the same at longer lag times.

Meteorological variables

The other meteorological variables (downward shortwave and longwave radiation, surface pressure, specific humidity and wind speed) were disaggregated from 2.0 degree to 1.0 degree using bilinear interpolation but with adjustments for differences in elevation between the two grids. The effects of elevation on near-surface meteorology have been well documented and the difference in elevation between the two grids, as shown in Figure 5, can be significant. The differences are most prominent in the foothills of mountain ranges where elevation may change by a few thousand meters within a 2.0 degree grid cell. Maximum differences are approximately 3000m in the Himalayas, 1300m in US Rockies and up to 3700m in the Andes. To account for the differences in elevation, air temperature is first adjusted to the new grid elevation using the environmental lapse rate (6.5 °C/km). Following the methods of Cosgrove et al. (2003), which assumes that the relative humidity is constant to avoid the possibility of super-saturation, the specific humidity, surface air pressure and downward longwave radiation are also corrected for elevation changes to ensure consistency. These corrections were applied whenever a dataset (reanalysis and observational) was interpolated from one grid to another, whether for upscaling or downscaling, using the following method. First, the data were elevation

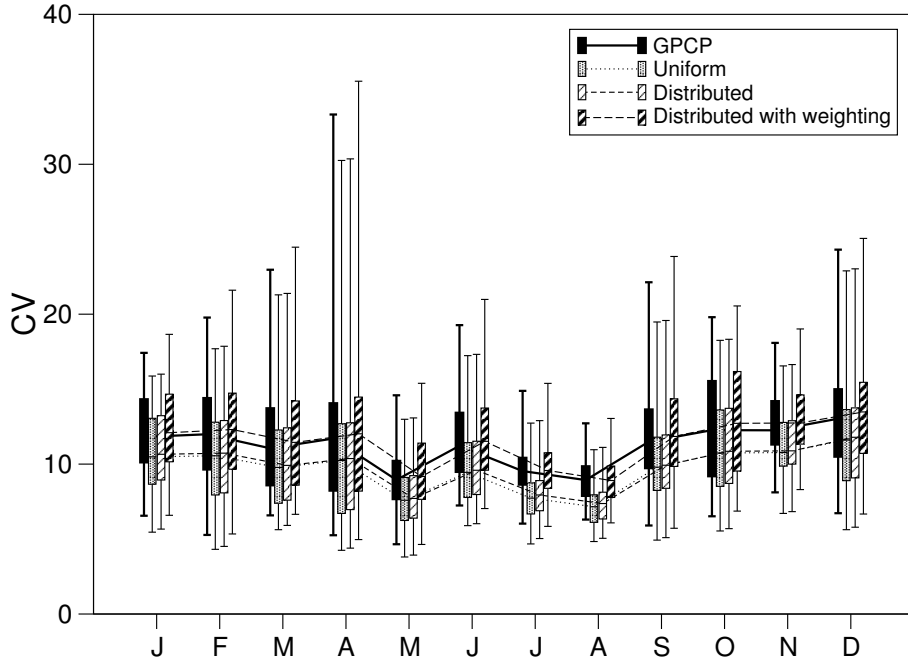


Figure 3.3: Average monthly distribution of the coefficient of variability for North America for the original daily, 1.0 degree GPCP data set and three data sets that were downscaled from a 2.0 degree aggregated version of the GPCP data to 1.0 degree using various downscaling methods. The uniform method assigns precipitation values uniformly to the higher resolution cells. The distributed approach uses a probabilistic method to determining the number of 1 degree grid cells within a 2 degree cell in which it is raining and distributes the 2 degree grid cell precipitation uniformly within these cells. The distributed with weighting method is the same as the distributed approach but weights the precipitation among the 1 degree grid cells based on the precipitation in neighboring cells. Similar results apply for the other continents.

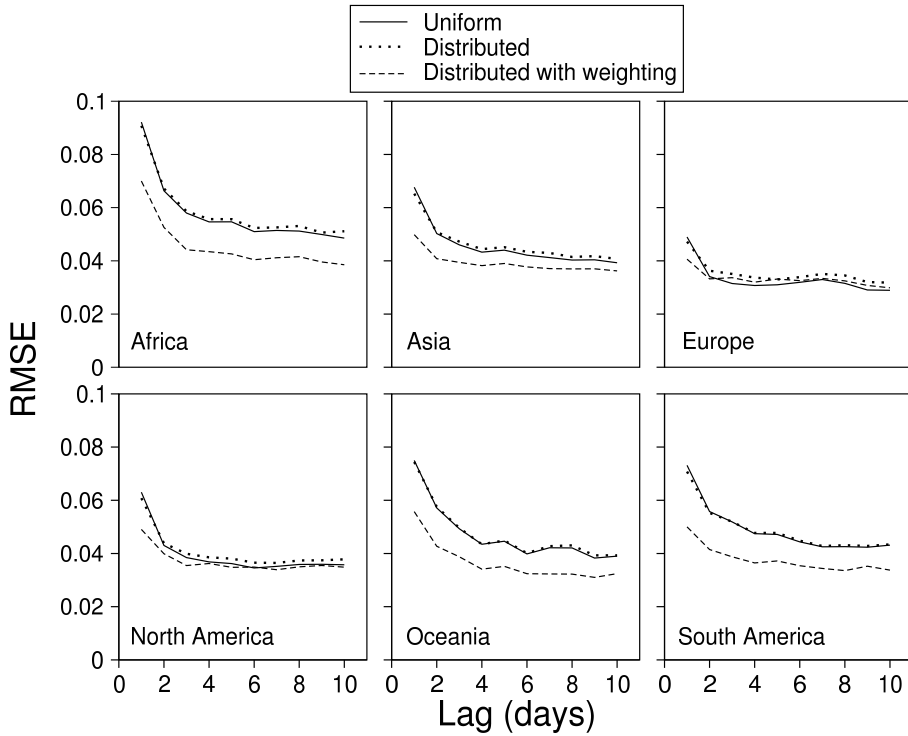


Figure 3.4: Root mean square error (RMSE) over the six continents in autocorrelation for various daily lag lengths between the original daily, 1.0 degree GPCP data set and three data sets that were downscaled from a 2.0 degree aggregated version of the GPCP data to 1.0 degree using various downscaling methods.

adjusted to sea-level (0.0m elevation) on its native grid. The data were then interpolated to the new grid resolution and elevation adjusted to the topography of the new grid. This ensures that the interpolation procedure is free of any elevation effects on the data. For the interpolation between the 2.0 degree and 1.0 degree grids, these elevation adjustments resulted in significant changes in some regions, with the maximum change in temperature of approximately 25°C, 160 W/m² for longwave radiation, 0.013 g/g for specific humidity and 38 KPa for surface air pressure.

3.3.3 Temporal downscaling

Precipitation

The diurnal variation of precipitation is generally significant over land areas, especially during the summer months where diurnal amplitudes can be greater than 50% of the daily mean value (Dai, 2001). High temporal resolution pre-

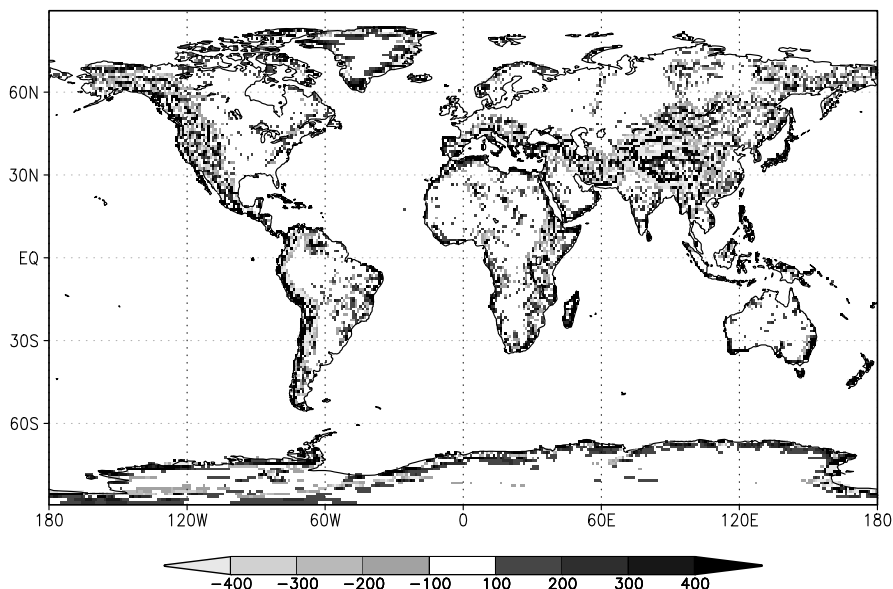


Figure 3.5: Difference in elevation (m) between the 2.0 degree and 1.0 degree grids. Elevation adjustments are made to air temperature, surface pressure, specific humidity and downward longwave radiation whenever data sets are interpolated between grids.

precipitation data (6-hourly or higher) are necessary to describe the diurnal cycle and are desirable for a multitude of hydrologic applications. Land surface hydrological processes are governed not only by the total amount of precipitation but also by the temporal structure of the precipitation, that is the storm duration and intensity and inter-storm length. Marani et al. (1997) showed the effect of the temporal structure of precipitation on land surface hydrological processes to be considerable because of the non-linear processes involved in partitioning precipitation. In the context of remotely-sensed precipitation, which may suffer from under sampling of the diurnal cycle, similar conclusions have been reached (e.g. Soman et al., 1995; Salby and Callaghan, 1997; Nijssen and Lettenmaier, 2004). Yet the availability of sub-daily precipitation data is intermittent in time and space, whether from gauges, radar or remote sensing, and thus downscaling is required for large scale applications. Direct use of the highest resolution NCEP precipitation data (6-hourly) is unwarranted, as it is acknowledged as being unreliable at scales less than monthly (Kalnay et al., 1996) and especially given the biases in the rain day statistics as described in section 3a. The biases in storm duration and storm frequency have been partially accounted for through the correction of monthly rain day frequencies (section 3a). However, to obtain reasonable estimates of the diurnal cycle of precipitation, disaggregation of the daily values to a 3-hourly time step is

necessary.

Temporal downscaling of precipitation has been attempted by many authors using a variety of techniques, including the use of probability distributions of precipitation statistics (e.g. Hershenhorn and Woolhiser, 1987; Connolly et al., 1998), multi-fractal cascade methods (e.g. Olsson, 1998; Gütner et al., 2001) and rectangular pulses stochastic rainfall generators (e.g. Bo et al., 1994; Cowpertwait et al., 1996). Here a simple stochastic sampling approach is used based on 3-hourly precipitation distributions extracted from the TRMM real time data set. This product provides one of the few large-scale, observation-based, gridded precipitation datasets at sub-daily resolution. The original TMI data suffer from under-sampling of the diurnal cycle because of orbit characteristics and can only adequately describe the diurnal cycle at coarse time and space resolutions (Negri et al., 2002). However the real time product used here combines the TMI data with IR data to produce near-continuous coverage in time and space. Other alternative data sets could be used, including the TRMM-based PERSIANN analysis (Hsu et al. 1997) and model-based products such as those from NASA’s Goddard Earth Observing System (GEOS), NCEP’s Global Data Assimilation System (GDAS) and the ECMWF.

The precipitation is downscaled from the daily NCEP product (with corrected rain day frequencies, section 3a) to a 3-hourly time step using a probabilistic approach based on sampling from the remote sensing based TRMM data set. The TRMM data set consists of 3-hourly data covering the latitude band 50S-50N (see Section 2). Monthly joint probability density functions (PDFs) of 3-hourly and daily precipitation amounts are derived from this data set for each 1.0 degree grid cell using information from the surrounding 2.0 degree window. 3-hourly precipitation amounts are then sampled at random from these distributions for each NCEP daily total and then the eight 3-hourly values in each day are scaled to match this daily total. For regions outside of 50S-50N where TRMM precipitation data are not available it is assumed that the PDFs are uniform across regional climate zones. Thus joint PDFs were created for each continent and climate zone (based on the Koppen climate classification, see Critchfield (1983)) and these were used to downscale the daily NCEP data outside of 50S-50N within the same climate zone and continent. This method was not feasible for regions within polar climate zones because there are no such regions within the 50S-50N latitude band. In this case, the probability distributions derived from cold climate zones were assumed to be representative of polar climates in the same continent.

The disaggregation method forces the statistics of the disaggregated data to match those of the TRMM dataset, whilst retaining the NCEP daily totals. The method was validated by recreating the TRMM product from its daily totals and indicated good performance in recreating the mean monthly diurnal cycle for different seasons and regions. The application of the disaggregation method is, however, dependent on the accuracy of the PDFs in representing actual diurnal cycles, and so is limited by the amount of data that contribute to them. The TRMM dataset used here has limited temporal coverage and may itself contain biases (Gottschalk et al., 2005). Updates from the TRMM

real time product and additional data from the retrospective version that start in 1998 will be added in the future to increase confidence in the PDFs and thus the resulting disaggregated values. Data from gauge-based datasets (Dai, 2001) that may be more reliable at regional scales could also be used.

Meteorological variables

The meteorological variables are simply downscaled from 6-hourly to 3-hourly resolution using linear interpolation. It is assumed that the diurnal cycle of these variables is represented adequately in the reanalysis, although the diurnal temperature range is adjusted to remove biases at the monthly scale (see section 3.d.2). No attempt is made to adjust these variables to make them consistent with the disaggregated 3-hourly precipitation as the relationships between precipitation and other meteorological variables are often weak. Downward solar radiation is interpolated with regard for the solar zenith angle to give a more realistic representation of the diurnal path of the sun. The type of the reanalysis variables (downward shortwave and longwave radiation are time average values; air temperature, pressure, humidity and windspeed are instantaneous values) is taken into account during the interpolation and all variables are converted into time average values.

3.3.4 Monthly bias corrections

As described in the introduction, systematic biases are inherent in the NCEP reanalysis (and other reanalysis products) at the monthly and seasonal scale. These biases are seasonally and regionally variable and will filter down into simulations of the land surface water and energy budgets. Adjustments are made to the reanalysis data (after downscaling and elevation corrections) so that the mean monthly values match those from available observation based datasets. Adjustments are not made to the specific humidity, air pressure and wind speed because global-scale, observation-based datasets for these variables do not exist.

Precipitation

The NCEP reanalysis precipitation is completely generated by the atmospheric forecast model and as such is acknowledged as being somewhat unreliable at the sub-monthly and local scale (Kalnay et al., 1996), although it does reveal useful information at larger space and time scales (Kalnay et al., 1996; Janowiak et al., 1998; Kistler et al., 2001). Biases in the NCEP reanalysis precipitation have been studied by many authors (e.g. Janowiak et al., 1998; Trenberth and Guillemot, 1998; Serreze and Hurst, 2000). Figure 6 shows the time series of global and continental average precipitation for the NCEP reanalysis and CRU data sets. The NCEP dataset is biased by 0.193 mm/day over global land areas excluding Antarctica which is equivalent to about 70 mm/yr. Errors in the NCEP reanalysis precipitation at monthly scales translate into errors in land surface fields like evapotranspiration, soil moisture and snow cover (Sheffield

et al., 2004). The effect on runoff generation has been investigated by Ngoduc et al. (2005) who found that biases in the NCEP reanalysis precipitation contributed the largest errors in resultant large basin river discharge when compared to biases in air temperature and radiation. To remove the biases in the NCEP product, the daily values are scaled so that their monthly totals match those of the CRU dataset before disaggregation to a 3-hourly time step as follows:

$$P_{NCEP,3hr}^* = \frac{P_{CRU,MON}}{P_{NCEP,MON}} \times P_{NCEP,3hr}, \quad (3.2)$$

where the asterisk indicates a corrected value, and the subscripts indicate the data source (NCEP or CRU) and the temporal resolution (3-hourly, daily, or monthly). Gauge-based precipitation measurements are often subject to losses from wind and wetting losses and due to solid precipitation (Goodison et al., 1998). Adam and Lettenmaier (2003) describe a global dataset of adjustment ratios that can be used for correcting gauge undercatch and can result in an increase in precipitation of about 12% globally. These catchment ratios can be applied to precipitation climatologies or to individual years in the reference period of the data set (1979-1998) (see Adam and Lettenmaier, 2003). For this study, the monthly CRU precipitation data set is adjusted using these catchment ratios before being used to scale the NCEP daily totals.

Figure 7 shows the effect of the monthly bias corrections on the NCEP reanalysis precipitation. These adjustments result in changes in global terrestrial precipitation (excluding Antarctica) of -8.8% (-0.19 mm/day or -70.3 mm/yr) after scaling to the CRU monthly values and -1.7% (-0.037 mm/day or 13.7 mm/yr) after also adjusting for gauge undercatch. Although the reduction in global precipitation by scaling to the CRU values is offset by the undercatch adjustment, there are substantial regional changes. Figure 7c shows the DJF biases in the NCEP dataset when compared to the CRU dataset. The largest biases in the reanalysis are over Greenland, central and southeast USA (for DJF only) and in northern India during JJA (not shown). There are large positive biases in mid and high northern latitudes during the summer (not shown), most notably in Canada and Alaska, central Europe, and throughout Eurasia to China. In the tropics the biases are spatially variable and seasonally dependent. For example, in Amazonia, the biases in the NCEP precipitation tend to be negative in the southwest during SON and DJF and shift northwards during the other part of the year. Conversely large positive biases occur generally in the east in an opposite pattern. This indicates the poor representation of the seasonal cycle of the tropical moisture patterns in the NCEP dataset (Trenberth and Guillemot, 1998). Of note is the correction to the spurious wavelike pattern in high northern latitudes as described in section 3.a. Figure 7d shows the mean DJF map of adjustments for gauge biases which are generally positive, with the largest increases in Greenland, central and northeast USA, parts of northern Eurasia and scattered regions in the Tropics.

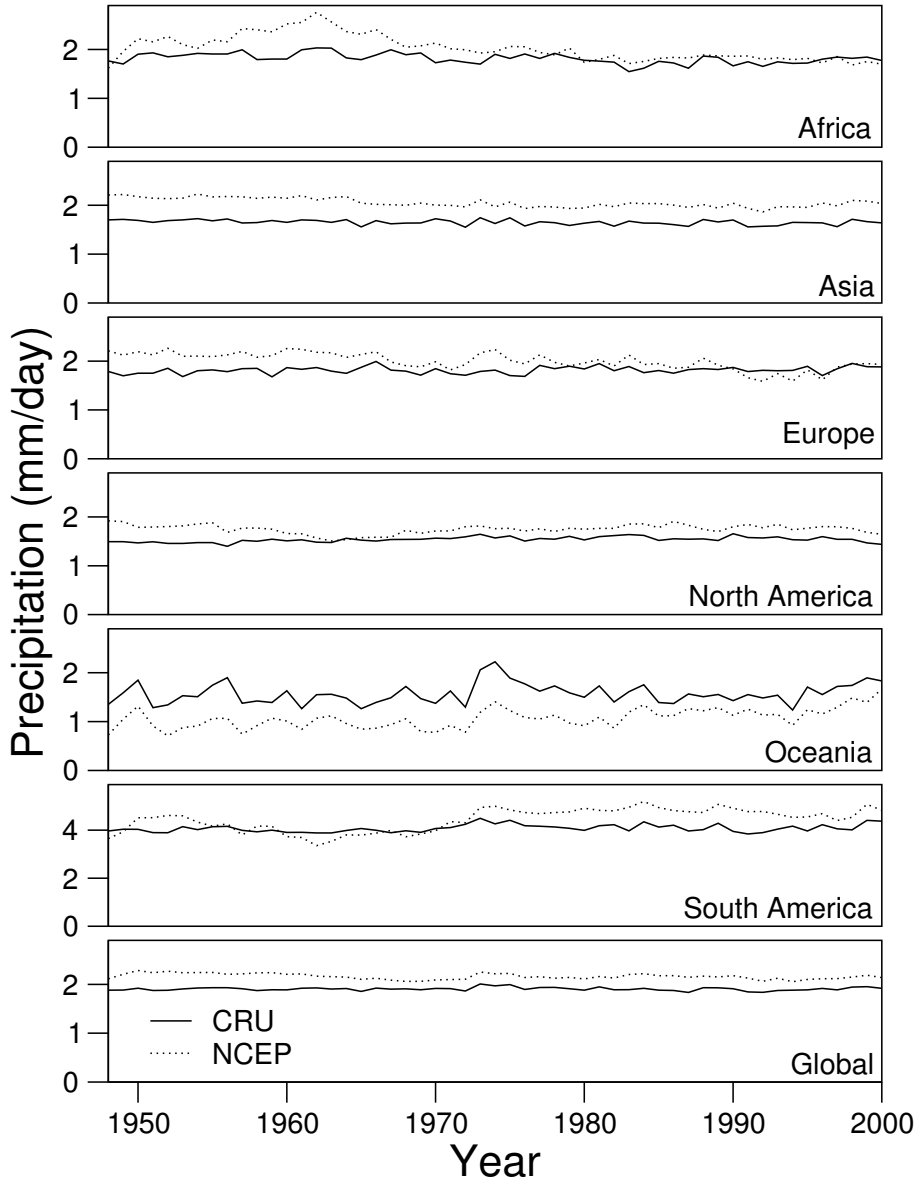


Figure 3.6: Annual time series of precipitation averaged over global and continental land areas excluding Antarctica for the NCEP and CRU data sets. NCEP global mean precipitation = 2.2 mm/day, CRU global mean precipitation = 2.0 mm/day, global mean bias in NCEP precipitation = 0.19 mm/day (70 mm/yr).

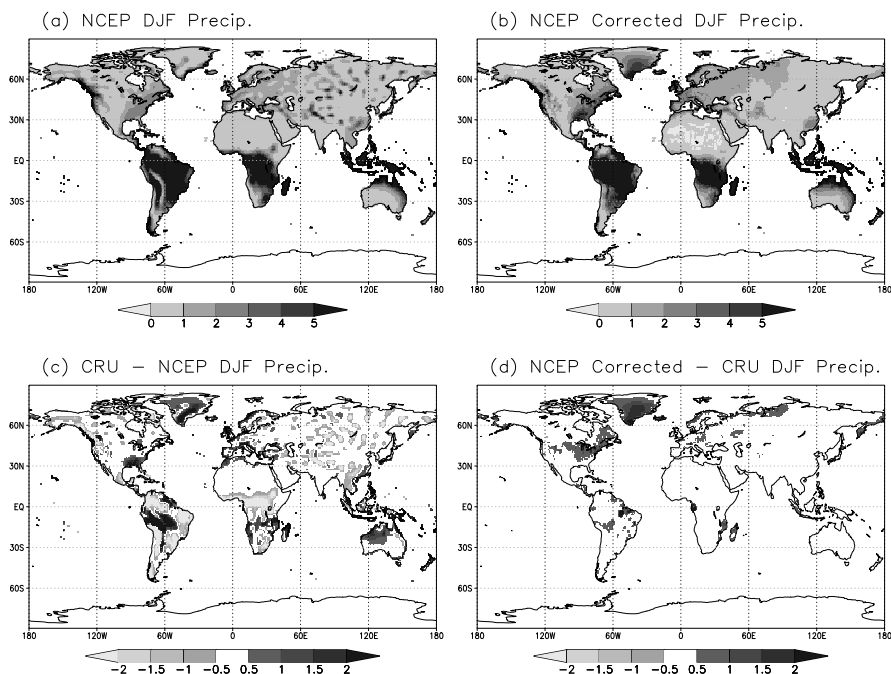


Figure 3.7: Average DJF precipitation (mm/day) for a) NCEP, b) NCEP scaled with the CRU dataset and adjusted for gauge biases c) difference between CRU and NCEP and d) difference between the NCEP scaled with the CRU dataset and adjusted for gauge biases and the CRU dataset.

Temperature

The NCEP air temperature is calculated from the modeled atmospheric variables, which are constrained by upper air observations and surface pressure, but no assimilation of screen level observations is carried out. It is a “B” class variable (Kalnay et al., 1996) in the reanalysis classification as it is strongly influenced by the model parameterization of surface energy fluxes. Kalnay and Cai (2003) compared NCEP surface air temperature with station based observations over the United States and found that the interannual variation was well represented although the upward trend over time was significantly less than that observed. Similar results were found by Kistler et al. (2001) at global scales. Simmons et al. (2004) looked at continental and regional scales and again found good agreement with interannual variability and generally lower warming trends in the northern hemisphere but distinct and probably incorrect regions of cooling in Australia and southern South America.

Figure 8 shows the mean annual time series of 2m air temperature for the NCEP and CRU datasets for global and continental land areas excluding Antarctica. The average annual global bias in the NCEP dataset is -0.56°C .

Comparison of the seasonal average air temperatures shows much larger regional and seasonal differences (see Figure 9). Most notably, in Siberia and Western Canada, and Alaska in the northern hemisphere winter, biases in the NCEP reanalysis can reach in excess of 5°C. Low biases are evident in the Himalayan range and Greenland, again of the order of 5°C, with smaller biases throughout the Tropics and scattered areas in northern Africa and central Asia. Biases in air temperature can be directly linked to changes in the land surface water budget through modifications of evaporation and thus soil moisture (e.g. Qu et al., 1998). To remove these biases the NCEP temperature data were adjusted to match the CRU monthly values by shifting the NCEP values by the difference between the NCEP and CRU monthly average values.

$$T_{NCEP,3hr}^* = T_{NCEP,3hr} + (T_{CRU,MON} - T_{NCEP,MON}) \quad (3.3)$$

In addition to scaling the 3-hourly values so that their monthly mean matched the CRU monthly values, the diurnal cycle of temperature for each day was scaled so that the monthly mean diurnal temperature range (DTR) matched the CRU monthly DTR values but the daily average value was unchanged as follows:

$$T_{NCEP,3hr}^* = T_{NCEP,DAILY}^* + \frac{DTR_{CRU,MON}}{DTR_{NCEP,MON}} (T_{NCEP,3hr}^* - T_{NCEP,DAILY}^*), \quad (3.4)$$

Adjustments were made to the specific humidity, surface air pressure and downward longwave radiation as outlined in section 3.2.2 to make them consistent with the new temperature values.

Downward short and longwave surface radiation

Incoming shortwave radiation incident at the earth's surface is the primary energy source for the land surface and drives evapotranspiration and snow melt. Therefore accurate specification of these forcing fluxes is essential for land surface modeling. Snow accumulation and melt is particularly sensitive to incoming longwave radiation (e.g. Schlosser et al., 2000), although Morrill et al. (1999) found that energy and water budgets were not sensitive to the diurnal cycle of longwave radiation. Downward surface short and longwave radiation are completely predicted by the NCEP reanalysis forecast model, and, as with precipitation and air temperature, contain systematic biases at seasonal time scales. Local scale comparisons indicate biases in both the long and shortwave products that may be systematic across geographic regions. Brotzge (2004) found that the NCEP dataset consistently overestimated downward surface shortwave radiation by 17-27% over 2000-2001 when compared to two Oklahoma Mesonet sites. Longwave radiation was also underestimated but by a lesser degree. Betts et al. (1996) found similar results when compared to data from the FIFE experiment for 1987 and concluded that these problems are generally attributed to the NCEP model atmosphere being too transparent and

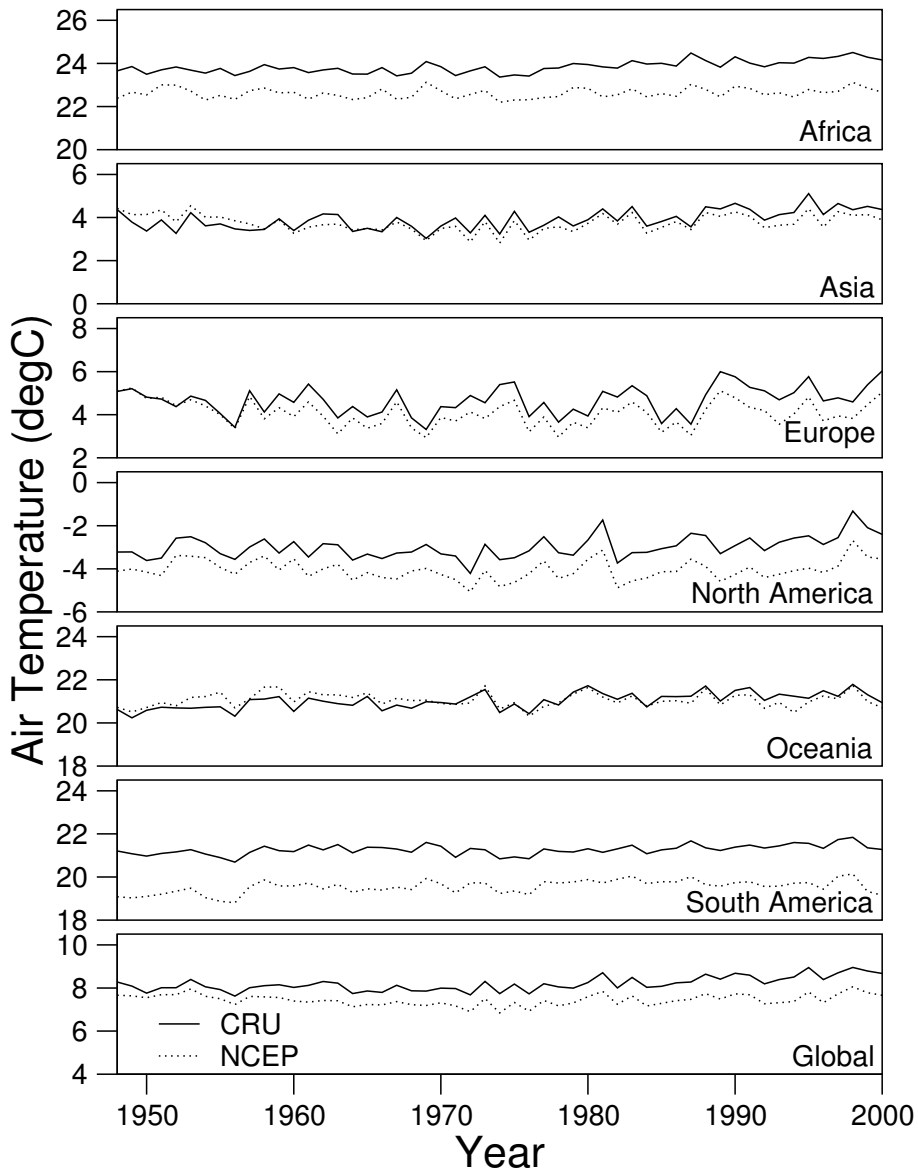


Figure 3.8: Annual time series of air temperature ($^{\circ}\text{C}$) averaged over global and continental land areas excluding Antarctica for the NCEP and CRU data sets. NCEP global mean air temperature = 7.6°C , CRU global mean air temperature = 8.1°C , global mean bias in NCEP air temperature = -0.6°C .

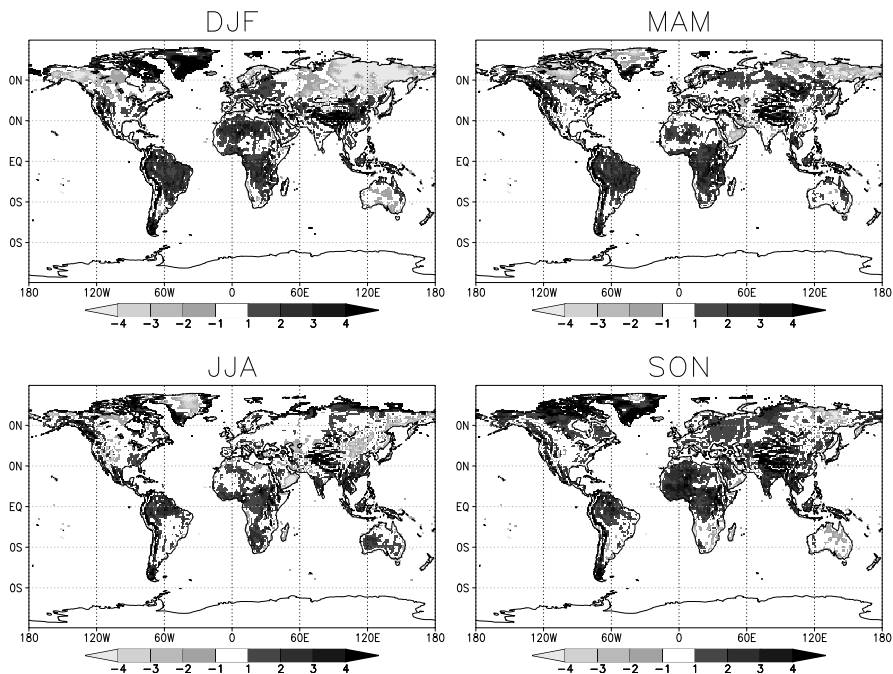


Figure 3.9: Average seasonal near-surface air temperature difference between the NCEP and CRU datasets ($^{\circ}\text{C}$).

too few clouds being produced, which may be systematic of large-scale atmospheric models in general. At larger scales, comparisons with remote sensing based data have revealed large-scale biases. For example, Berbery et al. (1999) found positive biases of $25\text{--}50\text{ W/m}^2$ over the United States when compared to the Geostationary Operational Environmental Satellite (GOES) based product of Pinker and Laszlo (1992).

Several global surface radiation budget (SRB) datasets have been developed in recent years including the GEWEX NASA Langley Surface Radiation Budget Project 1984-1995 product (Stackhouse et al., 2004) and the International Satellite Cloud Climatology Project (ISCCP) global 1983-2000 product (Zhang et al., 2004). These datasets provide surface short and longwave fluxes that have been validated against ground measurements. The latest version of the NASA Langley SRB product (release 2.0) is used here. Comparisons with ground-based measurements from the Baseline Surface Radiation Network (BSRN) indicate that errors are within measurement uncertainty. Comparison of the SRB and NCEP downward longwave data is shown in Figure 10 as seasonal averages for 1984-95. The mean bias in the NCEP dataset is 15.8 W/m^2 over global land areas excluding Antarctica. There are large regional biases of the order of $50\text{--}100\text{ W/m}^2$ across the Sahara, Middle East and Central Asia, the Andes and to a lesser extent in the western USA and Australia. The bi-

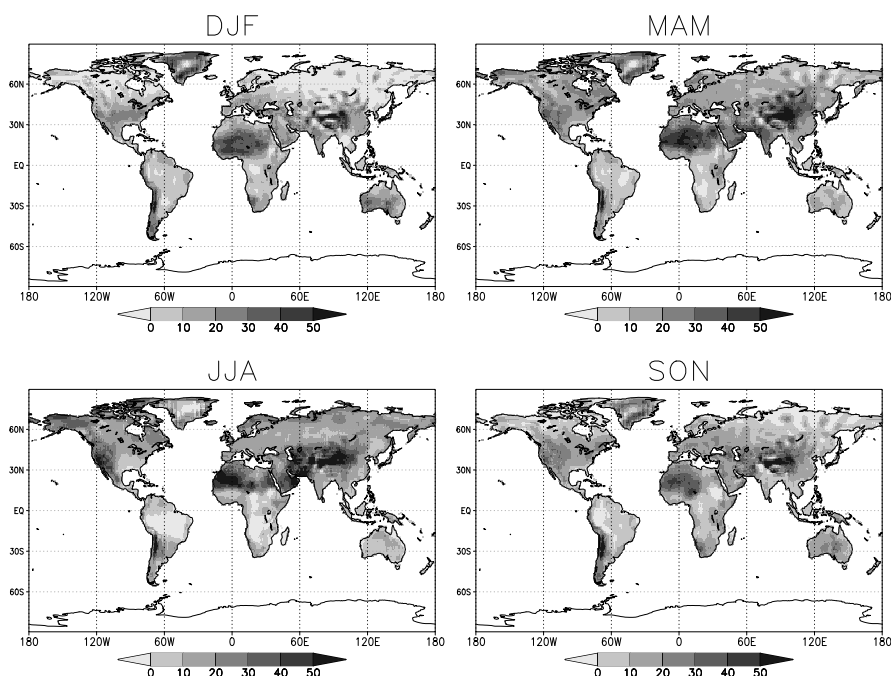


Figure 3.10: Average seasonal difference in downward longwave radiation between the NCEP and SRB datasets for 1984-94.

ases tend to be highest in the northern hemisphere spring and summer. The comparison of downward shortwave radiation is summarized in Figure 11. The mean bias in the NCEP shortwave data is -41.5 W/m^2 over global land areas. The biases tend to be larger in the spring and summer of each hemisphere in mid to high latitudes. These exceed -60 W/m^2 across the northern US and Canada, northern Europe, Siberia and Central Asia during the boreal summer and in the southern part of South America in the austral summer. In the tropics there is reasonable agreement throughout the year.

Analysis of station data have shown that shortwave radiation at the earth's surface has decreased over large regions during 1960-90 (Gilgen et al., 1998) that has been attributed to increases in cloud cover. More recently, studies of station data (Wild et al., 2005) and satellite measurements (Pinker et al., 2005) indicate that these downward trends have reversed over the past decade or so, possibly due to reductions in aerosols. However, the trend in global terrestrial shortwave radiation from the reanalysis shows a spurious upward trend (Figure 12b). Therefore, the reanalysis shortwave radiation is adjusted so that firstly, systematic biases are removed at the monthly scale so that it matches the mean of the SRB data for 1984-94, and secondly, trends over the full 50-yr period are consistent with observations.

Using the relationship between cloud cover and surface downward short-

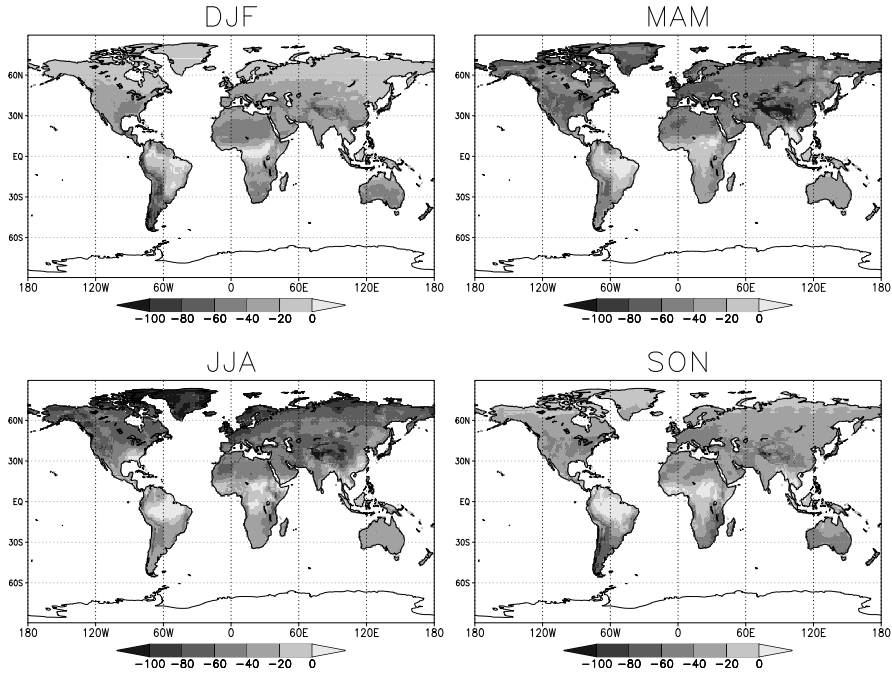


Figure 3.11: Average seasonal difference in downward shortwave radiation between the NCEP and SRB datasets for 1984-94. The bands of missing data in high northern latitudes are where SRB data are not available for all months.

wave radiation (Thornton and Running, 1999), a new time series of radiation is constructed that is consistent with observed trends. A linear regression was developed at each grid cell between the monthly anomalies of reanalysis cloud cover and shortwave radiation. This relationship was then used to predict monthly anomalies of shortwave radiation from observation-based estimates of cloud cover anomalies from the CRU dataset. The resultant time series was then converted to actual values whose monthly climatology over 1984-94 matched that of the SRB dataset. This was done by subtracting the mean monthly climatology for 1984-94 from the time series of anomalies and then adding the mean climatology of the SRB dataset. In this way the new time series is consistent with the SRB data over the limited period of overlap but imposes the long-term trends as derived from observed cloud cover. The NCEP 3-hourly values are then scaled so that their mean values match this new monthly time series as follows:

$$SW_{NCEP,3hr}^* = \frac{SW_{SRB+CRU,MON}}{SW_{NCEP,MON}} SW_{NCEP,3hr}, \quad (3.5)$$

where the subscript SRB+CRU indicates the time series of monthly SW

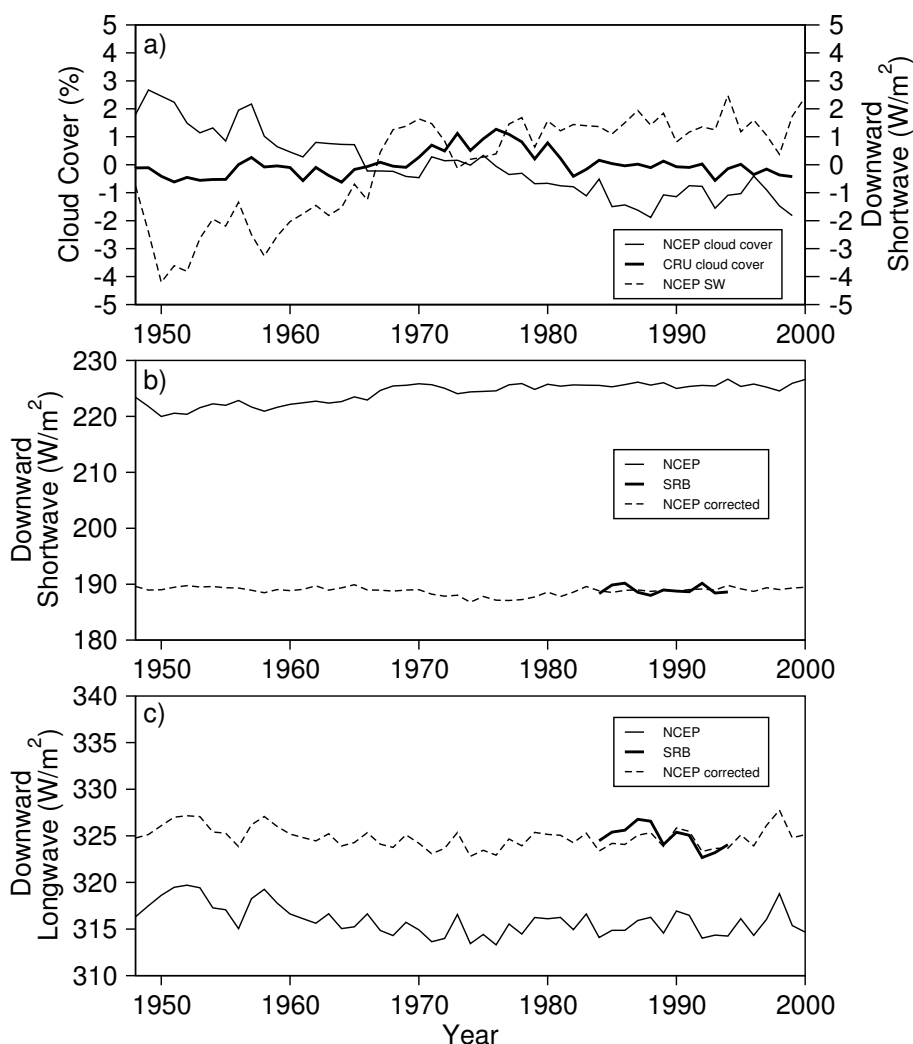


Figure 3.12: a) Annual anomalies of global mean cloud cover for the CRU dataset and cloud cover and downward shortwave radiation from the NCEP dataset. b) Annual time series of global mean downward shortwave radiation for the NCEP, SRB QCSW and NCEP corrected datasets. The corrected dataset has been scaled to be consistent with the SRB data and the long-term variation of the CRU cloud cover. c) Annual time series of global mean downward longwave radiation for the NCEP, SRB LW and NCEP corrected dataset. The corrected datasets has been scaled using the probability swap method to be consistent with the mean and variability of the SRB data whilst retaining the year-to-year variation of the NCEP dataset. Global means are calculated over terrestrial areas excluding Antarctica.

values derived from the CRU cloud cover and scaled to the SRB dataset.

Downward longwave radiation is bias corrected using a probability matching method that scales the reanalysis monthly values to match the mean and variability of the SRB values but retains the year-to-year variation of the NCEP data. Figure 12c shows no apparent global trend in the NCEP data which is consistent with station-based observations of long-term trends that are within the bounds of measurement error (Wild et al., 2001). Therefore, no attempt is made to alter the long-term trends in the NCEP monthly values. The probability matching method replaces each of the NCEP monthly mean values over 1948-2000 with a monthly value from the SRB time series that has the same cumulative probability as the NCEP value. The cumulative probabilities were calculated from PDFs of the NCEP and SRB monthly time series. The new monthly time series was then used to scale the NCEP 3-hourly values:

$$LW_{NCEP,3hr}^* = \frac{LW_{SRB,MON}}{LW_{NCEP,MON}} LW_{NCEP,3hr}, \quad (3.6)$$

Figure 12 shows the global mean monthly time series of downward short and longwave radiation for the NCEP, SRB and the scaled NCEP datasets.

3.4 Discussion and Conclusions

The goal of this study is to provide a global dataset of forcings that has long temporal and global coverage and is consistent in time and space. In this respect, the dataset makes use of the latest available global meteorological datasets and combines them with state of the art reanalysis to form a consistent, high quality dataset. Nevertheless, an essential part of the development of any dataset is validation against independent data sources, which will quantify the errors and known biases and hopefully instill confidence in the use of the data. This is a difficult task given the general lack of large-scale observations and the fact that potential validation datasets are better utilized in the development of the forcing dataset to produce the highest quality dataset possible.

The intended application of the forcing dataset is for long-term, large-scale modeling, where the focus of interest is on the variation of the land surface over seasonal to annual timescales and across regional and continental space scales. Here it is more important to ensure that the statistics of the forcing data are correct rather than trying to replicate the fine scale features of the historic record. For example, the forcing dataset is unlikely to recreate actual historic storm events partly because the correction of the daily precipitation frequencies may disrupt spatial coherence at the daily time scale. This is because the disaggregation and correction methodologies are designed to match the observed data only in a statistical sense whilst providing consistency among variables where possible, and any detrimental effects on the terrestrial water budget will be small at seasonal and regional scales.

The dataset can be evaluated by forcing a land surface model and comparing the resultant water and energy fluxes and states with observations, such as

streamflow records, snow cover extent and in situ soil moisture measurements. Several studies have shown that evaluating land surface model simulations over large areas requires detailed examination of all aspects of the modeling process (e.g. Nijssen et al., 2001a,b; PILPS2-E experiment: Nijssen et al., 2003, Bowling et al., 2003; the series of NLDAS papers: Mitchell et al., 2004a). In addition to the errors in the forcings, there are also uncertainties in the land surface model structure, physical parameterizations, and input parameters (vegetation, soils, etc) as well as in the observations themselves. The relative contribution of these factors to the differences from observations is difficult to discern without a detailed examination of all aspects of the modeling process and this is work in progress.

Nevertheless, it is possible to evaluate the dataset against similar bias corrected forcing products and this is done next by comparing against the GSWP-2 forcing dataset that uses a similar strategy to combine reanalysis with observations, although for a much shorter time period.

3.4.1 Comparison with GSWP-2 forcing dataset

The goal of GSWP-2 is to develop global datasets of soil moisture and other hydrologic variables from multiple land surface models and investigate the differences and sensitivities of these models. The GSWP forcing dataset has the same temporal (3-hourly) and spatial (1.0 degree) resolution but for a shorter time period (1986-1995), is based on the NCEP-DOE reanalysis and is described in detail by Zhao and Dirmeyer (2003). This section compares monthly mean values of precipitation, temperature, and radiation from the two datasets as absolute differences and using the non-parametric Wilcoxon signed ranks test of differences. The monthly mean diurnal temperature range and daily precipitation frequencies are also examined, as these generally have a significant impact on the hydrologic cycle. Figure 13 shows the mean annual differences and statistical significance of differences in the monthly means for these variables.

Monthly mean temperature

Comparison of the monthly temperatures revealed differences that are consistent with differences in the observations used to create the two datasets. Both use long-term monthly temperature from CRU but different versions (GSWP uses version 1.0 and this study uses the updated and extended version 2.0). Using the Wilcoxon signed ranks test, the null hypothesis was tested that the median difference of monthly means between the two datasets is zero for each grid cell at the 95% confidence level. Figure 13 shows that the null hypothesis can be rejected in the majority of regions, possibly due to changes in contributing gauges between the two versions of the CRU dataset and the effects of using different datasets to correct for elevation effects. The GSWP uses the ISLSCP elevation product and this study uses the National Geophysical Data Center (NGDC) 2-minute elevation dataset aggregated up to 1.0 degree reso-

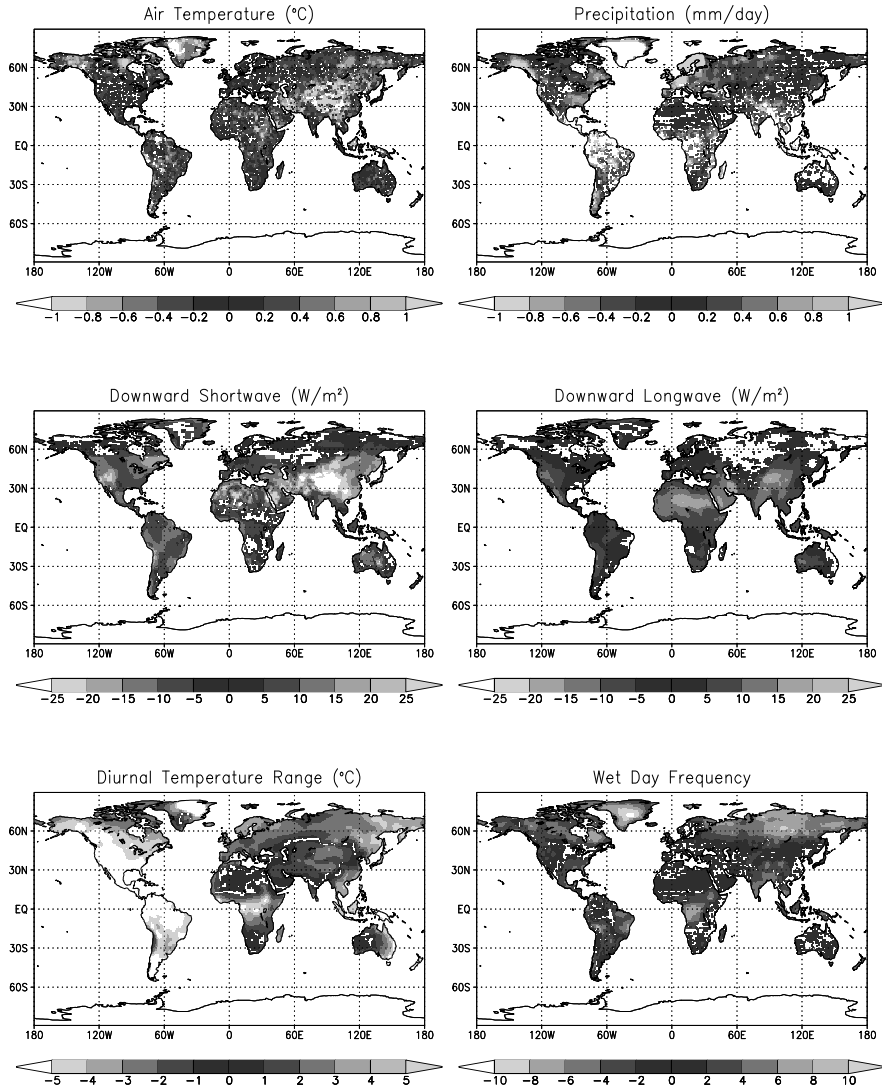


Figure 3.13: Difference of monthly mean values, averaged over 1986-1995, between the GSWP-2 forcing dataset and this study. Contours are critical values of the Wilcoxon signed ranks test statistic at the 95% level. Solid contours are where the GSWP data are greater, dashed contours are where GSWP are less. Regions where the two datasets are statistically similar are unshaded.

lution. The mean difference is 0.0965 °C over global land areas and maximum monthly differences of up to 4-5 °C occur in parts of the Himalayas and Tibetan plateau, Northern Greenland and in small isolated regions scattered across the globe.

Monthly mean precipitation

Monthly precipitation shows widespread differences that are statistically significant, which is to be expected given the independent sources of observation data used by each dataset. The GSWP data are based on Global Precipitation Climatology Centre (GPCC) monthly data which are used to scale the NCEP-DOE sub-monthly precipitation amounts. Corrections are also applied for gauge undercatch. Data from the Global Precipitation Climatology Project (GPCP) are blended in for regions where the density of contributing gauges for the GPCC product is low. For this study the CRU monthly means are used, with correction for gauge undercatch based on the analysis of Adam and Lettenmaier (2003). Several regions stand out as being coherently biased one way or the other. The GSWP dataset is generally greater across mid-latitudes in both hemispheres, with larger differences greater than 1.0 mm/day in Scandinavia, the Pacific Northwest and Alaska, the eastern US and southern South America. It is generally lower in the Tropics and high northern latitudes most notably in Central America and the Amazon basin, northern Canada and Greenland. The global mean annual bias in the GSWP is 0.0661 mm/day (24.1 mm./yr).

Monthly mean downward short and longwave radiation

For downward short and longwave radiation, both forcing datasets use SRB products, although different versions (this study uses the SRB-QCSW and SRB-LW datasets and GSWP uses the SRB-SW and SRB-QCLW datasets). Additionally, this study uses observed cloud cover data to adjust the inter-annual variability of the shortwave monthly means, whereas the GSWP uses the data as is because of the direct overlap with the SRB time period. The differences between the two datasets are consistent with the difference between the SRB-SW and SRB-QCSW datasets (global mean bias for GSWP is -8.2 W/m²). The GSWP is generally smaller with the greatest differences across a band stretching from northern Africa to Japan, and also in the western and northeast US. For longwave, the differences are again consistent with the differences between the SRB-LW and SRB-QCLW. The SRB-QCLW (GSWP) values tend to be larger (global mean bias of 6.0 W/m²), and distributed similarly to the shortwave differences, but are lower at high latitudes.

Diurnal temperature range

Both datasets use CRU DTR products to correct the air temperature. As for mean temperature the GSWP dataset uses CRU version 1.0 and version 2.0 is used here. For the GSWP dataset, the 3-hourly air temperature values are scaled by the ratio of the CRU to NCEP-DOE reanalysis DTR values but

with restrictions on the size of the ratio to avoid excessive values. A similar method is used here (section 3.d.2) but with no restriction on the ratio of CRU to NCEP values. The mean global bias for GSWP is -1.4°C and maximum monthly differences can exceed 5°C . GSWP is generally larger in the Western Hemisphere, the Tropics during the wet season and is lower predominantly over central Asia and other dry regions worldwide.

Daily precipitation frequency

The distribution of precipitation within a month in terms of the number of wet and dry days plays an important role in partitioning the monthly precipitation into runoff and evaporation (Sheffield et al., 2004). The GSWP2 dataset makes no adjustment to daily precipitation frequencies and so uses the NCEP-DOE as is. For this study, the NCEP-NCAR reanalysis daily data are resampled to match observation based datasets of precipitation frequencies. The GSWP2 has on average 0.48 fewer precipitation days per month globally. GSWP is generally greater in the humid Tropics (except for northwest South America) and in southwest South America and is smaller in most other regions, especially in higher northern latitudes. Maximum monthly differences are generally less than 4 precipitation days but can reach 10 precipitation days in small regions in Greenland, central Siberia and the humid Tropics.

3.4.2 Future improvements

Although the emphasis has been on using global scale observation datasets to ensure consistency in space, nevertheless, better quality data sets exist in terms of spatial and temporal resolution but with smaller spatial and temporal extents. For example, for the temporal disaggregation of precipitation at high northern latitudes, it was assumed, because of the lack of coverage by the TRMM dataset, that the diurnal cycle in cold, mid-latitude climates is representative of neighboring polar regions. Sub-daily station data from Canadian surface airways products and the Former Soviet Union (Razuvaev et al., 1998) are available for a significant number of high-latitude locations and can be used to derive the probability distributions used for the disaggregation. Furthermore, most monthly gridded precipitation datasets also do not allow for orographic effects. As the network of rain gauges that contribute to these data sets are generally not located in regions of complex and elevated topography, this usually results in an underestimation of precipitation, by as much as 3 times (Adam et al., 2006). The correction method of Adam et al. (2006) uses a simple catchment water balance method to calculate adjustments to precipitation. These changes may be incorporated into new versions of the dataset in the future, although concerns over consistency in time and space may make this somewhat counter-productive. In addition, as improved and extended versions of observation-based datasets used in this study become available these will be incorporated where applicable.

3.4.3 Dataset availability

The forcing dataset will be made available over the internet at <http://hydrology.princeton.edu> in the ALMA (Assistance for Land-surface Modelling activities) netcdf format (version 3) which is a standard data exchange format for land surface scheme forcing and output data. The development of the final 1.0 degree, 3-hourly dataset has gone through a number of intermediate stages in terms of spatial and temporal resolution and these intermediate products will also be added to the archive. The following products are available:

- Global, 2.0 degree, 1948-2000, daily
- Global, 1.0 degree, 1948-2000, daily
- Global, 2.0 degree, 1948-2000, 3-hourly
- Global, 1.0 degree, 1948-2000, 3-hourly

The variables are precipitation, air temperature, downward short and long-wave radiation, surface pressure, specific humidity and windspeed. Global coverage indicates terrestrial regions excluding Antarctica.

3.4.4 Concluding remarks

This paper describes a long-term, high resolution, near surface meteorological dataset that can be used for forcing hydrologic simulations of the land surface water and energy budgets. The necessity for accurate estimates of the spatial and temporal variation in terrestrial water and energy fluxes and states is evident and is the driving force in the development of high resolution and long-term hydroclimatological datasets. The development of the highest quality forcing datasets is a first and vital step towards this. Through research initiatives such as the World Climate Research Programme (WCRP) Climate Variability and Predictability (CLIVAR) program and Global Energy and Water Cycle Experiment (GEWEX) the emphasis has been on the development and enhancement of large scale datasets, through the use of increasingly better observational datasets and the use of new assimilation and modeling techniques. This study is intended to form a part of this process by providing a benchmark forcing dataset that combines state of the art reanalysis products with the most recent observation-based datasets. The goals in the development of this dataset are to provide consistency in time and space among variables from contributing datasets whilst trying to achieve the highest resolution that can be supported by the data. This dataset provides a significant improvement over the original reanalysis variables, and can be used for a wide variety of applications and diagnostic studies in the climatological, hydrological, and ecological sciences.

Acknowledgements

This study was carried out with funding from NASA grants NAG5-9414 and NAG8-1517. The NCEP/NCAR reanalysis data were provided by the NOAA-CIRES Climate Diagnostics Center, Boulder, Colorado, USA, from their web site at <http://www.cdc.noaa.gov/>. The GPCP dataset was downloaded from the World Data Center for Meteorology at <http://lwf.ncdc.noaa.gov/oa/wmo/wdcamet-ncdc.html>. The TRMM dataset was downloaded from the <ftp://aeolus.nascom.nasa.gov/pub/merged>. The CRU datasets were obtained from Dr. Tim Mitchell at the Climatic Research Unit (<http://www.cru.uea.ac.uk>) at the University of East Anglia, UK. The SRB dataset was downloaded from the NASA Langley Research Center Atmospheric Sciences Data Center at <http://eosweb.larc.nasa.gov>.

Chapter 4

Development of a global dataset of soil moisture and drought, 1950-2000

This chapter is a slightly modified version of: Sheffield, J., and E. F. Wood (2007), Characteristics of global and regional drought, 1950-2000: Analysis of soil moisture data from off-line simulation of the terrestrial hydrologic cycle, *J. Geophys. Res.*, *112*, D17115, doi:10.1029/2006JD008288.

Abstract

Drought occurrence is analyzed over global land areas for 1950-2000 using soil moisture data from a simulation of the terrestrial water cycle with the VIC land surface model, which is forced by an observation based meteorological dataset. A monthly drought index based on percentile soil moisture values relative to the 50-year climatology is analyzed in terms of duration, intensity and severity at global and regional scales. Short-term droughts (≤ 6 months) are prevalent in the Tropics and mid-latitudes, where inter-annual climate variability is highest. Medium term droughts (7-12 months) are more frequent in mid- to high-latitudes. Long term (12+ months) droughts are generally restricted to sub-Saharan Africa and higher northern latitudes. The Sahel region stands out for having experienced long-term and severe drought conditions. Severe regional drought events are systematically identified in terms of spatial coverage, based on different thresholds of duration and intensity. For example, in northern Europe, 1996 and 1975 were the years of most extensive 3- and 12-month duration drought, respectively. In northern Asia, severe drought events are characterized by persistent soil moisture anomalies over the wintertime. The drought index identifies several well-known events, including the 1988 US, 1982/83 Australian, 1983/4 Sahel and 1965/66 Indian droughts which are generally ranked as the severest and most spatially extensive in the record. Comparison with the PDSI shows general agreement at global scales and for these major events but they diverge considerably in cooler regions and seasons, and especially in latter years when the PDSI shows a larger drying trend.

4.1 Introduction

Drought is a pervasive climate phenomenon that is considered to be one of the most damaging natural hazards in terms of economic cost (Wilhite, 2000). It can cover extensive areas and last from months to multiple years and may have major impacts on agriculture, water supply and the environment. Historically drought has persistently affected human activity (e.g. Hodell et al., 1995, Stine, 1994) and impacts in every part of the globe in which habitation is possible. Despite its omnipresent nature our knowledge of the onset, development and recession of drought is deficient. This hampers our ability to predict its occurrence at seasonal and longer time scales. Part of the reason for this is the dearth of detailed data about its spatial and temporal variability across large scales and the impact on various environmental and social sectors.

To understand how drought varies, long-term observations of relevant variables, such as precipitation, streamflow and soil moisture, are required. Global datasets of these variables are lacking at high spatial resolution or are available only for limited time periods. Alternatively, models can provide spatially and temporally consistent fields of these variables at large scales when forced with observed boundary conditions and can be used for prediction at seasonal to decadal time scales when run in forecast mode. Furthermore, atmosphere-

ocean general circulation models (AOGCM) can be used to study decadal variability in drought when run in coupled mode, and may provide insights into the forcing mechanisms of historic drought events, such as the influence of sea surface temperature patterns (Hoerling and Kumar, 2003).

Historically, the Palmer Drought Severity Index (PDSI) (Palmer, 1965) has been the tool of choice when monitoring and analyzing drought occurrence. At continental to global scales its simplicity makes it an attractive choice for reconstructing drought records (Cook et al., 1999; Dai et al., 2004). However, it has been shown to be unsuitable for widespread application and suffers from simplifications in its physical basis (Alley, 1984; Heim, 2002). With the emergence of physically based models over the last decade that simulate the detailed processes of energy and water transfer at the earth's surface, including detailed soil moisture transport and snow processes, the potential for more accurate drought monitoring is evident (Sheffield et al., 2004a). Coupled with the growing availability of remote sensing products and detailed meteorological data at fine time and space scales to force these models with, both retrospectively and in real time, there is the potential for analyzing drought variability historically and for monitoring at regional and global scales.

Drought in its various forms has been analyzed at large scales by many authors in recent years. Sheffield et al. (2004a) used an approach based on simulated soil moisture data to analyze the spatial and temporal extent of national and regional drought over the US. Similarly, Andreadis et al. (2005) used severity-area-duration curves to investigate major US droughts over the 20th century. At similar scales, Van der Schrier et al. (2006a, 2006b) calculated summer PDSI over North America and Europe for 1901-2000 and identified the 1930s and 1950s as the driest periods of the record over North America and the late 1940s to early 1950s over Europe. Globally, Dai et al., (2004) calculated PDSI data from 1870 to 2002 and concluded that precipitation and temperature trends modulated by ENSO activity as the leading cause of variability. Peel et al. (2004, 2005) looked at 3863 precipitation station and 1236 stream flow gauge records globally to analyze the distribution of drought duration, magnitude and severity and found that both precipitation and streamflow showed similar distributions of drought duration globally except for the Sahel. McCabe and Palecki (2006) analyzed decadal variability in global PDSI and sea surface temperatures.

In this study, the spatial and temporal characteristics of global drought during the second half of the 20th century are analyzed using soil moisture data from an off-line land surface model simulation. Drought is defined conceptually as a sequence of soil moisture deficits relative to climatology. The simulation is driven by a hybrid forcing dataset derived by combining global atmospheric reanalysis with a suite of observational datasets to remove biases and spurious trends in the reanalysis (Sheffield et al., 2006). The output fields have been validated against observations of the terrestrial hydrologic budget, where available (Sheffield and Wood, *Evaluation of retrospective off-line simulation of the global terrestrial water budget*, 1950-2000, in preparation). This study focuses on the statistical properties of drought occurrence as derived from this

simulation, in terms of duration, magnitude and severity, and how these vary globally. This definition does not explicitly take into account the impacts of drought but these are generally small for short term droughts and increase with duration and magnitude. By providing a globally consistent picture of drought occurrence that is based on modeled physical processes and observation based boundary conditions, these analyses can help characterize historic droughts and thus form a basis for real time monitoring and prediction, including estimates of drought recovery. An analysis of the long-term variability and trends in drought characteristics over the latter half of the 20th century and the relationship with local and remote forcings will be reported elsewhere by the authors.

The paper is laid out as follows. First, the soil moisture dataset is described, including the land surface model and the meteorological forcings. Then methods for deriving the drought index are presented along with statistics for describing the attributes of drought and their temporal and spatial variation. These include the duration, magnitude (deviation from a threshold value), intensity (mean magnitude over the duration) and severity (intensity times duration). A general overview of the variation of soil moisture globally is given next, followed by a global and regional analysis of drought, its characteristics and their inter-relationships. Finally, the dataset is compared to the PDSI and the methods presented are used to identify major drought periods over the last 50 years and some examples of these are evaluated within the context of the statistical framework.

4.2 Datasets and methods

The analysis of drought is based on simulated soil moisture data derived from an off-line land surface hydrological model simulation. Soil moisture in the top meter or so provides a useful index of drought in that it provides an aggregate estimate of water availability from the balance of precipitation, evaporation and runoff processes and takes into account the delays caused by infiltration and drainage, snow accumulation and melt, and the impacts of anomalies in meteorological forcings such as temperature and radiation. In drought terminology, soil moisture falls somewhere in between meteorological drought (a period of precipitation deficit) and hydrological drought (a shortfall in stream-flow, reservoir and lake levels, groundwater, etc.) and may be representative of agricultural drought (deficient soil moisture relative to crop and plant demand) through its control on transpiration and thus vegetative vigor. The drought index is calculated as the deficit of soil moisture with respect to the model's seasonal climatology at a given location (Sheffield et al., 2004a). This allows us to quantify and compare drought characteristics between locations in a consistent manner. A drought is then defined as a period with a percentile soil moisture value less than a chosen level which represents the drought magnitude. This level reflects the rarity or extremeness of the event. The off-line simulation and the derivation of the drought index and related statistics are

described in detail next.

4.2.1 Off-line land surface simulation

The Variable Infiltration Capacity (VIC) land surface model (Liang et al., 1994, 1996; Cherkauer et al., 2002) was used to generate spatially and temporally consistent fields of soil moisture and other water budget flux and state variables. The VIC model simulates the terrestrial water and energy balances and distinguishes itself from other land surface schemes through the representation of sub-grid variability in soil storage capacity as a spatial probability distribution, to which surface runoff is related (Zhao et al., 1980), and by modeling base flow from a lower soil moisture zone as a nonlinear recession (Dumenil and Todini, 1992). The VIC model has been applied extensively at regional (Abdulla et al., 1996; Maurer et al., 2002) and global scales (Nijssen et al., 2001; Sheffield et al., 2004b), including snow and ice dominated regions (Bowling et al., 2003; Su et al., 2006).

Horizontally, VIC represents the land surface by a number of tiled land cover classes. The land cover (vegetation) classes are specified by the fraction of the grid cell which they occupy, with their leaf area index, canopy resistance, and relative fraction of roots in each of the soil layers. Evapotranspiration is calculated using a Penman-Monteith formulation with adjustments to canopy conductance to account for environmental factors. The subsurface is discretized into multiple soil layers. Movement of moisture between the soil layers is modeled as gravity drainage, with the unsaturated hydraulic conductivity a function of the degree of saturation of the soil. Cold land processes in the form of canopy and ground snow pack storage, seasonally and permanently frozen soils and sub-grid distribution of snow based on elevation banding are represented in the model. Seasonally and permanently frozen soils are represented in the VIC model according to the algorithm of Cherkauer and Lettenmaier (1999). Soil temperatures are calculated using a finite difference solution of the heat diffusion equation for a user-specified number of nodes that are independent of the soil moisture layers. Soil ice content is estimated based on node temperatures and infiltration and baseflow are restricted based on the reduced liquid soil moisture capacity.

Previously, soil moisture fields from a retrospective simulation with the VIC model for the USA (Maurer et al., 2002) have been analyzed in terms of drought occurrence by Sheffield et al. (2004a), who found that the simulated soil moisture values were able to represent historic drought events, display coherency and sufficient detail at small space scales, and compare well with standard drought indices such as the PDSI. In snow dominated regions the VIC based dataset and the PDSI dataset were found to diverge, likely due to inadequate representation of cold season processes in the calculation of the PDSI.

For this study, the VIC model was run globally at 1.0 degree spatial resolution and 3-hourly time step, for the period 1950-2000. Three soil layers were used in the simulation with the top layer being 30 cm thick. The second layer,

the main storage layer, was between 0.5 to 1.5 m and the lower layer, which provides moisture for subsurface runoff, was between 0.1m and 0.25m. These two layers are adjusted during the calibration process to result in routed streamflow that satisfactorily match observations at the large basin scale. The values of soil and vegetation parameters and their spatial distribution were specified following Nijssen et al. (2001). Soil textural information and bulk densities were derived by combining the 5-min Food and Agricultural Organization–United Nations Educational, Scientific, and Cultural Organization (FAO–UNESCO) digital soil map of the world (FAO 1995) with the World Inventory of Soil Emission Potentials (WISE) pedon database (Batjes 1995). The remaining soil characteristics, such as porosity, saturated hydraulic conductivity, and the exponent for the unsaturated hydraulic conductivity equation were based on Cosby et al. (1984). Vegetation types were taken from the Advanced Very High Resolution Radiometer (AVHRR)-based, 1-km, global land classification of Hansen et al. (2000). Vegetation parameters such as height, and minimum stomatal resistance were assigned to each vegetation class based on a variety of sources described in Nijssen et al. (2001). Monthly values of leaf area index were based on Myneni et al. (1997) and were kept constant from year to year.

This simulation was forced by a hybrid dataset of meteorological data derived from the National Centers for Environmental Prediction (NCEP)/National Center for Atmospheric Research (NCAR) reanalysis (Kalnay et al., 1996) and a suite of global observation based products. In effect, the sub-daily variations in the reanalysis are used to downscale the monthly observations. These observations, which are generally available at higher spatial resolution, are concurrently used to downscale the reanalysis in space. Known biases in the reanalysis precipitation and near-surface meteorology were corrected at the monthly scale using observation-based datasets of precipitation, air temperature and radiation. Corrections were also made to the rain day statistics of the reanalysis precipitation which have been found to exhibit a spurious wave-like pattern in high-latitude wintertime. Wind-induced undercatch of solid precipitation was removed using the results from the World Meteorological Organization (WMO) Solid Precipitation Measurement Intercomparison project (Adam and Lettenmaier, 2003). Other meteorological variables (downward short- and longwave, specific humidity, surface air pressure and wind speed) were downscaled in space with account for changes in elevation. The forcing dataset is described in detail by Sheffield et al. (2006). The simulation has been validated against available observations of terrestrial hydrology (Sheffield and Wood, *Evaluation of retrospective off-line simulation of the global terrestrial water budget, 1950-2000*, in preparation) including in-situ measurements of soil moisture, large basin streamflow and remote sensing based snow datasets.

4.2.2 Analysis of soil moisture and derivation of drought index

The drought index is calculated using the method of Sheffield et al. (2004a) and is briefly described here. Simulated soil moisture data at multiple model soil

layers are aggregated over the total soil column, converted to volumetric values and averaged to monthly values. The moisture in the total soil column is used as it reflects the totality of modeled processes, including plant transpiration, soil evaporation, infiltration, runoff, baseflow and snow accumulation and melt that act at various time scales. For each model grid cell and month, beta distributions are fitted to the 51 monthly values (1 value for each year in 1950-2000) by finding distribution shape parameters that minimize the error between the statistical moments of the simulation sample and that of the fitted theoretical distribution. The current level of drought or wetness for a particular month and point in space can then be gauged relative to this fitted distribution or climatology. A detailed description of these methods is given in Sheffield et al. (2004a) and a summary is given next.

Empirical moments of soil moisture

The statistical characteristics of hydrologic variables, including soil moisture can be best described by L-moments (Stedinger et al., 1993). Hydrologic variables are generally non-Gaussian and often possess extreme values or outliers which hinder conventional statistical description. The advantage of L-moments is that they are more robust to the presence of outliers and are able to characterize a wider range of distributions (Hosking, 1990). However, autocorrelation or trends in the monthly soil moisture data will invalidate the application of L-moments that assumes the variable to be random. The areal extent of statistically significant autocorrelation (0.01 level) in the data is between 12 and 17% depending on the month with about 50% of this area in drier regions (precipitation < 0.5mm/day) and the majority of the remainder in very high latitudes. Therefore, the area that potentially invalidates the assumption of randomness is small and generally restricted to drier regions, such as the Sahara, which we ignore in the analysis. L-moments can be written in terms of linear combinations of probability-weighted moments (PWMs). For values of a random variable X_j (X_1, X_2, \dots, X_n) sorted in decreasing order, unbiased estimators for the first three PWMs are:

$$\begin{aligned} b_0 &= \bar{X} \\ b_1 &= \sum_{j=1}^{n-1} \frac{(n-j)X_j}{n(n-1)} \\ b_2 &= \sum_{j=1}^{n-2} \frac{(n-j)(n-j-1)X_j}{n(n-1)(n-2)} \end{aligned} \tag{4.1}$$

The L-moments are calculated in terms of PWMs and are defined as

$$\lambda_1 = b_0 \quad (4.2)$$

$$\lambda_2 = 2b_1 - b_0 \quad (4.3)$$

$$\lambda_3 = 6b_2 - 6b_1 + b_0 \quad (4.4)$$

The sample estimates using the L-moments are defined for the first few moments as

$$L_{mean}(\mu_s) = \lambda_1 \quad (4.5)$$

$$L_{CV}(\sigma_s/\mu_s) = \frac{\lambda_2}{\lambda_1} \quad (4.6)$$

$$L_{skew}(\gamma_s) = \frac{\lambda_3}{\lambda_2} \quad (4.7)$$

where μ , σ and γ are the mean, standard deviation and skew, respectively and subscript s indicates the sample estimates of these statistics.

Soil moisture probability distributions

To simulate the continuous variation of soil moisture, beta probability distribution functions (PDF) are fitted to the simulated monthly soil moisture values. The beta distribution can represent a wide variety of shapes and is flexible enough to account for positive and negative skew values, which is necessary given the variation in soil moisture distributions globally. A generalized form of the beta distribution, defined on limits a and b , with $a < b$, is:

$$f(\theta) = \frac{1}{B(b-a)^{t-1}}(\theta-a)^{r-1}(b-\theta)^{t-r-1}, \quad a \leq \theta \leq b \quad (4.8)$$

where θ is the volumetric soil moisture content; the distribution shape parameters, r and t are constrained by $r > 0$ and $t > 0$ and $B = \Gamma(r)\Gamma(t-r)/\Gamma(t)$, where $\Gamma()$ is the gamma function. For soil moisture, the parameters a and b represent the lower and upper limit on soil moisture, respectively, which are dependent on soil type and climate. The parameters r and t do not have any direct physical significance but determine the shape of the distribution and its moments.

The parameters a , b , r and t were estimated for each grid location and month. Parameter a (b) was estimated by assuming that the first (last) 10% of the sorted soil moisture values are linearly related to its empirical cumulative distribution function. We also investigated setting a to zero and b to soil saturation and this gave similar results for the fitted distributions. To determine r and t , once a and b were estimated, the L-moment sample statistics were equated to the corresponding beta distribution moments and a “best-fit” solution for r and t was found by minimizing the objective function:

$$error = \frac{(\mu - \mu_s)^2}{\mu_s^2} + \frac{(\sigma^2 - \sigma_s^2)^2}{(\sigma_s^2)^2} + \frac{(\gamma - \gamma_s)^2}{\gamma_s^2} \quad (4.9)$$

using the shuffled complex evolution global optimization algorithm (SCE-UA) of Duan et al. (1993).

Calculation of the drought index

Equation 4.8 was used to estimate the PDF of monthly soil moisture, for each month and grid cell. The VIC drought index is then represented by the quantile, $q(\theta)$, corresponding to a soil moisture value θ , and is determined by integrating the PDF over (a, θ) . The integral of the PDF can be approximated as follows and is used to derive spatial fields of the drought index.

$$q(\theta) = \int_a^\theta f(\theta) d\theta \approx \sum_{i=1}^{i=M} f(a + (i-1) * \Delta\theta + \Delta\theta/2) * \Delta\theta \quad (4.10)$$

where $a \leq \theta \leq b$, M is a large integer (1000 in this study), and $\Delta\theta = (\theta - a)/M$.

4.2.3 Temporal and spatial drought statistics

To characterize the spatial and temporal variation of drought, a number of statistics are developed. Firstly, a drought is defined in general terms as a period of anomalously low soil moisture. In engineering design or water resources management, the anomaly is often described in terms of the deficit below a critical or demand level. For the soil moisture drought index, this is a threshold quantile, $q_0(\theta)$. The magnitude of drought is the deficit from this threshold level:

$$M = q_0(\theta) - q(\theta) \quad (4.11)$$

In line with other drought indices (e.g. the PDSI), the level of drought can be categorized based on different arbitrary threshold values. These categories are usually referred to as moderate, severe and extreme or similar. In this study, a threshold value of 10% soil moisture quantile is used for the majority of the analysis to discern between a drought and a non-drought. The study of Sheffield et al. (2004a) and sensitivity tests of the threshold value indicate that this value satisfactorily characterizes major drought conditions globally. This value is also comparable to that used by the US National Drought Monitor (<http://drought.unl.edu/dm>) to denote “severe” drought conditions. Other analyses carried out in this study investigate the continuous variation of the soil moisture and drought magnitude as a function of the threshold value. Recognizing that the meaning and impacts of drought are regionally and sector specific, we also investigate the occurrence of short-term, severe drought and

long-term, moderate drought (Section 4.4) as characterized by different values of $q_0(\theta)$ and duration.

Following Yevjevich (1972), the occurrence of drought can be analyzed using the theory of runs, which has been applied frequently to time series of anomalous hydrologic events, most often in streamflow analysis (e.g., Peel et al., 2004). A run is defined as a consecutive sequence of D data values, in this case soil moisture values θ , below the threshold $q_0(\theta)$ that is preceded and followed by at least one value $q(\theta) > q_0(\theta)$. The cumulative deficit or severity of a run of duration D starting at time t_1 is:

$$S = \sum_{t=t_1}^{t+D-1} q_0(\theta) - q(\theta)_t \quad (4.12)$$

which may also be written as

$$S = I \times D \quad (4.13)$$

where I is the intensity or average magnitude of the run. Thus a run may be termed “severe” if the magnitude is large and/or deficits of any magnitude last for multiple months. This recognizes that the impact of drought is a subtle balance between these two related factors. It should be noted that because the drought index is defined relative to the local climatology, the magnitude of a drought at one location may be higher than at another even though the absolute soil moisture value is higher. The distribution of run durations, within the time series of soil moisture quantiles can give insight into the stochastic or deterministic nature of drought occurrence. Further it can be used to understand the frequency of droughts and the probability of future occurrence, in terms of magnitude or severity. The mean run duration is given by

$$\bar{D} = \frac{1}{N} \sum_{t=1}^N D_t \quad (4.14)$$

where N is the total number of runs in the time series. Similarly, higher order statistics can be calculated that describe the spread in the distribution of runs (variance) and the bias towards longer or shorter runs (skew).

To facilitate general comparisons, a number of run duration classes, D_c , are defined as follows:

$$D_{1-3}, \text{ very short-term} : \quad 1 \leq D \leq 3, \quad q(\theta) \leq q_0(\theta) \quad (4.15)$$

$$D_{4-6}, \text{ short-term} : \quad 4 \leq D \leq 6, \quad q(\theta) \leq q_0(\theta) \quad (4.16)$$

$$D_{7-12}, \text{ medium-term} : \quad 7 \leq D \leq 12, \quad q(\theta) \leq q_0(\theta) \quad (4.17)$$

$$D_{12+}, \text{ long-term} : \quad D > 12, \quad q(\theta) \leq q_0(\theta) \quad (4.18)$$

The total number of runs of a particular duration class can then be calculated over the time series and the frequency of occurrence over a defined period

(e.g. number of medium-term runs per 30 years) used to compare with other locations.

All the above statistics can be calculated for time series of soil moisture at a model grid cell. It is of interest to know the global variation of these statistics across climate and land cover zones and their spatial correlation structure. The latter is important for understanding how the extent of drought develops and decays over space. The spatial extent of deficits (for a particular value of $q_o(\theta)$) over a region is defined as the ratio of the area in deficit to the total area of the region:

$$A = \frac{\sum_{i=1}^{N_{grids}} A(i) = \{q(\theta) \leq q_o(\theta)\}}{\sum_{i=1}^{N_{grids}} A(i)} \quad (4.19)$$

where $A(i)$ is the area of grid cell i weighted by the cosine of the grid cell latitude and N_{grids} is the total number of grid cells in the region of interest. We are also interested in the spatial extent of contiguous drought, A_C , which is calculated using a simple clustering algorithm based on Andreadis et al., (2005). Drought clusters of less than 10 grid cells (approximately 100,000 km²) are filtered out.

4.2.4 Some caveats and uncertainties

Sheffield et al. (2004a) lists some of the potential deficiencies in the approach applied here. These include errors in the model forcing (unknown systematic biases and spurious trends), simplifications and biases in the model physics, uncertainties in the soil and vegetation parameter data, and errors in the fitted soil moisture distributions. Although some of the uncertainties will be masked by spatial and temporal averaging and the use of summary statistics, the compound effect of errors in all stages of the modeling process will inevitably lead to errors in final analysis. Furthermore, the full representation of drought variability over global scales is a difficult task given that knowledge of the variability of even basic climate variables, such as precipitation and temperature, is lacking over much of the world at any scale. However, the use of a carefully constructed forcing dataset to drive a state of the art and physically based land surface model instills confidence in the soil moisture data (and other water budget variables), which are validated where observations are available. It should also be noted that the analysis does not take into account the direct influence of anthropogenic activities on the water budget such as irrigation and the potential response to climate variability and drought in terms of vegetation dynamics and land use change.

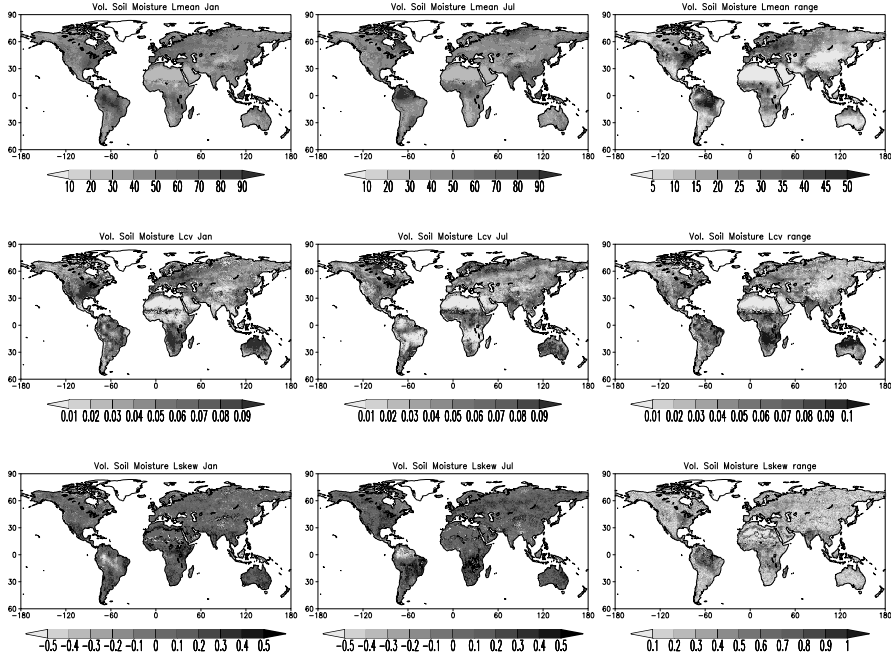


Figure 4.1: L-moment mean, variance and skew of monthly mean volumetric soil moisture for January and July. Also shown is the seasonal range for each statistic, calculated as the difference between the maximum and minimum monthly values.

4.3 Results

4.3.1 Global variation of soil moisture

The sample estimates of soil moisture statistics are derived using L-moments. Figure 4.1 shows the global variation in L_{mean} , L_{cv} and L_{skew} for January and July, and the seasonal global range for each statistic. High mean values of soil moisture occur in the Tropics and follow the seasonal undulation of the terrestrial Inter Tropical Convergence Zone (ITCZ), most notably in central Africa and in Amazonia where the mean soil moisture approaches saturation. The south-east Asian Monsoon is reflected in the soil moisture values, as is wetting up during the North American Monsoon. In mid-latitudes, soil moisture wets up in the Boreal winter and spring with extensive wetting across Europe and into Russia caused by low evaporation and melting snow pack. At higher northern latitudes, notable wet regions include near annually snow-covered regions of northern Quebec and Newfoundland in Canada and the northern parts of Ob-Yenisey basins in Siberia. Relatively low soil moisture values are spatially extensive and are found in perennially dry regions of the Sahara, the Middle East, central Asia, Australia and southern South America, among others.

The distribution of L_{cv} values is more interesting as it represents the inter-annual variability and thus gives an indication of the range in soil moisture values and the potential for higher drought frequency. Regions of high variability tend to be collocated or located near to regions of high mean soil moisture. For example, in the Amazon basin the region of high mean soil moisture is surrounded by a band of higher variability likely a result of the annually variable spatial extent of precipitation over the region. Similarly, in Africa, bands of high and low variability coincide with the central part and edges of the ITCZ seasonal footprint. The thin band of high variability over the Sahel shows the vulnerability of this region to wet and dry extremes. In the US, the high wintertime variability coincides with the region of high soil moisture in the southeast but is shifted slightly to the west.

The skewness of the distribution of soil moisture (L_{skew}) is highly variable across the world and shows seasonality as indicated in Figure 4.1. Soil moisture is bounded between wilting point and porosity, and so its distribution will typically become skewed as the mean approaches these boundaries (Western et al., 2002) with positive (negative) skew for dry (wet) soils. In general, northern mid- and high-latitudes show little or no skew in the winter but positive skew in the summer as the soil dries. The latter is indicative of the presence of a few extreme wet years that punctuate the time series, which is confirmed by inspection of individual grid cell histograms. Values tend to be higher in Tropical and sub-Tropical regions, most notably in the Amazon and central Africa, where high seasonality in precipitation forces soil moisture towards dry or wet conditions. Within the Amazon, regions of high and low variability tend to be collocated with regions of extreme skew values. For example, in January low variability is associated with negative skew and high variability with positive skew. In July, the dipole of negative and positive skew to the northeast and southwest, respectively, are some of the highest skew values globally. However these regions also have low variability indicating that the skewed monthly values are close to the mean and thus relatively unimportant. In Africa, positive skew is also associated with low variability.

4.3.2 Spatial extent of drought

The regionally averaged time series of soil moisture quantile and spatial extent of drought for $q(\theta) < 10\%$ (total and contiguous area) is illustrated in Figure 4.2. The regions are defined by Giorgi and Francisco (2000) with the addition of the northeast Canada region (NEC), and are shown in Figure 4.3 and defined in Table 4.1 in terms of area. These regions are chosen as they cover all land areas, are simple in shape, and have been used extensively in previous climate variability and change studies (e.g. Lopez et al., 2006; Kharin and Zwiers, 2005; Giorgi, 2002). Note that the time series in Figure 4.2 are smoothed to aid visualization, which will tend to diminish the extreme values. The maximum drought extent values from the original unsmoothed monthly time series are given in Table 4.1.

Globally, there is little variation in the extent of drought due to the spatial

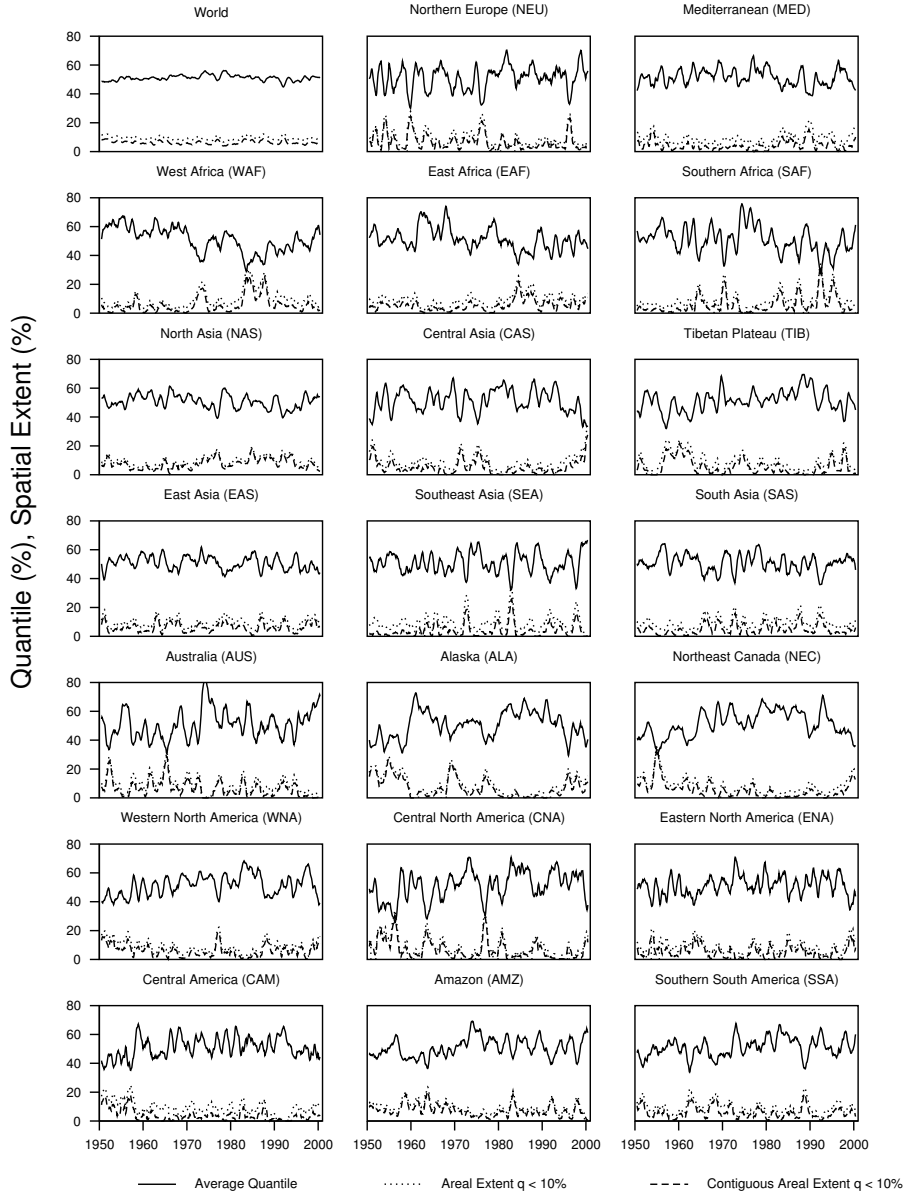


Figure 4.2: Time series of regionally averaged soil moisture quantile and areal extent of drought (total and contiguous) ($q(\theta) < 10\%$) for 1950-2000. The data are smoothed from the original monthly data with a 13-month moving average.

Region	Total Area (km ² x 10 ¹²)	A_{max} (%)	$A_{C,max}$ (%)
World	124.9	15.9	12.9
Northern Europe (NEU)	5.1	46.6	44.4
Mediterranean (MED)	6.3	38.4	36.6
Western Africa (WAF)	8.2	46.0	43.0
Eastern Africa (EAF)	8.6	32.6	28.8
Southern Africa (SAF)	6.2	50.7	49.8
Northern Asia (NAS)	14.7	26.3	24.6
Central Asia (CAS)	6.3	57.5	55.0
Tibetan Plateau (TIB)	4.7	33.3	30.1
East Asia (EAS)	8.5	34.6	31.9
Southeast Asia (SEA)	6.5	47.7	35.3
Southern Asia (SAS)	5.4	35.1	31.6
Australia (AUS)	8.6	61.9	59.8
Alaska (ALA)	3.5	40.5	36.8
Northeastern Canada (NEC)	4.5	42.9	41.1
Western North America (WNA)	5.6	39.7	38.9
Central North America (CNA)	3.4	74.7	74.4
Eastern North America (ENA)	2.7	53.5	52.3
Central America (CAM)	3.0	42.9	39.9
Amazon (AMZ)	12.9	48.2	46.2
Southern South America (SSA)	5.9	35.2	31.6

Table 4.1: List of regions used in this study, including their total area and maximum spatial extent of drought, A ($q_0(\theta) = 10.0\%$). The regions are taken from Giorgi and Francisco (2000) but exclude the Greenland region which has been replaced by the northeastern Canada (NEC) region.

averaging, with slightly less extensive drought in the 1970s. NEU shows higher variability than MED and dry conditions in NEU are at a maximum in the 1950s and the mid 1990s. WAF is dominated by the long-term drought period in the Sahel from the late 1960's to mid 1980's, also reflected but to a lesser extent in EAF. In SAF, there are a number of peaks that cover up to 40% of the region and a particularly extensive wet period in the 1970s. The size of the NAS region tends to dampen the variation in soil moisture and spatial extent although an underlying decadal variability is apparent. Spatially extensive drought conditions in the late 1950s to early 1960s over TIB are followed by increasingly wet conditions until the 1990s. SEA has experienced several periods of large drought extent in the early 1970s and 1980s. The AUS data are dominated by an extensive dry period in the 1950s and 1960s followed by an upward jump in soil moisture around 1973, also seen in the precipitation data. The extent of drought in WNA is relatively uniform but there is greater variability in CNA and a number of events that surpass 60% coverage. The data

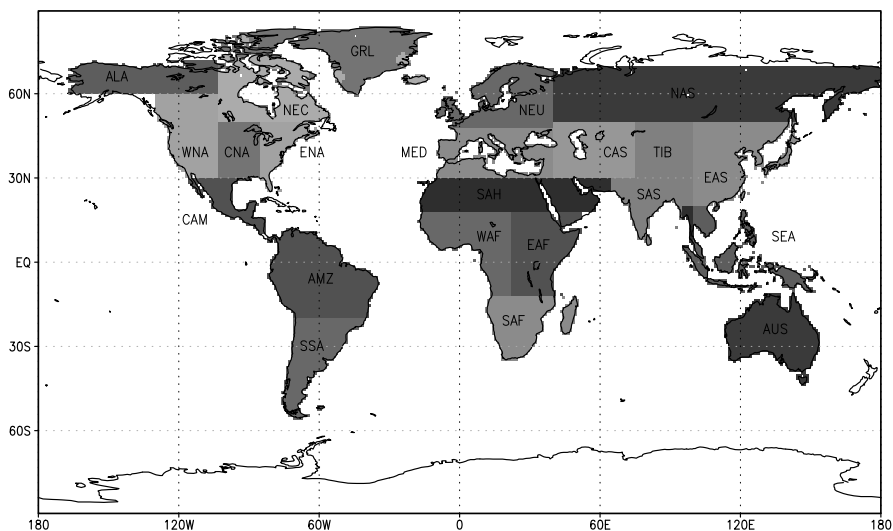


Figure 4.3: Map of regions used in the analysis as defined by Giorgi and Francisco (2000). The original GRL region is split into northeastern Canada (NEC) and Greenland for this study.

for the Amazon region are damped by the large area but show peak extents in the 1960s, 1980s and 1990s.

4.3.3 Run frequency and duration

The global distribution of frequencies of different duration runs ($q_o(\theta) = 10\%$) for 1950-2000 is shown in Figure 4.4. Very short-term runs (D_{1-3}) are most frequent in the eastern US, parts of the western Amazon, Argentina, Tropical Africa and southeast Asia with over 30 runs per 50 years. The highest frequencies of short-term runs (D_{4-6}) show much greater spatial variability and are generally located in mid-latitudes and parts of the Tropics. Medium term droughts (D_{7-12}) are at a maximum in high latitudes, especially northern Canada and eastern Siberia. These regions are characterized by freezing temperatures and thus are prone to persistent anomalies over the cold season. Long-term runs (D_{12+}) are restricted to a few areas including higher northern latitudes, central Asia and the Sahel and are notably absent in the Tropics.

The geographic variation of run duration can be characterized by a summary statistic such as the mean, median or higher moment. Figure 4.5 shows the total number of runs of any duration and the statistics (mean, standard deviation and skew) of run durations calculated using $q_o(\theta) = 10\%$. Note that the total time in deficit is equivalent to the total number of runs multiplied by the mean run length, with an expected value of 10% as defined by the threshold value. The total number of runs is minimal in dry regions. The highest values (> 25

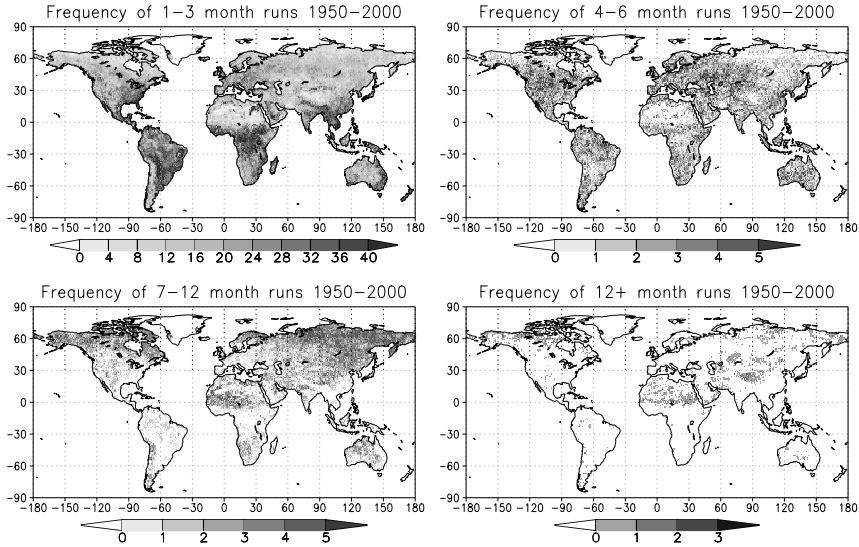


Figure 4.4: Frequency of occurrence of very short (D_{1-3}), short (D_{4-6}), medium (D_{7-12}), and long-term (D_{12+}) runs ($q_0(\theta) = 10\%$) for 1950-2000. The units are the number of runs over the whole time period.

runs) occur in more humid regions such as eastern North America, the Amazon and Paraná River basins, Tropical Africa, Europe and southeast Asia. The Sahel, scattered regions across central Asia and high northern latitudes stand out as having high mean run lengths, a result of the high frequency of long-term drought conditions. Regions of higher mean durations are generally collocated with regions of higher variability (standard deviation). Tropical latitudes tend to have the lowest standard deviations. The skew values are generally positive, indicating that the frequency of long duration runs is low.

4.3.4 Run intensity and severity

Figure 4.6 shows the distribution of run intensity and severity as calculated by equations 4.11 and 4.12. The data were calculated for a threshold value $q_0(\theta) = 50\%$ to capture the statistics of all events, but the results using other threshold values show similar patterns but different amplitudes. Mean run intensity, I_{mean} , is $\sim 15 - 25\%$ (departure below the threshold) for humid regions and $5 - 15\%$ for drier regions, explained by the greater frequency of short (long) term

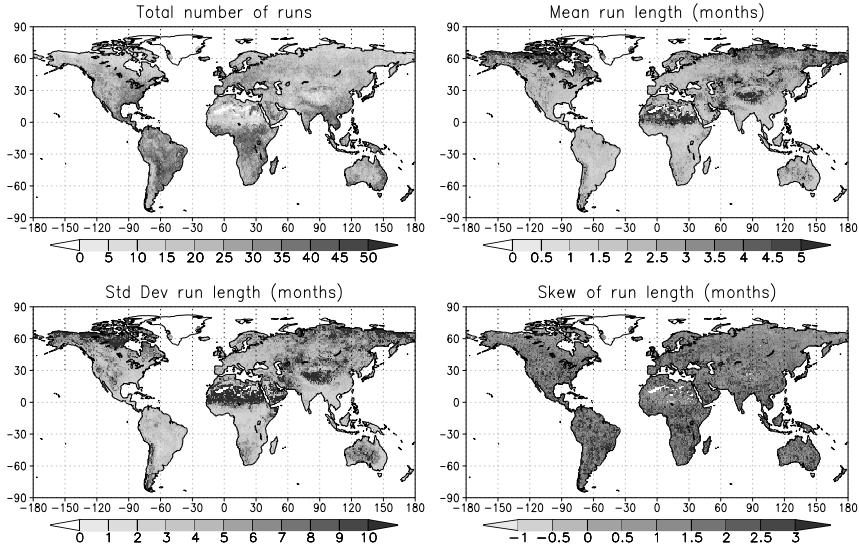


Figure 4.5: Global variation of a) total number of runs, and b) mean, b) standard deviation and c) skew of the distribution of run durations for $q_0(\theta) = 10\%$.

droughts in more humid (dry) regions. The eastern United States, central and eastern Europe, Southeast Asia, China and Tropical Africa exhibit the largest I_{mean} values. The pattern for maximum run intensity, I_{max} , is similar in terms of the general distribution of high and low values. The majority of values are clustered within the range 33 - 50%, with only the drier regions dropping below about 30%. For mean run severity, S_{mean} , the variation is much more distinct and several regions stand out as having experienced relatively severe conditions, driven more by long durations than by high intensities. S_{mean} is greater than 200% (cumulative departure below the threshold) over the Sahel, northern Canada, northern Siberia and the Taklamakan desert north of the Himalayas, with S_{mean} exceeding 500% for parts of the Sahel. Over much of the Tropics, $S_{max} < 400\%$, although in the northern half of Amazonia, $S_{max} \approx 800\%$. In the majority of regions elsewhere $S_{max} \approx 400 - 1200\%$. The regions of highest S_{mean} also have the highest S_{max} . In the Sahel, $S_{max} \approx 1000$ and reaches 4000% in parts.

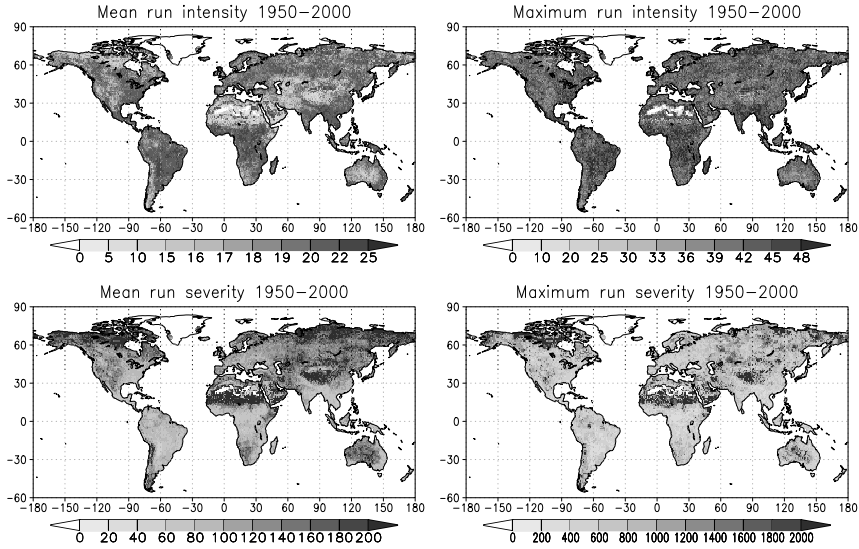


Figure 4.6: Global variation of statistics of run intensity and severity for $q_0(\theta) = 50\%$: a) mean and b) maximum run intensity; c) mean and d) maximum run severity.

4.3.5 Relationship between run duration and intensity

The relationship between D and I and thus the distribution of S is explored further in Figure 4.7 for three example regions, WNA, WAF and SAS. Neighboring regions show similar behavior. The figure shows scatter plots of coincident values of D and I for various values of $q_0(\theta)$. By definition, I cannot exceed the threshold value (i.e. $I \leq q_0(\theta)$) and this then forms an upper bound on the cloud of points. All plots show a wide range of values of I for short duration runs ($\sim D \leq 10$), but as D increases, I converges to approximately 50-75% of $q_0(\theta)$, most notably for WNA and for higher $q_0(\theta)$ values, for which runs are more numerous and longer durations ($D > 30$ months) are more probable. At lower thresholds ($q_0(\theta) = 10.0\%$), such a relationship may be equally valid, at least empirically, but is less tractable because of the smaller sample size.

For WAF, some very different behavior is apparent, in addition to the larger range in duration. Firstly, there is a clustering of points at regular intervals of duration, most notable for higher threshold values. The interval is approximately 12 months and is a result of the strong seasonal cycle in precipitation over this region. The seasonality ensures that long-term deficit conditions ($D >$

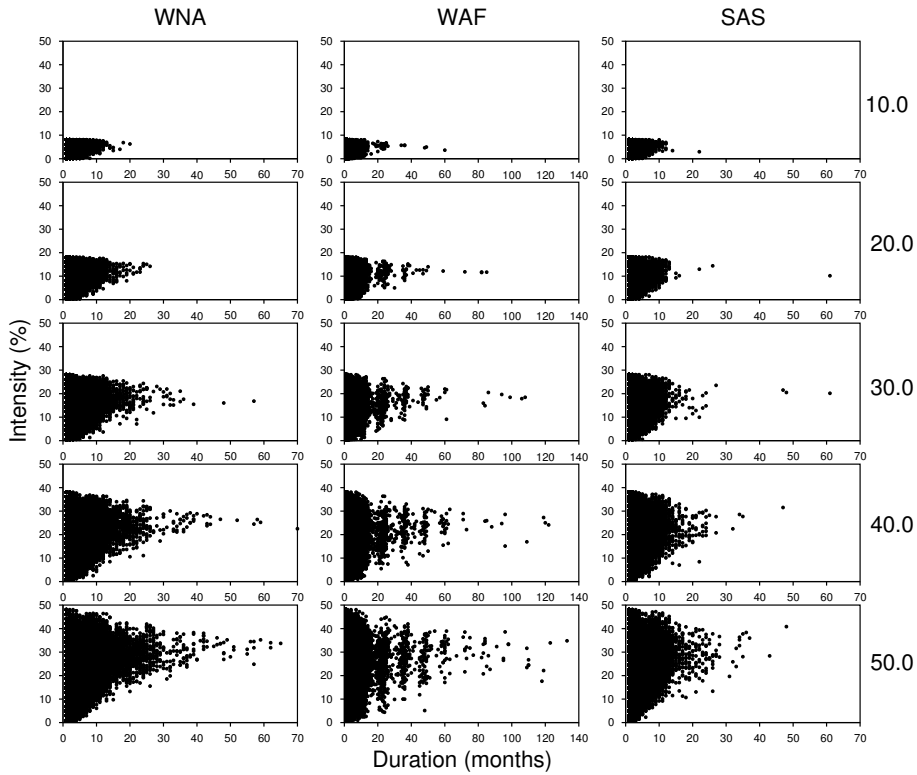


Figure 4.7: Run duration versus run intensity for the WNA, WAF and SAS regions. Each row corresponds to a different threshold value, $q_0(\theta)$, as indicated by the number to the far right. Each point represents a single run for a pixel. Note the extended x-axis for the WAF plot because of the existence of longer duration runs.

12) can be extended until at least the next rainy season as this is the only time of the year that the deficit can be dissipated. Secondly, the convergence to a small range of I at higher values of D is not as obvious for the WAF data. In fact there is considerable variability in I at high D , especially at higher $q_o(\theta)$ values. The reasons for this are unclear, although the greater number of long runs over WAF will tend to increase the variability in I .

4.4 Discussion

4.4.1 Comparison with the PDSI

The PDSI has been extensively analyzed and applied in research studies (e.g. Dai et al., 2004, Van der Schrier et al., 2006a,b) and is arguably the most prevalent drought index in operational use. It is a proxy for soil moisture

that correlates well with soil moisture and streamflow observations (Dai et al., 2004), but has been criticized for its hydrologic simplicity and lack of spatial consistency (Alley, 1984). In this section we compare the soil moisture index with a PDSI dataset driven by the same precipitation and temperature forcings and the PDSI dataset of Dai et al. (2004). To calculate the PDSI we use the self-calibrating algorithm of Wells et al. (2004) that removes the spatial inconsistency. At global scales the soil moisture index correlates well with both PDSI datasets (Figure 4.8) and all show decreasing tendencies since the mid-1970s. The soil moisture index shows greater month to month variability compared to the PDSI datasets. This has been attributed, in part, to the PDSI ignoring the daily variation of precipitation and the effects of snowmelt, and the use of time invariant vegetative cover, which will tend to dampen the index over seasonal scales (Sheffield et al., 2004a). At the grid scale, the datasets are generally well correlated but tend to diverge in cooler seasons and high latitudes and substantially so in dry regions (Figure 4.9), which is consistent with Sheffield et al., (2004a) who analyzed a similar soil moisture dataset generated at high resolution over the contiguous USA.

4.4.2 Identification of severe drought events

Figure 4.2 gives a general overview of the monthly spatial extent of drought on a regional basis but does not take into account the severity (combined intensity and duration) which are relevant for evaluating the impacts. Figure 4.10 shows regional time series of the spatial extent of drought in a similar manner to Figure 4.2, but filtered for high severity to reveal drought events that were either of long duration or high intensity. The filtering is applied at two scales: using a moving window of 3 month duration and 10% threshold ($D = 3$, $q_0(\theta) = 10.0\%$; short duration, high intensity droughts) and using a 12 month duration and 50% threshold ($D = 12$, $q_0(\theta) = 50.0\%$; long duration, low intensity droughts). The filtering process leaves only the severe events and could have been implemented in any number of ways using different combinations of duration and intensity. Nevertheless, Figure 4.10 reveals those events that are both severe and spatially extensive as derived from this dataset. In the following discussion, short duration, high intensity events are referred to as short-term. Long duration, low intensity events are referred to as long term. It should be noted that the spatial extent calculated here is not necessarily contiguous and this is more likely the case for larger regions as drought can occur in multiple disconnected locations at the same time.

Over North America, the 1950s were the decade of most spatially extensive and prolonged drought in the west and central regions, as expected, and would only be surpassed by the 1930s drought during this century (Andreadis and Lettenmaier, 2006). In terms of individual years, the winter drought of 1976/77 was considerably more extensive than the drought of 1988 that was purported to be the worst natural disaster in US history (Trenberth and Branstator, 1992).

The most extensive droughts in CAM occurred in the 1950s, which is consistent with reported conditions (Liverman, 1999) and with gauge based pre-

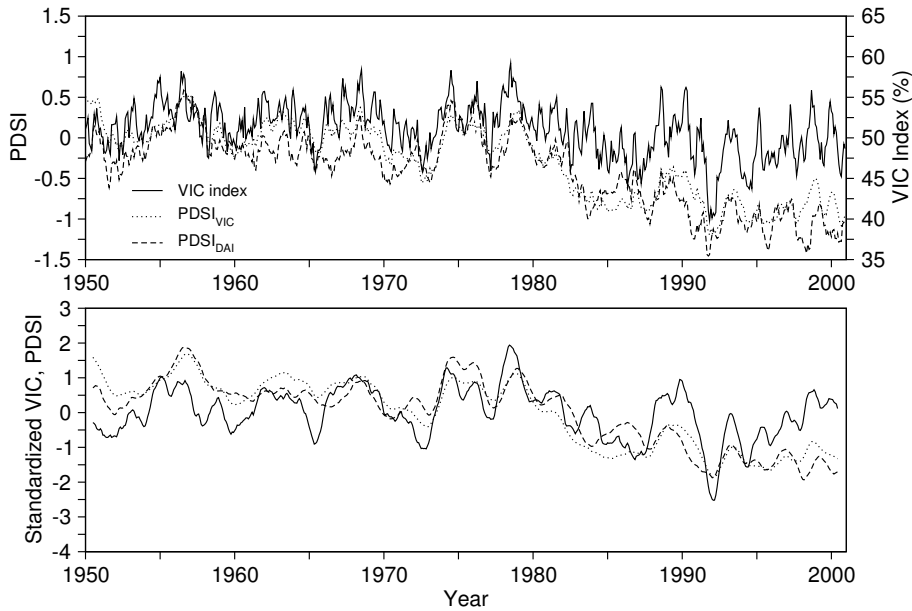


Figure 4.8: Time series of globally averaged VIC soil moisture index and two PDSI datasets for 1950-2000. The data are averaged over global land areas excluding Greenland and Antarctica. Bottom panel shows the data after standardization (subtract the mean and divide by the standard deviation) and filtering using a 13-month running mean. The $PDSI_{VIC}$ dataset is calculated using the self-calibrating algorithm of Wells et al. (2004) forced by the same precipitation and temperature data as the VIC soil moisture index. The $PDSI_{DAI}$ dataset is from the study of Dai et al. (2004).

precipitation records that show an increasing trend since the early 1960s (Aguilar et al., 2005). In the Amazon, maximum extent coincides quite satisfactorily with El Nino events, including 1957/8, 1972/3, 1992 and 1997, which are associated with dry and warm conditions, especially in the northern part of the region (Foley et al., 2002). In southern South America, 1962 and 1988 stand out as years of spatially extensive long term drought. These years coincide with La Nina events which are known to cause dry conditions in the east of this region (Boulanger et al., 2005), although curiously other La Nina events are not reflected in the drought record which requires further investigation.

The series for NAS is interesting for two reasons. Firstly, the extent of severe drought is much greater since the mid-1970s for short term droughts, possibly a result, in part, of the switch to a positive NAO phase (Visbeck et al., 2001). Secondly, the peaks tend to occur at regular intervals. Closer inspection of the data shows that these occur in the autumn and winter. As the soil column freezes, the soil moisture at any location tends to remain fairly constant over

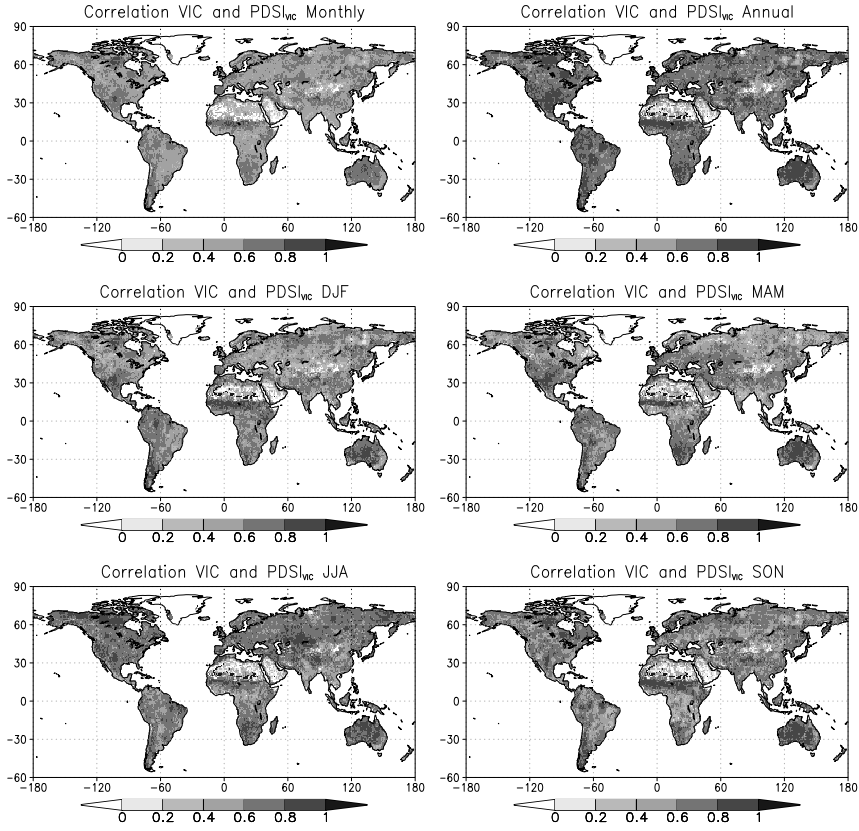


Figure 4.9: Correlation between the VIC soil moisture index and the PDSI_{VIC} dataset at monthly, annual and seasonal time scales.

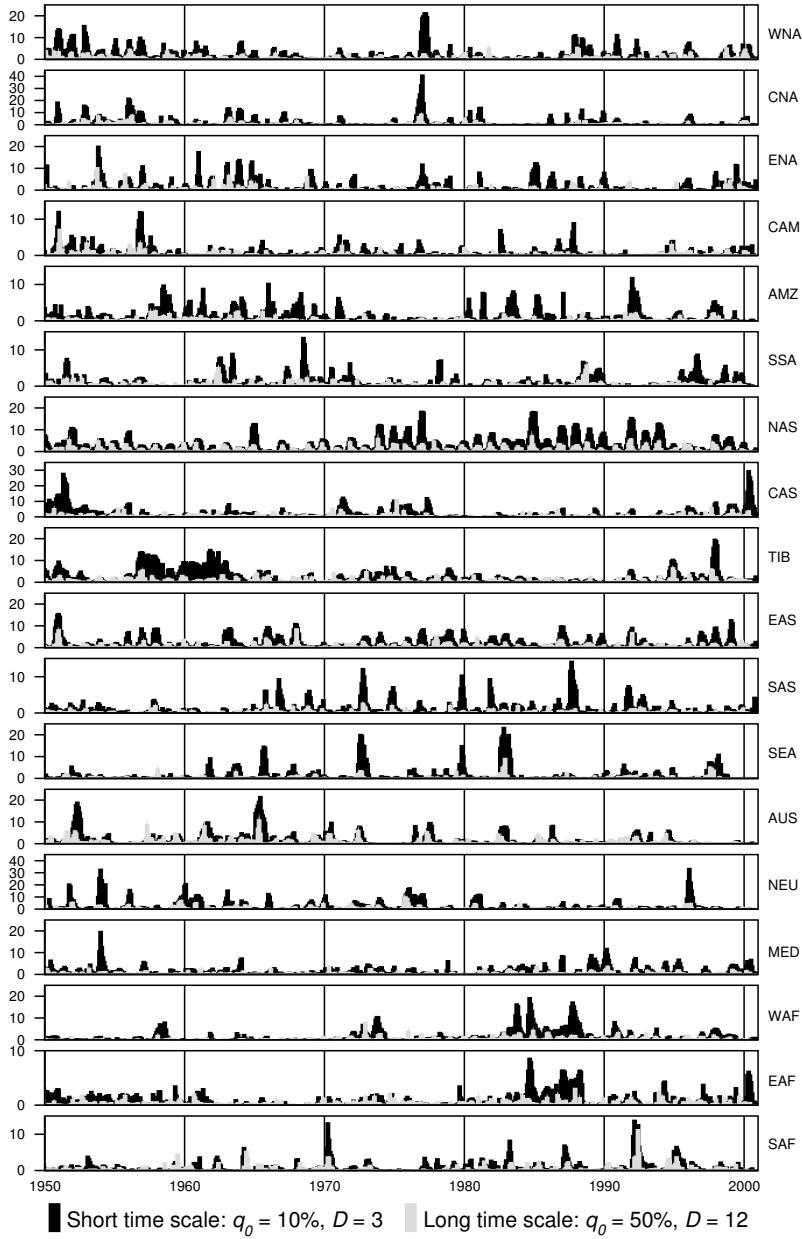


Figure 4.10: Time series of regional spatial extent of short (black bars) and long time scale (red bars) drought events. Short time scale droughts are defined as soil moisture quantile $q(\theta) < 10\%$ over a 3 month moving window $q_0(\theta) = 10.0, D = 3$. Long time scale droughts are defined as soil moisture quantile $q(\theta) < 50\%$ over a 12 month moving window $q_0(\theta) = 50.0, D = 12$. Note that the y-axis scales differ between regions.

the winter period, which will tend to prolong any preceding drought conditions. CAS shows major events in the early 1950s and at the end of the record, the latter analyzed by Barlow et al. (2002), with a spate of less extensive events in the 1970s. For TIB, the series of short-term drought is dominated by a prolonged event during the late 1950s to early 1960s, although peak spatial extent occurs in 1997 (short term) and 1994 (long term). In EAS, which covers most of eastern China and Japan, spatially extensive severe drought is limited at the short term but peak coverage for long term drought is evident in 1951, 1968 and 1992.

SAS shows a few major events which tend to occur in the middle part of the period. In SEA there are distinct major events in 1972, 1982/3, and 1997 at both time scales (short and long term) that coincide with major El Nino episodes. For AUS, drought events are more extensive in the earlier part of the period most notably in 1952 and 1965 for short term droughts and multiple years in the 1950s and 1960s for long term droughts, which may be due to changes in the influence on ENSO on Australian climate since the 1970s (Nicholls et al., 1996).

For Europe, NEU has far more spatially extensive droughts than the MED region. Spatially extensive short term droughts in NEU occur in 1954 and 1996. Other drought events, such as that in 1975/6, are less extensive but span multiple 3-month periods, and 1975 is the most extensive long term drought. 1954 is the most extensive short term drought year in the MED region, yet this stands alone in the first half of the period and drought appears to be much more extensive in the second half for both time scales, especially in the late 1980s and 1990s. This is generally consistent with Lloyd-Hughes and Saunders (2002) and van der Schrier et al. (2006b) who found that the 1950s and 1990s were the most drought prone periods across the whole of Europe in terms of PDSI and 3 and 12 month SPI.

WAF is dominated by prolonged drought in the 1970s and 1980s (Hulme, 1992; L'Hôte et al., 2002) that reached peak extent in 1984 and 1972. This is reflected in EAF but the spatial coverage is considerably lower. In SAF, peak events occur in 1970 and 1992 for short term drought and 1992 for long term drought which corresponds well with the SPI analysis of Rouault and Richard (2005) who determined that the majority of major drought events were coincident with El Nino episodes.

4.4.3 Analysis of selected major drought events

Several major drought events are selected for further analysis. These are chosen because of their documented socio-economic impacts and the large number of studies carried out into their origins and dynamics. We are interested in whether the hydrologic conditions, as represented by the soil moisture index, are good indicators of such events and how this compares with the PDSI. Other major droughts have been identified in the previous section but may not have impacted as greatly because of a sparse population or low agricultural activity, or may be less well reported. Snapshots of the spatial distribution of

soil moisture quantiles for four selected major historic regional drought events are shown in Figure 4.11: USA, 1988; the Sahel, 1983-84; India, 1965-66; and Australia, 1982-83. These four droughts are put in the context of the statistical analysis presented in Section 4.2 by determining the regional extent of drought for $q_0(\theta) = 10.0\%$ and the mean regional intensity and duration for $q_0(\theta) = 50.0\%$ on a seasonal basis. We compare this with the other years in the record and the results from the two PDSI datasets in Figure 4.12. The maximum values and years in which they occur are summarized in Table 4.2.

	VIC index	PDSI _{VIC}	PDSI _{DAI}
CNA			
A_{max} (%)	74.7 (1952)	70.4 (1956)	58.9 (1956)
A_{max} (%), JJA	36.7 (1988)	63.6 (1956)	50.5 (1956)
S_{max} (mo %), JJA	43.5 (1988)		
Sahel			
A_{max} (%)	68.8 (1984)	86.0 (1984)	92.0 (1984)
A_{max} (%), MJJASO	38.9 (1984)	69.5 (1984)	74.2 (1984)
S_{max} (mo %), MJJASO	70.8 (1986)		
India			
A_{max} (%)	46.7 (1987)	48.2 (1988)	55.1 (1966)
A_{max} (%), JJASON	37.1 (1987)	35.6 (1987)	48.2 (1966)
S_{max} (mo %), JJASON	78.4 (1987)		
East Australia			
A_{max} (%)	64.5 (1965)	77.1 (1983)	86.4 (1983)
A_{max} (%), SONDJF	46.7 (1982/3)	50.3 (1982/3)	59.0 (1982/3)
S_{max} (mo %), SONDJF	86.6 (1994)		

Table 4.2: Year and value of maximum regional drought extent, A_{max} , and severity, S_{max} , on a monthly and seasonal basis for four example regions as derived from the VIC soil moisture index and two PDSI datasets. The first value is the extent or severity. The value in parentheses is the year in which the maximum occurred.

USA 1988

The drought of 1988 over the central United States is estimated to have cost \$30 billion in agricultural losses alone and has been considered to be the worst natural disaster in U.S. history (Trenberth and Branstator, 1992). It is generally agreed that a combination of sea surface temperature (SST) anomalies, persistent stationary atmospheric circulation anomalies and soil moisture-precipitation feedbacks were key factors in the development and longevity of

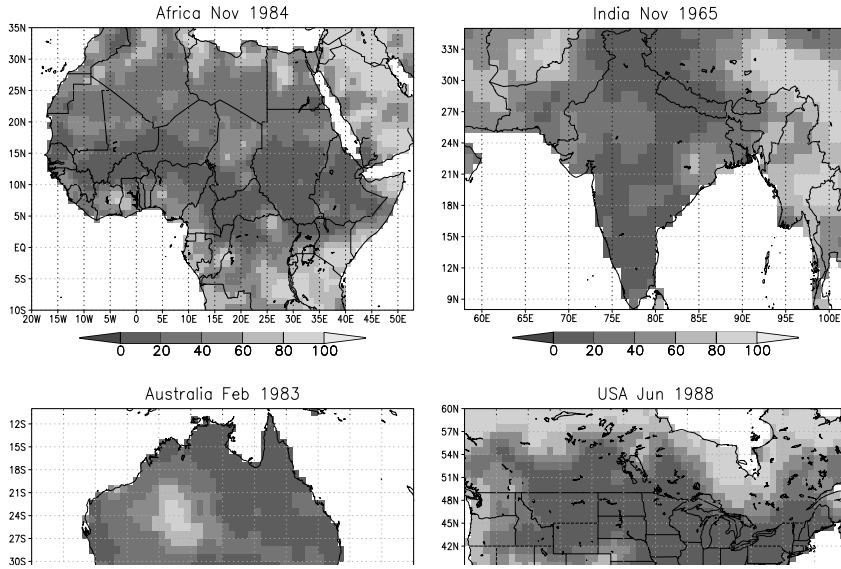


Figure 4.11: Examples of monthly soil moisture quantiles for four major regional droughts: a) the Sahel, 1983-84; b) northeast India, 1965-1966; c) Australia, 1983; d) USA, 1988.

the drought (Sud et al., 2003). Drought conditions, as derived from the soil moisture data, developed through the spring and summer of 1988, reaching a peak spatial extent in June 1988 (65.5% at $q_0(\theta) = 10.0\%$, region CNA) that was only exceeded by conditions in October 1952 (74.7%). In the context of the full time period (Figure 4.12), 1988 is ranked 1st, in terms of summer (JJA) drought extent, with 1980 and years of the early to mid 1950s ranked next. In terms of regional severity, defined as the regional intensity multiplied by the regional duration, 1988 is ranked 2nd with 1980 being the exceptional year by this definition. 1977 is ranked highly in annual terms, but dry conditions were manifested in the winter months (peak extent in January 1977 of 59.9%). The PDSI datasets exhibit similar spatial extent to the VIC index for 1988, but show 1956 to have a much greater spatial extent, also found by Van der Schrier et al. (2006a) (see their Figure 4.6).

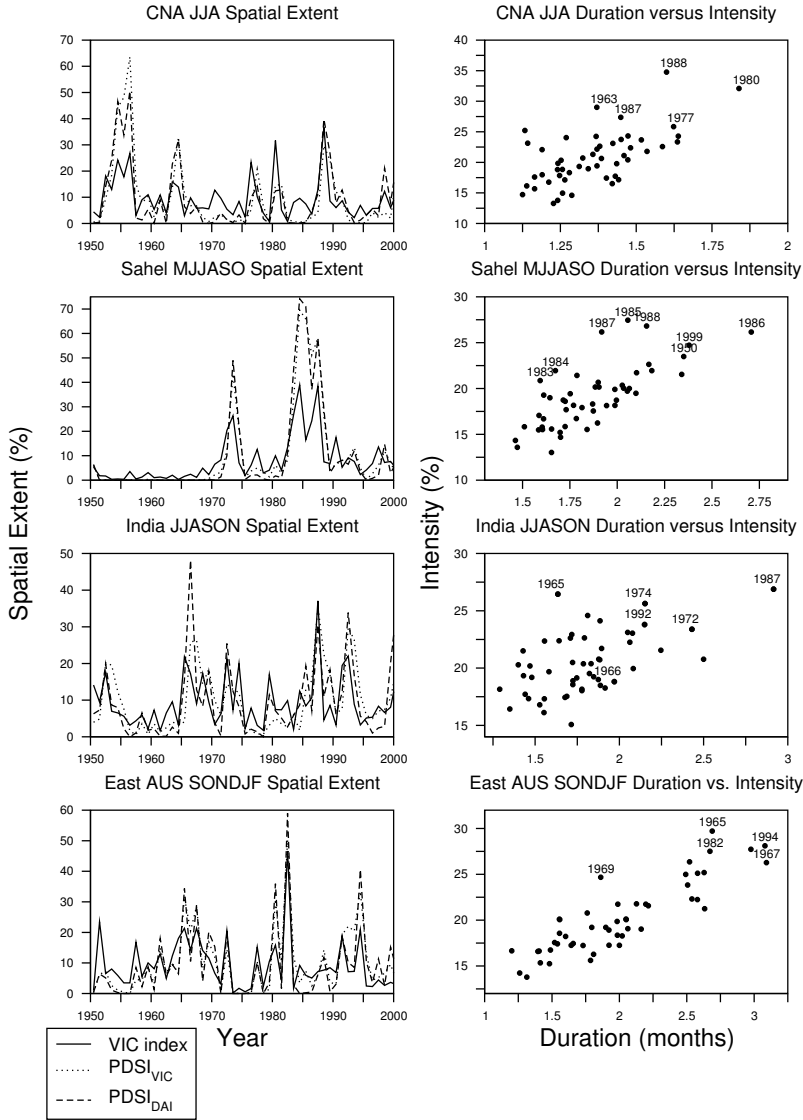


Figure 4.12: Regional time series of spatial extent of drought and scatter plots of average run duration versus intensity for the CNA, Sahel, India and east AUS regions. The spatial extent data calculated for $q_0(\theta) = 10\%$ and are shown for the VIC index, PDSI_{VIC} and PDSI_{DAI} datasets. The PDSI datasets are first transformed into quantile space. Each point in the scatter plots represents the average duration and intensity of runs for within each season averaged over all grid cells within the region. Selected historic drought event years are highlighted.

Sahel 1983-84

Long-term drought conditions in the Sahel region of Africa during the 1970s and 1980s had devastating social and environmental consequences (Mortimore and Adams, 2001; Tarhule and Lamb, 2003). Decreasing precipitation trends over the region have been well documented (Hulme, 1992; L'Hôte et al., 2002) but the forcing mechanisms have been the subject of debate. Previously, it was thought that overuse, in the form of overgrazing, deforestation and poor land management, was responsible. However, recent studies have shown that a combination of land-atmosphere interactions (Nicholson, 2000), ocean temperatures (Giannini et al., 2003) and anthropogenic forcing (Held et al., 2005) are likely causes. From the soil moisture data, the highest monthly spatial extent of drought over the Sahel region (10-20N, 20W-20E) occurred during September 1984 (68.7%). For the growing season average (May-October), 1984 also has the highest spatial extent (38.9%) closely followed by 1987 (38.5%). The PDSI spatial extent values are similarly ranked, although they are much higher (69.5 - 74.2%). The scatter plot of duration versus intensity (Figure 4.12) shows that 1983 was by far the severest drought year, with 1984 ranked 6th and showing particularly high intensities but relatively lower durations. For the encompassing WAF region, the maximum extent of drought conditions occurred during October 1983 (46.0%) and 18 out of the top 20 ranked months of spatial extent occurred in the 1980s.

India 1965-6

India has experienced a multitude of severe droughts over the last century, which are generally forced by inter annual variability in the Indian monsoon during June to September (Krishnamurthy and Shukla, 2000). In the last 50 years, the droughts of 1965/66, 1972 and 1987 have been the most widespread and damaging (OFDA/CRED, 2006). Conditions in 1965-66 were particularly devastating because of two consecutive years of drought. The soil moisture data reveal that the maximum monthly spatial extent of drought over India at $q_0(\theta) = 10.0\%$ was 35.3% in November 1965, although 1987 had five months with higher values up to 46.7%. The PDSI datasets are generally in agreement but show slightly larger values. Notably the PDSI_{DAI} dataset ranks the 1965 event highest, which may be due, in part, to the coarser spatial resolution and different source for the forcings. Figure 4.12 shows that, in terms of regional severity, 1965 and 1966 are not ranked highly within the full time period. However, this does not take into account multi-year droughts that spanned 1965-66 and it is conceivable that the overall impacts were compounded by consecutive years of severe drought conditions.

Australia 1982-3

Australia has experienced multiple drought events over the 20th century that are generally forced by variability at inter-annual and inter-decadal scales associated with El Nino (Chiew et al., 1998) and modified by Pacific inter-decadal

variability (Power et al., 1999). The strong El Nino of 1982/83 forced drought conditions that affected much of Australia during this time. Figure 4.11 shows a map of soil moisture quantiles in February 1983 indicating severe drought conditions in eastern Australia, the culmination of record low precipitation from July 1982 to February 1983. Drought conditions ($q_0(\theta) = 10.0\%$) covered more than 45% of the east AUS region on average from September 1982 to February 1983, with the maximum spatial extent of 62.1% during February 1983. Mean regional drought duration during the 1982/83 warm season (SONDJF) was 2.7 months and mean intensity was 27.5% and is ranked highly relative to the whole period. In terms of spatial extent, 1982/83 is easily the highest ranked year according to the VIC index and both PDSI datasets. Like other regions, the PDSI datasets tend to give larger values of spatial extent.

4.5 Summary and conclusions

A monthly soil moisture based drought index is developed for global terrestrial areas, excluding Greenland and Antarctica, from an off-line land surface model simulation forced by an observation based meteorological dataset. The index is used to investigate the occurrence and variability of drought globally over 1950-2000. Drought is described in terms of duration, intensity and severity, and various statistics that summarize their distributions in time and space. These variables are analyzed spatially, at global and regional scales, and temporally with respect to severity and spatial coverage. The inter-dependence of these correlated variables is also explored along with the sensitivity to the threshold soil moisture value that defines drought.

An analysis of the statistics of drought events reveals considerable global variability and some interesting relationships between drought characteristics. Based on a soil moisture quantile threshold of $q_o(\theta) = 10\%$, the frequencies of short-term droughts (6 months and less) and droughts of any length are highest in humid regions. Medium term droughts (6-12 months) are more prevalent in mid- to high-latitudes, which for the latter is a result in part of freezing temperatures causing static soil moisture conditions and forcing drought conditions to persist through the wintertime. Over the Sahel and parts of high northern latitudes, the frequency of long-term droughts is at a maximum.

Drought intensity is defined as the mean departure below the threshold soil moisture quantile over the drought duration and tends to be higher over humid regions. This is likely a result of the higher inter annual variability in soil moisture that tends to prevail in humid regions, even if the range in soil moisture is small in absolute terms. Drought severity, calculated as intensity times duration, tends to be lowest in more humid regions and is highest in regions of high mean duration, such that drought duration is a more dominant factor in severity for longer duration droughts. The Sahel region stands out globally for having long-term and severe drought conditions.

The relationship between duration and intensity, and thus the distribution

of severity, is of particular interest as this governs the impacts of drought. A more detailed analysis of the joint and conditional distributions of duration, intensity and severity (e.g. Kim et al., 2003) would be required to quantify the relationship between these highly correlated drought attributes, but some general remarks can be made nevertheless. The data shows that for some regions, the drought intensities will tend to converge to a small range of values at higher duration. This is consistent with the possibility that drought duration dominates severity at longer durations, as discussed previously. Elsewhere, strong seasonality in a region's climate may result in a wider spread of intensity values and cluster the distribution of long-term drought durations into annual and multi-annual lengths.

Severe drought events are systematically identified in terms of spatial coverage for various regions based on different thresholds of duration and intensity that relate to either high intensity, short duration droughts or low intensity, long duration droughts. For example, in northern Europe 1975 was the year of most spatially extensive drought at annual time scale and 1996 was the equivalent year at 3-month time scale. In northern Asia, severe drought events at short and long time scales are characterized by persistent soil moisture anomalies over the wintertime. Droughts in western and eastern Africa are dominated by events in the Sahel.

The drought index identifies several well-known drought events, including the 1988 USA, 1982/83 Australian, 1983/4 Sahel and 1965/66 Indian droughts, which are analyzed in more depth. These are generally ranked as the severest events in the record, although some are ranked relatively low and the severity of their reported impacts is likely compounded by socio-economic and other factors. Comparison of the results with those from two PDSI datasets shows general agreement, although the PDSI tends to give larger spatial extent values. Some events, however, (e.g. 1988 CNA and 1965 India) are ranked somewhat differently by each dataset that may be due to differences in scale and forcings, but is also likely a result of fundamental differences in the modeling approach between the VIC index and the PDSI. At global scales the VIC index and the PDSI are reasonably well correlated but this breaks down in cooler regions and seasons, and especially in the latter half of the 20th century, when the PDSI shows a larger drying trend. Given these comparisons, the known deficiencies and simplifications in the PDSI and the history of evaluations of the VIC model, we conclude that the VIC index is a good indicator of major drought events that is applicable to a wider range of climate regimes than the PDSI.

The overall analysis is inevitably subject to errors in the representation of the actual variation in soil moisture and drought occurrence, which are listed in Section 4.2.3 and Sheffield et al. (2004a). However, the soil moisture based index can provide a useful indicator of drought given its physical basis and consistent global coverage. The utility of a drought index is nevertheless, measured by how well it describes the development and recession of drought and whether this information can be used to monitor and react to drought. As the impacts of a certain magnitude and duration of soil moisture deficit are particular to the region, time of year and sector it is impossible to specify

whether drought is occurring as a simple yes or no. Rather it is more useful to present the actual deficit and duration and let the user decide the implications of this.

This dataset forms a climatology that provides a useful benchmark against which current and potential future changes in drought can be assessed. An increase in the number of droughts and/or drought severity is a possible outcome of future global warming and intensification of the water cycle (Wetherald and Manabe, 1999). Predicted temperature rise will lead to increased evaporation and thus reduced soil moisture, yet accompanying changes in precipitation, in terms of totals and statistics, may act to increase or decrease drought occurrence. Projections of precipitation changes are highly scenario and model dependent (Covey et al., 2003) and regional variability (Giorgi and Bi, 2005) compounds the uncertainty in future changes in drought regime. Recent increases in global temperatures may already have acted to change the global drought regime (Dai et al. 2004). An analysis of changes and trends in various drought statistics over the second half of the 20th century using this dataset is work in progress that will also examine the processes that force and modulate the temporal and spatial variation of drought at large scales.

Acknowledgements

This work has been supported by NOAA grants NA86GP0248 and NA0303AR4310001, NASA grant NAG5-9486 and DOE grant 983338. The VIC soil moisture data will be made available from <http://hydrology.princeton.edu> along with other water and energy balance variables from the 50-yr global simulations. We thank the three anonymous reviewers for their comments and suggestions that helped to improve the manuscript.

Chapter 5

Trends and variability in 20th century global drought

This chapter is a slightly modified version of: Sheffield, J., and E. F. Wood, Global trends and variability in soil moisture and drought characteristics, 1950-2000, from observation driven simulations of the terrestrial hydrologic cycle. J. Climate, in press.

Abstract

Global and regional trends in drought for 1950-2000 are analyzed using a soil moisture based drought index over global terrestrial areas, excluding Greenland and Antarctica. The soil moisture fields are derived from a simulation of the terrestrial hydrologic cycle driven by a hybrid reanalysis-observation forcing dataset. Drought is described in terms of various statistics that summarize drought duration, intensity and severity. There is an overall small wetting trend in global soil moisture, forced by increasing precipitation, which is weighted by positive soil moisture trends over the western hemisphere and especially in North America. Regional variation is nevertheless apparent and significant drying over West Africa, as driven by decreasing Sahel precipitation, stands out. Elsewhere, Europe appears to have not experienced significant changes in soil moisture, a trait shared by southeast and southern Asia. Trends in drought duration, intensity and severity are predominantly decreasing but statistically significant changes are limited in areal extent, of the order of 1.0 – 7.0% globally, depending on the variable and drought threshold and being generally less than 10% of continental areas. Concurrent changes in drought spatial extent are evident, with a global decreasing trend of between -0.021 and -0.035% yr^{-1} . Regionally, drought spatial extent over Africa has increased and is dominated by large increases over West Africa. Northern and East Asia show positive trends and central Asia and the Tibetan plateau show decreasing trends. In south Asia all trends are insignificant. Drought extent over Australia has decreased. Over the Americas, trends are uniformly negative and mostly significant.

Within the long-term trends there are considerable inter-annual and decadal variations in soil moisture and drought characteristics for most regions, which impact the robustness of the trends. Analysis of detrended and smoothed soil moisture time series reveals the leading modes of variability are associated with sea surface temperatures, primarily in the equatorial Pacific and secondly, in the north Atlantic. Despite the overall wetting trend there is a switch since the 1970s to a drying trend, globally and in many regions, especially in high northern latitudes. This is shown to be caused, in part, by concurrent increasing temperatures. Although drought is driven primarily by variability in precipitation, projected continuation of temperature increases during the 21st century indicate the potential for enhanced drought occurrence.

5.1 Introduction

Drought can be regarded as one of the most damaging of natural disasters in human, environmental and economic terms. It occurs as a result of extremes in climate that are driven by natural variability but may be exacerbated or dampened by anthropogenic influences. The variability of global climate is driven in the main by the El Nino Southern Oscillation (ENSO), which impacts the Tropics and many regions in mid-latitudes (Ropelewski and Halpert, 1987).

Other climate oscillations and modes of large-scale variability, such as the North Atlantic Oscillation (NAO), the Pacific Decadal Oscillation (PDO), and the Atlantic Multi-Decadal Oscillation (AMO), act on generally longer time scales and interact with ENSO or are the primary climate drivers elsewhere and more regional in their impacts. For example, the NAO is known to affect climate in eastern North America and Europe (Hurrell and VanLoon, 1997) as well as North Africa (Wang, 2003). The PDO (Mantua et al., 1997) is a primary driver of climate around the Pacific basin and interacts with ENSO resulting in modifications of climate globally (Newman et al., 2003; Verdon and Franks, 2005). The AMO (Kerr, 2000) impacts on the North Atlantic and especially on North American (Enfield et al., 2001; McCabe et al., 2004) and European climate (Sutton and Hudson, 2005), and is a potential modulating force of ENSO (Dong et al., 2006).

Of considerable interest is the change in variability and extremes under recent and future global warming and the potential acceleration of the water cycle which may act to alter the occurrence and severity of drought. As temperatures rise, the capacity of the atmosphere to hold moisture would increase as governed by the Clausius-Clapeyron equation (Held and Soden, 2000), with potential for increased evaporation and/or precipitation (Trenberth, 1999), although these may be limited by other factors such as available energy and aerosol concentration. Climate model studies have shown that variability is likely to increase under plausible future climate scenarios (Wetherald and Manabe, 2002), dependent upon climate sensitivity, with large regional changes in the water cycle. The potential for more droughts and of greater drought severity is a worrisome possibility (Wetherald and Manabe, 1999; Wang 2005).

Huntington (2006) reviews the observational evidence so far for water cycle intensification to date and concludes that despite some contradictions the overall picture points towards intensification. For drought specifically, trends have been analyzed over the past 50 to 100 years at regional (e.g. Lloyd-Hughes and Saunders, 2002; Rouault and Richard, 2005; Andreadis and Lettenmaier, 2006) and global scales (Dai et al., 2004). When analyzing the Palmer Drought Severity Index (PDSI) and the Standardized Precipitation Index (SPI) over Europe, Lloyd-Hughes and Saunders (2002) found insignificant change in the proportion of land experiencing medium to extreme drought during the 20th century. A drought analysis of South African SPI by Rouault and Richard (2005) found a substantial increase in 2-year droughts since the 1970s. They also found inter-decadal variability in the spatial extent of drought since the beginning of the century, most of the severest of which are associated with ENSO. Andreadis and Lettenmaier (2006) analyzed a long-term (1915-2003) hydrological simulation over the USA and found a general increasing trend in soil moisture, with concurrent decrease in drought duration and extent, except for the Southwest and parts of the West. Globally, Dai et al., (2004) showed the global pattern of trends in annual PDSI and found that generally drier conditions have prevailed since the 1970s.

In this paper, we investigate variability and trends in soil moisture and drought characteristics, globally and regionally over the second half of the 20th

century. The analysis is based on a global soil moisture dataset derived from a model simulation of the terrestrial hydrologic cycle. The simulation is driven by a hybrid observation/reanalysis based meteorological dataset and provides a globally consistent and physically based view of moisture availability. As drought can be described by any one or combination of characteristics, and these are important to varying degrees depending on the situation, we are interested in changes in a number of aspects of drought. These include duration, intensity and severity, which are dependent on the threshold for defining drought that is specific to the application. We focus on how soil moisture and drought characteristics vary at annual to decadal time scales, and whether there are any significant trends over the second half of the 20th century. Intuitively, changes in precipitation will be the primary driver of variability in drought but will be modified by temperature changes, which is especially relevant given recent and potential future increases in surface air temperature. We therefore investigate the direct (precipitation, temperature) and indirect (large-scale climate oscillations) forcing mechanisms to understand what is driving changes and variability in soil moisture and drought occurrence.

5.2 Datasets and methods

To represent drought globally, we use soil moisture fields from a land surface hydrological model simulation driven by observation-based meteorological forcings (Sheffield and Wood, 2007). Soil moisture balances the fluxes of precipitation, evapotranspiration and runoff and thus provides an aggregate measure of water availability and drought. In drought terminology, soil moisture falls somewhere in between meteorological and hydrological drought and may be representative of agricultural drought through its control on transpiration and thus vegetative vigor. We calculate an index of drought as the deficit of soil moisture relative to its seasonal climatology (Sheffield et al., 2004a). Wet spells can be calculated similarly but as the surplus of soil moisture. The simulation and the derivation of the drought index and related statistics are briefly described next. Further details can be found in Sheffield et al. (2004a).

5.2.1 Land surface hydrological simulation

The Variable Infiltration Capacity (VIC) land surface model (Liang et al., 1994; Cherkauer et al., 2002) was used to generate spatially and temporally consistent fields of soil moisture and other water budget flux and state variables. The VIC model simulates the terrestrial water and energy balances and distinguishes itself from other land surface schemes through the representation of sub-grid variability in soil storage capacity as a spatial probability distribution, to which surface runoff is related, and by modeling base flow from a lower soil moisture zone as a nonlinear recession. The VIC model has been applied extensively at regional (e.g. Maurer et al., 2002) and global scales (Nijssen et al., 2001; Sheffield et al., 2004b).

For this study, the VIC model was run globally at 1.0 degree spatial resolution and 3-hourly time step for the period 1950-2000. This simulation was forced by a hybrid dataset of precipitation, near-surface meteorological and radiation data derived from the National Centers for Environmental Prediction (NCEP)/National Center for Atmospheric Research (NCAR) reanalysis (Kalnay et al., 1996) and a suite of global observation-based products. In effect, the sub-daily variations in the reanalysis are used to downscale the monthly observations. These observations, which are generally available at higher spatial resolution, are concurrently used to downscale the reanalysis in space. Known biases in the reanalysis precipitation and near-surface meteorology were corrected at the monthly scale using observation-based datasets of precipitation, air temperature and radiation. Corrections were also made to the rain day statistics of the reanalysis precipitation which have been found to exhibit a spurious wave-like pattern in high-latitude wintertime. Other meteorological variables (downward short- and longwave, specific humidity, surface air pressure and wind speed) were downscaled in space with account for changes in elevation. The forcing dataset is described in detail by Sheffield et al. (2006). The simulation has been validated against available observations of terrestrial hydrology (J. Sheffield and E. F. Wood, Evaluation of retrospective off-line simulation of the global terrestrial water budget, 1950-2000, in preparation) including in-situ measurements of soil moisture, large basin streamflow and remote sensing based snow datasets.

Given recent and future potential increases in air temperature, we also carried out a second simulation to investigate the impact of trends in temperature on the drought trends. Higher temperatures will increase potential evapotranspiration and possibly result in increased drought occurrence, although actual changes will be controlled by available moisture from precipitation and be modified by temperature impacts on snow. Following Hamlet et al. (2006) and Dai et al. (2004) we forced the VIC model with climatological surface air temperature, instead of annually varying values. In this way, any differences in the trends in soil moisture and drought characteristics between the two simulations would be attributable to trends in temperature. In the discussion in section 5.5.2, the original simulation with annually varying air temperature forcing is referred to as TANN and the simulation with climatological air temperature as TCLIM.

5.2.2 Relationship with previous studies of drought using the VIC model

Previously, soil moisture fields from a retrospective simulation of the VIC model for the USA (Maurer et al., 2002) have been analyzed in terms of drought occurrence by Sheffield et al. (2004a), who found that the simulated soil moisture values were able to represent historic drought events, display coherency and sufficient detail at small space scales, and compare well with standard drought indices such as the PDSI. The PDSI is one of the most widespread used drought indices both operationally and in climate research (Dai et al., 2004; Burke et al.,

2006) and uses a generic two-layer soil model to describe the cumulative departure of moisture supply (Palmer, 1965). In snow dominated regions, Sheffield et al. (2004a) found that the VIC based dataset and the PDSI dataset diverged, likely due to inadequate representation of cold season processes in the calculation of the PDSI.

The simulations analyzed in Sheffield et al. (2004a) and in this paper were both generated by the VIC model (albeit slightly different versions) but differ substantially in terms of their domain (USA versus global), the meteorological forcings (gauge based versus a hybrid reanalysis/observation dataset), spatial resolution (0.125 degree versus 1.0 degree) and parameter data (different underlying datasets for the soil and vegetation distributions). Despite this, comparison of their representation of drought over the USA shows good agreement with respect to major drought events (not shown). Furthermore, the trends described in section 5.3 are consistent with Andreadis and Lettenmaier (2006) who used an extended version of the Maurer et al. (2002) USA dataset at 0.5 degree resolution. Work in progress has compared the 0.5 degree extended dataset with this global dataset in the framework of severity-area-duration curves (Andreadis et al., 2005) and shows close agreement that is encouraging given the differences in the simulations.

5.2.3 Soil moisture based drought index

The drought index is calculated using the method of Sheffield et al. (2004a) and is briefly described here. Simulated soil moisture data at multiple model soil layers are aggregated over the total soil column, converted to volumetric values and averaged to monthly values. For each model grid cell and month, a beta distribution is fitted to the 51 monthly values (1 value for each year in 1950-2000) using the method of moments. The current level of drought or wetness for a particular month and point in space can then be gauged relative to this fitted distribution or climatology. A drought is defined as a period of duration D months with a soil moisture quantile value, $q(\theta)$, less than an arbitrary threshold level, $q_0(\theta)$, preceded and followed by a value above this level. The departure below this level at any particular time is the drought magnitude:

$$M = q_0(\theta) - q(\theta) \quad (5.1)$$

and the mean magnitude over the drought duration is the intensity:

$$I = \frac{1}{D} \sum_{t=t_1}^{t_1+D-1} q_0(\theta) - q(\theta)_t \quad (5.2)$$

The product of duration and intensity gives the drought severity,

$$S = I \times D \quad (5.3)$$

or

$$S = \sum_{t=t_1}^{t+D-1} q_0(\theta) - q(\theta)_t \quad (5.4)$$

acknowledging that the impacts of drought are a balance between the length and the intensity of deficits. We also define classes of drought event based on their duration as follows:

$$D_{1-3}, \text{ very short-term} : \quad 1 \leq D \leq 3, \quad q(\theta) \leq q_0(\theta) \quad (5.5)$$

$$D_{4-6}, \text{ short-term} : \quad 4 \leq D \leq 6, \quad q(\theta) \leq q_0(\theta) \quad (5.6)$$

$$D_{7-12}, \text{ medium-term} : \quad 7 \leq D \leq 12, \quad q(\theta) \leq q_0(\theta) \quad (5.7)$$

$$D_{12+}, \text{ long-term} : \quad D > 12, \quad q(\theta) \leq q_0(\theta) \quad (5.8)$$

where the subscript to D indicates the range of drought duration in months. A climatological analysis of this dataset is given in Sheffield and Wood (2007).

5.3 Trends in soil moisture and drought

5.3.1 Trends in soil moisture

Trends are calculated using the non-parametric Mann-Kendall trend test (Mann, 1945; Kendall, 1975; Hirsch and Slack, 1984), which is robust and distribution independent. We tested for serial correlation in the monthly data, which would invalidate the assumption of independent data. The areal extent of statistically significant serial correlation (0.01 level) is between 12 and 17% depending on the month with about 50% of this area in drier regions and the majority of the remainder in very high latitudes. Therefore, the area that potentially invalidates the independence assumption is small and generally restricted to drier regions, such as the Sahara, which we ignore in the analysis. Figure 5.1 shows a map of the trends in annual volumetric soil moisture on a grid by grid basis. Results for the Sahara and other desert regions have been masked out based on a threshold of mean annual precipitation $< 0.5 \text{ mm.day}^{-1}$ to screen out serially correlated data and trend values that are essentially zero but are picked up by the ranked based test. Table 5.1 summarizes trends of regional averaged time series. The regions are defined by Giorgi and Francisco (2000) and are shown in Figure 5.2. For brevity, these regions may be referred to by acronyms that are defined in Chapter 4. The GRL region was originally defined as Greenland and northeastern Canada but as the VIC model is not designed to simulate permanent ice sheets and glaciers we exclude the interior of Greenland from the definition of the GRL region and rename it northeastern Canada (NEC). We discuss the trend results in relation to precipitation and temperature trends in the forcing dataset (Figure 5.3), which are calculated in the same manner as for the soil moisture quantiles.

At global scales, the trend in soil moisture is positive (wetting). Generally speaking, wetting trends occur in the Americas, Australia, Europe and western

Region	Soil Moisture (% yr ⁻¹)	Precipitation (mm dy ⁻¹ yr ⁻¹)	Air Temperature (K yr ⁻¹)
<i>World</i>	0.017 (1.137)	-0.001 (-0.999)	0.015 (5.166)
<i>Europe</i>			
NEU	0.096 (1.592)	0.003 (1.811)	0.018 (2.307)
MED	-0.048 (-0.780)	-0.002 (-1.430)	0.009 (2.201)
<i>Africa</i>			
WAF	-0.299 (-4.207)	-0.009 (-3.964)	0.008 (3.647)
EAf	-0.144 (-2.713)	-0.004 (-2.355)	0.016 (5.556)
SAF	-0.149 (-1.901)	-0.003 (-1.446)	0.012 (4.524)
<i>North Asia</i>			
NAS	-0.073 (-1.868)	-0.001 (-0.650)	0.023 (3.233)
CAS	-0.016 (-0.227)	-0.001 (-1.056)	0.018 (3.411)
TIB	0.133 (1.689)	-0.000 (-0.032)	0.021 (4.768)
EAS	-0.083 (-1.982)	-0.001 (-1.413)	0.016 (3.891)
<i>South Asia and Oceania</i>			
SEA	0.020 (0.211)	-0.006 (-1.040)	0.009 (4.776)
SAS	-0.055 (-1.251)	-0.007 (-2.534)	0.007 (2.843)
AUS	0.214 (2.079)	0.003 (1.218)	0.014 (4.427)
<i>North America</i>			
ALA	0.169 (1.527)	0.002 (2.339)	0.032 (3.947)
WNA	0.212 (2.713)	0.002 (1.933)	0.020 (3.281)
CNA	0.253 (2.892)	0.006 (1.998)	0.007 (1.162)
ENA	0.108 (1.836)	0.001 (0.569)	0.002 (0.528)
NEC	0.252 (2.437)	0.003 (2.485)	0.007 (1.007)
<i>South America</i>			
CAM	0.091 (1.429)	-0.002 (-0.877)	0.007 (2.063)
AMZ	0.152 (2.331)	0.004 (1.348)	0.009 (3.225)
SSA	0.184 (2.827)	0.005 (2.290)	0.004 (1.998)

Table 5.1: Non-parametric trends in regional average soil moisture quantile, precipitation and surface air temperature. Trends values in bold are significant at the 0.05 level. Statistical test values are given in parentheses.

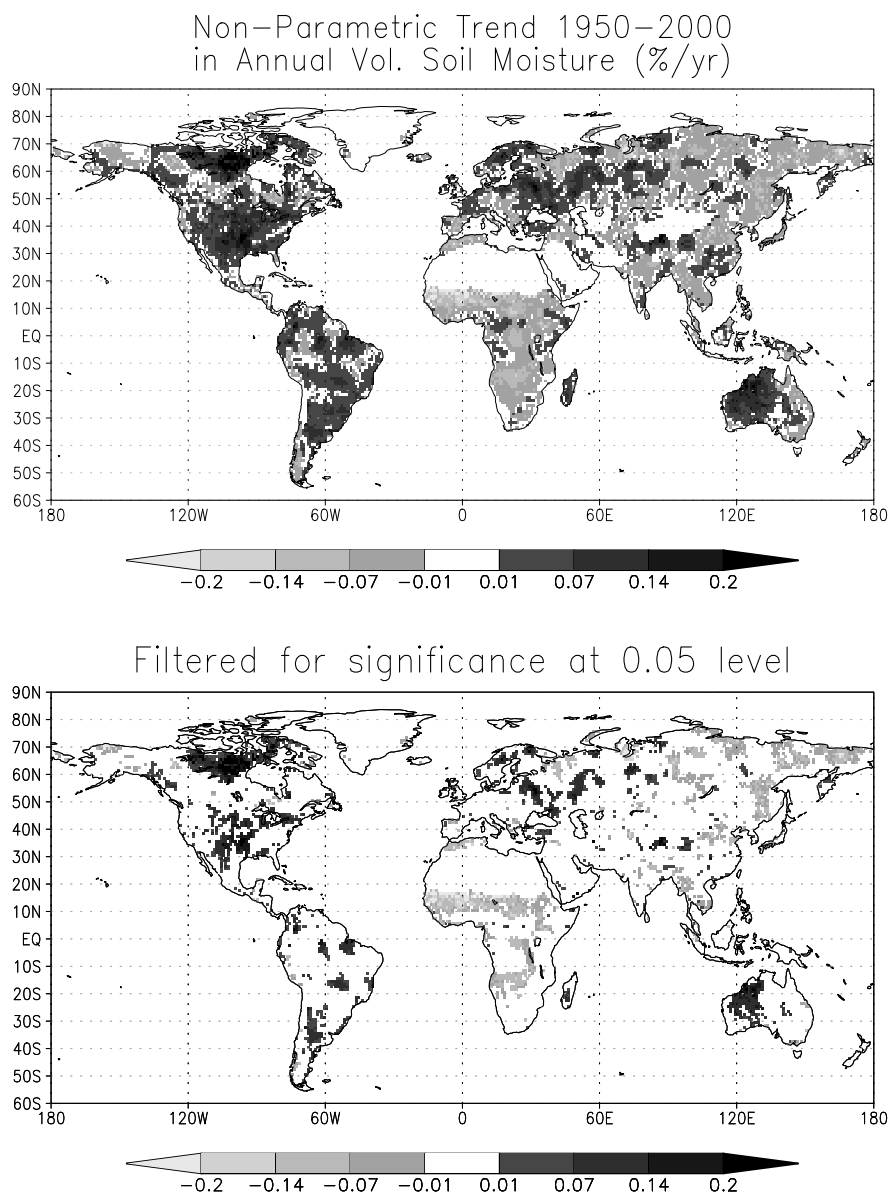


Figure 5.1: Global distribution of linear trends in annual mean volumetric soil moisture, 1950–2000, calculated using the Mann-Kendall non-parametric trend test. Regions with mean annual precipitation less than 0.5mm day^{-1} have been masked out because the VIC model simulates small drying trends in desert regions that, despite being essentially zero are identified by the non-parametric test. The trends in the bottom panel have been filtered for significance at the 0.05 level.

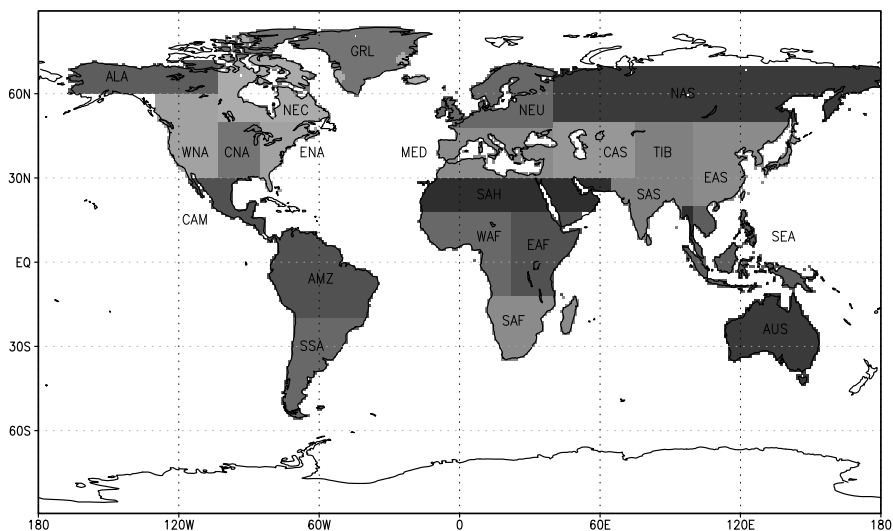


Figure 5.2: Map of regions used in the analysis as defined by Giorgi and Francisco (2000). The GRL region has been modified from its original definition that covered Greenland and eastern Canada to exclude the interior of Greenland. This is because the VIC model is not designed to simulate permanent ice caps and glaciers. The region is renamed northeastern Canada (NEC).

Asia and negative trends (drying) occur in Africa and parts of eastern Asia. The trends are generally collocated with equivalent trends in precipitation (Figure 5.3). Statistically significant trends in soil moisture at the 0.05 level are, however, restricted to relatively small sub-areas of these continents. Regions of wetting trends are evident in the central Northern Territories of Canada (up to $0.2 \text{ \%vol yr}^{-1}$), central USA ($0.05 - 0.2 \text{ \%vol yr}^{-1}$) and northern Mexico ($< 0.1 \text{ \%vol yr}^{-1}$). These are coincident with statistically significant increasing trends in precipitation (Figure 5.3). For northern Canada, increased precipitation has also been noted by Zhang et al. (2000) and McBean (2005). Nevertheless, the simulated increase in soil moisture (and increase in precipitation) appears contradictory to decreasing river discharge into the Arctic and North Atlantic from Canadian rivers since the mid 1960s (D ry and Wood, 2005a). This could be explained by increasing evapotranspiration driven by higher temperatures (Zhang et al., 2000) that results in increased precipitation and decreased streamflow, although changes to snow will complicate this. However, calculation of soil moisture trends over a similar period (1964-2000) as used by D ry and Wood (2005a) shows widespread decreasing (but not always significant) trends over much of northern Canada that is consistent with decreasing streamflow. This indicates the large influence of increasing moisture during 1950-1963 on the overall trend, which is further discussed in general in section 5.4.2. The trends

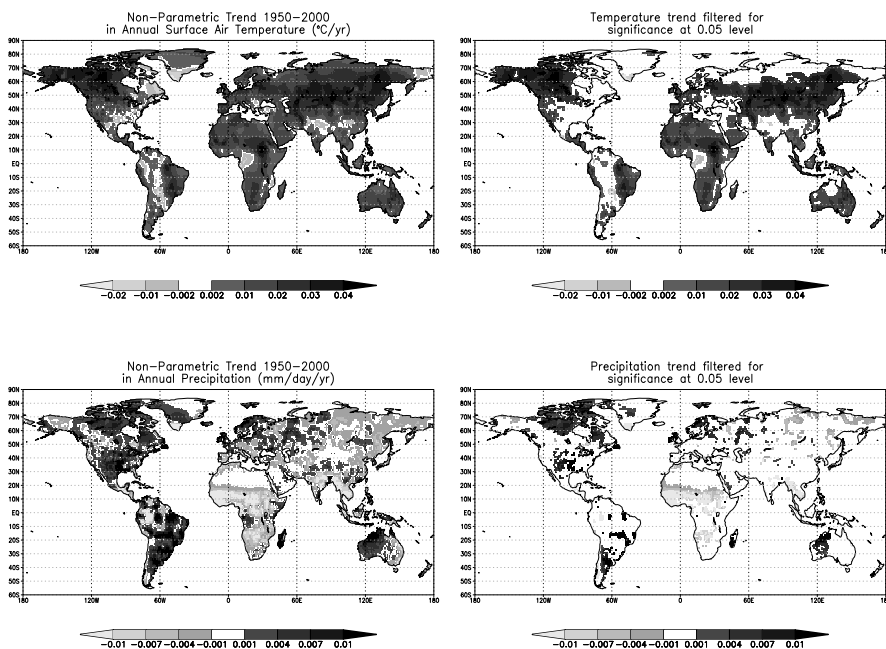


Figure 5.3: Global distribution of linear trends, 1950-2000, in surface air temperature and precipitation as used to force the VIC model. The data are taken from the dataset of Sheffield et al. (2006) which are based on the CRU TS2.0 dataset of Mitchell and Jones (2005). The trends in the right hand panels have been filtered for significance at the 0.05 level.

over the USA are also consistent with increases in precipitation and soil wetness during the 20th century reported by Groisman et al. (2004) and Andreadis and Lettenmaier (2006). Scattered regions in Brazil and Columbia, and a large part of central Argentina show increasing trends up to 0.1 %vol yr⁻¹. These are generally collocated with increasing precipitation trends, and the trends are consistent with increased streamflow in large South American basins (Garcia and Mechoso, 2005) and increased precipitation and streamflow in the La Plata basin (Berbery and Barros, 2002). In the western hemisphere, parts of Scandinavia, eastern Europe and western Russia show increasing trends (up to 0.2 %vol yr⁻¹). A few small regions of significant increasing trend of up to 0.4 %vol yr⁻¹ occur in western China in the northern Tibetan plateau. In western Australia there are significant increasing trends up to 0.25 %vol yr⁻¹. These trends are generally consistent with increasing precipitation in these regions, also noted over the 20th century by Dai et al. (1997).

Drying trends are most prominent in the Sahel (up to -0.6 %vol yr⁻¹ for individual grid cells), which has been well documented in terms of precipitation deficits during the 1970s and 1980s (Hulme, 1992; L'Hôte et al., 2002). Also, significant decreasing trends occur in parts of central Africa and in south-

ern Africa (up to -0.15 %vol yr $^{-1}$ through Angola and Zambia) that coincide with the southern extent of the ITCZ and are again collocated with decreasing trends in precipitation. Although the Arctic as a whole has likely experienced increased precipitation over the latter half of the 20th century (McBean et al., 2005), several regions show significant drying trends, such as northern and southeastern Alaska. The majority of northeastern Asia shows drying trends (up to -0.2 %vol yr $^{-1}$) that are coincident with decreasing precipitation as shown in Figure 5.3 and reported by McBean (2005), although the area of statistically significant values is relatively small, being restricted to the central Yenesei and eastern Amur basins and far northeastern Siberia. The consistency of these trends with observed changes in related variables is unclear, as there is lack of consistency between increasing Arctic discharge from Siberian rivers (Peterson et al, 2002; Shiklomanov et al., 2006) and precipitation (Berezovskaya et al., 2004) and much debate over the impact of other processes such as changes in permafrost and fires (McClelland et al., 2006). Significant drying trends are also apparent in northern China and parts of southeast Asia, up to -0.2 %vol yr $^{-1}$. This is consistent with Zou et al. (2005) who analyzed trends in PDSI data in China during 1951-2003 and found no significant changes except for northern regions.

To investigate whether the trends vary by season, which is more likely in monsoonal regions and continental interiors where inter-seasonal climate variability is relatively high, we also calculated trend values for each season separately (Figure 5.4). Over the USA, the overall increasing trend is most prominent in winter months. In South America, the tendency is for higher trends in Argentina during the Austral summer and autumn (DJF, MAM) whereas trends in Brazil and elsewhere in the north are greater in the drier seasons (JJA, SON). Over Africa, the largest trends tend to coincide with the peak or retreat of the ITCZ (JJA and SON over the Sahel; DJF and MAM in central and southern Africa). The few scattered regions of significant trends in Europe are mainly restricted to the winter months. Decreasing trends in far northeastern Siberia are dominant in the summer, whereas increasing trends east of the Urals are dominant in the spring. Decreasing trends in China are highest in the DJF-MAM, and decreasing trends in northern India and southeast Asia are highest in the Monsoon season (JJASON). In Australia, increasing trends in the west are highest in the Austral summer (DJF).

5.3.2 Global trends in drought characteristics

Next we investigate trends in droughts characteristics (duration, magnitude, and severity) over the 50-yr period. Trends are again calculated using the Mann-Kendall non-parametric test. Individual drought events are assumed to be independent and the period between events is calculated from the beginning of an event to the beginning of the next. We tested for serial correlation in the characteristics of events and found that about 5% or less of grid cells had significant values (0.05 level) and, similar to the results for soil moisture, that most of these were located in the Sahara region which we ignore in the analysis.

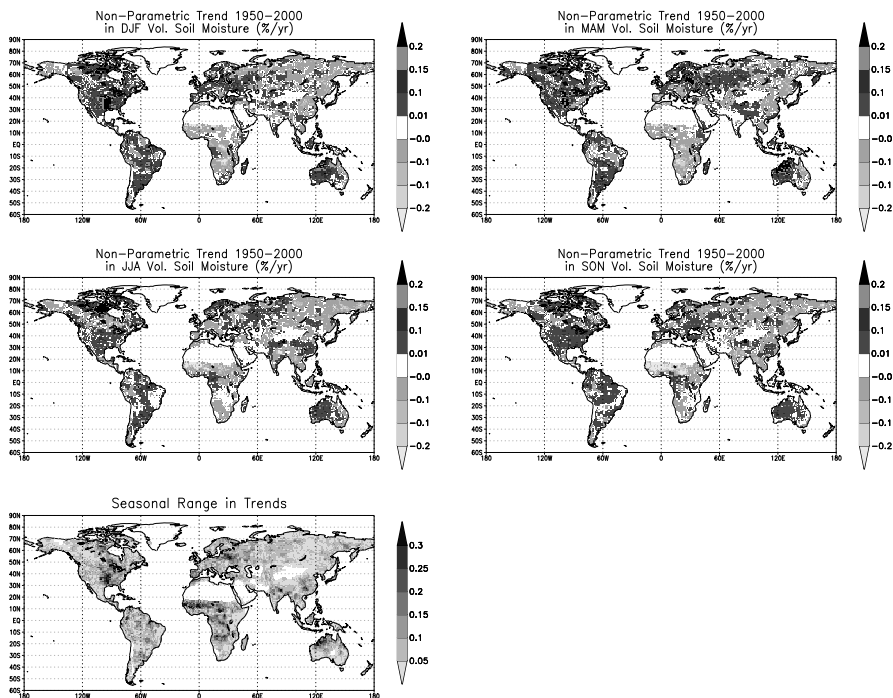


Figure 5.4: Global distribution of linear trends in seasonal mean volumetric soil moisture, 1950-2000, calculated using the Mann-Kendall non-parametric trend test. Regions with mean annual precipitation less than 0.5mm day^{-1} have been masked out in the same way as for Figure 5.1. The bottom panel shows the seasonal range in trends calculated as the maximum minus the minimum trend of the four seasonal values at each grid cell.

The geographic distribution of trends in drought duration, intensity and severity is shown in Figure 5.5 for statistically significant trends only, at the 0.05 level for soil moisture quantile threshold $q_0(\theta) = \{10.0, 50.0\}$, corresponding to severe and mild drought respectively. Table 5.2 shows the percent area of each continent that has statistically significant trends in drought characteristics. In general, hydrological and meteorological variables exhibit spatial correlation, which reduces the number of independent data points over a region. To determine the field significance of the area of significant trends, we estimated the distribution of trend areas using a bootstrap approach in which we generate 1000 time series of soil moisture fields by resampling from the original dataset. Tests over a single region showed that 1000 samples were sufficient to give stable results. The area of significant trends was then calculated for each resampled series and the 95th percentile calculated from the total sample. If the original trend area is greater than this percentile value then it is field significant.

	D		I		S	
	+ve	-ve	+ve	-ve	+ve	-ve
	$q_0(\theta) = 10\%$					
World	0.6 (19)	1.8 (80)	1.8 (74)	3.1 (91)	1.9 (69)	2.6 (60)
Africa	0.8 (95)	1.7 (97)	1.7 (70)	2.3 (71)	2.4 (89)	2.1 (48)
Asia	0.9 (74)	1.3 (19)	2.1 (92)	2.8 (64)	2.4 (95)	1.7 (5)
Europe	0.4 (25)	3.3 (90)	1.6 (47)	3.9 (75)	1.0 (23)	4.0 (75)
N. America	0.3 (2)	2.7 (95)	1.3 (13)	4.2 (98)	1.3 (19)	4.1 (94)
Oceania	0.3 (15)	0.8 (7)	2.1 (77)	2.8 (57)	1.4 (37)	3.1 (71)
S. America	0.2 (19)	1.7 (45)	2.1 (80)	2.8 (72)	1.8 (33)	2.1 (36)

	$q_0(\theta) = 50\%$					
World	1.9 (98)	6.8 (100)	3.0 (97)	6.0 (99)	4.1 (100)	6.6 (99)
Africa	4.1 (99)	7.4 (98)	6.8 (100)	4.5 (81)	10.4 (100)	4.6 (80)
Asia	2.2 (96)	4.5 (85)	3.2 (85)	4.0 (69)	4.5 (99)	4.0 (69)
Europe	1.0 (63)	9.6 (100)	0.9 (31)	6.4 (98)	1.1 (43)	8.2 (97)
N. America	1.1 (43)	8.3 (99)	1.9 (38)	7.6 (99)	2.0 (35)	9.4 (99)
Oceania	0.7 (29)	5.2 (83)	0.7 (15)	10.3 (96)	1.0 (20)	7.8 (91)
S. America	0.5 (36)	8.1 (98)	2.0 (43)	8.1 (96)	1.8 (40)	9.7 (96)

Table 5.2: Percent area with statistically significant positive or negative trends in drought duration (D), intensity (I) and severity (S) for $q_0(\theta) = \{10.0, 50.0\%\}$. The values in parentheses are field significance calculated using a bootstrap resampling approach.

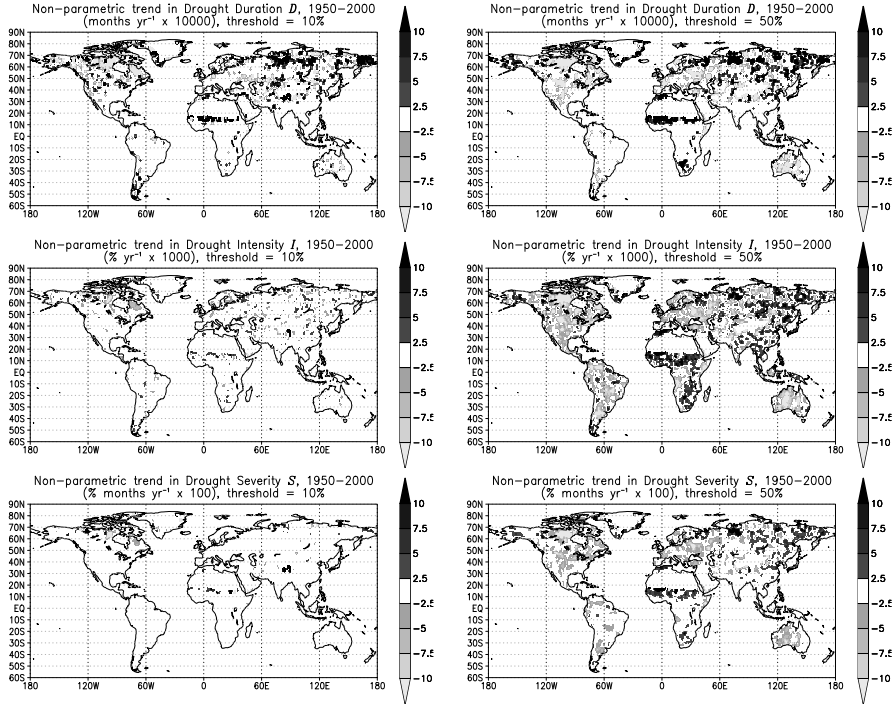


Figure 5.5: Non-parametric trend in drought duration D , intensity I and severity S for $q_0(\theta) = \{10.0, 50.0\}$ threshold values for 1950-2000. Note that the units have been scaled by 10000, 1000 and 100, respectively. Regions with average precipitation $< 0.5\text{mm day}^{-1}$ have been masked out.

Overall, the area that has undergone statistically significant changes in drought characteristics is small (Table 5.2). In general, the area of negative trends is greater than that of positive trends, a result of the global wetting trend in soil moisture. Significant trends are more spatially extensive for $q_0(\theta) = 50\%$, a result influenced by the greater number of droughts at this threshold value. Also, the area of significant trends in drought severity is generally greater than that for drought intensity, which is in turn greater than that for duration. Globally, only 0.6 - 4.1% of the land has experienced increasing trends in duration, intensity and severity, and 1.8 - 6.8% has experienced decreasing trends. At continental scales, Africa is dominated by significant increasing trends in drought severity (area = 10.4% for $q_0(\theta) = 50\%$). Over Asia, the areas of significant decreasing trends at $q_0(\theta) = 50\%$ are highest for duration (4.5%), intensity (4.0%) and severity (4.0%). Negative trends tend to dominate over Europe, especially for drought duration (area = 9.6% for $q_0(\theta) = 50\%$). Elsewhere, decreasing trends are more prevalent in North America (e.g. area of decreasing trends in duration = 8.3%) and Oceania especially for

drought intensity (area = 10.3% for $q_0(\theta) = 50\%$). In South America, the area of decreasing trends is dominant, especially for $q_0(\theta) = 50\%$ (8.1, 8.1 and 9.7% for duration, intensity and severity respectively).

5.3.3 Regional trends in drought spatial extent

Table 5.3 gives trends in the spatial extent of drought for the world and regionally, for various threshold values. Globally, there is an overall decreasing trend in drought extent of -0.021 to -0.035 % yr^{-1} , although only for a threshold $q_0(\theta) \leq 20\%$ are the trends statistically significant at the 0.05 level. Regionally there are distinct differences in the sign of the trends as well as the magnitude and statistical significance that are consistent with the trends in soil moisture. Over northern Europe the tendency is for a decrease in spatial extent, although only trends for $q_0(\theta) \leq 20.0$ are significant and in the Mediterranean region all trends are positive but essentially statistically zero. Lloyd-Hughes and Saunders (2002) analyzed PDSI and SPI over Europe, and similarly found generally insignificant change in the proportion of land experiencing medium to extreme drought during the 20th century. West Africa is dominated by events in the Sahel, which result in large increases in spatial extent that are approximately proportional to the threshold. For example, for $q_0(\theta) = 50\%$ the trend is 0.527 % yr^{-1} , which translates into about 28% increase over the full period. Although eastern Africa shows consistently increasing trends also (up to 0.15% yr^{-1}), they are only significant for $q_0(\theta) \geq 40\%$. In southern Africa (SAF), positive trends of $0.038 - 0.234$ % yr^{-1} are only significant at the 0.1 level.

Over the northern part of Asia (regions NAS, CAS, TIB and EAS) the picture is mixed, with positive and significant trends over northern Asia, positive but insignificant trends over eastern Asia and negative trends over central Asia and the Tibetan Plateau, although only over TIB are the majority of the trends significant. All trends in southern Asia are insignificant with negative trends for SEA and positive for SAS. The Australian region trends are negative and all significant ranging from -0.08 to -0.32% yr^{-1} . For north America, the trends in spatial extent are uniformly negative and almost always significant (the exceptions are in WNA for $q_0(\theta) = \{10, 20\}$, ENA for $q_0(\theta) = \{10, 20, 30\}$ threshold and ALA for $q_0(\theta) = \{40, 50\}$ threshold). The largest trends are in CNA for $q_0(\theta) = 50\%$ (approx. -0.4% yr^{-1} or 19% decrease in spatial extent over the full period) and NEC for $q_0(\theta) = 50\%$ (approx. -0.5 % yr^{-1} or 26% decrease). Over south America, all trends are negative, with all AMZ trends significant, but only trends for $q_0(\theta) \leq 30\%$ significant in CAM and for $q_0(\theta) \geq 30\%$ in SSA.

5.3.4 Epochal changes in drought frequency

We next calculated the change in drought statistics between the first (1950-75) and second (1976-1999) halves of the simulation period (Figure 5.6), which shows that the number of droughts has tended to decrease over most parts

Region	Trend in Drought Spatial Extent (% yr ⁻¹)				
	10.0	20.0	$q_0(\theta)$ 30.0	40.0	50.0
<i>World</i>	-0.021	-0.032	-0.035	-0.027	-0.021
<i>Europe</i>					
NEU	-0.102	-0.143	-0.139	-0.139	-0.140
MED	0.014	0.022	0.022	0.026	0.022
<i>Africa</i>					
WAF	0.068	0.179	0.319	0.435	0.527
EAF	0.029	0.064	0.088	0.117	0.154
SAF	0.038	0.090	0.150	0.203	0.234
<i>North Asia</i>					
NAS	0.055	0.102	0.129	0.139	0.140
CAS	-0.049	-0.098	-0.151	-0.176	-0.203
TIB	-0.063	-0.130	-0.166	-0.208	-0.206
EAS	0.011	0.023	0.053	0.083	0.093
<i>South Asia and Oceania</i>					
SEA	-0.011	-0.016	-0.026	-0.031	-0.009
SAS	0.022	0.031	0.037	0.032	0.032
AUS	-0.082	-0.191	-0.258	-0.319	-0.318
<i>North America</i>					
ALA	-0.115	-0.206	-0.238	-0.241	-0.207
WNA	-0.052	-0.113	-0.195	-0.248	-0.279
CAN	-0.108	-0.199	-0.264	-0.325	-0.376
ENA	-0.050	-0.108	-0.152	-0.177	-0.185
NEC	-0.181	-0.315	-0.407	-0.481	-0.509
<i>South America</i>					
CAM	-0.060	-0.118	-0.139	-0.130	-0.111
AMZ	-0.069	-0.125	-0.172	-0.216	-0.238
SSA	-0.034	-0.090	-0.155	-0.214	-0.258

Table 5.3: Trends in the spatial extent of drought for various $q_0(\theta)$ values. The trends are calculated using the Mann-Kendall non-parametric test. Trend values in bold are significant at the 0.05 level.

of the world. For short-term droughts, D_{4-6} , mid-latitudes are dominated by decreases, most notably in central and eastern Europe, Australia, southern South America and central North America. Increases are evident across southern Canada, southwest Europe and across northern Russia and most of Siberia, although these are localized. The pattern for medium-term (D_{6-12}) droughts is more organized with large and spatially coherent decreases across most of Alaska and northern Canada, eastern Europe and western Russia, sub-Tropical Asia and central Australia. Conversely, a large expanse of increased frequency traverses Siberia. The number of long-term droughts (D_{12+}) in both epochs is limited to a few regions (northern Canada, Tibetan plateau) and the changes are all decreasing. Mean drought duration has decreased in northern mid-latitudes and northern Canada, but has increased over the Northwest US and large regions of Siberia. In Africa, mean drought duration increased in the Sahel and southern Africa. For drought intensity, the changes are generally small and localized and where they are more prominent, tend to collocated with regions of large changes in mean drought length. For drought severity, the distribution of changes is similar to that for mean drought duration, and given that changes in mean drought intensity are relatively small, the indication is that changes in drought severity are driven mainly by changes in drought duration.

5.4 Temporal variability of soil moisture and drought

5.4.1 Regional temporal variability

Within the long-term linear trends identified there is considerable variability at interannual to decadal time scales. Figure 5.7 shows the temporal variation of several drought characteristics (mean drought duration, \bar{D} for $\{q_0(\theta)=50.0\%\}$; number of very short, high intensity droughts $\{q_0(\theta)=10.0\%, D = D_{1-3}\}$; number of long, low intensity droughts $\{q_0(\theta)=50.0\%, D = D_{12+}\}$; spatial extent of drought $\{q_0(\theta)=50.0\%, D = D_1\}$ calculated for an 11-yr moving window. The drought characteristics are averaged over each region. The time series for long, low intensity droughts is multiplied by a factor of 3 to aid visualization. At global scales, there is little variation over the time period in drought duration and frequency, although the spatial extent of drought has swung from the high of the 1950s, through a low in the 1960-70s and back up again in recent years.

Figure 5.8 shows the spatial loadings of the first three principal components of monthly soil moisture quantiles and represents the major modes of variability in global drought and wet spells. Figure 5.9 shows smoothed time series of these principal components. Although the variance explained by the first three components is small, the value decreases rapidly for higher order components, and so we show only the first three components for brevity. PC1 explains 8.1% of the global variability in soil moisture and is negative in the

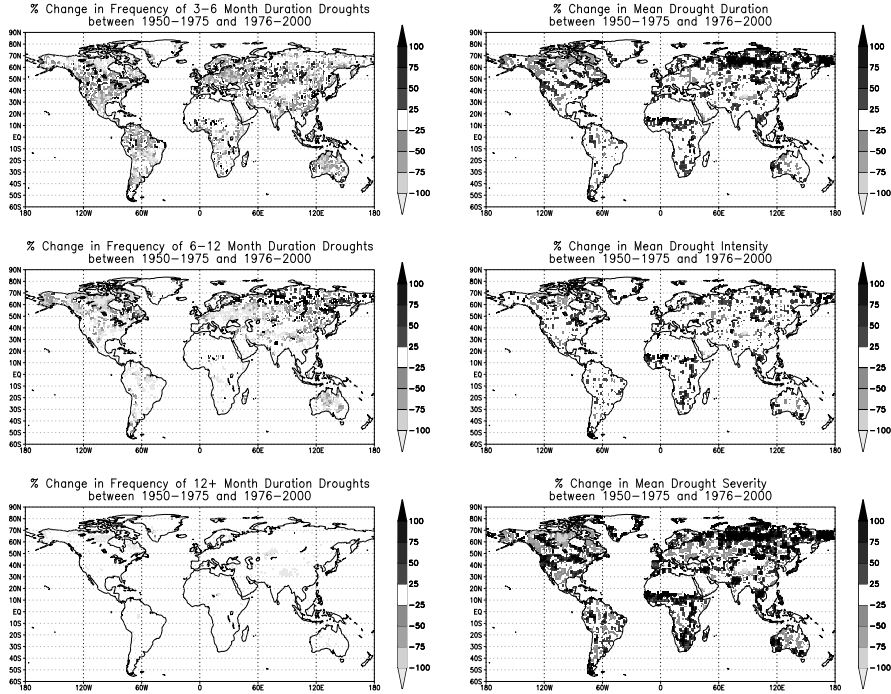


Figure 5.6: Percent change in frequency of short- (D_{4-6}), medium (D_{6-12}), and long-term (D_{12+}) duration droughts and mean drought duration (\bar{D}), intensity (\bar{I}) and severity (\bar{S}) for $q_0(\theta) = 10.0\%$, between 1950-75 and 1976-99.

Amazon, the Sahel, southern Africa, northeastern Siberia, southeast Asia and Australia among other places. It is positive in southern South America, central and southern US, northern Canada and central and eastern Asia. The distribution of loadings for PC1 reminisce ENSO impacts. In fact the time series in Figure 5.9 is correlated with Nino 3.4 SST variability ($r = 0.50$) and so, notwithstanding the variability associated with the overall trend, tropical Pacific temperatures appear to be the primary driver of global variability in soil moisture, a result also shown by Dai et al. (2004) for PDSI data. PC2 explains 6.4% of the variance and shows strong positive loadings over northern Canada, the Amazon, southern Africa and central Australia. Negative loadings are highest in Alaska, northern Europe and far eastern Asia. The time series of PC2 shows a low frequency multidecadal oscillation that covaries well with the AMO index ($r = 0.67$) and is consistent with the PDSI analysis of McCabe and Palecki (2006). The third component, PC3, explains 6.0% of the variance and shows strong positive loadings over central Europe through Russia, Australia, south America and Alaska, and strong negative loadings over northern Siberia, east Africa and northeast Canada. The decadal variability follows the NAO

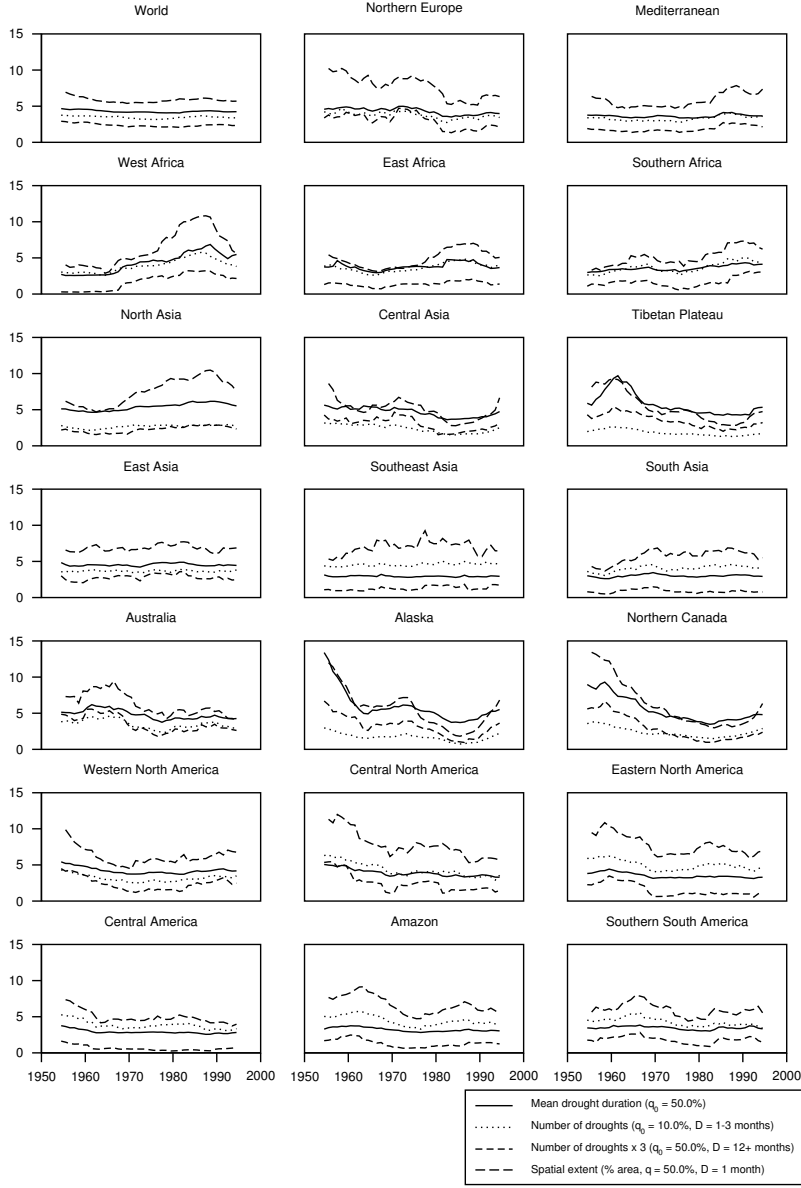


Figure 5.7: Regional average time series of various drought statistics: mean duration of drought $\{q_0(\theta)=50.0\%\}$, number of droughts $\{q_0(\theta)=10.0\%, D = D_{1-3}\}$, number of droughts $\{q_0(\theta)=50.0\%, D = D_{12+}\}$ and spatial extent of drought $\{\% \text{ area}, q_0(\theta)=50.0\%, D = D_1\}$. The statistics are calculated over an 11-year moving window and are plotted at the center of the window. The data series for the number of long-term droughts $\{q_0(\theta)=50.0\%, D = D_{12+}\}$ are multiplied by 3 for ease of comparison.

somewhat (Figure 5.9), however the correlation is insignificant ($r = 0.21$) and especially weak during the mid-1980s to mid-1990s.

Regionally, considerable variation in drought characteristics is evident (Figure 5.7) and we can also relate the variations in soil moisture to large scale climate oscillations that act at inter-annual to decadal time scales. Table 5.4 shows the correlation between regional principal components of smoothed monthly soil moisture quantiles and various climate indices. The soil moisture data are detrended to avoid spurious correlations at multi-decadal time scales and the PCs are smoothed using a 13-month moving window. It should be noted that the large extent of some regions may hide any strong connectivity at smaller scales.

In northern Europe a decadal oscillation, most evident in the spatial extent, underlies the small decreasing trend in drought (Section 5.3.3), with peaks in the 1950s, 1970s and 1990s (Figure 5.7). Lloyd-Hughes and Saunders (2002) and van der Schrier et al. (2006) also found the 1950s and 1990s to be the most drought prone periods in terms of PDSI and 3 and 12 month SPI. For the Mediterranean, although overall trends are insignificant, there is a slight decreasing trend until the early 1980s when there is a sharp increase in frequencies, especially for drought spatial extent. The underlying soil moisture variability in the Mediterranean appears to be weakly correlated with the NAO ($r=0.56$), as documented previously (e.g. Rodo et al., 1997). The relationship in northern Europe is insignificant ($r=-0.19$, Table 5.4) which may be a result of the variability in strength of connectivity across the region and seasonally (Uvo, 2003).

The change in the number of droughts over West Africa is dominated by the increasing trend up to the mid-1980s but there is a large reversal in trend in the following years. Correlations between the detrended soil moisture time series and the AMO are modest ($r= -0.46$ for PC1) but are consistent with observational and model based studies (Zhang and Delworth, 2006). Previous studies have shown that NAO has some influence over the climate in this region (Oba et al., 2001), although there is contradictory evidence (Wang, 2003) and the correlation here is weakly significant ($r= -0.43$ for PC2) which reflects this uncertainty. A similar, but less pronounced picture is apparent in East Africa, with a noticeable decrease in drought frequency in the 1950-60s. The AMO and Nino3.4 SSTs provide the highest, but weak, correlations ($r= 0.43$ and 0.48 , respectively). In southern Africa, peaks occur in the late 1960s and early 1990s which overlays the positive trend in drought characteristics and decreasing soil moisture trend. Rouault and Richard (2005) analyzed South African SPI and found a substantial increase in 2-year droughts since the 1970s. They surmised that the change was likely driven by stronger connections with ENSO, although correlations here with the Nino3.4 index are low, likely due to the large size of the SAF region.

A decadal oscillation in north Asia (NAS) overlays the general increasing trend for all characteristics that is consistent with decreasing soil moisture. Of note is the increase in the number of long, low intensity droughts during the 1980s and 1990s, which may be related to the switch to a positive NAO phase

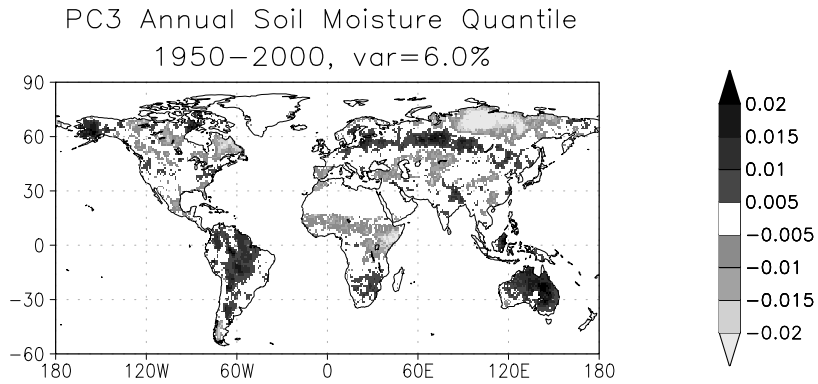
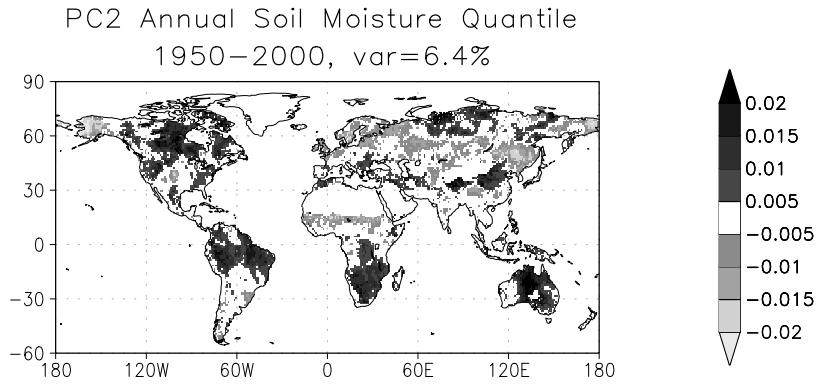
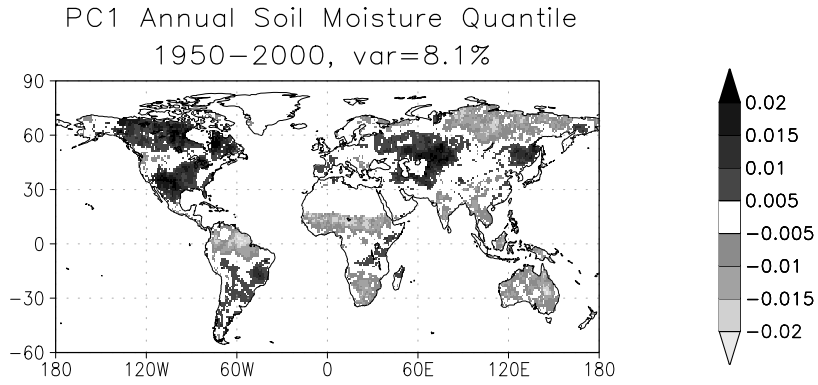


Figure 5.8: Spatial loadings of the first three principal components of annual soil moisture quantile for 1950–2000. The amount of variance explained by each component is also given.

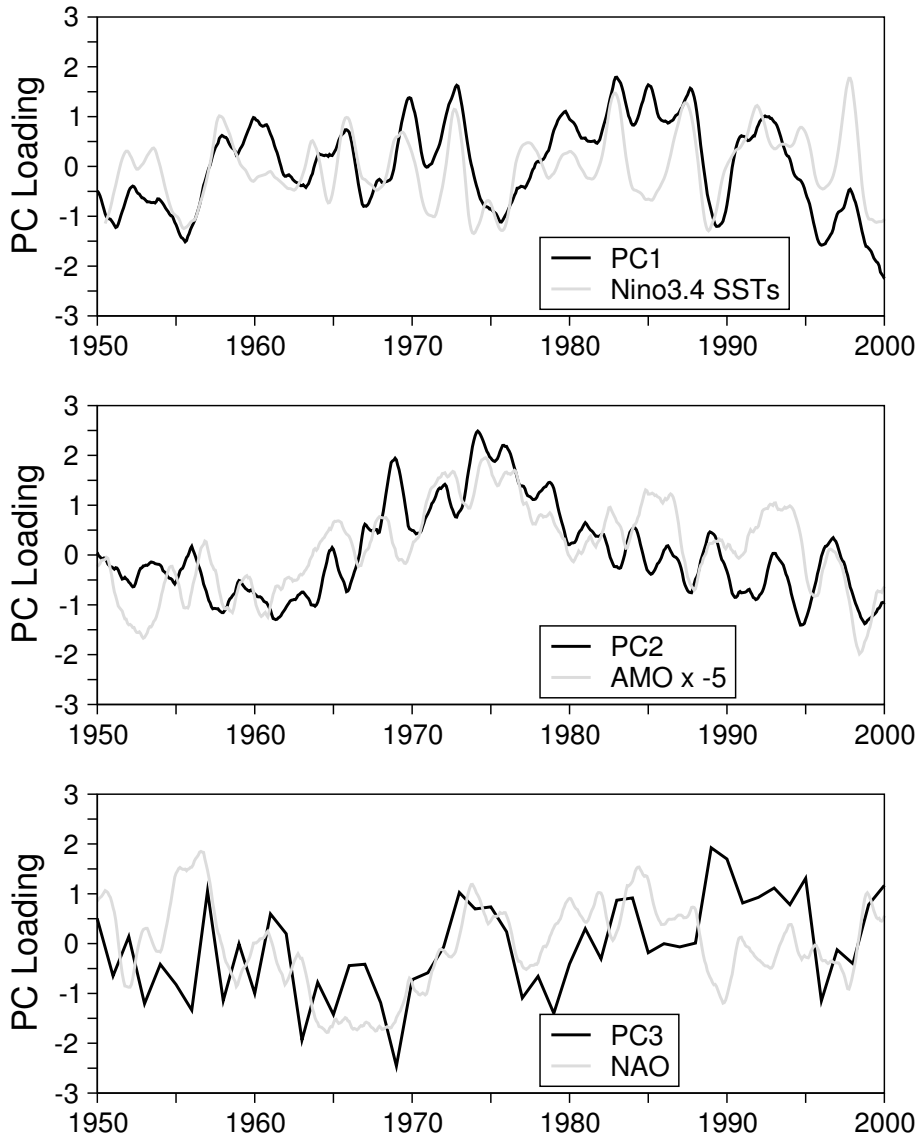


Figure 5.9: Smoothed time series of the first three principal components of monthly soil moisture quantile for 1950-2000 compared to climate indices. Nino3.4 SSTs are defined as over 5.0S-5.0N, 120.0-170.0W. AMO: Atlantic multidecadal oscillation defined as detrended area weighted average SSTs over the North Atlantic, 0 to 70N. NAO: DJFM wintertime North Atlantic Oscillation defined as the difference of normalized sea level pressure between stations in Portugal and Iceland.

Region	Climate Index			
	<i>Nino3.4</i>	<i>PDO</i>	<i>AMO</i>	<i>NAO</i>
<i>World</i>	-0.50	-0.22	-0.67	-0.21
<i>Europe</i>				
NEU	-0.20	0.23	0.24	-0.19
MED	0.21	0.19	-0.20	0.56
<i>Africa</i>				
WAF	-0.16	-0.17	-0.46	-0.43
EAF	-0.48	-0.16	0.43	-0.32
SAF	-0.39	0.16	-0.36	0.18
<i>North Asia</i>				
NAS	-0.17	-0.08	0.16	-0.16
CAS	-0.46	-0.22	-0.49	-0.13
TIB	0.08	-0.23	0.42	-0.24
EAS	0.42	0.17	-0.28	0.22
<i>Southern Asia and Oceania</i>				
SEA	-0.87	-0.17	-0.12	0.04
SAS	0.39	0.12	-0.20	-0.14
AUS	-0.49	-0.13	0.20	-0.04
<i>North America</i>				
ALA	-0.12	0.12	0.46	0.33
NEC	-0.34	-0.19	0.49	-0.18
WNA	0.38	0.22	0.45	0.23
CNA	0.39	-0.12	0.26	-0.15
ENA	0.24	-0.09	0.32	-0.12
<i>South America</i>				
CAM	0.36	0.22	0.42	-0.22
AMZ	0.72	0.11	-0.37	-0.23
SSA	0.33	-0.1	-0.18	-0.21

Table 5.4: Correlation between regional principal components of detrended annual soil moisture quantile and various climate indices. The climate indices are also annual values and are compared year for year (51 values) with no lag relative to the soil moisture data. The correlations are the maximum values for the first three PCs and those in bold are statistically significant at the 0.01 level. Nino3.4: SST anomalies in the Nino3.4 region, 5.0S-5.0N, 120.0-170.0W. PDO: Pacific decadal oscillation defined as the leading PC of monthly SST anomalies in the North Pacific Ocean, poleward of 20N. AMO: Atlantic multidecadal oscillation defined as detrended area weighted average SSTs over the North Atlantic, 0 to 70N. NAO: DJFM wintertime North Atlantic Oscillation defined as the difference of normalized sea level pressure between Portugal and Iceland.

(Visbeck et al., 2001), although correlations of soil moisture with climate indices are insignificant. Central Asian droughts also follow a decadal cycle, peaking in the 1970s and ending with an upward trend in the 1990s. Correlations with climate indices are weak but greatest with the Nino3.4 and AMO indices. Over the Tibetan plateau, the series are dominated by a peak in all variables around 1960, and a decreasing trend thereafter until the early 1990s, when there are slight increases again, which has continued into recent years (Barlow et al., 2002). The AMO provides the only significant, although weak, correlation ($r = 0.42$). Drought in East Asia shows little variation over the 50 years as seen before and is most closely tied to Nino3.4 variability.

For southeast and south Asia, there are small but increasing trends over much of the period with a slight decreasing trend in the 1990s. Note the high and expected correlation ($r = -0.87$, PC1) with the Nino3.4 index. The decreasing trends over Australia are dominated by a large amplitude decadal variation that peaks in the 1960s and late 1980s. The correlation with Nino3.4 is expected ($r = -0.49$, PC1) but is weak, likely owing to the size of the AUS region.

Over North America, the overall wetting trend is reflected in decreasing trends in all drought variables, yet there is large variability within this. Alaska and Northeastern Canada show large decreases since the 1950s but an upturn in the 1990s with weak correlation between soil moisture and the AMO ($r = 0.46$ and 0.49 , respectively, PC1). The number and spatial extent of droughts in western North America decreases until the early 1970s, at which time they increase to the end of the record. In central North America there is an overall decreasing trend, although both the western and central regions exhibit an upward jump in longer duration drought frequencies during the 1970s. In eastern North America the series are dominated by decadal variability overlaid by a decreasing trend. Low values occur during the 1970s and for a brief period around the early 1990s. The changes across these three latter regions are generally consistent with the overall decreasing drought trends found by Andreadis and Lettenmaier (2006) for the USA.

A decreasing trend is apparent in Central America, most prominently at the beginning of the period. The Amazon is dominated by a decadal cycle, peaking in the early 1960s and mid 1980s that relates to Nino3.4 SSTs ($r = -0.72$). In southern South America there are similar oscillations with peaks in frequencies and extent in the mid-1960s followed by a drop until the early 1980s and then increasing conditions thereafter.

5.4.2 Variation and robustness of trends

The regional time series of soil moisture and drought statistics show large variability within the long-term trends identified in Section 5.3. Of interest is how these variations affect the robustness of the global wetting trend, especially as we move into the 21st century and the potential impacts of global warming. Recent increases in global temperatures (e.g. Jones et al., 1999; Jones and Moberg, 2003; Hansen et al., 1999; Brohan et al., 2006) may have already

caused an acceleration of the water cycle (Huntington, 2006) and intensification of drought. For example, many regions show decadal variations that switch during the 1970s, that has been reported previously (Dai et al., 2004; Rouault and Richard, 2005), which may be indicative of temperature impacts on drought, either directly or indirectly through intensification of climate drivers such as ENSO (Hunt, 1999; Herbert and Dixon, 2003). Nevertheless, evidence of increasing summertime soil moisture across Asia despite increasing temperatures (Robock et al., 2000) and forcing of increased drought by large scale climate anomalies (e.g. decreased late-spring precipitation in China driven by a shift to positive phase of the NAO (Xin et al., 2006)) add to the uncertainty of current and future drought response to changing temperatures.

Figure 5.10 shows a time series of trends in regional mean soil moisture quantile calculated over an 11-yr moving window. The trends are color coded according to the sign of the trend and the statistical significance at the 0.05 level. At the global scale the trends oscillate from wetting to drying around the mid-1970s with peak drying trends in the mid-1980s and subsequent reduction in magnitude towards the end of the century. Over northern Europe, mostly insignificant wetting trends are separated by drying trends at the beginning and end of the series. In the Mediterranean, initially increasing soil moisture is overwhelmed by decreasing trends from the mid-1960s onwards. For Africa, generally decreasing trends dominate (with a spate of increasing trends centered on 1970 in southern Africa) although all regions begin to experience increasing trends at the end of the time period. Over northern Asian regions, mostly increasing trends are juxtaposed with decreasing trends in the last 20 years, although the north Asia region shows drying trends since the mid 1960s. The decadal oscillation in trends over southeast and southern Asia, Australia and the Amazon indicating a consistency over most of the Tropics which mirrors the variation at the global scale as well. Over the Americas, all regions (except the Amazon) end the period with decreasing trends, although there is considerable variability previously in some regions (e.g. central North America). Of particular note are the large trends in Alaska and Northern Canada in the last 10-20 years that are concurrent with increasing temperatures (not shown).

These results indicate a switch to drying trends in soil moisture in many regions and more generally at global scales, despite a long-term wetting trend. Although there is considerable variability over the whole period, we hypothesize that this is caused in part by warming temperatures that act to increase evapotranspiration and/or early snowmelt and therefore the occurrence of drought. This is despite the possibility of concurrent increases in precipitation, although this is unlikely in some regions because of the anti-correlation of precipitation and temperature (Dèry and Wood, 2005b). We explore the relationship between soil moisture/drought and precipitation and temperature variability next and then address the impact of warming trends.

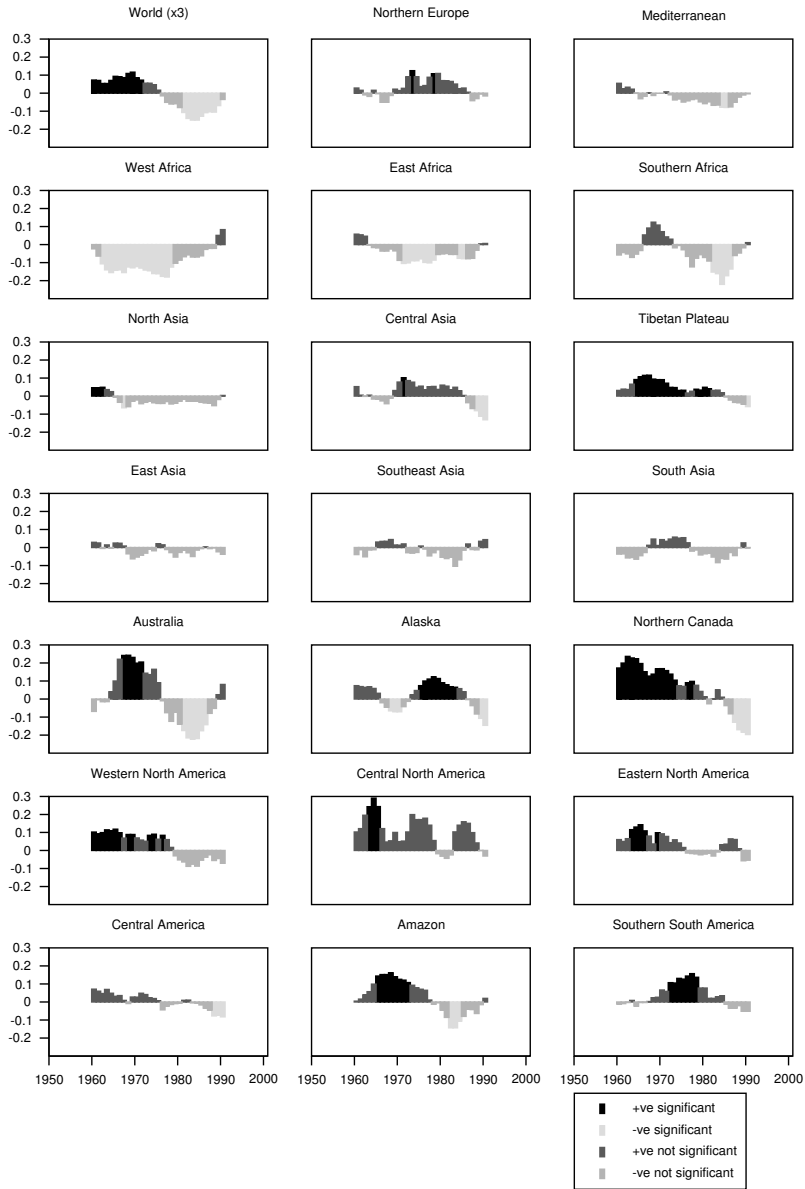


Figure 5.10: Trends in regional average soil moisture for a 21-yr moving window. The x-axis indicates the middle date over which the trend is calculated. Trends that are significant at the 0.05 level are shaded in darker colors. Positive (negative) trend values are shaded in warm (cool) colors. The values for “world” have been multiplied by 3 for ease of visualization.

5.5 Relationships with meteorological forcings

5.5.1 Relationship with precipitation and temperature variability

Drought is driven primarily by lack of precipitation, but this is accentuated or diminished by associated changes in temperature and other meteorological processes. Anomalously high temperatures will tend to increase evapotranspiration, while low precipitation will obviously reduce recharge of the soil column. These processes may interact in complex and non-linear ways such that drought can be, for example, induced by many months of below normal rainfall, be prolonged by high temperatures and then be alleviated by a single storm. These relationships may also have implications for the occurrence of drought under future climates that are likely to be warmer but with associated changes in precipitation that are regionally dependent and may show increase or decreases. Drought development may also lag anomalies in precipitation and other meteorological forcings but this relationship is not well understood. For example, months of anomalously low precipitation may not result in drought conditions until some time later. A subsequent return to normal conditions may similarly be delayed as moisture takes time to filter through the hydrologic system and replenish depleted stores. These processes are complicated by seasonal variations where precipitation may dominate in cool seasons and be modified in warm seasons by temperature effects.

Figure 5.11 shows scatter plots of the trends in precipitation and temperature stratified by trends in soil moisture quantile for several regions chosen to represent a diversity of climates. Wetting (drying) trends that are significant at the 0.05 level in soil moisture are associated with positive (negative) trends in precipitation in all regions. Of note is the small spread in the distribution of precipitation trends and clear delineation between wetting and drying soil moisture trends in high latitude regions (ALA and NAS). Tropical and southern hemisphere regions (e.g. AMZ, SAF, SAS) show larger spread in precipitation trends and some overlap in the range of positive soil moisture trends with negative precipitation trends. The relationship between soil moisture and temperature is somewhat unclear, however (in part, because decreasing temperature trends are uncommon). As significant trends in soil moisture (wetting and drying) are generally associated with positive temperature trends, indicating that increasing temperatures do not necessarily hinder increasing soil moisture and conversely, that they may enhance decreasing soil moisture.

At seasonal scales, the relationship between soil moisture, precipitation and temperature is more complex, especially for cooler regions where snow pack storage and seasonally frozen soil water play an important role. As an example, the results for the NAS region (Figure 5.12) show very different relationships between trends in soil moisture and those in the forcing variables. During summer (JJA) and autumn (SON), drying (wetting) soil moisture trends are generally associated with decreasing (increasing) precipitation. However, in the cooler months (DJF and MAM) this distinction is not apparent and the

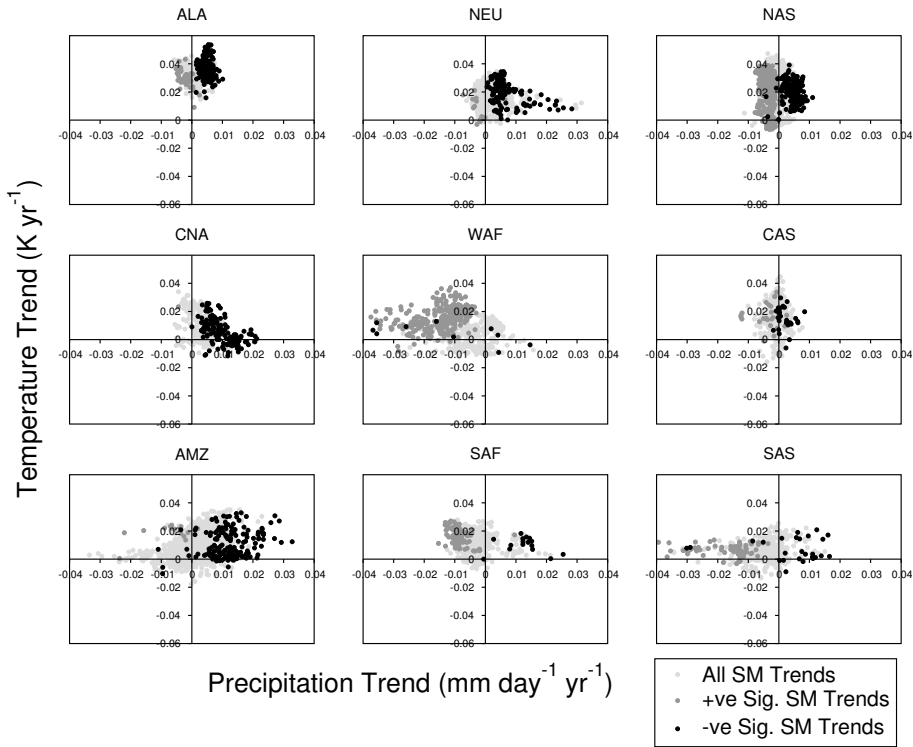


Figure 5.11: Scatter plot of trends in precipitation and surface air temperature, stratified by trends in soil moisture for selected regions. Blue (red) symbols represent positive (negative), significant trends in soil moisture at the 0.05 level.

sign of trends in soil moisture is independent of the sign of the precipitation trend. Springtime soil moisture is dominated by snowmelt which, although driven in part by springtime temperatures and precipitation, is a function of the snowpack accumulated over the preceding winter. As a comparison, humid regions such as the Amazon (not shown) show little seasonal variability in the precipitation-temperature-soil moisture relationships.

5.5.2 Sensitivity of drought to temperature trends

To further investigate the impact of temperature on soil moisture and drought trends we compare the results of the TANN (annually varying temperature forcing) and the TCLIM (climatological temperature forcing) simulations. Figure 5.13 shows the difference between the two simulations in terms of mean soil moisture and trends in soil moisture, and indicates where changes are attributable to trends in temperature. Regions of maximum differences in mean soil moisture tend to occur in the northern Hemisphere, in mid to high latitudes,

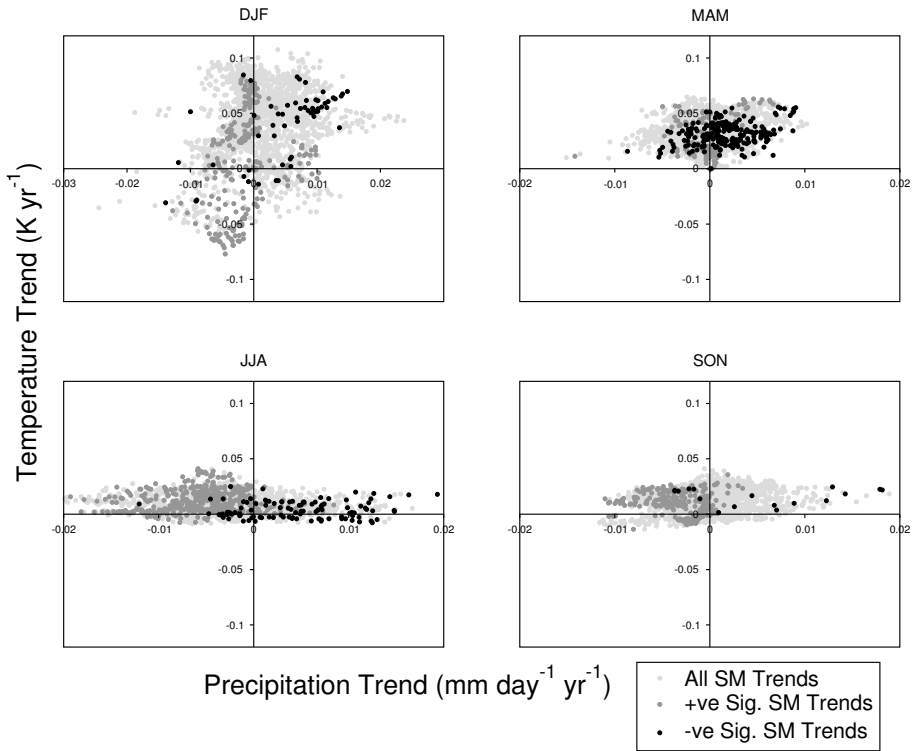


Figure 5.12: Scatter plot of seasonal trends in precipitation and surface air temperature, stratified by trends in soil moisture for the NAS region. Blue (red) symbols represent positive (negative), significant trends in soil moisture at the 0.05 level.

with TANN driving increases in soil moisture in eastern Europe, northern Eurasia, southern Alaska and southeastern Canada and decreases in eastern USA, Pacific Northwest, eastern Canada and small parts of central Europe, central Asia and eastern Siberia. Globally, the tendency is for equal areas of increases and decreases in the Northern Hemisphere and a ratio of 3:2 in favor of increases in the southern hemisphere. The differences in trends between the two simulations are small (of the order of $0.002\% \text{ yr}^{-1}$ or less), although this is the trend over the full 50 years ($\approx 0.1\% \text{ 50yr}^{-1}$). The largest differences are found in high northern latitudes, with increased trend magnitude for TCLIM over northern Canada and northern Europe and decreased trend magnitude for from eastern Europe through to central Siberia. Eastern Siberia also shows decreased magnitudes. Elsewhere, the northern half of the Andes shows lower magnitudes in Peru and higher magnitudes in Columbia.

In Figure 5.14, the differences between the two simulations are shown for 11-yr moving averages in trends in regional mean soil moisture quantile. For the majority of regions the differences are generally less than $1\% \text{ yr}^{-1}$. However,

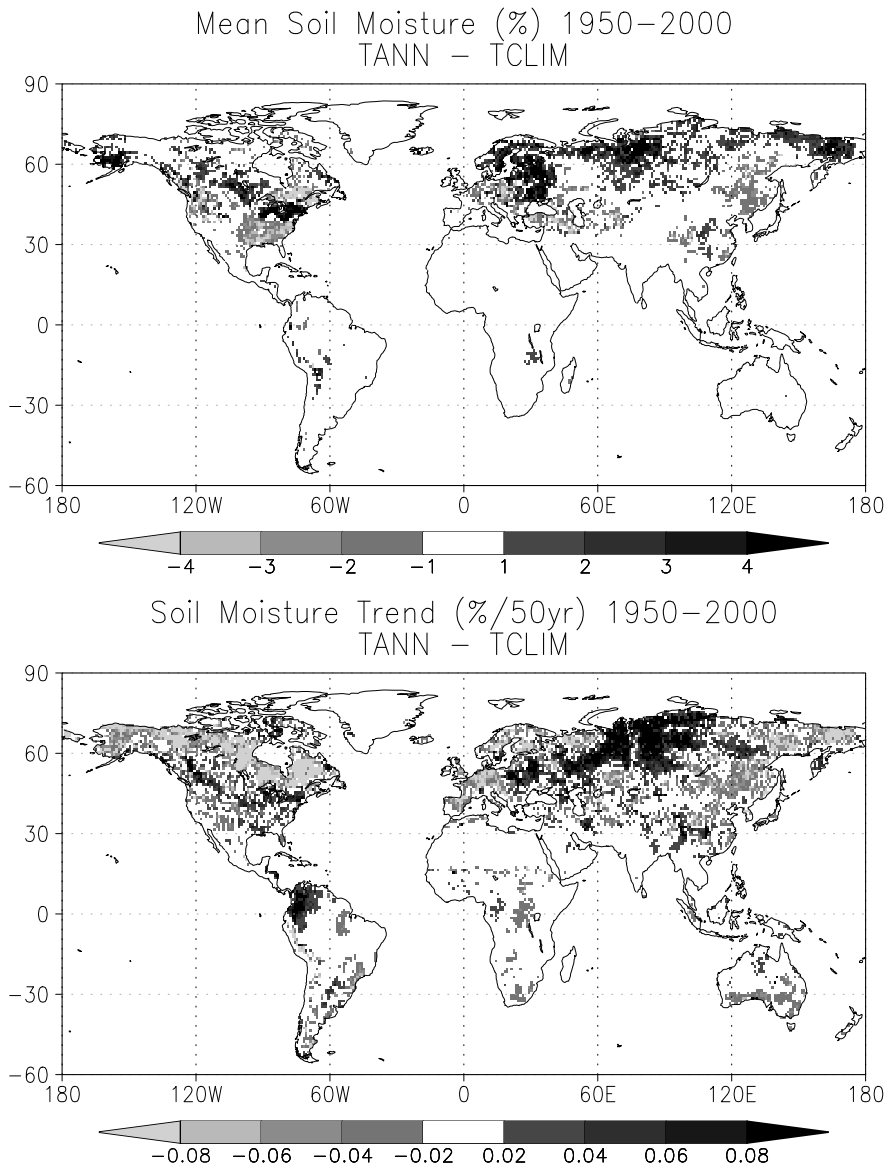


Figure 5.13: Comparison of soil moisture between the original simulation with annually varying air temperature forcing (TANN) and that with time invariant or climatological air temperature (TCLIM). Top panel: difference in mean soil moisture, 1950–2000. Bottom panel: difference in soil moisture trend, 1950–2000.

outstanding are a few regions with differences up to $6\% \text{ yr}^{-1}$ (ALA, NEC) and $2\text{-}3\% \text{ yr}^{-1}$ (NEU, NAS). Note that these are differences in trends over 11-yr windows and will generally be much higher than the 50-yr trends. Of particular interest are the large differences in regions ALA and NEC during the last 20 years of the record that indicate that decreasing soil moisture is exaggerated by the increasing trend in air temperature. The temperature trend is particularly pronounced during 1990-2000 (not shown). Similar behavior in the latter years of the record exists for other regions, such as EAS, WNA, ENA and SSA but the magnitude of the differences are considerably smaller. Even at the global scale a difference is noticeable in the last 20 years. Despite some long term variability over the full period in most regions, the evidence points towards a temperature effect in recent years that tends to exaggerate or force decreasing trends in soil moisture.

5.6 Discussion and conclusions

5.6.1 Uncertainties in the meteorological forcings and hydrologic modeling

The trends discussed are only as robust as the meteorological data that forces the simulation and the land surface model that is used to derive the soil moisture data. It has been shown that modeled land surface hydrology is sensitive to the forcing dataset that drives it, and especially precipitation (Ngo-Duc et al., 2003; Fekete et al., 2004; Berg et al., 2004; Sheffield et al., 2004b; Guo et al., 2006). Fekete et al. (2004) showed that the uncertainty in precipitation datasets was of the order of interannual variability and that the impact of precipitation uncertainties on the terrestrial water budget was of at least the same magnitude, especially in semi-arid regions where the hydrologic response is highly non-linear. In the second Global Soil Wetness Project (GSWP-2) multi-model comparison, Guo et al. (2006) found that uncertainties in the forcings were as large as differences between land surface models. The first order drivers of drought, monthly precipitation and temperature, are derived in this study from the Climatic Research Unit (CRU) TS2.0 gauge based dataset (Mitchell and Jones 2005). For time periods when station observations are limited or non-existent the CRU dataset relies on climatological values, or so-called “relaxation to climatology” (Mitchell and Jones, 2005). Additionally, the gauge density that contributes to a grid cell may force errors in the simulated hydrology for densities of the order of less than 30 gauges per 10^6 km^2 (Oki et al., 1999).

It is therefore likely that errors in the forcing dataset used here will result in errors in the representation of drought and that the reliability of the time series at the grid scale (1.0 degree) may be reduced (Patz et al., 2002), although this can be alleviated through spatial and temporal averaging (Giorgi, 2002). Nevertheless, at larger scales, and especially in data-poor regions, we argue that this is our best estimate. In data rich regions such as the USA and

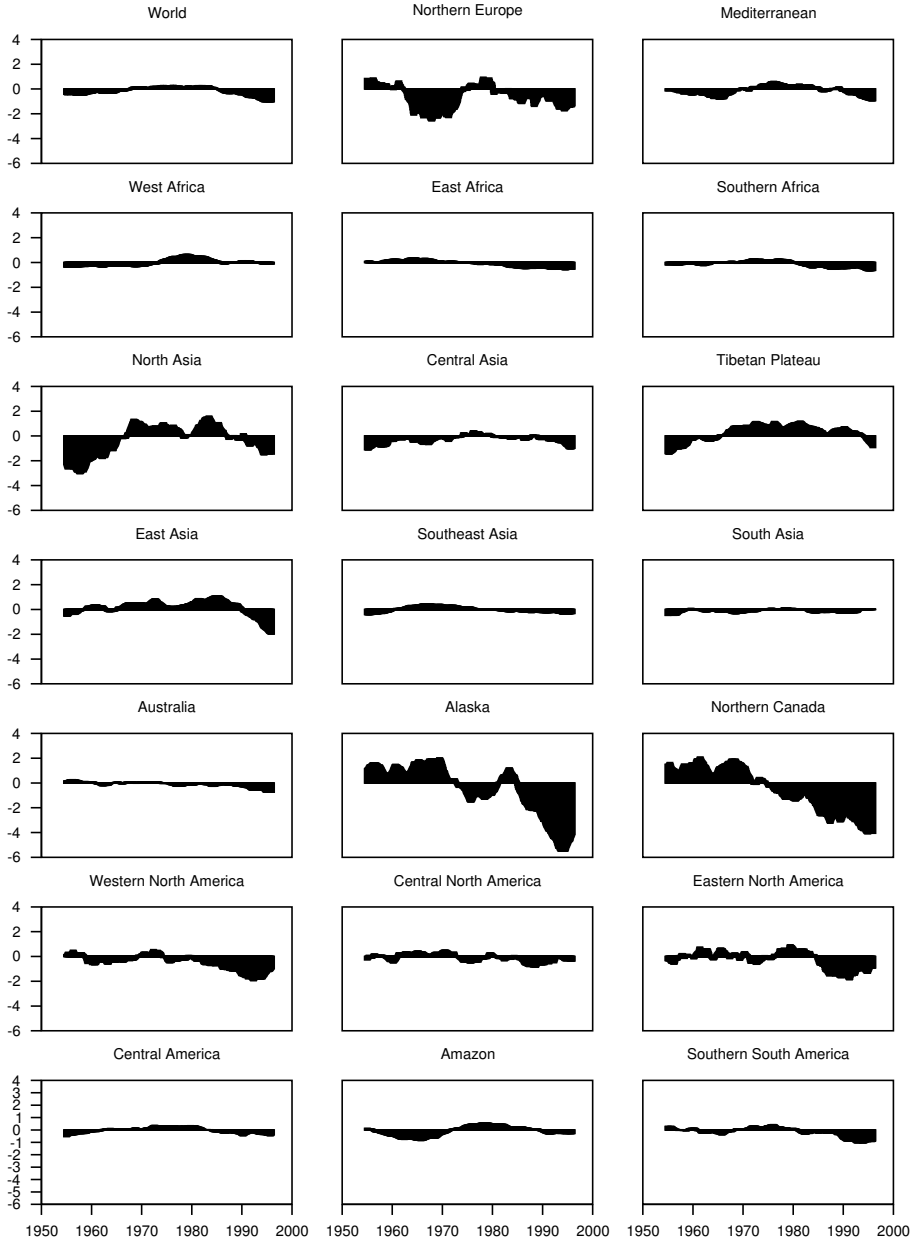


Figure 5.14: Difference in 11-yr moving window trends in soil moisture quantile between the TANN and TCLIM simulations. The TANN simulation was forced with annually varying surface air temperature. The TCLIM simulation was forced with climatological surface air temperature.

Europe, our estimates may compare less favorably against that obtained when using data from dense station networks. For example, Decharme and Douville (2006) showed that the GSWP-2 forcing dataset drastically overestimated precipitation compared to data from a dense network in France with resulting impacts on modeled river discharge and that this overestimation was systematic globally. However, comparisons of drought characteristics derived from the dataset in this paper and datasets based on higher spatial resolution modeling forced with gauge-based observations (Sheffield et al. (2004a), Andreadis et al., 2005; Andreadis and Lettenmaier, 2006) are encouraging (section 5.2.2). Furthermore, biases in the modeling of the land surface budgets, through simplifications in the modeling and uncertainties in the parameter data, may result in errors in the trends (Sheffield et al., 2004a). These biases are generally unquantifiable but most importantly are systematic and therefore uniform over time. Therefore it is likely they will not impact the sign or strength of the calculated trends appreciably. We similarly argue that comparable results would be obtained if we used a different model. Inter-comparison of land surface models driven by the same forcings has been carried out regionally (Wood et al., 1998; Mitchell et al., 2004) and globally (Guo and Dirmeyer, 2006) and have concluded that although the models do poorly at reproducing the absolute values of observed soil moisture they do reasonably well at mimicking the anomalies and interannual variability. They may, therefore, provide useful information on drought occurrence and trends when viewed with respect to their own climatologies.

The PDSI can be considered as another type of model but designed specifically to monitor drought (although much simpler in its treatment of physical processes when compared to hydrologic land surface models) and has been used to assess trends in global drought previously (Dai et al., 2004; Burke et al., 2006). Burke et al. (2006) looked at trends in PDSI over the second half of the 20th century as calculated from i) the observation driven PDSI data set of Dai et al. (2004) and ii) a PDSI dataset driven by precipitation and temperature from coupled and uncoupled runs of the Hadley climate model. They found that the two datasets show a global drying trend of between -0.2 and -0.3 decade⁻¹ in PDSI units. This is at odds with the results of this paper that shows a small wetting trend globally, although the pattern of regional trends is similar (compare Figure 5.1 with their Figure 3). The difference is mainly because of the larger drying trend in the PDSI datasets for the last 20 years as shown by Burke et al. (2006) and Sheffield and Wood (2007) and is systematic of the PDSI, whether driven by the Burke et al. (2006), the Dai et al. (2004), or the VIC forcings (Sheffield and Wood, 2007). This may be due to a number of differences in the PDSI and VIC modeling approaches, such as the model time step (PDSI is monthly, VIC is 3hourly), the sensitivity of the model to precipitation and temperature changes (e.g., the PDSI uses the Thornthwaite method to calculate PE that may be biased for higher temperatures (Burke et al., 2006)), and the fundamental physical processes that are modeled (e.g. the PDSI does not include snow processes) and requires further investigation.

There are also a number of non-meteorological boundary conditions, such

as land cover, that are assumed time invariant (although vegetation parameters such as leaf area index do vary seasonally) but may actually have an appreciable impact on the trends. For example, anthropogenic factors, including irrigation, water withdrawals and land use change, and natural processes such as vegetation dynamics and wildfire, are not modeled explicitly and the impact of these may vary in time also, thus affecting the trends. Estimates of current day irrigation are that 16.3% of cultivated regions are equipped for irrigation (Siebert et al., 2005) which can have a significant impact on the water cycle (Haddeland et al., 2007), although historically this may have been offset by changes in land use. Land cover has changed dramatically over the past 300-years (Foley and Ramakutty, 1999) and more so in tropical/developing regions over the 20th century (Goldewijk, 2001). The impact that this has had on the water cycle may be substantial (Zhang and Schilling, 2006; Scanlon et al., 2007), likely reducing evapotranspiration and increasing runoff with possible implications for the results presented here. Furthermore, elevated levels of CO₂ and increased growing season length may be responsible for recent increases in net primary productivity (NPP) and thus transpiration (Friend et al., 2007), although stomatal closure response to elevated CO₂ levels may have had the opposite effect (Gedney et al., 2006).

5.6.2 Summary and conclusions

Global and regional trends in drought over the past 50 years are analyzed using a soil moisture based drought index over global terrestrial areas, excluding Greenland and Antarctica. Drought is described in terms of various statistics that summarize drought duration, intensity and severity. Trends in soil moisture and drought characteristics were calculated using a non-parametric trend test on a grid cell basis and for regional averages. Despite some uncertainties in the forcings and the modeling process we have confidence in the results as derived from a validated dataset, especially at larger scales and when put in context of other studies.

An overall increasing trend in global soil moisture, driven by increasing precipitation underlies the whole analysis, which is reflected most obviously over the western hemisphere and especially in North America. Regional variation is nevertheless apparent and significant drying over West Africa, as driven by decreasing Sahel precipitation, stands out. Elsewhere, Europe appears to have not experienced significant changes in soil moisture, a trait shared by southeast and southern Asia. Trends in drought characteristics are predominantly decreasing but statistically significant changes are limited in areal extent, of the order of 1.0 – 7.0% globally, depending on the drought threshold and variable and being generally less than 10% of continental areas. Concurrent changes in drought spatial extent are evident, with a global decreasing trend of -0.021 to -0.035% yr⁻¹. Regionally, drought extent over Africa has increased and is dominated by large increases over West Africa. Northern and East Asia show positive trends and central Asia and the Tibetan plateau show decreasing trends. In south Asia all trends are insignificant. Drought extent over Australia has decreased.

Over the Americas, trends are uniformly negative and mostly significant.

Within the long-term trends there are interannual and decadal variations in soil moisture and drought characteristics that are apparent in many regions. Globally, variations are driven mainly by ENSO variability, although the AMO appears to play an important role globally and in many regions, such as west and east Africa, central Asia and the high latitudes of North America. However, the short length of record relative to the scale of the AMO precludes any definite conclusions. High correlation values are found between the Mediterranean and the NAO, and southeast Asia and the Amazon basin and Nino3.4 SSTs. Stronger connection are likely at scales smaller than the regions examined here and by using seasonal and lagged correlations. The decadal variations in soil moisture and drought characteristics impact the robustness of the long-term trends. In general, they are responsible for diminishing the long-term trends. In fact, despite the overall wetting trend, there is a switch in later years to a drying trend, globally and in many regions, which is concurrent with increasing temperatures. Although drought is driven primarily by variability in precipitation, temperature has an effect that appears to be exaggerated in the last decade or so especially in high northern latitudes. This is most pertinent within the context of potential continued temperature increases during the 21st century.

Future climate projections from coupled models predict increases in global temperatures and generally increasing temperatures over land regions for most emission scenarios (e.g. Giorgi and Bi, 2005). The range in predictions varies among scenarios but is generally increasing. If temperature is a secondary forcing of drought (precipitation being the primary forcing) in most regions then the implication is that droughts will increase in the future, especially given the magnitude of predicted temperature increases. On the other hand, predicted changes in precipitation are highly variable in space and are scenario dependent to the extent that precipitation is predicted to increase in some regions and decrease in others (Giorgi and Bi, 2005). Temperature driven changes in drought will be modified by the changes to precipitation, although the fact that precipitation and temperature are anti-correlated in many regions (Trenberth and Shea, 2005; D  ry and Wood, 2005b), may lead to enhanced drought occurrence.

Acknowledgements

This work has been supported by NOAA grants NA86GP0248 and NA0303AR4310001 and NASA grant NAG5-9486. We thank three anonymous reviewers for their useful comments and suggestions.

Chapter 6

Projected changes in 21st century drought

This chapter is a slightly modified version of: Sheffield J., and E. F. Wood, Projected changes in drought occurrence under future global warming from multi-model, multi-scenario, IPCC AR4 simulations. *Clim. Dynam.*, in press.

Abstract

Recent and potential future increases in global temperatures are likely to be associated with impacts on the hydrologic cycle, including changes to precipitation and increases in extreme events such as droughts. We analyze changes in drought occurrence using soil moisture data for the SRES B1, A1B and A2 future climate scenarios from eight AOGCMs that participated in the IPCC AR4. The models show decreases in soil moisture globally for all future scenarios with a corresponding doubling of the spatial extent of severe soil moisture deficits and frequency of short-term (4-6 month duration) droughts from the mid 20th century to the end of the 21st. Long-term (more than 12 month duration) droughts become three times more common. Regionally, the Mediterranean, west African, central Asian and central American regions show large increases most notably for long term frequencies as do mid latitude North American regions but with larger variation between scenarios. In general, changes under the higher emission scenarios, A1B and A2 are the greatest, and despite following a reduced emissions pathway relative to the present day, the B1 scenario shows smaller but still substantial increases in drought, globally and for most regions. Increases in drought are driven primarily by reductions in precipitation with increased evaporation from higher temperatures modulating the changes. In some regions, increases in precipitation are offset by increased evaporation. Although the predicted future changes in drought occurrence are essentially monotonic increasing globally and in many regions, they are generally not statistically different from natural variability for multiple decades, in contrast to primary climate variables, such as global mean surface air temperature and precipitation. On the other hand, changes in annual and seasonal means of terrestrial hydrologic variables, such as evaporation and soil moisture, are essentially undetectable within the 21st century. Changes in the extremes of climate and their hydrological impacts may therefore be more detectable than changes in their means.

6.1 Introduction

The climate varies naturally in response to external forcings, such as solar radiation (Christensen and Lassen, 1991) and atmospheric aerosols (Robock and Mao, 1995), and because of internal interactions between components of the climate system (Trenberth and Hurrell, 1994). The extremes of these variations have consequences on the terrestrial water cycle that impact human activities in terms of changes to the availability or absence of water, e.g. flooding or drought (Higgins et al., 2000; Dai et al., 1998). When coupled with potential climate change, which may impact regionally and exaggerate the influence of natural variability, the extremes of climate may become more pronounced (Easterling et al., 2000; Palmer and Räisänen, 2002). To design and implement strategies to minimize climate change or mitigate against the detrimental impacts (Hasselmann, 2003), it is essential to be able to detect whether climate

change is actually occurring and to what extent. This is problematic because the climate change signal may be small relative to the natural variability of the climate system (Hulme et al., 1999) and may thus be undetectable, at least over the short term. The possibility then arises that by the time the signal becomes detectable, adverse impacts may have already occurred and it may be too late to reverse the change or even adapt to it (Pittock, 1999; King, 2004).

Climate change is often measured by changes in primary climate variables such as global surface air temperature and precipitation. These variables are first order drivers of climate impacts, inducing changes in weather extremes, sea ice thinning and glacier retreat, and thus are appropriate for studying the broader issues in climate change. They are also the best observed variables over large scales with relatively long historical records. Recent changes in climate may be large enough to be detectable now, although this will depend on the climate variable and our level of confidence in detecting change (Hergerl et al., 2006). Analysis of the instrumental record indicates that recent increases in global annual temperature are anomalous and more rapid compared to the long-term record (e.g. Jones et al., 1999; Hansen et al., 1999, Brohan et al., 2006) and model results suggest that this cannot be due to natural variability alone (Jansen et al., 2007). However, changes in global variables may bear little relation to regional changes, especially for precipitation (Giorgi and Bi, 2005) and thus changes in, for example, droughts and floods that may have serious impacts on human and environmental welfare.

The potential acceleration of the hydrologic cycle under recent and future global warming is of considerable interest (Huntington, 2006), especially in terms of changes in regional variability and extremes. Of all natural disasters, the economic and environmental consequences of drought are among the highest, due primarily to the longevity and widespread spatial extent of many droughts (Wilhite, 2000). Thus the potential impacts of climate change on drought are most pertinent. As temperatures rise, the capacity of the atmosphere to hold moisture would increase as governed by the Clausius-Clapeyron equation (Held and Soden, 2000), with potential for increased evaporation and/or precipitation (Trenberth, 1999), although these may be limited by other factors such as available energy and aerosol concentration. Climate model studies have shown that variability is likely to increase under plausible future climate scenarios (Wetherald and Manabe, 2002), dependent upon climate sensitivity, with large regional changes in the water cycle. The potential for more droughts and of greater severity is a worrisome possibility (Gregory et al., 1997; Wetherald and Manabe, 1999; Wang 2005).

Several studies using climate models have suggested that the interior of the northern hemisphere continents will become drier over the next century, especially in the summer (Rind et al, 1990; Gregory et al., 1997; Wetherald and Manabe 1995; 1999; 2002). Gregory et al. (1997) analyzed summer drought over southern Europe and central North America in terms of precipitation and soil moisture from a single integration of the Hadley climate model forced by $1\% \text{ yr}^{-1}$ increasing CO_2 concentrations. They found increases in multivariate drought statistics that were driven primarily by evaporation

through increased temperatures but also decreased precipitation in the form of fewer events. Wetherald and Manabe (1999) analyzed soil moisture from the GFDL climate model for three scenarios: increasing greenhouse gases, increasing sulphate-aerosol and combination of both. They similarly found summer dryness and winter wetness in North America and southern Europe as well as other semi-arid regions, although high latitudes showed increasing wetness. Based on a threshold of one standard deviation, changes in soil moisture did not become detectable for several decades. In summarizing such studies, the third Intergovernmental Panel on Climate Change (IPCC) report (IPCC, 2001) concluded that increased drought risk over these regions was “likely”.

More recently, Giorgi (2006) analysed a set of IPCC 4th Assessment Report (AR4) simulations and calculated a climate change index based on changes in precipitation and temperatures means and variability. He found major climate change “hot-spots” in the Mediterranean and Northern Europe, followed by high northern latitudes and Central America. Other hot-spots occur in Southern Equatorial Africa, the Sahara and eastern North America. Wang (2005) analyzed a large set of IPCC AR4 models in terms of consensus changes in precipitation, temperature and soil moisture and found inter-model consistency in some regions of northern mid- and high-latitudes in predicting summer dryness and winter wetness. In terms of drought, Burke et al. (2006) calculated the Palmer Drought Severity Index (PDSI), a commonly used drought index, from the latest version for the Hadley centre climate model for the SRES A2 scenario and found regionally strong wetting and drying, but a net global drying trend resulting in an increase in the area of extreme drought from 1% to 30% by end of this century. The conclusion of the latest IPCC report (IPCC, 2007, chapter 10, pg 783) was that “In a warmer future climate, most Atmosphere-Ocean General Circulation Models project increased summer dryness and winter wetness in most parts of the northern middle and high latitudes. Summer dryness indicates a greater risk of drought.”

The consensus from these and other studies into the hydrologic impacts of future warming and the synthesis conclusions of the past two IPCC reports point towards a greater risk of drought during the 21st century. In this paper we investigate how drought is expected to change in the future by analyzing soil moisture and drought characteristics over global land areas, excluding Antarctica, from a suite of climate model simulations carried out under the auspices of the IPCC AR4. We quantify the change in global and regional drought occurrence relative to the pre-industrial era as represented by climate model control simulations. We take into account the uncertainty in regional climate change by using data from multiple climate models and for three future climate scenarios that represent a range of plausible emission pathways.

Although global warming is expected to accelerate the hydrologic cycle and thus the occurrence and severity of drought, the changes may not become detectable for several decades (Wetherald and Manabe, 1999). The detectability of climate change can be quantified by how long we have to monitor for to detect significant changes against the background of natural variability, which is basically a signal to noise problem (McCabe and Wolock, 1997; Zheng and

Basher, 1999; Ziegler et al., 2003). The greater the variability, the harder it is to detect a signal. We use this concept to evaluate the detectability of potential future changes by applying statistical analyses to time series of drought occurrence to determine when and where changes will become detectable. Detectability is a function of the natural variability of the system, the magnitude of the change we are interested in and the level of risk we are prepared to accept in statistical testing, among others factors, and we carry out a set of sensitivity experiments to evaluate their impact.

This study is the first that we are aware of that analyzes potential changes in drought under future global warming, as characterized by persistence in severe soil moisture deficits, from multiple models and scenarios. Previous studies have assessed predicted changes in mean climate and specifically soil moisture (Wetherald and Manabe, 2002; Wang 2005) that will likely (but not necessarily) induce changes in drought. Here, we take into consideration changes in the full distribution of pertinent variables and not just the mean or some other tendency measure. Furthermore, we analyze actual model output as opposed to derived products such as the PDSI that may suffer from inadequacies which will enhance uncertainty in the results. In terms of models and scenarios analyzed, previous studies have focused on single models and/or single scenarios (e.g. Wetherald and Manabe, 2002; Wang 2005; Burke et al., 2006). To instill confidence in the robustness of assessment of future change, it must take into account the uncertainty in future climates because of model differences as well as the diversity of possible emission pathways as represented by the different scenarios. Nevertheless, uncertainties are inherent in this study, such as biases induced by the specific models and approaches we take and we highlight these where relevant.

The paper is laid out as follows. After presenting the datasets and methods we briefly evaluate how well the models represent drought during the 20th century against off-line estimates. We then show how drought is expected to change over the 21st century for the three future climate scenarios, globally and regionally, and where these changes are statistically significant relative to natural variability as derived from pre-industrial control simulations. Mechanisms for the expected changes are presented next, that show how changes in evaporation, as forced by increasing temperatures, modify the primary impacts of precipitation changes and how this can be altered by changes in snow at higher latitudes. In section 6.4 we investigate the detectability of these changes and how this depends on the time period, drought characteristic, level of significance and background variability against which the change is quantified. This section also looks at how drought detectability compares to that for other hydro-climatic variables and whether we are likely to detect changes in extremes, such as drought, earlier than changes in the mean of primary climate variables, such as annual precipitation.

6.2 Datasets and methods

6.2.1 Climate model simulations

To estimate potential future climate change we use data from the IPCC AR4 General Circulation Model (GCM) simulations. The range of future climates predicted by GCMs is large and regionally dependent (NRC, 2003; Giorgi and Bi, 2005) and we therefore use data from multiple GCMs and three scenarios: the Special Report on Emissions Scenarios (SRES) A2, A1B and B1 (Nakicenovic et al., 2000). Each scenario represents different mixes of changes in population, economic output, land use, and energy and technology use, among others, but can be generally characterized by maximum atmospheric CO₂ concentrations. B1 represents relatively slow population growth and an emphasis on environmental protection, with CO₂ concentrations stabilized at 550ppm by the end of the century. A1B describes a future of very rapid economic growth, global population that peaks in mid-century and declines thereafter, and the rapid introduction of new and more efficient technologies with a balance between fossil and non-fossil energy sources and is characterized by maximum concentrations of 720ppm. A2 describes a heterogeneous world with continuously increasing global population and regionally orientated economic development and fragmented technological change and is generally regarded as a worst-case scenario that sees a four to five fold increase in CO₂ emissions over 2000-99 during which CO₂ concentrations increase from about 350 to 850ppm. We also use data from the corresponding pre-industrial control (PICNTRL) and 20th century simulations (20C3M), which were also run in coupled mode, i.e. with a free-running ocean component. The 20C3M simulations are driven by prescribed historical greenhouse gas concentrations, sulphate-aerosol loadings and other forcings since the start of the industrial revolution. We use data for eight models (Table 6.1) which were selected as those which had soil moisture and ancillary data available for all these scenarios. Where ensemble simulations for a particular scenario were available we use the first ensemble member but it should be noted that single simulations were available more often than not.

6.2.2 Drought estimation

We define drought occurrence as an extended period of anomalously low soil moisture. The amount of water in the soil provides a useful indicator of drought as it reflects the aggregate effect of all hydrologic processes from changes in short-term precipitation events and temperature swings to long-term changes in climate, and can represent the status of agriculture and potential hydrologic recharge to rivers and reservoirs (Sheffield et al., 2004). Empirical probability distributions are derived for the modelled soil moisture fields for each month from the pre-industrial control simulations and the current state of drought is characterized by the quantile of the current soil moisture value in relation to the control period distribution. A drought is defined as a consecutive sequence of months of length D with soil moisture quantile values, $q(\theta)$, less than a

Model Name	Modeling Group	Country
CGCM3.1(T47)	Canadian Centre for Climate Modelling & Analysis	Canada
GFDL-CM2.1	US Dept. of Commerce / NOAA / Geophysical Fluid Dynamics Laboratory	USA
GISS-ER	NASA / Goddard Institute for Space Studies	USA
INM-CM3.0	Institute for Numerical Mathematics	Russia
IPSL-CM4	Institut Pierre Simon Laplace	France
MIROC3.2(medres)	Center for Climate System Research (The University of Tokyo), National Institute for Environmental Studies, and Frontier Research Center for Global Change (JAMSTEC)	Japan
MRI-CGCM2.3.2	Meteorological Research Institute	Japan
ECHAM5/MPI-OM	Max Planck Institute for Meteorology	Germany

Table 6.1: Models used in this study, which have monthly soil moisture data available for the PICNTRL, 20C3M and SRES B1, A1B and A2 scenarios.

chosen threshold, $q_0(\theta)$. Here we use a value of 10%, which reflects conditions that occur only once every 10 years for a particular month on average and so reflects rare events, and has been shown to be applicable to identifying historic events at global scales (Sheffield and Wood, 2007). We are particularly interested in how individual dry months are organized into sequences of consecutive dry months that can then be considered a drought with associated deleterious impacts. Drought can be characterized in various ways and we define a number of statistics based on duration (D), intensity (I), severity (S) and areal extent (A) that are also dependent on $q_0(\theta)$:

$$I = \frac{1}{D} \sum_{t=t_1}^{t+D-1} q_0(\theta) - q(\theta)_t \quad (6.1)$$

$$S = I \times D \quad (6.2)$$

Intensity is the mean magnitude over the duration of the drought and severity is the time integrated deficit below the threshold. We also define three classes of drought depending on their duration: short-term (4-6 months), medium term (7-12 months), and long-term (longer than 12 months).

$$D_{4-6}, \text{ short-term} : \quad 4 \leq D \leq 6, \quad q(\theta) \leq q_0(\theta) \quad (6.3)$$

$$D_{7-12}, \text{ medium-term} : \quad 7 \leq D \leq 12, \quad q(\theta) \leq q_0(\theta) \quad (6.4)$$

$$D_{12+}, \text{ long-term} : \quad D > 12, \quad q(\theta) \leq q_0(\theta) \quad (6.5)$$

The spatial extent of drought, A , is defined as follows:

$$A = \frac{\sum_{i=1}^N A(i) = \{q(\theta) \leq q_0(\theta)\}}{\sum_{i=1}^N A(i)} \quad (6.6)$$

where $A(i)$ is the area of grid cell i weighted by the cosine of the grid cell latitude and N is the total number of grid cells in the region of interest.

6.2.3 Statistical methods

Changes in the occurrence of drought are calculated between the pre-industrial control and future climate simulations from the ensemble of climate models. To show how future changes compare to modeled present day conditions, we also show results relative to the 20th century simulations in section 6.4.4. For each model, we calculated the frequency of drought and other statistics in each 30-year period within the control simulation and in 30-year periods in the future climate simulation. In this way we take into account the uncertainty due to model differences and the natural variability of the climate system as represented by the control simulations. To account for the differences in simulation length among models, which would bias the results towards a model with a longer control simulation, we averaged the results over the 30-yr periods in the control simulations.

Changes in drought are identified by testing the null hypothesis that the distribution of a drought statistic across all models has the same mean as the distribution across all models during a future time period. The Student's t-test statistic, which is a measure of the ratio of the difference in means to the combined variance of the two distributions, is calculated at each grid cell and the null hypothesis is rejected for t-test values greater than the critical value at confidence level α (usually taken as 0.05 or 95%). In this case we conclude that a statistically significant change has occurred. Application of the test assumes that the means of the two samples do not deviate substantially from a normal distribution.

6.2.4 Data preparation

We focus on monthly values for all calculations, which is the smallest time scale for which data are available for the complete period of each simulation from the IPCC database. Monthly values of soil moisture for each model are available as

depths of water and are normalized to volumetric values by dividing by the field capacity, which is given for each model as a fixed field. This ensures that the soil moisture data for each model are analyzed with respect to their dynamic range as governed by soil characteristics and meteorological conditions, and are thus inter-comparable. The volumetric data are then interpolated from each model's native grid to a 2.0 degree regular grid, which is a representative scale across the set of models. Ancillary variables (e.g. precipitation) that are used in subsequent analysis of drought forcing are interpolated in the same manner.

6.3 Results

First, we evaluate the representation of drought in the climate models by considering i) the natural occurrence of drought as derived from the control simulations and ii) drought under contemporary climate from the 20th century simulations. In section 6.3.2 we compare the 20th century results with observation-based data to determine whether the models are capable of reproducing our best estimates of large scale contemporary drought occurrence.

6.3.1 Natural variability of drought from GCM control simulations

Figure 6.1 shows the global distribution of drought statistics in terms of the multi-model ensemble mean. The statistics are the frequency of D_{4-6} and D_{12+} droughts, the mean drought duration, D_{mean} , and the mean drought severity, S_{mean} . For each model, the drought statistics are calculated over 30-yr blocks within the control period and then the mean is calculated over all blocks. The maps in Figure 6.1 show the multi-model mean and standard deviation (inter-model variability) of the individual model means.

For D_{4-6} droughts, the highest frequencies are located in mid-latitudes and the Tropics, with peak values of about 1-2 droughts per 30 years in the Pacific northwest and eastern United States, central Europe and Asia, China and central Africa. Low frequencies (< 0.5 droughts 30 yr⁻¹) occur in arid regions where soil moisture is persistently low and does not change much from year to year, and in high latitudes where freezing temperatures and snow cover prolong soil moisture anomalies (Wang, 2005; Sheffield and Wood, 2007). The standard deviation or inter-model variability of is largest in regions of high seasonality, such as the edges of the footprint of the Inter Tropical Convergence Zone (ITCZ) in Africa and lowest in dry regions and high latitudes.

The distribution of D_{12+} frequencies is generally the opposite of that for short-term droughts, with maxima in central and northern North America, eastern south America, Siberia, and eastern Asia among others. High values are also prevalent in dry regions although as the range in soil moisture is so small, the absolute magnitude of drought is also very small. Minima are mostly located in regions with more seasonally uniform climates such as central tropical Africa, parts of southeast Asia and the eastern and Pacific northwest coasts of

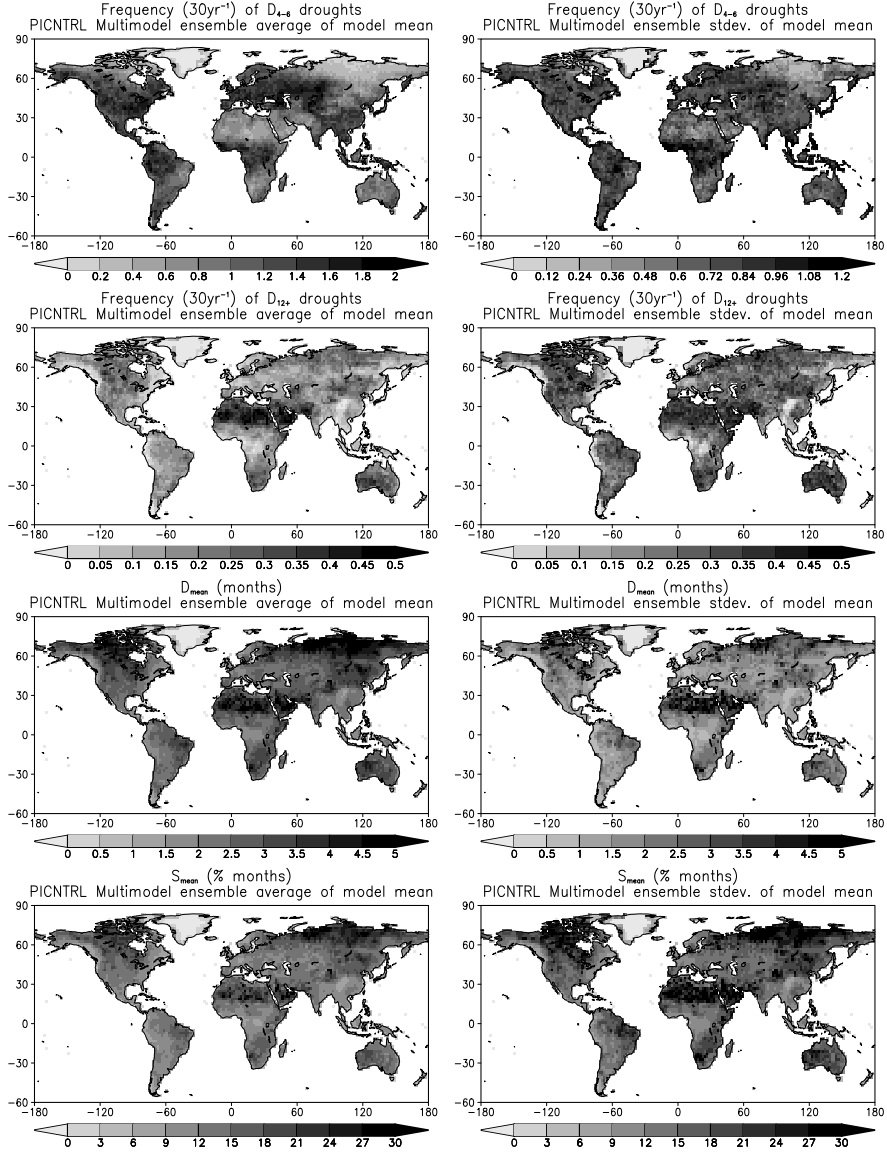


Figure 6.1: Multimodel ensemble drought statistics for the pre-industrial control (PICNTRL) simulation. The statistics are number of 3-6 month duration droughts (30yr⁻¹), number of 12+ month duration droughts (30yr⁻¹), mean drought duration (months) and mean drought severity (% months). The statistics are calculated for 30-yr periods within the each models control period and then averaged all 30 year periods. The multimodel ensemble mean and standard deviation are shown on the left and right hand side respectively.

North America. The standard deviation values are also at a maximum in high latitudes and globally are relatively high compared with the mean, possibly indicating a lack of consensus across models in how drought varies on longer time scales. Mean drought duration and severity are similarly distributed being that severity is dominated by drought duration at low threshold values. Mean drought duration is at a maximum in high latitudes, central North America, Brazil, southern Africa and Australia.

6.3.2 20th century drought and comparison with off-line modeling

Comparison of soil moisture data from the IPCC AR4 20C3M simulations with field measurements have been carried out by Li et al., (2007) over small regions in the Northern Hemisphere based on the database of Robock et al. (2002). They found that the models simulated the seasonal cycles for Ukraine, Russia, and Illinois adequately, but were generally poor for Mongolia and China. Importantly, all models failed to replicate observed summer drying in Russia and the Ukraine during the latter part of the 20th century. Here we are interested in the large-scale, long-term statistics of drought as characterized by persistent soil moisture deficits. A comparison of global and regional averaged drought characteristics from the 20C3M simulations with observation-based estimates is shown in Figure 6.2. The regions are defined by Giorgi and Francisco (2000) with the inclusion of the northeast Canada region (NEC) in place of the Canadian-Greenland (GRL) region. We also define the WORLD region as continental land areas excluding Greenland and Antarctica. The observation-based statistics are derived from off-line simulations using the Variable Infiltration Capacity (VIC) land surface model (Sheffield and Wood, 2007), forced by an observation-based meteorological dataset (Sheffield et al., 2006). Because of the lack of large scale, long-term monitoring of soil moisture, observation forced off-line modeling provides the best possible estimate of historic soil moisture values at continental to global scales (Maurer et al., 2002; Sheffield et al., 2006, Guo and Dirmeyer, 2006).

The climate model values in Figure 6.2 generally encapsulate observation-based values, although the spread among models and the occurrence of outliers can be large depending on the region and statistic (e.g. CAM for D_{4-6} , SAS for D_{12+} , AUS for D_{mean}). For D_{4-6} droughts the agreement is remarkably good and the observation-based values fall within the maximum and minimum range for all regions and generally lie within the inter-quartile range of the model distribution. This is consistent with Seneviratne et al., (2006) who, as part of the Global Land Atmosphere Coupling Experiment (GLACE), showed that AGCMS were capable of distinguishing between observed regions of high and low soil moisture memory on monthly time scales. For the other drought statistics, the climate model values tend to be higher, most notably for D_{12+} frequencies and S_{mean} , although for the former this is a result, in part, of the zero lower bound in most regions. The general overestimation by the models of long term drought frequencies and mean drought duration points to an under-

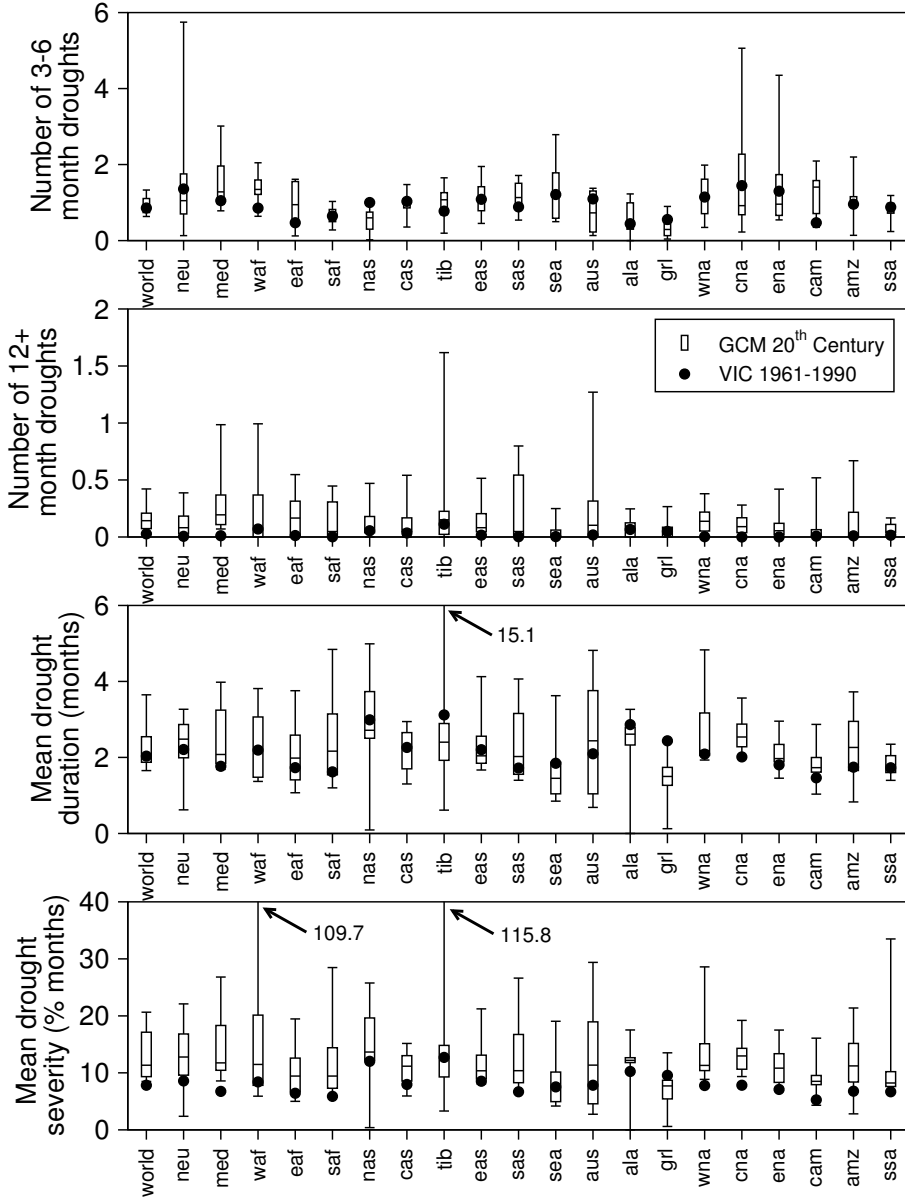


Figure 6.2: Regionally averaged D_{4-6} and D_{12+} frequencies, D_{mean} and S_{mean} for 1961-1990 from the 20th century (20C3M) simulations (box and whispers) and an observation forced land surface model simulation (black dots). The box and whispers represent the inter-quartile range and the range (maximum and minimum values) of the set of GCMs.

estimation of climate variability that has been noted previously (e.g. Collins et al., 2002; Hunt, 2006).

6.3.3 Global and regional drought under future climate scenarios

Next we investigate how soil moisture and drought are predicted to change under future climates. Global averaged time series of monthly mean soil moisture and drought characteristics for the three future climate scenarios are shown in Figure 6.3. For these models, the future climate simulations were initialized from the end of the 20C3M simulation and we prepend these data (in terms of the multi-model distribution) to the future scenario time series. Globally, soil moisture decreases under all scenarios, with corresponding increases in drought spatial extent. Note that the spatial extent of drought may not be contiguous which is more likely for larger regions. Corresponding changes in drought statistics (frequency of D_{4-6} and D_{12+} droughts and S_{mean}) are all increasing. In general, the increases in drought statistics are greatest under the higher emissions scenario, A2, and least under the lower emissions scenario, B1 (Table 6.2). The global spatial extent of drought across all models roughly doubles by 2070-99 under all scenarios relative to the control scenario. The frequency of D_{4-6} droughts also doubles and D_{12+} droughts become over three times more frequent. The spread in model projections as quantified by the inter-quartile range (IQR) is, however, fairly large, even at the beginning of the 21st century (also noted previously in the 20th century comparisons in section 6.3.2) and this increases by the end of the century, such that the lower bound on projections shows little change over the century, although these are invariably increases.

Figures 6.4-6.6 show the multi-model mean, regionally averaged time series of D_{4-6} and D_{12+} frequencies and A . Similar to the global results, most regions show increases in drought statistics, but with large variation between regions and across scenarios. In particular, the MED, WAF, CAS and CAM regions show large increases, most notably for D_{12+} frequencies. The mid latitude North American regions (WNA, CNA, ENA) also show increases but with larger variation between scenarios. Changes over high latitudes (ALA, NEC, NEU, NAS), eastern mid-latitude Asia (EAS, TIB) and regions bordering the Indian ocean (EAF, SAS, SEA) are relatively small. The frequency of D_{12+} droughts actually decreases in NEU. Again, changes under the B1 scenario are the least and the A1B and A2 results are similar.

6.3.4 Statistical significance of changes

We next evaluated the statistical significance of changes in drought by the end of the 21st century with respect to natural variability as represented by the model control simulation (Figures 6.7 and 6.8). In general, D_{4-6} drought frequency increases globally between the control and the future period (Figure 6.7). Large areas experience greater than 5 short-term droughts per 30 years (averaged over all models) that are statistically significant at the 95% level, in-

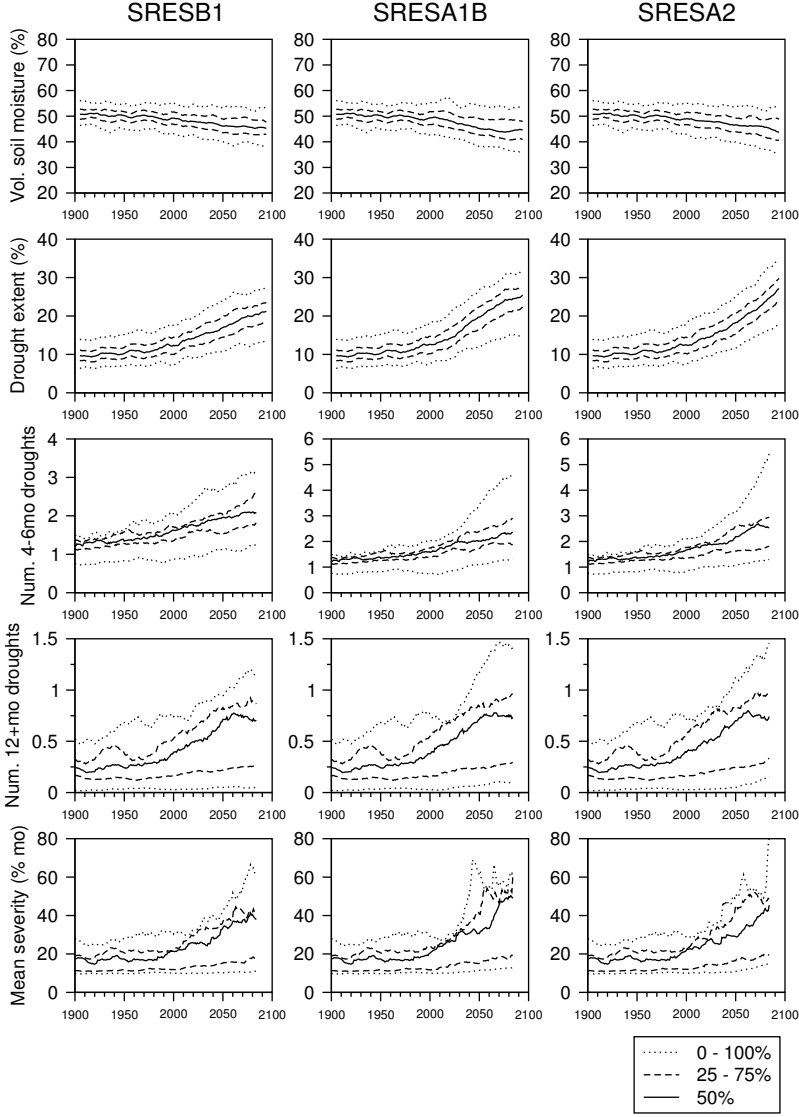


Figure 6.3: Global average time series of soil moisture and various drought statistics for the 21st century for the SRESB1, SRESA1B and SRESA2 scenarios. Monthly soil moisture and drought extent ($q_0(\theta) = 10.0\%$) is shown as the 121-month running mean. The frequency of 3-6 month duration droughts ($q_0(\theta) = 10.0\%$), 12+ month duration droughts ($q_0(\theta) = 50.0\%$) and the maximum severity (defined as the drought intensity times the drought duration) are calculated over a 30-yr moving window. The data are shown as the 0, 25, 50, 75 and 100% percentiles of the distribution of the multimodel ensemble of soil moisture and drought statistics.

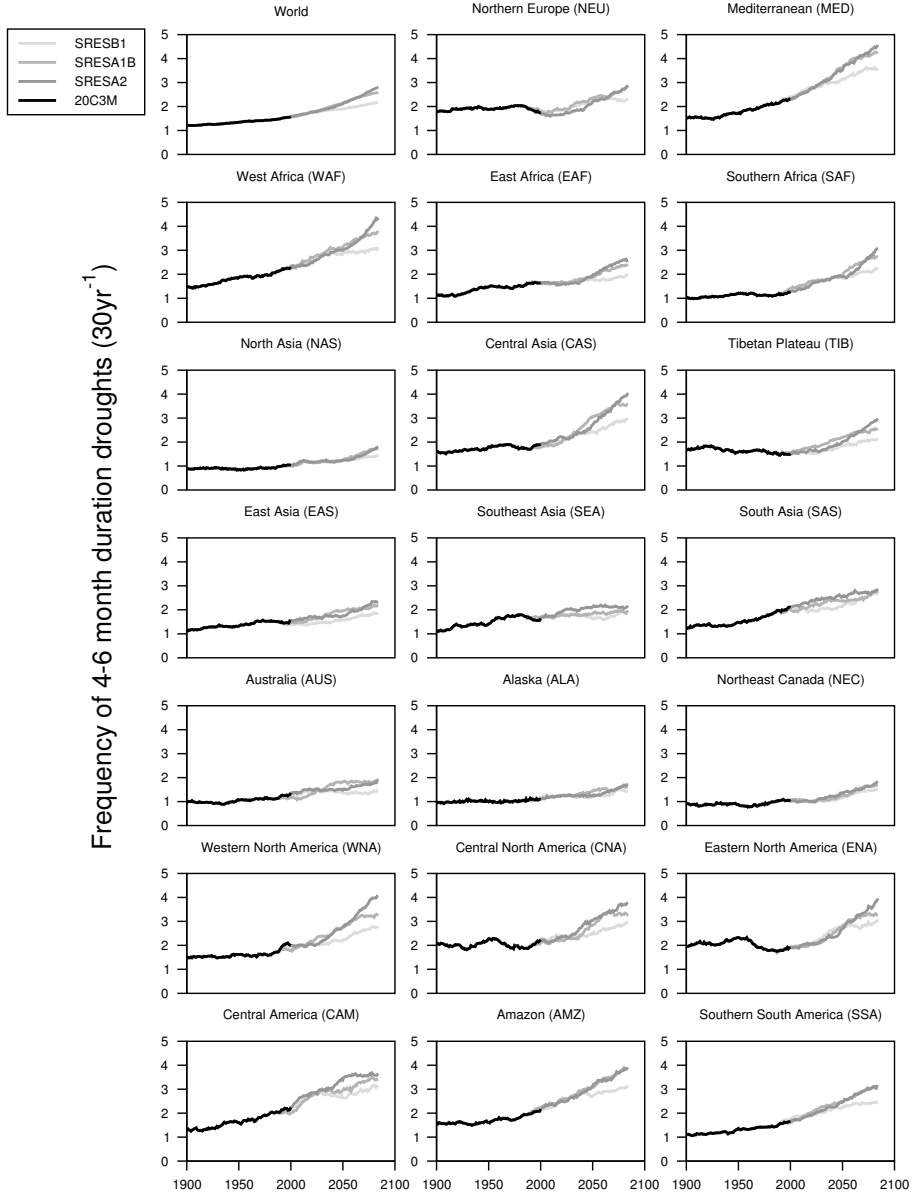


Figure 6.4: Regional time series of multimodel ensemble mean of frequency of short-term droughts (D_{3-6} , $q_0(\theta) = 10.0\%$) for the 21st century for the SRESB1, SRESA1B and SRESA2 scenarios. The values are calculated over a 30-yr moving window and then averaged over each region.

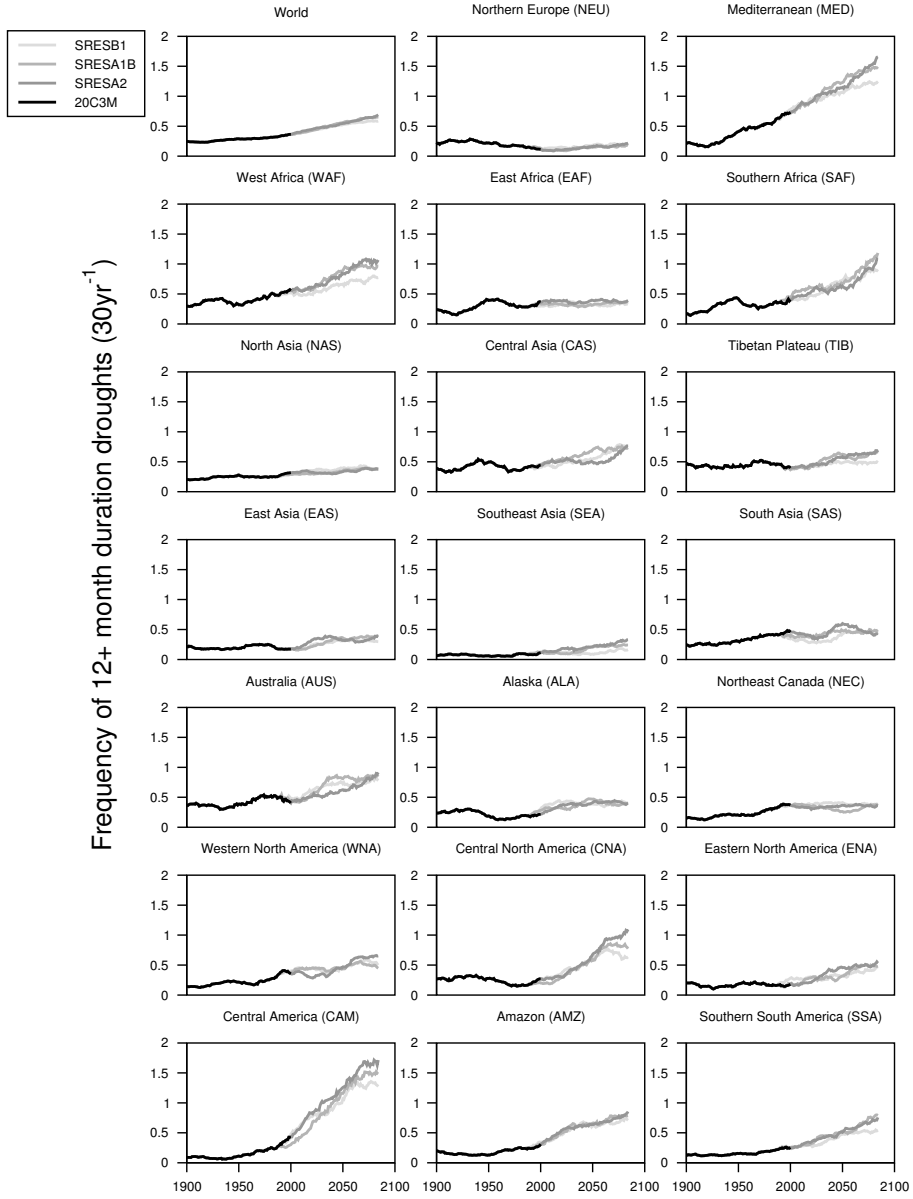


Figure 6.5: As Figure 6.4 but for long-term (D_{12+}) drought frequency.

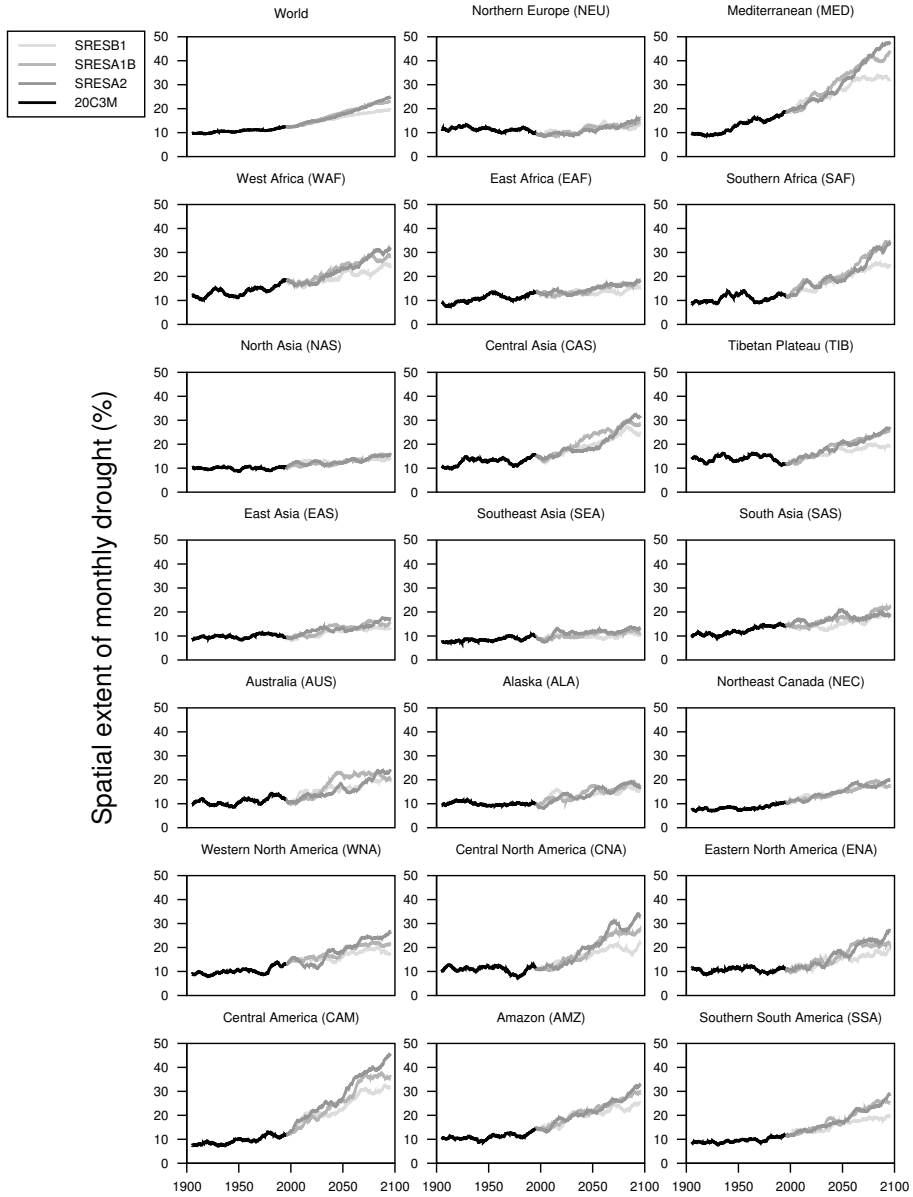


Figure 6.6: As Figure 6.4 but for the spatial extent of monthly drought, $q_0(\theta) = 10\%$.

	PICNTRL	20C3M (1961-90)	SRES B1 (2070-99)	SRES A1B (2070-99)	SRES A2 (2070-99)
SM (%)	50.8, 0.9	49.8, 3.8	45.8, 5.6	44.7, 7.4	44.9, 7.3
A (%)	9.2, 1.0	11.2, 3.5	18.9, 6.2	22.3, 7.2	18.9, 6.7
D_{4-6} ($30yr^{-1}$)	1.2, 8.3	1.4, 0.3	2.1, 0.8	2.4, 1.0	2.5, 1.1
D_{12+} ($30yr^{-1}$)	0.2, 2.1	0.3, 0.2	0.7, 0.6	0.7, 0.7	0.7, 0.6
D_{mean} (mos.)	3.0, 2.0	3.2, 1.7	5.4, 3.3	6.6, 4.9	6.3, 3.6
S_{mean} (mos. %)	14.8, 9.9	17.2, 9.3	38.0, 22.2	48.9, 40.7	45.3, 29.3

Table 6.2: Summary of multi-model global mean soil moisture and drought characteristics for the PICNTRL, 20C3M and future climate SRES B1, A1B and A2 scenarios. The first of each pair of values is the multi-model mean and the second is the multi-model IQR. The individual model PICNTRL values are calculated as the average over the whole simulation period, which varies among models and is between 330 and 500 years.

cluding southern Europe, large parts of the US and Central America, southern South America, central west Africa and parts of southern Asia. Statistically significant changes in D_{12+} drought frequency are less spatially extensive (Figure 6.8), with both increases and decreases scattered across the globe. Decreases are mostly restricted to high latitudes and generally result in zero frequencies. Increases in the southern US, Central America, the Mediterranean and southern Africa, are of the order of 2 droughts $30yr^{-1}$. The spatial distribution of changes is fairly robust across scenarios, but with magnitudes greatest under the A2 scenario, and lowest under B1. Figure 6.9 and Table 6.3 summarize the regionally averaged D_{4-6} and D_{12+} drought frequencies and spatial extent of drought for the PICNTRL simulation and the predicted changes and their statistical significance for the 20C3M (1961-1990) and the three future climate scenarios (2070-2099). Note that increases in D_{4-6} drought frequency and spatial extent are statistically significant for most regions and scenarios. Significant changes in D_{12+} frequencies are restricted to the MED, WAF, SAF, CAS, CAM, SSA and WORLD regions for all scenarios and in TIB and CNA for the higher emission scenarios only. In particular the MED region shows more than 3, 6 and 4 times increase in D_{4-6} and D_{12+} drought frequency and A, respectively.

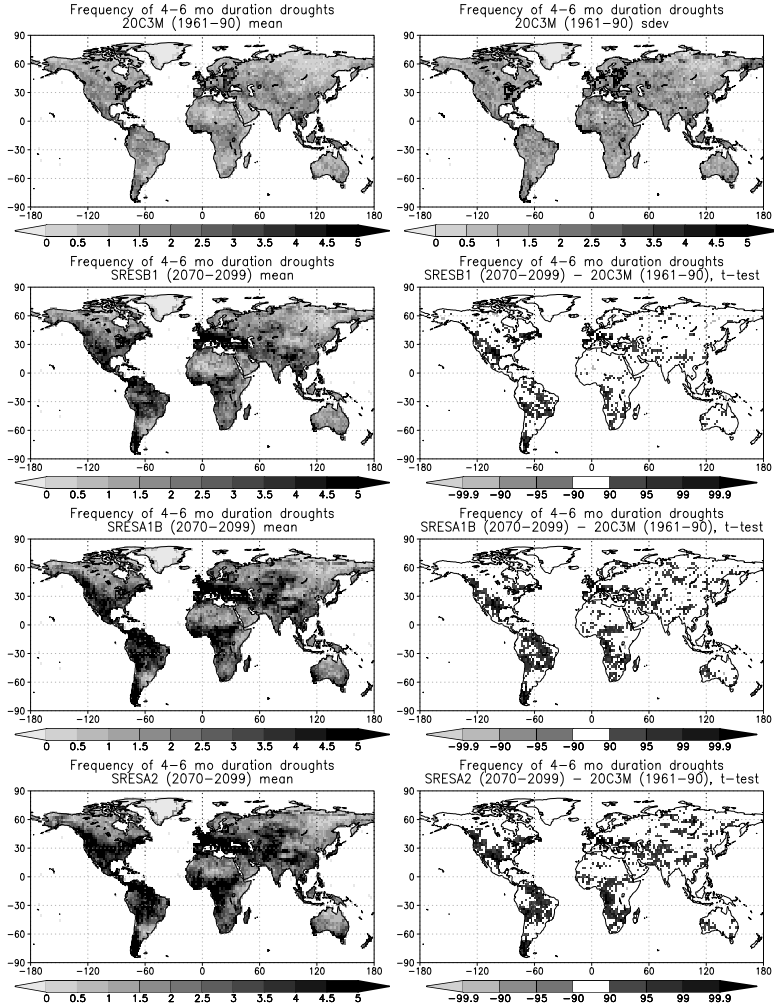


Figure 6.7: Multimodel ensemble mean of frequency of D_{4-6} droughts in the control simulation (PICNTRL) and for 2070-99 in the SRESB1, SRESA1B and SRESA2 future climate scenarios. Also shown are the standard deviation of the PICNTRL multimodel ensemble and the statistical significance of the difference in ensemble means between the PICNTRL simulation and the future climate predictions. Statistically significant changes were estimated by calculating t-test statistics under the null hypothesis that the mean of distribution of control period drought frequency equals the mean of distribution for the future climate period. Results are shown for significance levels of 90.0, 95.0, 99.0 and 99.9% with negative values indicating a decrease in the frequency of drought.

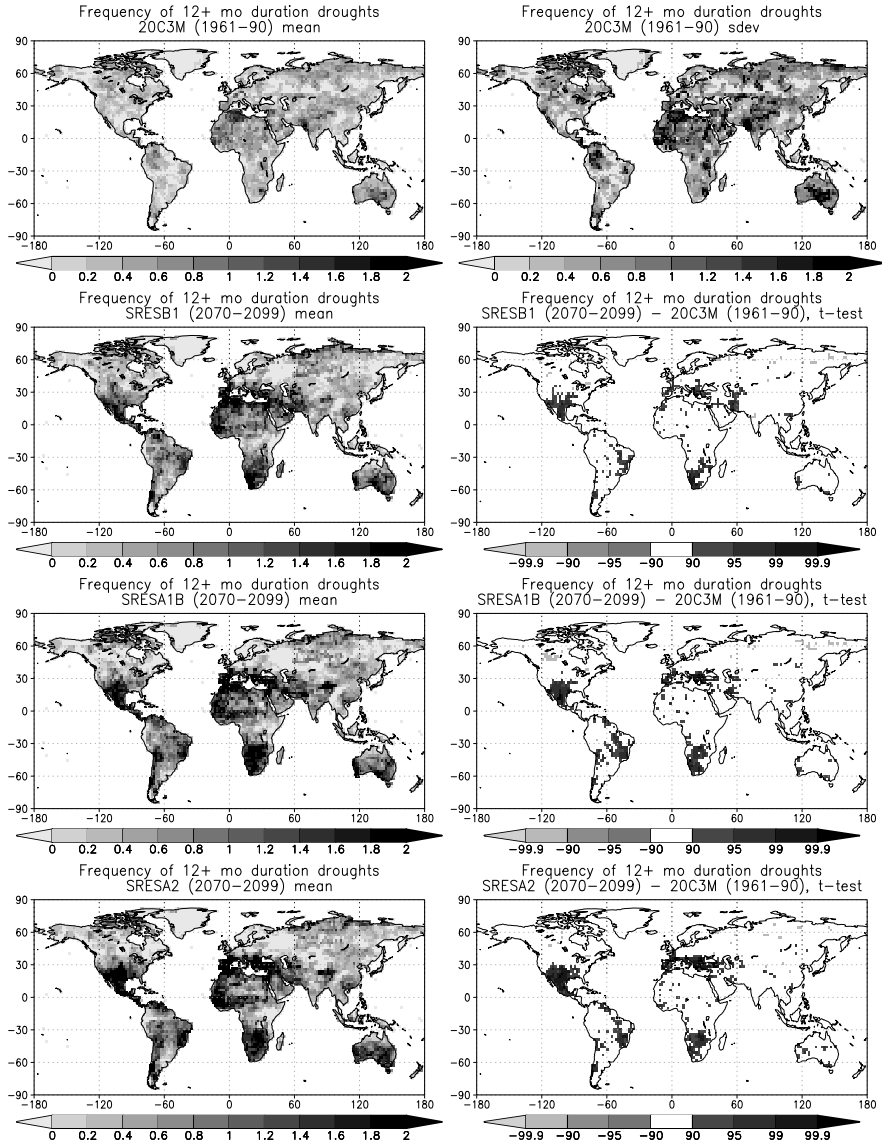


Figure 6.8: As for Figure 6.7, but for frequency of D_{12+} droughts.

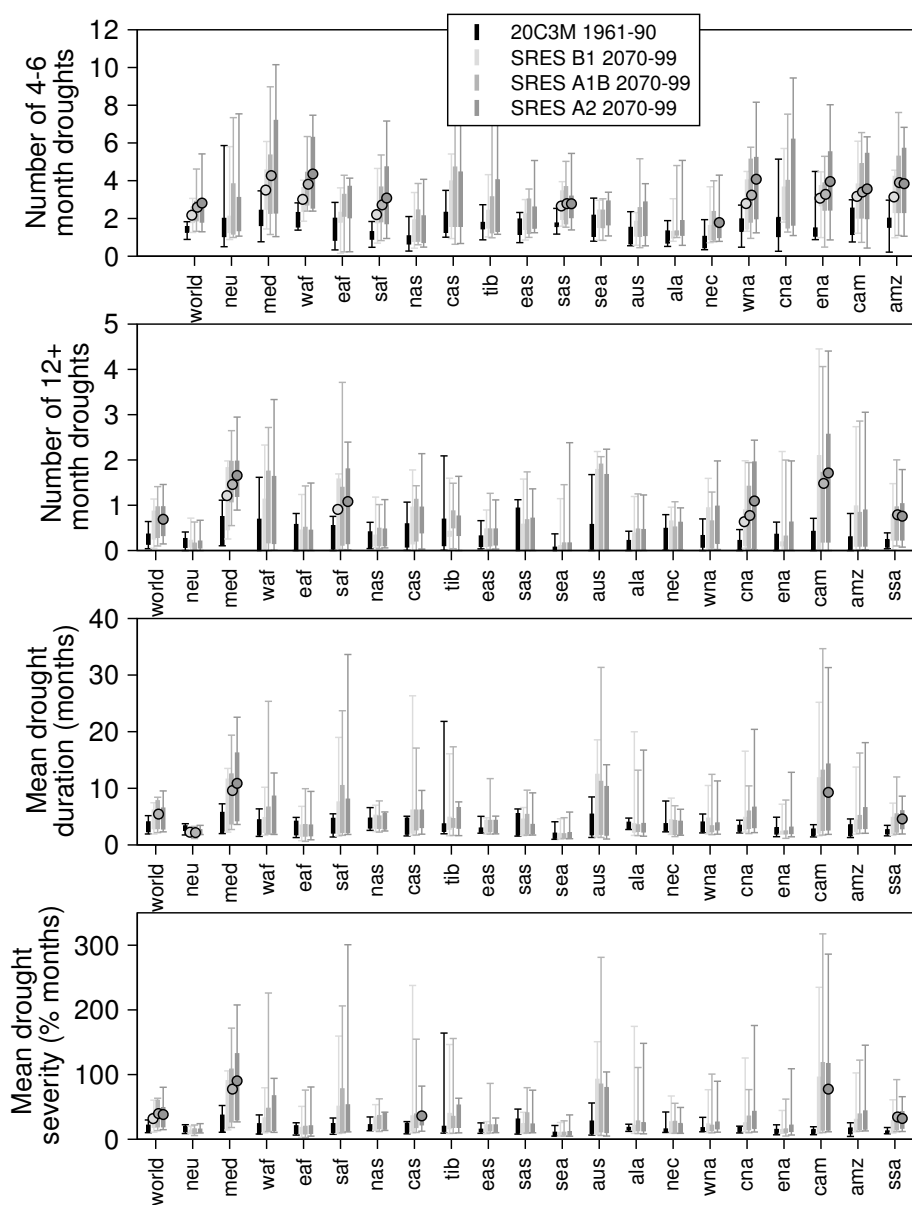


Figure 6.9: Regionally averaged drought statistics for 1961-90 (20C3M) and three future climate scenarios for 2070-99 (SRES B1, SRES A1B, SRES A2). Drought statistics are frequency of 3-6 month duration droughts, frequency of 12+ month duration droughts, mean drought duration and mean drought severity. Box and whiskers represent the inter quartile range and maximum and minimum values of the set of models. The mean model value is shown as colored circles if the change is statistically significant at the 95% level relative to the control simulation (PICNTRL).

	D_{4-6}					D_{12+}					A				
	PIC	20C	B1	A1B	A2	PIC	20C	B1	A1B	A2	PIC	20C	B1	A1B	A2
WORLD	1.1	1.4	2.2	2.6	2.8	0.2	0.3	0.6	0.7	0.7	9.2	11.2	18.9	22.3	23.0
NEU	1.4	2.0	2.3	2.9	2.9	0.1	0.2	0.2	0.2	0.2	9.2	11.1	12.3	13.3	14.1
MED	1.2	2.1	3.5	4.3	4.6	0.2	0.5	1.2	1.5	1.7	8.7	15.7	32.7	41.4	44.7
WAF	1.3	2.0	3.0	3.8	4.4	0.2	0.5	0.8	1.0	1.1	9.9	15.1	23.0	27.9	30.2
EAF	1.2	1.5	2.0	2.4	2.6	0.2	0.3	0.3	0.4	0.4	9.7	11.2	14.5	16.9	17.1
SAF	0.9	1.1	2.2	2.7	3.1	0.2	0.3	0.9	1.2	1.1	9.4	10.3	24.3	31.7	30.7
NAS	1.0	0.9	1.5	1.7	1.8	0.2	0.2	0.4	0.4	0.4	9.8	9.9	13.6	15.0	14.9
CAS	1.4	1.8	2.9	3.6	4.0	0.2	0.4	0.7	0.7	0.8	9.9	12.8	25.0	27.9	29.2
TIB	1.5	1.7	2.1	2.6	3.0	0.2	0.5	0.5	0.7	0.7	10.0	14.8	19.4	24.1	24.4
EAS	1.3	1.5	1.8	2.2	2.3	0.2	0.2	0.3	0.4	0.4	9.3	10.5	13.1	15.5	15.7
SAS	1.3	1.7	2.7	2.8	2.8	0.2	0.4	0.5	0.5	0.4	9.4	14.0	17.9	20.4	18.5
SEA	1.2	1.7	1.9	2.0	2.2	0.1	0.1	0.2	0.2	0.3	7.2	9.0	10.4	11.6	12.6
AUS	1.0	1.2	1.5	1.9	1.8	0.3	0.5	0.8	0.9	0.9	9.3	12.2	20.2	22.1	22.4
ALA	1.1	1.0	1.4	1.6	1.7	0.1	0.1	0.4	0.4	0.4	9.6	9.8	15.5	17.4	17.7
NEC	1.0	0.9	1.5	1.7	1.8	0.1	0.3	0.4	0.4	0.4	8.8	8.8	17.3	18.3	18.2
WNA	1.5	1.6	2.8	3.2	4.1	0.2	0.2	0.5	0.4	0.7	9.9	10.8	18.8	21.3	24.8
CNA	1.6	2.0	3.0	3.2	3.8	0.2	0.2	0.6	0.8	1.1	9.9	9.7	20.3	26.3	30.5
ENA	1.5	1.8	3.1	3.3	4.0	0.1	0.2	0.5	0.5	0.5	8.9	10.4	18.2	21.1	24.1
CAM	1.3	1.9	3.2	3.4	3.7	0.1	0.2	1.3	1.5	1.7	8.5	10.8	30.6	36.0	41.1
AMZ	1.4	1.7	3.1	3.9	3.8	0.2	0.2	0.7	0.8	0.9	9.7	11.8	23.8	28.0	29.0

Table 6.3: Regionally averaged, multi-model mean values of short- (D_{4-6}) and long (D_{12+}) term drought frequencies and spatial extent of drought (A), for the PICNTRL, 20C3M (1961-90) and SRES B1, A1B, A2 (2070-99) scenarios. Values in bold are statistically significant, relative to the PICNTRL simulation, at the 0.05 level with DF=14.

6.3.5 Drivers of changes in drought occurrence

Figure 6.10 shows how predicted changes in regional drought are skewed towards the warm season. The figure shows the multi-model mean of regional averaged, monthly frequency of occurrence of soil moisture deficits for $q_0(\theta) < 10.0\%$ for the PICNTRL, 20C3M and the three future climate scenarios. By definition the PICNTRL frequencies are 10% for all months. The 20C3M and SRES frequencies are progressively larger, with $20C3M < B1 < A1B < A2$ as noted previously. Warm season increases are nearly always greater than those in cooler seasons. For southern hemisphere regions, such as SAF, AMZ, SSA and AUS, the largest changes are predominantly in the austral spring. In cooler regions (NAS, ALA, NEC), increased frequencies tend to be concentrated in the warm season and increases in the cool season, especially for ALA and NAS, are minimal.

Precipitation and temperature are the primary drivers of drought. Increases in temperature will potentially increase transpiration and direct evaporation from the soil through increased atmospheric demand, while increases in precipitation will tend to increase soil moisture. Conversely, decreases in temperature and precipitation will tend to increase and decrease soil moisture respectively. However the contribution of future changes in temperature and precipitation to changes in drought occurrence under future climates is not straightforward because of the complex interactions between these forcing variables and hydrologic processes at the earth's surface. This is complicated further by changes in mean precipitation versus changes in precipitation frequency and intensity and the seasonality of changes, especially in snow dominated regions. Apart from precipitation, the key linkage between climate change and changes in soil moisture is evaporation. Although temperature increases will tend to increase potential evaporation, actual evaporation may be enhanced or diminished by precipitation increases and decreases respectively.

Model projections of future climates show increases in temperature globally and for all regions whereas changes in precipitation are regionally and often scenario dependent as shown for three example regions in Figure 6.11. These regions were chosen as they show diversity in changes in future drought. The MED region shows some of the largest increases in drought frequency that is robust across models (section 6.3.3). This can be directly attributed to reductions in precipitation totals, especially in the warm season, accompanied by reductions in runoff and soil moisture (Figure 6.11). Changes in evaporation are limited to small decreases in the summer, driven by reduced precipitation that is not offset by increased atmospheric demand from higher temperatures in an already water limited environment. In the CNA region, drought occurrence is expected to increase but changes in other variables are mixed. Precipitation is expected to increase in the spring but decrease in the summer. Coupled with increased temperature, this leads to increased evaporation in the spring but little change in the summer as decreased precipitation likely outweighs any increases in potential evaporation.

Changes in drought in the NAS region are modest but are focused on the

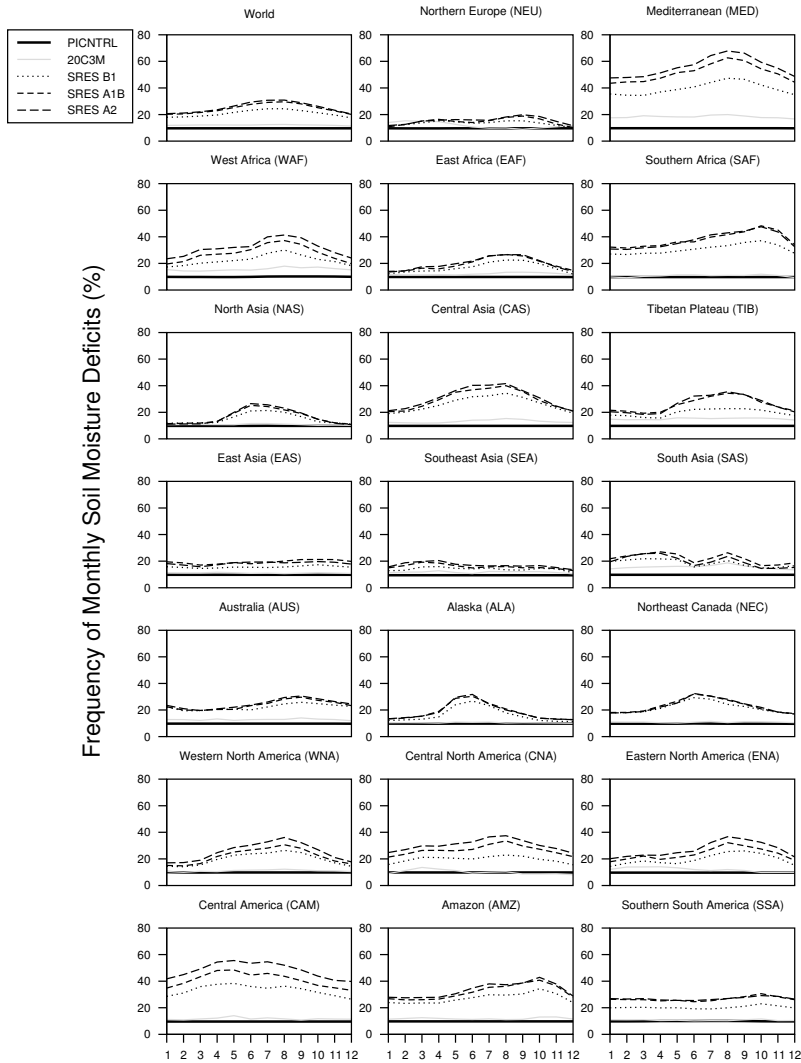


Figure 6.10: Multimodel regional average of frequency of monthly soil moisture deficits for the PICNTRL, 20C3M, SRES B1, A1B and A2 scenarios, relative to the 10th percentile of the PICNTRL simulations. For each model, the number of months with soil moisture deficits below the 10th percentile soil moisture value of the PICNTRL simulation are summed and averaged across all models and the region and converted to a percentage. The values are calculated separately for each month. The PICNTRL data are by definition equal to 10% for all months. The 20C3M data are calculated for 1961-1990. The future climate SRES scenarios are calculated for 2070-99.

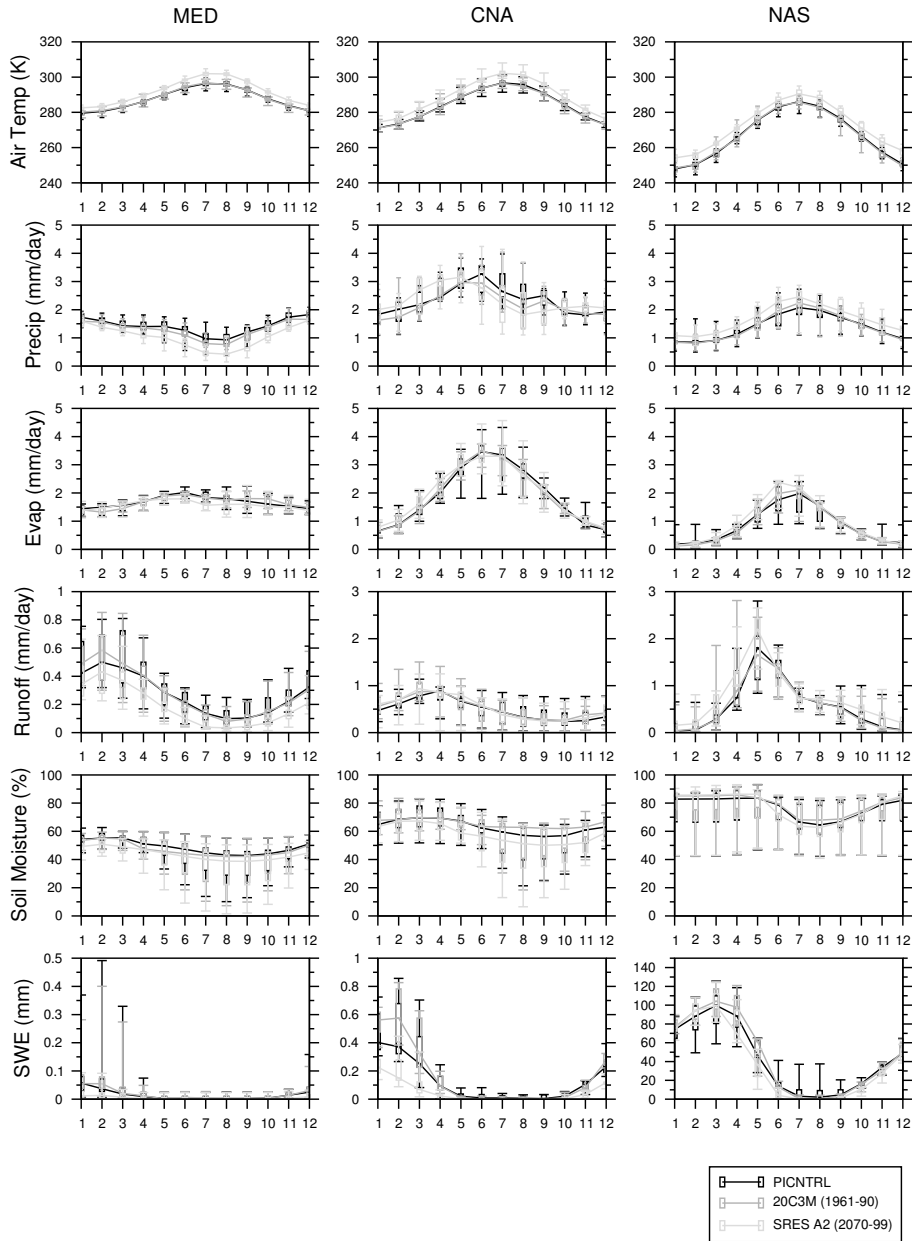


Figure 6.11: Mean seasonal cycle of air temperature and the main components of the terrestrial hydrological cycle for the MED, CNA and NAS regions for the PICNTRL, 20C3M (1961-90) and SRES A2 (2070-99) scenarios. The boxes and whiskers represent the inter-quartile range and range, respectively across the models.

summertime and are generally representative of other high latitude regions. The hydrology in these regions is dominated by snow and ice processes which, given increases in air temperature in these regions, can explain the seasonally disproportionate changes in soil moisture deficits. Warmer temperatures tend to reduce the snow cover through melting of the existing pack and increasing the ratio of rainfall to snowfall. Precipitation is also predicted to increase in the winter (and throughout the rest of the year). Rain falling on the existing snow pack will also increase the rate of melting. This will in turn shift the spring melt earlier. These changes force wetter soil moisture conditions in the winter and spring, although this is offset somewhat by increased evapotranspiration due to higher temperatures. During the summer, soil moisture is reduced, despite increased precipitation, because of earlier spring melt that is compounded by evapotranspiration increases as a result of increased temperatures. The frequency of soil moisture deficits therefore increases disproportionately in the summer time compared to the wintertime.

6.4 Detectability of changes in drought

The detection of statistically significant changes in drought is dependent upon, among other factors, the strength of the change (signal) against the background of natural variability (noise). As these factors vary, a change will be detected earlier or later, and the time of detection can be used to quantify detectability (e.g. Ziegler et al., 2003). The above analysis shows that statistically significant changes are predicted to occur in many regions by the end of this century, in particular the MED, SAF, CNA and CAM regions. However, these changes may actually have become significant at earlier times and there may be other regions where changes become significant or detectable at later time periods (if simulation data are available).

6.4.1 Examples of regional detectability

Figure 6.12 shows some examples of the detectability of drought occurrence for the A2 scenario for the WORLD and five regions (MED, CNA, TIB, AMZ and SEA). These regions were chosen as they represent a variety of increasing drought responses (some regions, such as NEU and NAS, show no statistically significant changes). As the mean change in drought occurrence increases over time, because of, for example, decreasing precipitation, the statistical significance of the change generally also increases. Whether the changes in drought occurrence are statistically significant is dependent on the region, drought characteristic and scenario, although we only show results here for A2 (results for all scenarios are shown in section 6.4.2). The variance (or spread) among models is also a factor. For some regions (e.g. MED) the changes are already detectable in the 20th century or early 21st century. In others, such as WORLD, changes at the same confidence level vary by several decades between drought characteristics. Elsewhere, changes can flip between being detectable or not (e.g.

CNA for D_{12+} frequency) or between two levels of significance (e.g. SEA for D_{4-6} frequency), which has implications for decision making based on discrete thresholds. In general, D_{4-6} frequency is more detectable than D_{12+} frequency, although the TIB region shows the opposite behaviour and in the AMZ region only changes in D_{4-6} frequency are detectable. Changes in D_{4-6} droughts in the SEA region become detectable relatively early (around 2010) despite their small magnitude.

6.4.2 Detectability under different scenarios

Table 6.4 summarizes the detectability of changes in regional drought for the three future climate scenarios. Detectability is quantified as the mid year of the 30-yr period in which the mean change in the regional average drought characteristic first becomes statistically significant (at the 0.05 level), although in reality we would not be able to make an assessment until the end of the period once observations had been made. An earlier year of detection represents higher detectability in the predicted changes. Because of decadal variability during the 20th century there are periods of high drought occurrence that are statistically detectable but are followed by periods of non-detectability. We therefore look for the first detectable year after any period of decadal variability.

Table 6.4 indicates that changes in D_{4-6} frequencies are more detectable than the other drought characteristics. D_{mean} changes are undetectable in most regions. Changes in regions such as MED, CAM and the WORLD are detectable for all drought characteristics and scenarios (shown previously in the end of century summary, Figure 6.9). For some regions (e.g. NEU, ALA, NAS), the changes are undetectable within the simulation period. Calculations with data from lower emission scenarios, such as B1, tend to increase the time to detection as the magnitude of the changes are lower (although variance may decrease if models show more consensus and tend to increase detectability). Detectability under higher emission scenarios is increased (detection time decreases) because the magnitude of change increases (increased signal to noise ratio), although this is complicated by the possibility that the uncertainty in future changes under higher greenhouse gas concentrations may increase the spread in model projections.

6.4.3 Detectability as a function of risk

The time of detection is also inherently controlled by the level of risk that one is willing to take in making the determination. The estimates in section 6.3.3 and section 6.4.2 are made using a conservative, low-risk probability ($\alpha = 0.05$) of making an error in detection. This low risk value could be representative of a conservative attitude to global warming in which more time is needed for detection before taking steps toward mitigating the impacts of global warming; higher risk values imply less time is required for detection. Figure 6.13 shows the sensitivity of detection times to the test significance. As we instil more confidence in the detection process and α decreases, our willingness to

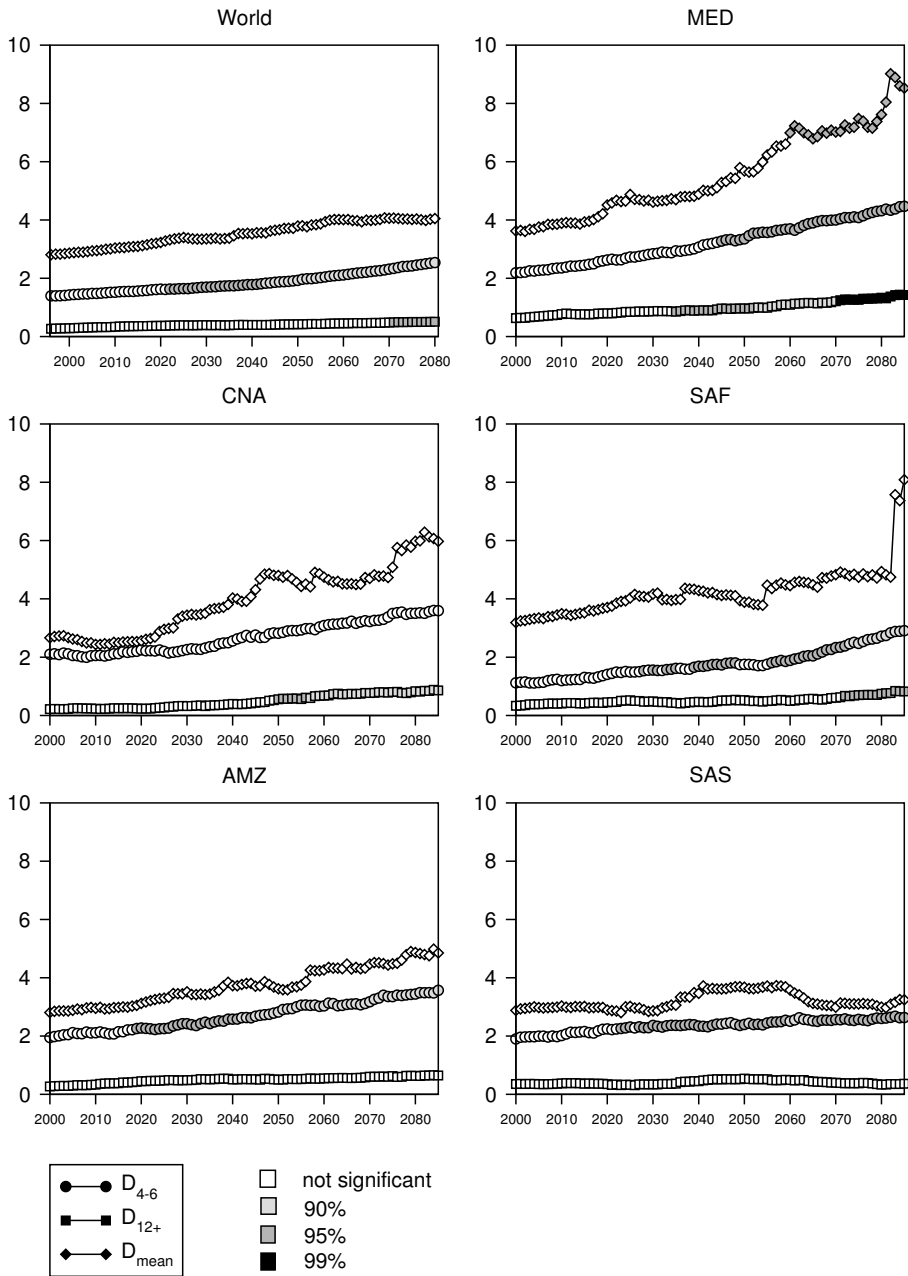


Figure 6.12: Detectability of changes in drought occurrence for the world and five selected regions. The frequency of D_{4-6} and D_{12+} droughts, and the mean drought duration D_{mean} in a 30-year moving window centred on the year is averaged over each region. The colours indicate statistical significance of the changes in drought occurrence relative to the climate model control period values at 90.0, 95.0 and 99.0% confidence levels.

	D_{4-6}			D_{12+}			A		
	B1	A1B	A2	B1	A1B	A2	B1	A1B	A2
WORLD	1972	1972	1972	2013	2013	2011	1920	1920	1920
NEU	-	-	-	-	-	-	-	-	-
MED	1941	1941	1941	1956	1956	1956	1943	1943	1943
WAF	1964	1964	1964	2073	2012	2052	1913	1913	1913
EMF	-	2068	2058	-	-	-	-	-	-
SAF	2015	2013	2019	2073	2081	2072	1998	1995	1998
NAS	-	-	-	-	-	-	2002	2060	2051
CAS	2055	2032	2049	2068	2059	2073	2054	2029	2056
TIB	-	-	2081	-	2037	2052	2045	2031	2018
EAS	2073	2069	2064	-	-	-	2056	2064	2017
SAS	1969	1969	1969	-	-	-	1945	1945	1945
SEA	2072	2067	2014	-	-	-	-	2079	-
AUS	-	-	2083	-	-	-	2012	2021	2011
ALA	-	-	-	-	-	-	-	-	-
NEC	-	-	-	-	-	-	2046	2049	2046
WNA	2055	2022	2038	-	-	-	2003	2002	2023
CNA	2072	2051	2083	-	-	2056	2012	2018	2024
ENA	2025	2034	2022	-	-	-	2022	2009	2009
CAM	1977	1977	1977	2052	2050	2037	1996	1980	1980
AMZ	1996	1995	1998	-	-	-	1994	1993	2000
SSA	1999	2005	2011	2050	2054	2045	1990	1989	1989

Table 6.4: Year of detection of statistically significant changes in drought frequency between the control and the B1, A1B and A2 scenarios from the multi-model ensemble. Dash symbols indicate that the change is undetectable within the simulation period. Statistical significance is calculated using the Students t-test for a significance level of 0.05. Drought frequencies are calculated over 30-yr periods and the year of detection is the middle of such a period. Note that detection times for a drought characteristic for periods that fall completely within the 20th century are derived from the 20C3M simulations only and are thus the same for all future scenario columns in the table.

falsely detect a change when none is occurring decreases. Therefore the size of the change has to be larger for us to be confident that it is statistically different from background variability, which generally implies that we have to wait longer to detect the change and thus detectability decreases. At $\alpha = 0.05$ the detection times for changes in drought characteristics vary widely depending on the region and variable, and changes for some variables are essentially undetectable (e.g. NAS for all variables). Detection times for lower confidence levels are earlier, as expected, although often not substantially different from the 95% values. However, above the 99% level, the changes generally become undetectable within the simulation period. For example, detection times for changes in D_{12+} frequency over CNA increase from about 2050 at 95% and below, to undetectable for 99% and above. Note that some changes are detectable during the early part of the 20th century (e.g. NEU for D_{12+} frequency and S_{mean}), but reflect decadal variability rather than a global warming induced long-term trend.

6.4.4 Detectability relative to the 20th Century

Detection of change is dependent on the background noise used to quantify the natural variability of the system. The results shown so far are relative to the model control simulations, which represent a “pristine” climate without anthropogenic influence. Variability in these simulations results from a number of sources including variability in solar output and internal variability of the coupled atmosphere-ocean-land system. Our perception of change, however, may be better realized relative to contemporary climate as this encompasses observed climate variability, including the occurrence of drought of which we have first hand experience. Figure 6.14 gives the detection times when using either the PICNTRL or the 20C3M (1961-90) data to estimate the background variability. Detectability generally decreases when using the 20C3M data as would be expected, as drought frequency has already increased relative to the control simulation (as shown in the regional time series in Figures 6.4-6.6 and the 20th century detection times for many regions in section 6.4.2). It should be noted though that decadal variability within the 20th century means that for some regions 1961-90 is a wet period and the changes become detectable earlier than when using the PICNTRL data.

6.4.5 Multi-Model ensemble versus single model detectability

Given the uncertainty in future climate projections by a single model, this study is based on a multi-model ensemble. This enables us to capture the uncertainty in the representation of climate processes. However we have chosen to use a single model simulation as representative of each particular model despite the variability among same model simulations that differ only by their initial conditions. To assess how detectability differs when using the predicted climate of a single model we calculated the year to detection for each of the five available

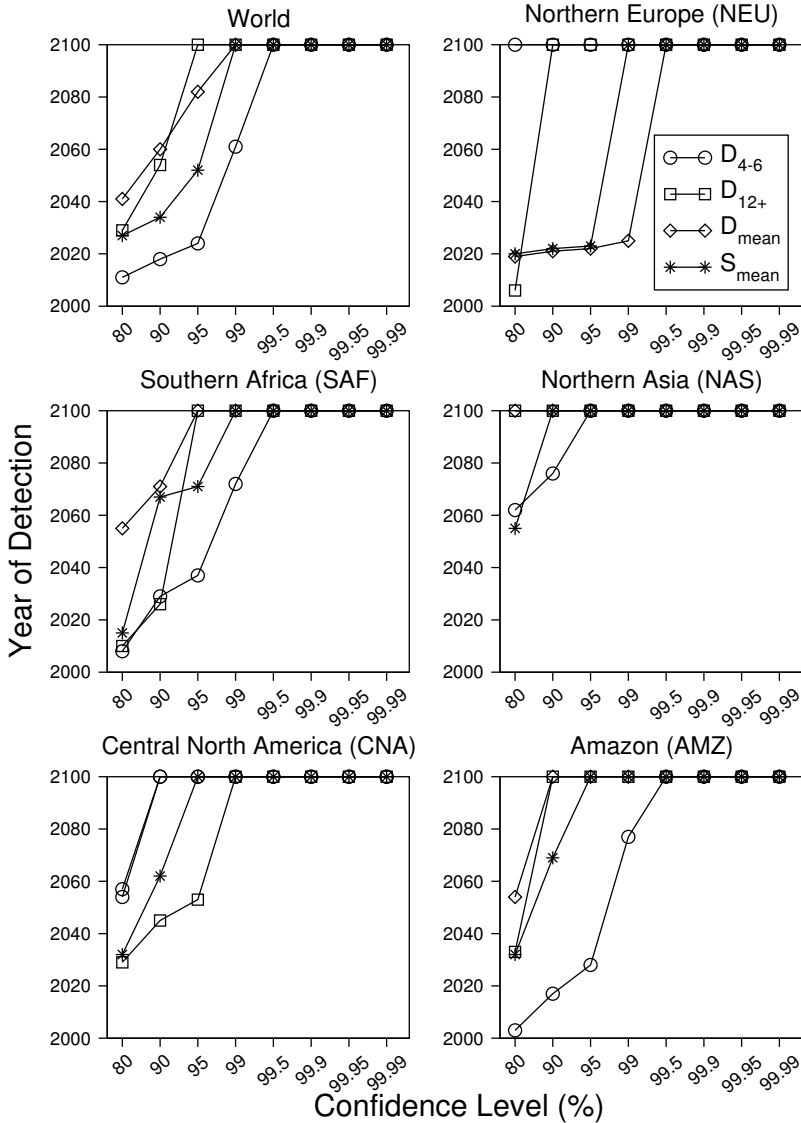


Figure 6.13: Detectability as a function of statistical significance for the world and selected regions for the SRES A1B scenario. The year of detection is calculated as the mid year of the 30-yr period in which the model mean change in the drought variable is statistically different at the given significance level relative to the control (PICNTRL) simulation. Detection years equal to 2100 indicate that the change is not detectable within the period of the simulation. The minimum possible detection time is 1900, which is the mid point of the first 30-yr period, and changes may have become detectable before this time.

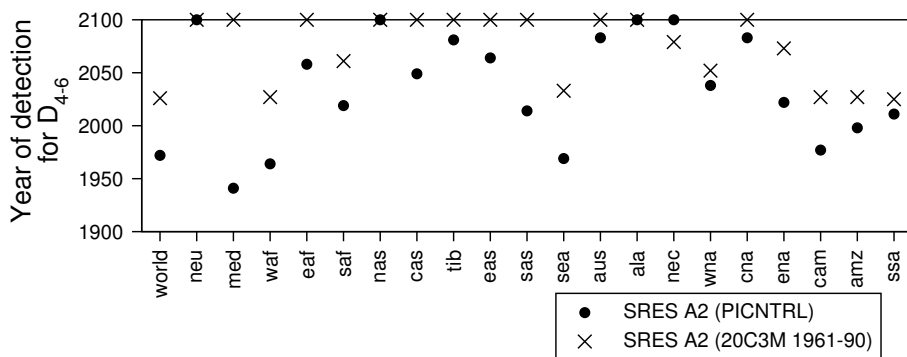


Figure 6.14: Comparison of detection times for different estimates of natural variability. Detection times are when regional average changes in drought characteristics for the SRES A2 scenario become statistically different at the 0.05 level from natural variability estimated from either the PICTNRL scenario or the 20C3M scenario (1961-90).

ensemble members for the CGCM3.1(T47) model for the A2 scenario (Figure 6.15). This model was chosen because of the availability of a relatively large number of ensemble members and it is assumed that similar results would be obtained when using other models if multiple members were available. As multiple integrations of the control simulation are not available for a single model, we represent the natural variability of the climate system by the variation between 30-year periods in the control simulation. The results show reasonable agreement (within 25 years) for Europe, parts of Asia and the Americas but large differences in detectability elsewhere. For example, the SAF region shows differences up to 150 years, although this is because of detectable changes at the start of the 20C3M scenario for the single model. The time series of mean values for the single and multi-model ensembles are actually similar and it is the larger magnitude of the change for the single model ensemble that results in the large differences in detectability. For the WORLD the single model year of detection is 2008 and the multi-model values is 1963. Assuming that a multi-model ensemble gives a better estimate of the magnitude and detectability of future changes in drought occurrence (as is seen in multi-model comparisons with observations, e.g. Guo and Dirmeyer, 2006), the implication is that a single model estimate may be considerably biased in some regions.

6.4.6 Comparison with detection times of primary climate variables

Climate change is usually described in terms of primary climate variables, such as global mean temperature and precipitation. Current estimates indicate that recent trends in temperature are statistically unusual compared with the historic (Jones and Moberg, 2003) and paleoclimatic records (Osborn and Briffa,

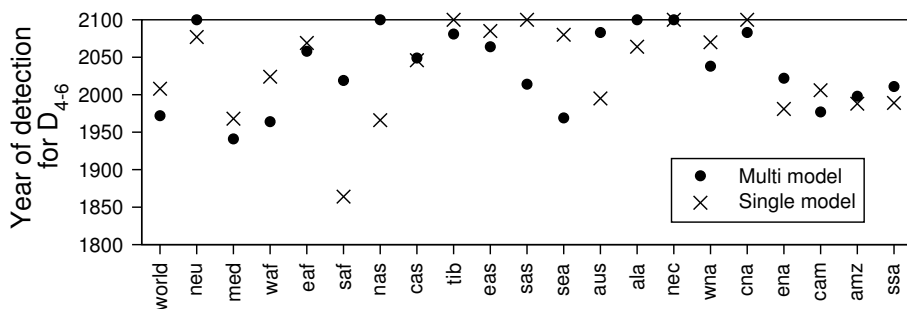


Figure 6.15: Comparison of detection times for statistically significant changes (0.05 level) in regionally averaged frequency of D_{4-6} droughts for the multi model ensemble and the single model ensemble means.

2006). For precipitation, observations are generally less extensive in time and space and are plagued by errors due to, among other factors, measurement error (e.g. wind induced undercatch), orographic effects, temporal inconsistencies, and spatial sampling errors, especially in data sparse regions (Hulme and New, 1997). Table 6.5 shows the year of detection for statistically significant changes in annual and seasonal values of surface air temperature and the main components of the terrestrial water balance for the MED region under the A2 scenario. We also repeat the detection values for drought. Air temperature changes are detectable within the first half of the 21st century at all time scales. Changes in precipitation and runoff are also detectable, except for DJF, but at later times. For evaporation and soil moisture, changes are only detectable in JJA and DJF respectively and not until beyond mid century. The MED region was chosen as it shows some of the largest increases in drought and corresponding detectable changes in other variables. Few other regions show detectable changes and changes at global scales are only detectable for air temperature which is consistent with observed trends in relation to estimates of natural variability (Hansen et al., 2006; Osborn and Briffa, 2006). In fact, changes in air temperature are detectable for all regions and time scales between 1991 and 2043. Changes in snow as represented by snow water equivalent (SWE) are only detectable in mid-latitudes of North America (WNA, CAN, ENA) and Asia (CAS, EAS) where variability in snow cover is higher than more northerly regions and thus likely to experience detectable changes earlier.

6.5 Discussion and conclusions

We have analyzed soil moisture data for three future climate scenarios from eight AOGCMs that participated in the IPCC AR4. The models show decreases in soil moisture at global scales for the future scenarios with a corresponding doubling of the spatial extent of severe soil moisture deficits and frequency of short-term (D_{4-6}) droughts from the mid 20th century to the end of the 21st.

	Annual/ No season	DJF	MAM	JJA	SON
T	2025	2031	2024	2034	2028
P	2040	-	2061	2043	2036
Q	2075	-	-	2063	2051
E	-	-	-	2060	-
SM	-	2071	-	-	-
D_{4-6}	1941				
D_{12+}	1956				
A	1943				

Table 6.5: Year of detection of statistically significant changes in annual and seasonal mean surface air temperature and the main components of the terrestrial water cycle (precipitation (P), evapotranspiration (E), runoff (Q), and soil moisture (SM), and three drought characteristics for the MED region under the SRES A2 scenario. Also shown are the detection times for drought characteristics repeated from Table 6.3. Note that a drought may span multiple seasons.

Long-term (D_{12+}) droughts become three times more common. Regionally, the MED, WAF, CAS and CAM regions show large increases, most notably for D_{12+} frequencies as do mid latitude North American regions (WNA, CNA, ENA) but with larger variation between scenarios. Changes elsewhere are generally increasing but relatively small. Changes under the B1 scenario are the least and the A1B and A2 results are similar. We tested the statistical significance of changes at the end of the 21st century relative to natural variability as represented by the pre-industrial control simulations and found significant increases in D_{4-6} drought frequency globally and in most regions. Significant changes in D_{12+} frequency are less spatially extensive with increases for the MED, WAF, SAF, CAS, CAM and SSA regions for all scenarios and for TIB, CAN and AMZ for the higher emission scenarios only. Statistically significant decreases in D_{12+} frequency exist but are restricted to small areas of high latitudes.

A number of other studies have analyzed the current IPCC and other climate model simulations in terms of changes in soil moisture and drought at large scales and the results presented here are generally consistent with these. Although these studies were based on either different models (Gregory et al., 1997) and/or versions (Wetherald and Manabe, 2002) or different sets of the IPCC AR4 models (Wang, 2005; Burke et al., 2006) and use different metrics for defining changes in soil moisture or droughts, there is general consensus that global drying of soil moisture will occur. Wetherald and Manabe's (2002) analysis of an earlier version of the GFDL coupled model showed annual reduction in soil moisture and large reduction in summertime soil moisture in some semi-arid regions including southern North America and the Mediterranean. This is consistent with our study in terms of soil moisture (see Figure 6.11 for

the MED and CNA regions) and reflected in the particularly large increases in drought occurrence for the MED, CNA and CAM regions (section 6.3.4). They also noted summer time reductions in soil moisture in mid-continental middle to higher latitudes but increases in winter, which we see, for example, in the NAS region (Figure 6.11).

The study of Wang (2005) has considerable overlap with this study in terms of the data used, although we use fewer models but more scenarios (Wang analyzed data from 15 models for the SRES A1B scenario) and we analyze the occurrence of drought as opposed to changes solely in the soil moisture mean. Wang found significant variation in the global pattern of changes in soil moisture, despite the direction of changes in precipitation being quite consistent across models, perhaps indicating the complexity of the soil moisture response and/or the variation across models in how they simulate surface fluxes that has been extensively noted in off-line land surface model comparisons (Wood et al., 1998; Mitchell et al., 2004; Guo and Dirmeyer, 2006). This may also be a result of differences in the sub-monthly statistics, for example, the simulated storm frequencies and intensities. Only in some regions of northern mid- and high-latitudes did Wang find consistency in predicting summer dryness and winter wetness (again consistent with this study and the study of Wetherald and Manabe, 2002). Elsewhere, the general consensus is for drier soils. Regions where the models were unanimous in predicting drying include southwest North America, Central America, the Mediterranean, South Africa, and Australia. This is reflected in our results that find statistically significant changes in drought occurrence in these regions (with the exception of Australia, which for our analysis showed large mean changes but with high uncertainty across models).

In terms of changes in drought specifically, Gregory et al. (1997) and Burke et al. (2006) analyzed earlier and current versions of the Hadley climate model. Despite looking at different metrics to quantify drought (Gregory et al. (1997) looked at changes in the frequency of low summer precipitation, length of dry spells and frequency of dry soils; Burke et al. (2006) looked at the PDSI as driven by climate model predicted precipitation and temperature) and different scenarios (a $1\% \text{ yr}^{-1}$ increasing CO_2 concentration and the SRES A2 scenario, respectively) they found substantial drying at global scales and similar changes to this study in most regions. In both cases, a single model and single future climate scenario were considered. Crucially, both studies note that these results need to be corroborated by other climate models. The analysis of detectability from a single model (section 6.4.5) shows how different the result can be when using one model, although the sign of changes is likely to be the same even under different scenarios. This is reflected in multi-model analyses of soil moisture from off-line modelling, where individual models are generally capable of mimicking observed anomalies and trends (Guo and Dirmeyer, 2006), but importantly, multi-model means do better at replicating observations than almost any individual model (Guo et al., 2007).

Wetherald and Manabe (2002) and earlier papers referenced within, provide mechanisms for summer time drying in mid-latitudes that are supported

by Wang (2005). We find the same mechanisms are at play here, with reductions in precipitation the primary forcing of increased drought with increased evaporation driven by higher temperatures modulating the changes. In some regions, increases in precipitation are offset by increased evaporation. At higher latitudes where snow processes have a dominant role we see evidence for redistribution of soil moisture from spring to winter forced by earlier spring melt and a likely increased rain to snow ratio during the cooler seasons. This has a knock-on effect during the summer when reduced soil moisture persistence from the spring coupled with increased evaporative demand from increased temperatures conspires to reduce soil moisture, also found by Wang (2005).

Although the predicted future changes in drought occurrence are essentially monotonic increasing globally and in many regions, they are generally not statistically different from natural variability for multiple decades. Detectability of change is however dependent on many factors, including the magnitude of the change, and the background noise or natural variability as estimated from the control simulations, which in turn depend on the type of drought statistic. It also depends on the chosen level of significance in the statistical testing or risk that one is willing to take in detecting the impacts of climate change. As this is generally an arbitrary choice the implication is that this can by itself introduce great uncertainty in the detection of climate change. A 95% confidence level is ubiquitous in the scientific literature, but a 90 or 99% confidence level could just as easily be used with dramatic changes in the results as seen for the example of CNA in Figure 6.13.

In contrast to primary climate variables, such as global mean surface air temperature, changes in drought are predicted to become detectable only after multiple decades, if at all. This lag can be crucial with respect to implementing mitigative or adaptive measures against such changes (Pittock, 1999). On the other hand, changes in annual and seasonal means of terrestrial hydrologic variables, including soil moisture, are essentially undetectable within the 21st century. Although related studies of future drought occurrence (e.g. Wetherald and Manabe, 2002; Wang, 2005) focused on changes in the mean, such as mean monthly precipitation or soil moisture, it has been noted (Gregory et al., 1997; Kharin and Zwiers, 2005) that changes in the mean are accompanied by lengthening of distribution tails and larger changes in extremes, such as drought as shown here. The implication is that changes in the extremes of climate and their hydrological impacts may be more detectable than changes in mean climate, although observing and quantifying extreme events, and comparing them to model output, is much harder in practice (Hergerl et al., 2006).

Despite the robustness of the changes in drought, globally and across many regions, and for all scenarios, there are still many uncertainties in this study that arise not only from our approach but also from the simulations themselves. Firstly, we have by necessity used eight models to represent the uncertainty across models, although 24 models contributed data for one or more scenarios to the IPCC AR4. The error in doing this is difficult to quantify but our estimates are consistent with results for a larger set of models for a single scenario (Wang, 2005). Secondly, the models themselves may be biased because

of inadequacies in the modelled physical processes and parameterizations and because of processes that are not included in the modelling. Evaluation of the models' ability to replicate observed climate variability and the terrestrial water cycle has been addressed elsewhere with mixed results (e.g. Dai, 2006; Frei and Gong, 2005; Lau et al., 2006; Li et al., 2007; Swenson and Milly, 2006). For drought specifically, we have shown that the models do reasonably well in replicating our best estimates of 20th century drought statistics at regional scales yet with large spread among the models. Although they may do better at replicating atmospheric and large scale climate variability (e.g. AchutaRao and Sperber, 2006), the uncertainty in modelled land surface processes and soil moisture in particular, coupled with the uncertainties in future climate projections is reason to incorporate as many models as possible in any assessment of future change.

Processes that have a direct impact on drought occurrence but are not present in the models include anthropogenic forcings such as irrigation, water diversion and land use and natural processes such as vegetation dynamics and wildfire. Anthropogenic processes are difficult to quantify, even historically. Estimates of current day irrigation are that 16.3% of cultivated regions are equipped for irrigation (Siebert et al., 2005) which can have a significant impact on the water cycle (Haddeland et al., 2007), although historically this may have been offset by changes in land use. The impact of vegetation dynamics, through feedbacks with climate and interactions with climate induced changes in plant phenology and species composition may have a profound impact on drought occurrence through controls on water use, with potential positive feedbacks from natural deforestation (Cox et al., 2000; Gullison et al., 2007).

Notwithstanding the uncertainties in detectability, we can make some final general observations regarding the results. The consensus among this set of the latest GCM projections of future climates is that drought frequency will increase relative to the control period but will not show statistically significant changes for several decades, indicating that the impacts of climate change will not be felt immediately at regional scales. In general, there is a greater propensity to increased warm season drought which may be especially pertinent when specific impacts are taken into consideration, such as drought effects on agriculture that are most important during the growing season. Drought is shown to increase under all scenarios, including the B1 scenario that follows a reduced greenhouse gas emission pathway through the 21st century relative to the present day. The implication is that drought occurrence will increase, despite future emission reductions and this will be exacerbated by the thermal inertia of the oceans (Wigley et al., 2005; Meehl et al., 2005) and already accumulated greenhouse gases, which in turn will increase the time to stabilization of concentrations. Under high emission pathways (A1B and A2), the magnitude of the drought changes are expected to be even higher, but more worrisome is that these scenarios may already be underestimating observed changes as has been seen since the IPCC Third Assessment Report simulations (Rhamstorf et al., 2007).

Acknowledgements

This work was partly supported by U.S. Department of Energy grant 983338. We acknowledge the modeling groups for making their simulations available for analysis, the Program for Climate Model Diagnosis and Intercomparison (PCMDI) for collecting and archiving the CMIP3 model output, and the WCRP's Working Group on Coupled Modelling (WGCM) for organizing the model data analysis activity. The WCRP CMIP3 multi-model dataset is supported by the Office of Science, U.S. Department of Energy.

Chapter 7

Synthesis

7.1 Summary

Drought is a pervasive and costly natural hazard that inflicts substantial social, environmental and economic cost globally. As part of the general scientific effort to quantify and understand the occurrence of drought and potential future changes, this work has described the analysis of retrospective and future projected soil moisture data in terms of drought occurrence, its trends and variability. This section summarizes the conclusions of each chapter and is followed by some final remarks and future directions.

An integral part of the analysis of historic drought occurrence was the development of the retrospective dataset and the meteorological forcings that drove the off-line simulation. In itself the forcing dataset provides a useful resource for studies of the variability of the large scale water cycle and the evaluation of coupled models, among other applications. Chapters 2 and 3 described the development of the forcing dataset and the steps taken to provide long temporal and global coverage, and ensure its consistency and accuracy in time and space. In this respect, the dataset made use of the latest available global meteorological datasets and combined them with state of the art reanalysis to form a consistent, high quality dataset, globally for 1948-2000, at 3-hourly, 1.0 degree resolution.

In Chapter 2, the initial development of the forcing dataset was described. This work was motivated by the identification of a spurious wave-like pattern identified in the monthly precipitation statistics of the NCEP/NCAR reanalysis dataset (which formed the basis for the daily variability of the forcings) over terrestrial areas in high latitudes in winter. Comparison with three observation based precipitation datasets verified the anomaly and other regional biases in the reanalysis precipitation field. The rain day anomaly was corrected using a re-sampling approach to replicate the monthly precipitation statistics from each of the three comparison datasets. The resulting daily precipitation values were then scaled so that their monthly totals matched those of the CRU dataset, which had the longest temporal extent. The monthly statistics of the resulting

corrected datasets matched well the statistics of the respective dataset used for the correction but the degree to which it did this depended on the statistical similarity of the reanalysis and correcting dataset.

In the context of land surface modeling, the need for the correction was clear, as the high latitude anomalous pattern was reflected in the modeled land surface states using the VIC model. A number of experiments were carried out to investigate the effect of the correction on the land surface by forcing the model with the original and corrected reanalysis datasets. The results showed that the land surface water budget is sensitive to the sub-monthly distribution of precipitation. Simulations forced with identical monthly precipitation totals but different rain day statistics differed significantly in the partitioning of precipitation into canopy evaporation and throughfall with implications for the level of accuracy required of the correcting dataset. Ultimately, the choice of the correcting dataset would be based on the level of confidence in the data and the accuracy of the rain day statistics at the grid scale. However, attention must also be paid to the temporal extent of the data and whether it is representative of the long-term variability over the multiple decades of the reanalysis dataset period. In the absence of a single dataset that fulfills these criteria it may be that a hybrid dataset would have to be used.

This hybrid approach was taken in the development of the full meteorological forcing dataset described in Chapter 3. The dataset was constructed by combining a suite of global observation-based datasets with the reanalysis. Known biases in the reanalysis precipitation and near-surface meteorology have been shown to exert an erroneous effect on modeled land surface water and energy budgets, and were thus corrected using observation-based datasets of precipitation, air temperature and radiation. As described in Chapter 2, corrections were also made to the rain day statistics of the reanalysis precipitation. Wind-induced undercatch of solid precipitation was removed using the results from the WMO Solid Precipitation Measurement Intercomparison. Precipitation was disaggregated in space to 1.0 degree by statistical downscaling using relationships developed with the GPCP daily product. Disaggregation in time from daily to 3-hourly was accomplished similarly, using the TRMM 3-hourly real-time dataset. Other meteorological variables (downward short- and longwave, specific humidity, surface air pressure and wind speed) were downscaled in space with account for changes in elevation. The dataset was evaluated against the bias-corrected forcing dataset of the GSWP-2, a similar product developed for a much shorter period.

In Chapter 4, a monthly soil moisture based drought index was developed for global terrestrial areas from an off-line land surface model simulation forced by the meteorological dataset. The index was used to investigate the climatological aspects of drought occurrence, globally over 1950-2000. The variability and trends in drought, and its forcings were explored in Chapter 5. Drought was described in terms of duration, intensity and severity, and various statistics that summarize their distributions in time and space. These variables were analyzed spatially, at global and regional scales, and temporally with respect to severity and spatial coverage. The inter-dependence of these correlated variables was

also explored along with the sensitivity to the threshold soil moisture value that defines drought.

An analysis of the statistics of drought events revealed considerable global variability and some interesting relationships between drought characteristics. Based on a soil moisture quantile threshold of 10%, the frequencies of short-term droughts (6 months and less) and droughts of any length were found to be highest in humid regions. Medium term droughts (6-12 months) are more prevalent in mid- to high-latitudes, which for the latter is a result in part of freezing temperatures causing static soil moisture conditions and forcing drought conditions to persist through the wintertime. Over the Sahel and parts of high northern latitudes, the frequency of long-term droughts was at a maximum. Drought intensity, defined as the mean departure below the threshold soil moisture quantile over the drought duration, tended to be higher over humid regions. This is likely a result of the higher inter annual variability in soil moisture that tends to prevail in humid regions, even if the range in soil moisture is small in absolute terms. Drought severity, calculated as intensity times duration, tended to be lowest in more humid regions and highest in regions of high mean duration, such that drought duration is a more dominant factor in severity for longer duration droughts. The Sahel region stands out globally for having long-term and severe drought conditions.

Severe drought events were systematically identified in terms of spatial coverage for various regions based on different thresholds of duration and intensity that relate to either high intensity, short duration droughts or low intensity, long duration droughts. In northern Asia, severe drought events at short and long time scales were found to be characterized by persistent soil moisture anomalies over the wintertime. Droughts in western and eastern Africa are dominated by events in the Sahel. The drought index identified several well-known drought events, including the 1988 USA, 1982/83 Australian, 1983/4 Sahel and 1965/66 Indian droughts, which were analyzed in more depth. These events were generally ranked as the severest events in the record, although some were ranked relatively low and the severity of their reported impacts was likely compounded by socio-economic and other factors. Comparison of the results with those from two PDSI datasets showed general agreement, although the PDSI tended to give larger spatial extent values. Some events, however, (e.g. 1988, central North America and 1965, India) were ranked somewhat differently by each dataset that may be due to differences in scale and forcings, but is also likely a result of fundamental differences in the modeling approach between the VIC index and the PDSI. At global scales the VIC index and the PDSI were reasonably well correlated but this breaks down in cooler regions and seasons, and especially in the latter half of the 20th century, when the PDSI showed a larger drying trend. The simplified temperature based approach for calculating potential evaporation in the PDSI may have contributed to this trend. Given these comparisons, the known deficiencies and simplifications in the PDSI and the history of evaluations of the VIC model, this chapter concluded that the VIC index is a good indicator of major drought events that is applicable to a wider range of climate regimes than the PDSI.

In Chapter 5, trends and variability in the retrospective soil moisture and drought index were analyzed. Trends were calculated using a non-parametric trend test on a grid cell basis and for regional averages. An overall increasing trend in global soil moisture, driven by increasing precipitation underlay the whole analysis, which was reflected most obviously over the western hemisphere and especially in North America. Regional variation was nevertheless apparent and significant drying over West Africa, as driven by decreasing Sahel precipitation, stood out. Elsewhere, Europe has not experienced significant changes in soil moisture, a trait shared by southeast and southern Asia. Trends in drought characteristics were predominantly decreasing but statistically significant changes were limited in areal extent, of the order of 1.0 to 7.0% globally, depending on the drought threshold and variable and being generally less than 10% of continental areas. Concurrent changes in drought spatial extent were found, with a global decreasing trend of -0.021 to -0.035% yr^{-1} . Regionally, drought extent over Africa has increased and is dominated by large increases over West Africa. Northern and East Asia showed positive trends, and central Asia and the Tibetan plateau showed decreasing trends. In south Asia all trends were found to be insignificant. Drought extent over Australia has decreased. Over the Americas, trends were uniformly negative and mostly significant.

Within the long-term trends we found interannual and decadal variations in soil moisture and drought characteristics in many regions. Globally, variations were driven mainly by ENSO variability, although the AMO appears to play an important role globally and in many regions, such as west and east Africa, central Asia and the high latitudes of North America. However, the short length of record relative to the scale of the AMO precluded any definite conclusions. High correlation values were found between Mediterranean soil moisture and the NAO, and between soil moisture in southeast Asia and the Amazon basin and Nino3.4 SSTs. Stronger connections are likely at scales smaller than the regions examined and by using seasonal and lagged correlations. The decadal variations in soil moisture and drought characteristics were found to impact the robustness of the long-term trends. In general, they were responsible for diminishing the long-term trends. In fact, despite the overall wetting trend, there is a switch in later years to a drying trend, globally and in many regions, which is concurrent with increasing temperatures. Although drought is driven primarily by variability in precipitation, temperature has an effect that, given the results of a simulation forced by climatological temperature, appears to be exaggerated in the last decade or so especially in high northern latitudes.

Finally, Chapter 6 extended the work of the retrospective analyses of Chapters 4 and 5 to explore the projected changes in drought over the 21st century. An increase in the number of droughts and/or drought severity is a possible outcome of future global warming and intensification of the water cycle. To evaluate projected changes, we focused on data from climate models. Soil moisture data were analyzed for three future climate scenarios (B1, A1B, A2) from eight AOGCMs that participated in the IPCC AR4. The models showed decreases in soil moisture at global scales for the future scenarios with a corresponding doubling of the spatial extent of severe soil moisture deficits and frequency of

short-term (4-6 month duration) droughts from the mid 20th century to the end of the 21st. Long-term (longer than 12 month duration) droughts were found to become three times more common. Regionally, the Mediterranean, West African, Central Asian and Central American regions showed large increases, most notably for long-term frequencies, as did mid latitude North American regions but with larger variation between scenarios. Changes elsewhere were generally increasing but relatively small. Changes under the B1 scenario were the least and the A1B and A2 results were similar. Tests of the statistical significance of changes at the end of the 21st century relative to natural variability as represented by the pre-industrial control simulations showed significant increases in short-term drought frequency globally and in most regions. Significant changes in long-term frequency were less spatially extensive with increases for the Mediterranean, West African, South African, Central Asian and Central American and southern South American regions for all scenarios and for the Tibetan plateau, central North America and the Amazon for the higher emission scenarios only. Statistically significant decreases in long-term frequency existed but were restricted to small areas of high latitudes.

Although the projected future changes in drought occurrence were found to be essentially monotonic increasing globally and in many regions, they were generally not statistically different from natural variability for multiple decades. Detectability of change is, however, dependent on many factors, including the magnitude of the change, and the background noise or natural variability as estimated from the control simulations, which in turn depend on the type of drought statistic. It also depends on the chosen level of significance in the statistical testing or risk that one is willing to take in detecting the impacts of climate change. As this is generally an arbitrary choice, the implication is that this can by itself introduce great uncertainty in the detection of climate change. A 95% confidence level is ubiquitous in the scientific literature, but a 90 or 99% confidence level could just as easily be used with dramatic changes in the results. In contrast to primary climate variables, such as global mean surface air temperature, changes in drought were predicted to become detectable only after multiple decades, if at all. This lag can be crucial with respect to implementing mitigative or adaptive measures against such changes. On the other hand, changes in annual and seasonal means of terrestrial hydrologic variables, including soil moisture, were essentially undetectable within the 21st century. Although other studies of future drying have focused on changes in the mean, such as mean monthly precipitation or soil moisture, it was noted in Chapter 6 that changes in the mean are accompanied by lengthening of distribution tails and larger changes in extremes, such as drought. The implication is that changes in the extremes of climate and their hydrological impacts may be more detectable than changes in mean climate, although observing and quantifying extreme events, and comparing them to model output, is much harder in practice.

Notwithstanding the uncertainties in detectability, the consensus among this set of the latest GCM projections of future climates is that drought frequency will increase relative to the control period but will not show statistically

significant changes for several decades, indicating that the impacts of climate change will not be felt immediately at regional scales. In general, there is a greater propensity to increased warm season drought which may be especially pertinent when specific impacts are taken into consideration, such as drought effects on agriculture that are most important during the growing season. Drought is shown to increase under all scenarios, including the B1 scenario that follows a reduced greenhouse gas emission pathway through the 21st century relative to the present day. The implication is that drought occurrence will increase, despite future emission reductions and this will be exacerbated by the thermal inertia of the oceans and already accumulated greenhouse gases, which in turn will increase the time to stabilization of concentrations. Under high emission pathways (A1B and A2), the magnitude of the drought changes are expected to be even higher, but more worrisome is that these scenarios may already be underestimating observed changes as has been seen since the IPCC Third Assessment Report simulations.

7.2 Conclusions and Future Directions

One of the greatest challenges in the hydrologic sciences is the quantification of the large scale water cycle because of the importance of water not only as a resource but also as a potential hazard. This is especially pertinent in the context of potential future global warming in which the strength of the water cycle is expected to change, with impacts on the availability of water and the occurrence and severity of extreme events. Drought is one of the key manifestations of water cycle variability but poses some of the most difficult questions in terms of our understanding of its occurrence, driving mechanisms and predictability. In particular we wish to know how drought has varied historically, what are the mechanisms that are associated with its initiation, persistence and recovery, and what changes can be expected in the future. Progress towards answering these questions is a long-term goal of many research initiatives and it is hoped that this thesis provides some added knowledge to this process and is a platform for further work in this area.

Overall, we have shown that retrospective off-line simulation of the global terrestrial water cycle is a feasible tool for recreating historic soil moisture variability and analyzing the occurrence of drought. A crucial part of this has been the development of the meteorological forcing dataset, which has also formed the basis of a multitude of other research activities in progress. In fact, in the past 18 months since its release, this dataset has been downloaded over 100 times by various research groups and individuals, with stated purposes ranging from evaluation of land surface models, to assessments of glacier melt, to studies of regional land-atmospheric coupling. The development of this dataset was originally motivated by the necessity for accurate estimates of the spatial and temporal variation in terrestrial water and energy fluxes and states that require the development of high resolution and long-term hydroclimatological datasets. The development of the highest quality forcing datasets is a first and vital step

towards this. Through research initiatives such as the World Climate Research Programme (WCRP) Climate Variability and Predictability (CLIVAR) program and Global Energy and Water Cycle Experiment (GEWEX) the emphasis has been on the development and enhancement of large scale datasets, through the use of increasingly better observational datasets and the use of new assimilation and modeling techniques. The work described in Chapters 2 and 3 is intended to form a part of this process by providing a benchmark forcing dataset that combines state of the art reanalysis products with the most recent observation-based datasets. The goals in the development of this dataset are to provide consistency in time and space among variables from contributing datasets whilst trying to achieve the highest resolution that can be supported by the data. The dataset provides a significant improvement over the original reanalysis variables, and can be used for a wide variety of applications and diagnostic studies in the climatological, hydrological, and ecological sciences. The final product provides a long-term, globally-consistent dataset of near-surface meteorological variables that can be used to drive models of the terrestrial hydrologic and ecological processes for the study of seasonal and inter-annual variability and for the evaluation of coupled models and other land surface prediction schemes.

Future improvements in the forcing dataset are recommended for a number of reasons. Although the emphasis has been on using global scale observation datasets to ensure consistency in space, better quality data sets do exist in terms of spatial and temporal resolution but with smaller spatial and temporal extents. For example, for the temporal disaggregation of precipitation at high northern latitudes, it was assumed, because of the lack of coverage by the TRMM dataset (restricted to 50S - 50N), that the diurnal cycle in cold, mid-latitude climates is representative of neighboring polar regions. Sub-daily station data from Canadian surface airways products and the Former Soviet Union (Razuvaev et al., 1998) are available for a significant number of high-latitude locations and can be used to derive the probability distributions used for the disaggregation. Furthermore, most monthly gridded precipitation datasets do not allow for orographic effects. As the network of rain gauges that contribute to these data sets are generally not located in regions of complex and elevated topography, this usually results in an underestimation of precipitation, by as much as three times (Adam et al., 2006). The correction method of Adam et al. (2006) uses a simple catchment water balance method to calculate adjustments to precipitation. These changes could be incorporated into new versions of the dataset in the future, although concerns over consistency in time and space may make this somewhat counter-productive. In addition, as improved and extended versions of observation-based datasets used in this study become available these can be incorporated where applicable.

At present, one degree is relatively high spatial resolution at global scales, especially in comparison to climate model grids. Nevertheless, one grid cell still represents a large area (approximately 100km in mid-latitudes) which can encompass large variation in physiography and climate. The associated spatial variability of soil moisture can also be high (Western et al., 2002) with impli-

cations for the development of drought. Higher resolution forcing data may therefore provide added information of the finer scale variations in drought and how drought develops as a spatially connected process. In terms of the temporal extent, the dataset covers the period 1948-2000 and so the derived hydrologic simulation captures many historically important regional drought events and some decadal variability in soil moisture. Nevertheless, this period still misses some significant drought events, such as the 1930s US drought and the series of early 20th century droughts in China and the Soviet Union that had such severe consequences. Extensions to the forcing dataset will add further information on drought occurrence and the long-term variability of the water cycle in general. Of course, the availability and density of observations during the first half of the 20th century and earlier is reduced, which increases the uncertainty in the associated forcings. Additionally, before 1950, the lack of reanalysis data means that most variables would have to be modeled or derived from predictive relationships with observed precipitation and temperature.

Moisture availability and drought are also inextricably linked to anthropogenic influences and other non-meteorological boundary conditions. For example, anthropogenic factors including irrigation, water withdrawals and land use change, and natural processes such as vegetation dynamics and wildfire, are not modeled explicitly. The impact of these may also vary in time, thus affecting the estimates of drought occurrence and the estimated trends. Estimates of current day irrigation are that 16.3% of cultivated regions are equipped for irrigation (Siebert et al., 2005) which can have a significant impact on the water cycle (Haddeland et al., 2007), although historically this may have been offset by changes in land use. Land cover has changed dramatically over the past 300-years (Foley and Ramakutty, 1999) and more so in tropical/developing regions over the 20th century (Goldewijk, 2001). The impact that this has had on the water cycle may be substantial (Zhang and Schilling, 2006; Scanlon et al., 2007), likely reducing evapotranspiration and increasing runoff with possible implications for the results presented here. Furthermore, elevated levels of CO₂ and increased growing season length may be responsible for recent increases in net primary productivity (NPP) and thus transpiration (Friend et al., 2007), although stomatal closure response to elevated CO₂ levels may have had the opposite effect (Gedney et al., 2006). Further investigation of these processes and their impact on drought are required. In particular, the contribution of changes in land use and irrigation to changes in soil moisture and drought are needed, especially in the context of future global warming and our ability to adapt to potential changes.

Despite these uncertainties, the retrospective drought index has been shown to be consistent with previous studies and captures well historic major drought events. It has been shown to be comparable to the most ubiquitous drought index in use, the PDSI. The weight of evidence as to the deficiencies of the PDSI, coupled with the availability of forcing data and computing power, indicate that state of the art land surface models are a viable alternative in retrospective analyses and realtime drought monitoring activities. We have shown that drought is driven mainly by precipitation variability, which has been modu-

lated in recent years by increases in temperature. The results also hint that the PDSI may have over-predicted the drying trend over the recent decades but this needs further investigation. At broader scales, soil moisture variability is connected to large scale climate variability, most notably the ENSO, AMO and NAO. This has important implications for understanding the mechanisms of drought occurrence and the potential for seasonal prediction, although the mechanisms that link large scale oscillations to drought occurrence are not fully clear. In addition, this is confounded by the trends in the data and compound impacts of multiple modes of climate variability. Further analysis is required to understand the driving forces of drought, at local and remote scales, and this is the focus of intensive research at present.

One of the greatest uncertainties in the depiction of historic drought is the lack of data describing its variation. At present off-line retrospective modelling driven by observation based forcings is the most promising source, yet uncertainties still remain, as noted above. Furthermore, estimates of the terrestrial hydrology have been shown to vary widely among models, even when driven by the same boundary conditions (e.g. Mitchell et al., 2004) with sometimes up to a factor of two difference in the calculated hydrologic variables. The VIC model used here is just one of many land surface schemes available. Our probabilistic approach for describing drought occurrence may overcome some of the systematic differences, but the non-linear nature of the hydrologic cycle means that drought may develop quite differently between models. One of the recommendations of this thesis is that multi-model retrospective datasets of global water cycle variability are constructed, analyzed and compared to get a better sense of uncertainties in the representation of historical drought.

As we look to the future, drought is expected to become more frequent, more extensive and more severe in many regions, with obvious impacts on agriculture and water availability. Some of these changes may happen despite any immediate efforts to reduce greenhouse gas emissions because of already elevated concentrations in the atmosphere and the thermal inertia of the oceans. However, there is still great variation in these projections because of uncertainty in the models and the processes and feedbacks that they describe. The wide variation in the sign and magnitude of regional precipitation change is one example of this. Our reliance on climate models to provide believable projections of the future is based on their ability to replicate observations or at least off-line estimates of the historic water cycle, in terms of its mean, variability and extremes. Therefore, future directions should seek greater understanding of the ability of climate models to reproduce historic drought and the retrospective dataset provides one benchmark against which they can be assessed. The greatest uncertainty may, however, be which emissions pathway we take in the future.

Bibliography

- Abdulla, F. A., D. P. Lettenmaier, E. F. Wood, and J. A. Smith, 1996: Application of a macroscale hydrologic model to estimate the water balance of the Arkansas-Red river basin, *J. Geophys. Res.*, **101**(D3), 7449–7459.
- AchutaRao, K., and K. R. Sperber, 2006: ENSO Simulation in Coupled Ocean-Atmosphere Models: Are the Current Models Better?. *Climate Dynamics*, 10.1007/s00382-006-0119-7.
- Adam, J. C., and D. P. Lettenmaier, 2003: Adjustment of global gridded precipitation for systematic bias. *J. Geophys. Res.*, 108, 4257, doi:10.1029/2002JD002499.
- Adam, J. C., E. A. Clark, D. P. Lettenmaier, and E. F. Wood, 2006: Correction of global precipitation products for orographic effects, *J. Clim.*, **19**(1), 15–38.
- Aguilar, E., and 35 co-authors, 2005: Changes in precipitation and temperature extremes in Central America and northern South America, 1961–2003, *J. Geophys. Res.*, **110**, D23107, doi:10.1029/2005JD006119.
- Alley, W. M., 1984: The Palmer Drought Severity Index: Limitations and assumptions, *J. Clim. Appl. Meteorol.*, **23**, 1100–1109.
- Andreadis, K. M., and D. P. Lettenmaier, 2006: Trends in 20th century drought over the continental United States, *Geophys. Res. Lett.*, **33**, L10403, doi:10.1029/2006GL025711.
- Andreadis, K. M., E. A. Clark, A. W. Wood, A. F. Hamlet, and D. P. Lettenmaier, 2005: Twentieth-century drought in the conterminous United States. *Journal of Hydrometeorology*, **6**, 985–1001.
- Barkstrom, B. R., E. F. Harrison, and G. L. Smith, 1989: Results from the Earth Radiation Budget Experiment (ERBE), *Adv. Space Res.*, **9**, 775–782.
- Barlow, M., H. Cullen, and B. Lyon, 2002: Drought in central and southwest Asia: La Nina, the warm pool, and Indian Ocean precipitation. *J. Climate*, **15**(7), 697–700.
- Batjes, N. H., 1995: A homogenized soil data file for global environmental research: A subset of FAO, ISRIC and NCRS profiles. Rep. 95/10, International Soil Reference and Information Centre, Wageningen, Netherlands, 50 pp. [Available from ISRIC, P.O. Box 535, 6700 AJ Wageningen, Netherlands.].

- Berberly, E. H. and V. R. Barros, 2002: The hydrologic cycle of the La Plata basin in South America. *Journal of Hydrometeorology*, **3**, 630-645.
- Berberly, E. H., K. E. Mitchell, S. Benjamin, T. Smirnova, H. Ritchie, R. Hogue, and E. Radeva, 1999: Assessment of land-surface energy budgets from regional and global models, *J. Geophys. Res.*, **104**(D16), 19,329–19,348.
- Berezovskaya, S., D. Q. Yang, and D. L. Kane, 2004: Compatibility analysis of precipitation and runoff trends over the large Siberian watersheds. *Geophys. Res. Lett.*, **31**(21), 4.
- Berg, A. A., J. S. Famiglietti, J. P. Walker, and P. R. Houser, 2003: Impact of bias correction to reanalysis products on simulations of North American soil moisture and hydrological fluxes, *J. Geophys. Res.*, **108**(D16), 4490, doi:10.1029/2002JD003334.
- Betts, A. K., J. H. Ball, and P. Viterbo, 2003a: Evaluation of the ERA-40 surface water budget and surface temperature for the Mackenzie River basin. *J. Hydrometeor.*, **4**(6), 1194-1211.
- Betts, A. K., J. H. Ball, M. Bosilovich, P. Viterbo, Y. C. Zhang, and W. B. Rossow, 2003b: Intercomparison of water and energy budgets for five Mississippi subbasins between ECMWF reanalysis (ERA-40) and NASA Data Assimilation Office fvGCM for 1990-1999. *J. Geophys. Res.*, **108**(D16): Art. No. 8618.
- Betts A. K., P. Viterbo, and E. Wood, 1998: Surface energy and water balance for the Arkansas Red River basin from the ECMWF reanalysis. *J. Climate*, **11**(11), 2881-2897.
- Betts, A. K., S.-Y. Hong, H.-L. Pan, 1996: Comparison of NCEP-NCAR reanalysis with 1987 FIFE data. *Mon. Weather Rev.*, **124**, 1480-1498.
- Boulanger, J. P., J. Leloup, O. Penalba, M. Rusticucci, F. Lafon, and W. Vargas, 2005: Observed precipitation in the Parana-Plata hydrological basin: long-term trends, extreme conditions and ENSO teleconnections. *Climate Dynamics*, **24**(4), 393-413.
- Bowling, L.C., D.P. Lettenmaier, B. Nijssen, L.P. Graham, et al. 2003, Simulation of high latitude hydrological processes in the Torne-Kalix basin: PILPS Phase 2(e) 1: Experiment description and summary intercomparisons, *J. Global Planet. Change*, 38(1-2), 1-30.
- Bo, Z., S. Islam, and E. A. B. Eltahir, 1994: Aggregation-disaggregation properties of a stochastic rainfall model. *Water Resour. Res.*, **30**, 3423-3435.
- Brohan, P., J. J. Kennedy, I. Haris, S. F. B. Tett and P. D. Jones, 2006: Uncertainty estimates in regional and global observed temperature changes: a new dataset from 1850. *J. Geophysical Research*, 111, D12106, doi:10.1029/2005JD006548.
- Brotzge, J. A., 2004: A two-year comparison of the surface water and energy budgets between two OASIS sites and NCEP–NCAR reanalysis data. *J. Hydromet.*, **5**, 311-326.
- Burke, E. J., S. J. Brown, and N. Christidis, 2006: Modeling the recent evolution of global drought and projections for the twenty-first century with the hadley centre climate model. *Journal of Hydrometeorology*, **7**, 1113-1125.

- Cherkauer, K. A., and D. P. Lettenmaier, 1999: Hydrologic effects of frozen soils in the upper Mississippi River basin, *J. Geophys. Res.*, **104**(D16), 19,599–19,610.
- Cherkauer, K. A., L. C. Bowling, and D. P. Lettenmaier, 2002: Variable Infiltration Capacity (VIC) cold land process model updates, *Global Planet. Change*, **38**, 151–159.
- Chiew, F. H. S., T. C. Piechota, J. A. Dracup, and T.A. McMahon, 1998: El Niño/Southern Oscillation and Australian rainfall, streamflow and drought: links and potential for forecasting. *J. Hydrology*, **204**: 138–149.
- Christensen, E., and K. Lassen, 1991: Length of the solar cycle: an indicator of solar activity closely associated with climate. *Science*, **254**, 698–700.
- Collins, M., T. J. Osborn, S. F. B. Tett, K. R. Briffa, and F. H. Schweingruber, 2002: A comparison of the variability of a climate model with paleotemperature estimates from a network of tree-ring densities. *Journal of Climate*, **15**, 1497–1515.
- Connolly, R. D., J. Schirmer, and P. K. Dunn, 1998: A daily rainfall disaggregation model. *Agric. Forest Meteorol.*, **92**, 105–117.
- Cook, E. R., D. M. Meko, D. W. Stahle, and M. K. Cleaveland, 1999: Drought reconstructions for the continental United States, *J. Climate*, **12**(4), 1145–1162.
- Cosby, B. J., G. M. Hornberger, R. B. Clapp, and T. R. Ginn, 1984: A statistical exploration of the relationships of soil moisture characteristics to the physical properties of soils. *Water Resour. Res.*, **20**, 682–690.
- Cosgrove, Brian A., et al., 2003: Real-time and retrospective forcing in the North American Land Data Assimilation System (NLDAS) project, *J. Geophys. Res.*, **108**(D22), 8842, doi:10.1029/2002JD003118.
- Covey, C., K. M. AchutaRao, U. Cubasch, P. Jones, S. J. Lambert, M. E. Mann, T. J. Phillips, and K. E. Taylor, 2003: An overview of results from the Coupled Model Intercomparison Project, *Global Planet. Change*, **37**, 103–133.
- Cowpertwait, P. S. P., P. E. O’Connell, A. V. Metcalfe, and J. A. Mawdsley, 1996: Stochastic point process modeling of rainfall. II. Regionalisation and disaggregation. *J. Hydrol.*, **175**, 47–65.
- Cox, P. M., R. A. Betts, C. D. Jones, S. A. Spall, and I. J. Totterdell, 2000: Acceleration of global warming due to carbon-cycle feedbacks in a coupled climate model. *Nature*, **408**, 184 – 187.
- Critchfield, H. J., 1983: *General Climatology*. 4th ed. Prentice Hall, 453 pp.
- Cullather, R. I., D. H. Bromwich and M. C. Serreze, 2000: The atmospheric hydrologic cycle over the Arctic Basin from reanalyses. Part I: Comparison with observations and previous studies. *J. Climate*, **13**, 923–937.
- Dai, A., 2001: Global precipitation and thunderstorm frequencies. Part II: Diurnal variations, *J. Climate*, **14**, 1112–1128.
- Dai, A., 2006: Precipitation characteristics in eighteen coupled climate models. *J. Climate*, **19**, 4605–4630.
- Dai, A., I. Y. Fung, and A. D. DelGenio, 1997: Surface observed global land precipitation variations during 1900–88. *J. Climate*, **10**(11), 2943–2962.

- Dai, A., K. E. Trenberth, and T. Qian, 2004: A global data set of Palmer Drought Severity Index for 1870-2002: Relationship with soil moisture and effects of surface warming. *J. Hydrometeor.*, **5**, 1117-1130.
- Dai, A., K. E. Trenberth, and T. R. Karl, 1998: Global variations in droughts and wet spells: 1900-1995. *Geophys. Res. Lett.* **25**(17), 3367-3370.
- Darnell, W. L., W. F. Staylor, S. K. Gupta, N. A. Ritchey, and A. C. Wilber, 1992: Seasonal variation of surface radiation budget derived from International Satellite Cloud Climatology Project C1 data. *J. Geophys. Res.*, **97**, 15741-15760.
- Decharme, B. and H. Douville, 2006: Uncertainties in the GSWP-2 precipitation forcing and their impacts on regional and global hydrological simulations. *Climate Dynamics*, **27**, 695-713.
- Déry, S. J., and E. F. Wood, 2005a: Decreasing river discharge in northern Canada. *Geophys. Res. Lett.*, **32**(10), 4.
- Déry, S. J., and E. F. Wood, 2005b: Observed twentieth century land surface air temperature and precipitation covariability, *Geophys. Res. Lett.*, **32**, L21414, doi: 10.1029/2005GL024234.
- Dirmeyer, P. A., X. Gao, M. Zhao, Z. Guo, T. Oki and N. Hanasaki, 2005: The Second Global Soil Wetness Project (GSWP-2): Multi-model analysis and implications for our perception of the land surface. COLA Technical Report 185 [Available online at: <ftp://grads.iges.org/pub/ctr/ctr.185.pdf>], 46 pp.
- Dong, B. W., R. T. Sutton, and A. A. Scaife, 2006: Multidecadal modulation of El Nino-Southern Oscillation (ENSO) variance by Atlantic Ocean sea surface temperatures. *Geophys. Res. Lett.*, **33**(8), 4.
- Duan, Q., V. K. Gupta, and S. Sorooshian, 1993: A shuffled complex evolution approach for effective and efficient global minimization, *J. Optimization Theory Appl.*, **76**(3), 501- 521.
- Dumenil, L., and E. Todini, 1992: A rainfall-runoff scheme for use in the Hamburg climate model, in *Advances in theoretical hydrology, A tribute to James Dooge*. P. O’Kane, ed., European Geophysical Society Series on Hydrological Sciences 1, Elsevier, Amsterdam.
- Easterling, D. R., G. A. Meehl, C. Parmesan, S. A. Changnon, T. R. Karl, and L. O. Mearns, 2000: Climate extremes: Observations, modeling, and impacts. *Science*, **289**, 2068-2074.
- Eltahir, E. A. B., and R. L. Bras, 1993: Estimation of the fractional coverage of rainfall in climate models. *J. Climate*, **6**, 639-644.
- Enfield, D. B., A. M. Mestas-Nunez, and P. J. Trimble, 2001: The Atlantic multidecadal oscillation and its relation to rainfall and river flows in the continental US. *Geophys. Res. Lett.*, **28**(10), 2077-2080.
- FAO, 1995: The Digital Soil Map of the World, Version 3.5. United Nations Food and Agriculture Organization, CD-ROM. [Available from Food and Agriculture Organization of the United Nations, Viale delle Terme di Caracalla, 00100 Rome, Italy].
- Fekete, B. M., C. J. Vörösmarty, J. O. Roads, and C. J. Willmott, 2004: Uncertainties in precipitation and their impacts on runoff estimates. *J. Climate*,

- 17, 294-304.
- Foley, J. A., A. Botta, M. T. Coe, and M. H. Costa, 2002: El Nino-Southern Oscillation and the climate, ecosystems and rivers of Amazonia. *Global Biogeochemical Cycles*, **16**(4), 27.
- Frei, A., and G. Gong, 2005: Decadal to century scale trends in North American snow extent in coupled Atmosphere-Ocean General Circulation Models. *Geophysical Research Letters*, **32**, L18502.
- Friend, A. D., A. Arneth, N. Y. Kiang, M. Lomas, J. Ogee, C. Rodenbeckk, S. W. Running, J. D. Santaren, S. Sitch, N. Viovy, F. I. Woodward, and S. Zaehle, 2007: FLUXNET and modelling the global carbon cycle. *Global Change Biology*, **13**, 610-633.
- Fu, Q., K. N. Liou, M. C. Cribb, T. P. Charlock, A. Grossman, 1997: Multiple scattering parameterization in thermal infrared radiative transfer. *J. Atmos. Sci.*, **54**, 2799-2812.
- Garcia, N. O., and C. R. Mechoso, 2005: Variability in the discharge of South American rivers and in climate. *Hydrological Sciences Journal*, **50** (3), 459-478.
- Gedney, N., P. M. Cox, R. A. Betts, O. Boucher, C. Huntingford, and P. A. Stott, 2006: Detection of a direct carbon dioxide effect in continental river runoff records. *Nature*, **439**, 835-838.
- Giannini, A., R. Saravanan, and P. Chang, 2003: Oceanic forcing of Sahel rainfall on interannual to interdecadal time scales. *Science*, **302**, 1027-1030.
- Gibson, J. K., P. Kallberg, S. Uppala, A. Hernandez, A. Normura and E. Serrano, 1997: ERA description. ECMWF Re-Analysis Project Rep. Ser. 1, 72 pp. ECMWF, Reading, UK.
- Gilgen, H, Wild, M, Ohmura, A., 1998: Means and trends of shortwave irradiance at the surface estimated from global energy balance archive data. *J. Climate*, **11**, 2042-2061.
- Giorgi, F., 2002: Variability and trends of sub-continental scale surface climate in the twentieth century. Part 1: observations. *Clim. Dyn.*, **18**, 675-691.
- Giorgi F., and R. Francisco, 2000: Uncertainties in regional climate change predictions. A regional analysis of ensemble simulations with the HADCM2 GCM. *Clim. Dyn.*, **16**, 169-182.
- Giorgi F., and X. Q. Bi, 2005: Updated regional precipitation and temperature changes for the 21st century from ensembles of recent AOGCM simulations. *Geophys. Res. Lett.*, **32**, L21715, doi:10.1029/2005GL024288.
- Goldewijk, K. K., 2001: Estimating global land use change over the past 300 years: The HYDE Database. *Global Biogeochemical Cycles*, **15**, 417-433.
- Gong, G., D. Entekhabi, and G. D. Salvucci, 1994: Regional and seasonal estimates of fractional storm coverage based on station precipitation observations. *J. Climate.*, **7**, 1495-1505.
- Goodison, B. E., P. Y. T. Louie, and D. Yang, 1998: WMO solid precipitation measurement intercomparison, final report, WMO/TD-872, WMO, Geneva, 212pp.

- Gottschalck, J., J. Meng, M. Rodell, P. Houser, 2005: Analysis of multiple precipitation products and preliminary assessment of their impact on Global Land Data Assimilation System land surface states. *J. Hydrometeor.*, **6**, 573-598.
- Gregory, J. M., J. F. B. Mitchell, and A. J. Brady, 1997: Summer drought in northern midlatitudes in a time-dependent CO₂ climate experiment. *Journal of Climate*, **10**, 662-686.
- Groisman, P. Y., R. W. Knight, T. R. Karl, D. R. Easterling, B. M. Sun, and J. H. Lawrimore, 2004: Contemporary changes of the hydrological cycle over the contiguous United States: Trends derived from in situ observations. *J. Hydrometeor.*, **5**(1), 64-85.
- Gullison, R. E., P. C. Frumhoff, J. G. Canadell, C. B. Field, D. C. Nepstad, K. Hayhoe, R. Avissar, L. M. Curran, P. Friedlingstein, C. D. Jones, and C. Nobre, 2007: Tropical Forests and Climate Policy. *Science* **316** (5827), 985. [DOI: 10.1126/science.1136163]
- Guo, Z. C., and P. A. Dirmeyer, 2006: Evaluation of the Second Global Soil Wetness Project soil moisture simulations: 1. Intermodel comparison, *Journal of Geophysical Research-Atmospheres*, 111(D22), 14.
- Guo, Z. C., P. A. Dirmeyer, Z. Z. Hu, X. Gao, and M. Zhao, 2006: Evaluation of the Second Global Soil Wetness Project soil moisture simulations: 2. Sensitivity to external meteorological forcing. *Journal of Geophysical Research-Atmospheres*, **111**, 11.
- Guo, Z., P. A. Dirmeyer, X. Gao, and M. Zhao, 2007: Improving the quality of simulated soil moisture multi-model ensemble approach. *Q. J. R. Meteorol. Soc.*, **133**: 731-747, DOI: 10.1002/qj.48
- Gupta, S. K., N. A. Ritchey, A. C. Wilber, C. H. Whitlock, G. G. Gibson, and P. W. Stackhouse, 1999: A climatology of surface radiation budget derived from satellite data, *J. Climate*, **12**, 2691-2710.
- Gupta, S. K., W. L. Darnell, and A. C. Wilber, 1992: A parameterization for longwave surface radiation from satellite data: Recent improvements. *J. Appl. Meteor.*, **31**, 1361-1367.
- Gütner, A., J. Olsson, A. Calver, and B. Gannon, 2001: Cascade-based disaggregation of continuous rainfall time series: the influence of climate. *Hydrol. Earth System Sci.*, **5**(2), 145-164.
- Haddeland, I., T. Skaugen, and D.P. Lettenmaier, 2007: Hydrologic effects of land and water management in North America and Asia: 1700-1992, *Hydrol. Earth Sys. Sci.*, **11**(2), 1035-1045.
- Hahmann, A. N., 2003: Representing spatial subgrid-scale precipitation variability in a GCM. *J. Hydrometeor.*, **4**, 891-900.
- Hall, F. G., G. Collatz, S. Los, E. Brown de Colstoun, and D. Landis, eds., 2005: ISLSCP Initiative II. NASA. DVD/CD-ROM. NASA.
- Hamlet, A. F., P. W. Mote, M. P. Clark, and D. P. Lettenmaier, 2007: Twentieth-century trends in runoff, evapotranspiration, and soil moisture in the western United States. *Journal of Climate*, **20**, 1468-1486.

- Hansen, J., M. Sato, R. Ruedy, K. Lo, D. W. Lea, and M. Medina-Elizade, 2006: Global temperature change. *Proceedings of the National Academy of Sciences of the United States of America*, **103**, 14288-14293.
- Hansen, J., R. Ruedy, J. Glascoe, and M. Sato 1999. GISS analysis of surface temperature change. *J. Geophys. Res.* **104**, 30997-31022, doi:10.1029/1999JD900835.
- Hansen, M. C., R. S. DeFries, J. R. G. Townshend, and R. Sohlberg, 2000: Global land cover classification at 1 km spatial resolution using a classification tree approach. *Int. J. Remote Sens.*, **21**, 1331-1364.
- Hasselmann, K., M. Latif, G. Hooss, C. Azar, O. Edenhofer, C. C. Jaeger, O. M. Johannessen, C. Kemfert, M. Welp, and A. Wokaun, 2003: The challenge of long-term climate change. *Science*, **302**, 1923-1925.
- Hegerl, G. C., T. J. Crowley, M. Allen, W. T. Hyde, H. N. Pollack, J. Smerdon, and E. Zorita, 2007: Detection of human influence on a new, validated 1500-year temperature reconstruction. *Journal of Climate*, **20**, 650-666.
- Hegerl, G. C., T. R. Karl, M. Allen, N. L. Bindoff, N. Gillett, D. Karoly, X. B. Zhang, and F. Zwiers, 2006: Climate change detection and attribution: Beyond mean temperature signals. *Journal of Climate*, **19**, 5058-5077.
- Heim, R. R., Jr., 2002: A review of twentieth century drought indices used in the United States, *Bull. Am. Meteorol. Soc.*, **83**(8), 1149-1165.
- Held, I. M., and B. J. Soden, 2000: Water vapor feedback and global warming. *Ann. Rev. Energy Env.*, **25**, 441-475.
- Held, I. M., T. L. Delworth, J. Lu, K. L. Findell, and T. R. Knutson, 2005: Simulation of Sahel drought in the 20th and 21st centuries. *Proc. Nat. Acad. Science*, **102**, 17891-17896.
- Herbert, J. M. and R. W. Dixon, 2003: Is the ENSO phenomenon changing as a result of global warming? *Physical Geography*, **23**, 196-211.
- Hershenhorn, J., and D. A. Woolhiser, 1987. Disaggregation of daily rainfall. *J. Hydrol.*, **95**, 299-322.
- Higgins, R. W., A. Leetmaa, Y. Xue, and A. Barnston, 2000: Dominant factors influencing the seasonal predictability of US precipitation and surface air temperature. *J. Climate* **13**, 3994-4017.
- Hirsch, R. M., and J. R. Slack, 1984: A Nonparametric Trend Test For Seasonal Data With Serial Dependence. *Water Resources Research*, **20**(6), 727-732.
- Hodell, D. A., Curtis, J. H. and Brenner, M. 1995: Possible role of climate in the collapse of the Classic Maya Civilization. *Nature*, **375**, 391-394.
- Hoerling, M., and A. Kumar, 2003: The perfect ocean for drought. *Science*, **299** (5607), 691-694, DOI: 10.1126/science.1079053
- Hosking, J. R. M., 1990: L-moments: analysis and estimation of distributions using linear combinations of order statistics, *J. R. Stat. Soc.*, **52**(1), 105-124.
- Hsu, K., X. Gao, S. Sorooshian, and H. V. Gupta, 1997: Precipitation estimation from remotely sensed information using artificial neural networks. *J. of App. Met.*, **36**, 1176-1190.
- Huffman, G. J., R. F. Adler, E. F. Stocker, D. T. Bolvin, and E. J. Nelkin, 2003: Analysis of TRMM 3-hourly multi-satellite precipitation estimates

- computed in both real and post-real time. Combined Preprints CD-ROM, 83rd AMS Annual Meeting. Paper P4.11 in 12th Conf. on Sat. Meteor. and Oceanog., 9-13 Feb. 2003, Long Beach, CA, 6 pp.
- Huffman, G. J., R. F. Adler, M. M. Morrissey, D. T. Bolvin, S. Curtis, R. Joyce, B. McGavock and J. Susskind, 2001: Global precipitation at one-degree daily resolution from multisatellite observations. *J. Hydrometeor.*, **2**(1), 36-50.
- Huffman, G. J., R. F. Adler, P. Arkin, A. Chang, R. Ferraro, A. Gruber, J. Janowiak, A. McNab, B. Rudolf and U. Schneider, 1997: The Global Precipitation Climatology Project (GPCP) combined precipitation dataset. *Bull. Amer. Meteor. Soc.*, **78**, 5-20.
- Hulme, M., 1992: Rainfall changes in Africa — 1931-1960 to 1961-1990. *Int. J. Climatology*, **12**, 685-699.
- Hulme, M., 1995: Estimating global changes in precipitation. *Weather*, **50**, 34-42.
- Hulme, M. and M. New, 1997: Dependence of large-scale precipitation climatologies on temporal and spatial sampling. *Journal of Climate*, **10**, 1099-1113.
- Hulme, M., E. M. Barrow, N. W. Arnell, P. A. Harrison, T. C. Johns, and T. E. Downing, 1999: Relative impacts of human-induced climate change and natural climate variability. *Nature*, **397**, 688-691.
- Hunt, A. G., 1999: Understanding a possible correlation between El Nino occurrence frequency and global warming. *Bulletin of the American Meteorological Society*, **80**, 297-300.
- Hunt, B. G., 2006: The Medieval Warm Period, the Little Ice Age and simulated climatic variability. *Climate Dynamics*, **27**, 677-694.
- Huntington, T. G., 2006: Evidence for intensification of the global water cycle: Review and synthesis. *J. Hydrology*, **319**(1-4), 83-95.
- Hurrell, J. W., and H. VanLoon, 1997: Decadal variations in climate associated with the north Atlantic oscillation. *Climatic Change*, **36**(3-4), 301-326.
- IPCC, 2001: *Climate Change 2001: The Scientific Basis. Contribution of Working Group I to the Third Assessment Report of the Intergovernmental Panel on Climate Change*, Houghton, J. T., et al. Eds., Cambridge University Press, Cambridge, UK, 944 pp.
- IPCC, 2007: *Climate Change 2007: The Physical Science Basis. Contribution of Working Group I to the Fourth Assessment Report of the Intergovernmental Panel on Climate Change*, Solomon, S., D. Qin, M. Manning, Z. Chen, M. Marquis, K.B. Averyt, M. Tignor and H.L. Miller (eds.). Cambridge University Press, Cambridge, United Kingdom and New York, NY, USA, 996 pp.
- Janowiak, J. E., A. Gruber, C. R. Kondragunta, R. E. Livezey and G. J. Huffman, 1998: A comparison of the NCEP-NCAR reanalysis precipitation and the GPCP rain gauge-satellite combined dataset with observational error considerations. *J. Climate*, **11**(11), 2960-2979.
- Jansen, E., J. Overpeck, K.R. Briffa, J.-C. Duplessy, F. Joos, V. Masson-Delmotte, D. Olago, B. Otto-Bliesner, W.R. Peltier, S. Rahmstorf, R.

- Ramesh, D. Raynaud, D. Rind, O. Solomina, R. Villalba and D. Zhang, 2007: Palaeoclimate. In: *Climate Change 2007: The Physical Science Basis. Contribution of Working Group I to the Fourth Assessment Report of the Intergovernmental Panel on Climate Change* [Solomon, S., D. Qin, M. Manning, Z. Chen, M. Marquis, K.B. Averyt, M. Tignor and H.L. Miller (eds.)]. Cambridge University Press, Cambridge, United Kingdom and New York, NY, USA.
- Johnson, K. D., D. Entekhabi, and P. S. Eagleson, 1993: The implementation and validation of improved land-surface hydrology in an atmospheric general circulation model. *J. Climate*, **6**, 1009–1026.
- Jones, P. D., and A. Moberg, 2003: Hemispheric and large-scale surface air temperature variations: An extensive revision and an update to 2001. *J. Climate*, **16**(2), 206–223.
- Jones, P. D., M. New, D. E. Parker, S. Martin, and I. G. Rigor, 1999: Surface air temperature and its variations over the last 150 years. *Reviews of Geophysics*, **37**, 173–199.
- Kalnay, E., and M. Cai, 2003: Impact of urbanisation and land-use change on climate, *Nature*, **423**, 528– 531.
- Kalnay, E., M. Kanamitsu, R. Kistler, W. Collins, D. Deaven, L. Gandin, M. Iredell, S. Saha, G. White, J. Woollen, Y. Zhu, A. Leetmaa, R. Reynolds, M. Chelliah, W. Ebisuaki, W. Higgins, J. Janowiak, K. C. Mo., R. Jenne and D. Joseph, 1996: The NCEP/NCAR 40-Year Reanalysis Project. *Bull. Amer. Meteor. Soc.*, **77**, 437–471.
- Kanamitsu, M., W. Ebisuzaki, J. Woollen, S-H. Yang, J. J. Hnilo, M. Fiorino, and G. L. Potter, 2002: NCEP–DOE AMIP-II Reanalysis (R-2). *Bull. Amer. Meteor. Soc.*, **83**, 1631–1643.
- Kendall, M. G., 1975: *Rank Correlation Methods*. Charles Griffin, London, 202 pp.
- Kerr, R. A., 2000: A North Atlantic climate pacemaker for the centuries. *Science*, **288**(5473), 1984–1986.
- Kharin, V. V., and F. W. Zwiers, 2005: Estimating extremes in transient climate change simulations. *J. Climate*, **18** (8): 1156–1173.
- Kim, T.-W., J. B. Valdés, and C. Yoo, 2003: Nonparametric approach for estimating return periods of droughts in arid regions, *J. Hydrologic Engrg.*, **8**(5), 237–246.
- King, D. A., 2004: Climate change science: Adapt, mitigate, or ignore? *Science* **303**, 176–177.
- Kistler, R., E. Kalnay, W. Collins, S. Saha, G. White, J. Woollen, M. Chelliah, W. Ebisuzaki, M. Kanamitsu, V. Kousky, H. Dool, R. Jenne and M. Fiorino, 2001: The NCEP–NCAR 50–Year Reanalysis: Monthly Means CD-ROM and Documentation. *Bull. Amer. Meteor. Soc.*, **82**: 247–268.
- Krishnamurthy, V., and J. Shukla, 2000: Intraseasonal and interannual variability of rainfall over India. *J. Climate*, **13** (24), 4366–4377.
- Lau, K.-M., S. Shen, K.-M. Kim, and H. Wang, 2006: A Multi-model Study of the 20th Century Simulations of Sahel Drought from the 1970s to 1990s. *Journal of Geophysical Research*, **111**, D0711, doi:10.1029/2005JD006281.

- Lau, K. -M, V. M. Mehta, Y. C. Sud, and G. K. Walker, 1994: Climatology and natural variability of the global hydrologic cycle in the GLA atmospheric general circulation model, *J. Geophys. Res.*, **99**(D1), 1329-1345.
- Lenters, J. D., M. T. Coe, and J. A. Foley, 2000: Surface water balance of the continental United States, 1963-1995: Regional evaluation of a terrestrial biosphere model and the NCEP/NCAR reanalysis. *J. Geophys. Res.*, **105**(D17), 22393-22425.
- Levis, S., M. T. Coe, and J. A. Foley, 1996: Hydrologic budget of a land surface model: a global application, *J. Geophys. Res.*, **101**(D12), 16,921-16,930.
- L'Hôte Y., G. Mahé, B. Somé, and J. P. Triboulet, 2002: Analysis of a Sahelian annual rainfall index from 1896 to 2000; the drought continues. *Hydrological Sciences Journal-Journal Des Sciences Hydrologiques*, **47**, 563-572.
- Liang, X., D.P. Lettenmaier, E.F. Wood, and S.J. Burges, 1994: A simple hydrologically based model of land surface water and energy fluxes for general circulation models. *J. Geophys. Res.*, **99**(D7), 14,415-14,428.
- Liang, X., E. F. Wood, and D. P. Lettenmaier, 1996: Surface soil moisture parameterization of the VIC-2L model: Evaluation and modifications, *Global Planet. Change*, **13**, 195- 206.
- Li, H., A. Robock, and M. Wild, 2007: Evaluation of Intergovernmental Panel on Climate Change Fourth Assessment soil moisture simulations for the second half of the twentieth century. *J. Geophys. Res.*, **112**, D06106, doi:10.1029/2006JD007455.
- Liverman, D. M., 1999: Vulnerability and adaptation to drought in Mexico. *Natural Resources Journal*, **39**(1), 99-115.
- Lloyd-Hughes, B. and M. A. Saunders, 2002: A Drought Climatology for Europe, *International Journal of Climatology*, **22**, 1571-1592.
- Lopez, A., C. Tebaldi, M. New, et al., 2006: Two approaches to quantifying uncertainty in global temperature changes. *J. Climate*, **19** (19): 4785-4796.
- Mann, H. B., 1945: Non-parametric test against trend. *Econometrika* **13**, 245-259.
- Mantua, N. J., S. R. Hare, Y. Zhang, J. M. Wallace, and R. C. Francis, 1997: A Pacific interdecadal climate oscillation with impacts on salmon production. *Bulletin Of The American Meteorological Society*, **78**(6), 1069-1079.
- Marani, M., G. Grossi, M. Wallace, F. Napolitano, and D. Entekhabi, 1997: Forcing, intermittency, and land surface hydrological partitioning. *Water Resour. Res.*, **33**, 1671-175.
- Maurer, E. P., A. W. Wood, J. C. Adam, D. P. Lettenmaier, and B. Nijssen, 2002. A long-term hydrologically-based data set of land surface fluxes and states for the conterminous United States, *J. Clim.*, **15**, 3237-3251.
- Maurer, E. P., G. M. O'Donnell, D. P. Lettenmaier and J. O. Roads, 2001: Evaluation of NCEP/NCAR Reanalysis Water and Energy Budgets using Macroscale Hydrologic Simulations, In: *Land Surface Hydrology, Meteorology, and Climate: Observations and Modeling*, AGU series in Water Science and Applications, V. Lakshmi, J. Albertson and J. Schaake (eds.), pp. 137-158.

- Maurer, E. P., G. M. O'Donnell, D. P. Lettenmaier, and J. O. Roads, 2001: Evaluation of the Land Surface Water Budget in NCEP/NCAR and NCEP/DOE Reanalyses using an Off-line Hydrologic Model, *J. Geophys. Res.*, **106**(D16), 17,841-17,862.
- McBean, G.A., 2005: Arctic Climate – Past and Present, in *Arctic Climate Impact Assessment (ACIA)*. Cambridge University Press, Cambridge, United Kingdom and New York, NY, USA.
- McCabe, G. J., and M. A. Palecki, 2006: Multidecadal climate variability of global lands and oceans. *Int. J. Climatology*, **26**(7), 849-865.
- McCabe, G. J., Jr., and D. M. Wolock, 1997: Climate change and the detection of trends in annual runoff. *Climate Res.* **8**, 129-134.
- McCabe, G. J., M. A. Palecki, and J. L. Betancourt, 2004: Pacific and Atlantic Ocean influences on multidecadal drought frequency in the United States. *Proceedings Of The National Academy Of Sciences Of The United States Of America*, **101**(12), 4136-4141.
- McClelland, J. W., S. J. Dery, B. J. Peterson, R. M. Holmes, and E. F. Wood, 2006: A pan-arctic evaluation of changes in river discharge during the latter half of the 20th century. *Geophys. Res. Lett.*, **33**(6), 4.
- Meehl, G. A., et al., 2005: How much more global warming and sea level rise? *Science* **307** (5716), 1769-1772.
- Meeson, B. W., F. E. Corprew, J. M. P. McManus, D. M. Myers, J. W. Closs, K. -J. Sun, D. J. Sunday, P. J. Sellers, 1995: ISLSCP Initiative I-Global Data Sets for Land-Atmosphere Models, 1987-1988. Volumes 1-5. Published on CD by NASA.
- Mitchell, K. E., and 22 coauthors, 2004: The multi-institution North American Land Data Assimilation System (NLDAS): Utilizing multiple GCIP products and partners in a continental distributed hydrological modeling system, *J. Geophys. Res.*, **109**, D07S90, doi:10.1029/2003JD003823.
- Mitchell K. E., D. Lohmann, P. R. Houser, E. F. Wood, J. C. Schaake, A. Robock, D. P. Lettenmaier, B. A. Cosgrove, J. Sheffield, Q. Duan, L. Luo, R. W. Higgins, R. T. Pinker, J. D. Tarpley, C. H. Marshall, J. K. Entin, M. Pan, W. Shi, J. Meng, B. H. Ramsay, and A. Bailey, 2004a: The multi-institution North American Land Data Assimilation System (NLDAS) project: Utilizing multiple GCIP products and partners in a continental distributed hydrological modeling system., *J. Geophys. Res.*, **109**, D07S90, doi: 10.1029/2003JD003823.
- Mitchell, T. D., and P. D. Jones, 2005: An improved method of constructing a database of monthly climate observations and associated high-resolution grids. *International Journal of Climatology*, **25**(6), 693-712.
- Mitchell, T. D., T. R. Carter, P. D. Jones, M. Hulme, and M. New, 2004b: A comprehensive set of high-resolution grids of monthly climate for Europe and the globe: the observed record (1901-2000) and 16 scenarios (2001-2100). *J. Climate*, submitted.
- Morrill, J. C., R. E. Dickinson and A. N. Hahmann, 1999: Sensitivity of a land surface model to the diurnal distribution of downward longwave radiation. *J. Meteor. Soc. Jpn.*, **77**(1B), 265–279.

- Mortimore, M. J., and W. M. Adams, 2001: Farmer adaptation, change and 'crisis' in the Sahel. *Global Environmental Change*, **11**, 49–57.
- Myneni, R. B., R. R. Nemani, and S. W. Running, 1997: Estimation of global leaf area index and absorbed PAR using radiative transfer models. *IEEE Trans. Geosci. Remote Sens.*, **35**, 1380–1393.
- Nakicenovic, N., O. Davidson, G. Davis, A. Grübler, T. Kram, E. L. L. Rovere, B. Metz, T. Morita, W. Pepper, H. Pitcher, A. Sankovski, P. Shukla, R. Swart, R. Watson, and Z. Dadi, 2000: *Emissions scenarios—summary for policymakers*. Intergovernmental Panel on Climate Change, Geneva, Switzerland.
- Negri, A. J., T. L. Bell, and L. Xu, 2002: Sampling of the diurnal cycle of precipitation using TRMM, *J. Atmos. Ocean. Tech.*, **19**, 1333–1344.
- Newman M., G. P. Compo, and M. A. Alexander, 2003: ENSO-forced variability of the Pacific decadal oscillation. *J. Climate*. **16**: 3853–3857.
- New, M. G., M. Hulme, and P. D., Jones, 1999: Representing twentieth century space-time climate variability. Part 1: development of a 1961–90 mean monthly terrestrial climatology. *J. Climate*, **12**, 829–856.
- New, M. G., M. Hulme, and P. D. Jones, 2000: Representing twentieth-century space-time climate variability. Part II: Development of 1901–1996 monthly grids of terrestrial surface climate. *J. Climate*, **13**, 2217–2238.
- Ngo-Duc, T., J. Polcher, and K. Laval, 2005: A 53-year forcing data set for land surface models. *J. Geophys. Res.*, **110**, D06116, doi:10.1029/2004JD005434.
- Nicholls, N., B. Lavery, C. Frederiksen, W. Drosowsky, and S. Torok, 1996: Recent apparent changes in relationships between the El Nino - Southern oscillation and Australian rainfall and temperature. *Geophys. Res. Lett.*, **23** (23), 3357–3360.
- Nicholson, S., 2000: Land surface processes and Sahel climate. *Reviews of Geophysics*, **38**, 117–139.
- Nijssen, B., and D. P. Lettenmaier, 2004: Effect of precipitation sampling error on simulated hydrological fluxes and states: Anticipating the Global Precipitation Measurement satellites, *J. Geophys. Res.*, **109**, D02103, doi:10.1029/2003JD003497.
- Nijssen, B., G. M. O'Donnell, D. P. Lettenmaier, D. Lohmann, E. F. Wood, 2001b: Predicting the discharge of global rivers. *J. Climate*, **14**, 3307–3323.
- Nijssen, B., R. Schnur, and D. P. Lettenmaier, 2001a: Global retrospective estimation of soil moisture using the Variable Infiltration Capacity land surface model, 1980–1993. *J. Climate*, **14**, 1790–1808.
- Nijssen N., L.C. Bowling, D.P. Lettenmaier, D. B. Clark, M. E. Maayar et al, 2003, Simulation of high latitude hydrological processes in the Torne-Kalix basin: PILPS Phase 2(e) 2: Comparison of model results with observations, *J. Global Planet. Change*, 38(1–2), 31–53.
- NRC, 2003: *Understanding climate change feedbacks*. Report of the Panel on Climate Change Feedbacks, National Research Council. National Academies Press, Washington D.C., 166pp.

- Oba, G., E. Post, and N. C. Stenseth, 2001: Sub-saharan desertification and productivity are linked to hemispheric climate variability. *Global Change Biology*, **7**(3), 241-246.
- OFDA/CRED, 2006: *EM-DAT: The OFDA/CRED International Disaster Database* (available online at www.em-dat.net). Université Catholique de Louvain, Brussels, Belgium.
- Oki, T., T. Nishimura, and P. Dirmeyer, 1999: Assessment of annual runoff from land surface models using Total Runoff Integrating Pathways (TRIP), *J. Meteorol. Soc. Jpn.*, **77**, 235-255.
- Olsson, J., 1998: Evaluation of a cascade model for temporal rainfall disaggregation. *Hydrol. Earth System Sci.*, **2**, 19-30.
- Osborn, T. and K. R. Briffa, 2006: The spatial extent of 20th-century warmth in the context of the past 1200 years. *Science*, **311**, 841-844.
- Palmer, T. N., and J. Räisänen, 2002: Quantifying the risk of extreme seasonal precipitation events in a changing climate. *Nature* **415**, 512-514.
- Palmer, W., 1965: *Meteorological drought*, Res. Pap. 45, 58 pp., U.S. Dep. of Commerce, Washington, D. C.
- Pan, M., and E. F. Wood, 2004: Water budget estimation by assimilating multiple observations and hydrological modeling using constrained ensemble Kalman filtering. *Eos Trans. AGU*, **85**(17), *Jt. Assem. Suppl.*
- Pan, M., J. Sheffield, E. F. Wood, K. E. Mitchell, P. R. Houser, J. C. Schaake, A. Robock, D. Lohmann, B. A. Cosgrove, Q. Duan, L. Luo, R. W. Higgins, R. T. Pinker, and J. D. Tarpley, 2003: Snow process modeling in the North American Land Data Assimilation System (NLDAS): 2. Evaluation of model simulated snow water equivalent, *J. Geophys. Res.*, **108**(D22), 8850, doi:10.1029/2003JD003994.
- Patz, J. A., M. Hulme, C. Rosenzweig, T. D. Mitchell, R. A. Goldberg, A. K. Githeko, S. Lele, A. J. McMichael, D. Le Sueur, 2002: Climate change - Regional warming and malaria resurgence. *Nature*, **420**(6916), 627-628.
- Peel, M. C., G. G. S. Pegram, and T. A. McMahon, 2004: Global analysis of runs of annual precipitation and runoff equal to or below the median: run length. *Int. J. Climatol.*, **24**, 807-822.
- Peel, M. C., T. A. McMahon, and G. G. S. Pegram, 2005: Global analysis of runs of annual precipitation and runoff equal to or below the median: run magnitude and severity. *Int. J. Climatol.* **25**: 549-568.
- Peterson, B. J., Holmes, R. M., McClelland, J. W., Vorosmarty, C. J., Lambers, R. B., Shiklomanov, A. I., I. A. Shiklomanov, S. Rahmstorf, 2002: Increasing river discharge to the Arctic Ocean. *Science*, **298**(5601), 2171-2173.
- Pinker, R. T., and I. Laszlo, 1992: Modeling surface solar irradiance for satellite applications on a global scale, *J. Appl. Meteor.*, **31**, 194-211.
- Pinker, R. T., B. Zhang, and E. G. Dutton, 2005: Do satellites detect trends in surface solar radiation? *Science*, 6 May, 850-854.
- Pinker, R. T., et al., 2003: Surface radiation budgets in support of the GEWEX Continental-Scale International Project (GCIP) and the GEWEX Americas Prediction Project (GAPP), including the North American Land Data

- Assimilation System (NLDAS) project, *J. Geophys. Res.*, **108**(D22), 8844, doi:10.1029/2002JD003301.
- Pittock, A. B., 1999: Climate change: The question of significance. *Nature* **397**, 657-658.
- Power, S., T. Casey, C. Folland, A. Colman, and V. Mehta, 1999: Inter-decadal modulation of the impact of ENSO on Australia. *Climate Dynamics*, **15**, 319-324.
- Qu, W., A. Henderson-Sellers, A. J. Pitman, T. H. Chen, F. Abramopoulos, A. Boone, S. Chang, F. Chen, Y. Dai, R. E. Dickinson, L. Dümenil, M. Ek, N. Gedney, Y. M. Gusev, J. Kim, R. Koster, E. A. Kowalczyk, J. Lean, D. Lettenmaier, X. Liang, J.-F. Mahfouf, H.-T. Mengelkamp, K. Mitchell, O. N. Nasonova, J. Noilhan, A. Robock, C. Rosenzweig, J. Schaake, C. A. Schlosser, J.-P. Schulz, A. B. Shmakina, D. L. Verseghy, P. Wetzel, E. F. Wood, Z.-L. Yang, and Q. Zeng, 1998: Sensitivity of latent heat flux from PILPS land-surface schemes to perturbations of surface air temperature. *J. Atmos. Sci.*, **55**, 1909-1927.
- Rahmstorf, S., A. Cazenave, J. A. Church, J. E. Hansen, R. F. Keeling, D. E. Parker, and R. C. J. Somerville, 2007: Recent climate observations compared to projections. *Science*, **316** (5825), 709.
- Ramankutty, N. and J. A. Foley, 1999: Estimating historical changes in global land cover: Croplands from 1700 to 1992. *Global Biogeochemical Cycles*, **13**, 997-1027.
- Razuvaev, V. N., E. G. Apasova, and R. A. Martuganov. 1998: Six- and Three-hourly Meteorological Observations from 223 U.S.S.R. Stations. ORNL/CDIAC-108, NDP-048/R1. Carbon Dioxide Information Analysis Center, Oak Ridge National Laboratory, Oak Ridge, Tennessee.
- Rind, D., R. Goldberg, J. Hansen, C. Ruedy, and C. Rosenzweig, 1990: Potential evapotranspiration and the likelihood of future drought. *J. Geophys. Res.*, **95**, 9983-10004.
- Roads, J., E. Raschke, and B. Rockel, 2002a: BALTEX water and energy budgets in the NCEP/DOE reanalysis II. *Boreal Environment Research*, **7** (4), 307-317.
- Roads J., M. Kanamitsu, and R. Stewart, 2002b: CSE water and energy budgets in the NCEP-DOE Reanalysis II. *J. Hydrometr.*, **3** (3), 227-248.
- Roads J., R. Lawford, E. Bainto, E. Berbery, S. Chen, B. Fekete, K. Gallo, A. Grundstein, W. Higgins, M. Kanamitsu, W. Krajewski, V. Lakshmi, D. Leathers, D. Lettenmaier, L. Luo E. Maurer, T. Meyers, D. Miller, K. Mitchell, T. Mote, R. Pinker, T. Reichler, D. Robinson, A. Robock, J. Smith, G. Srinivasan, K. Verdin, K. Vinnikov, T. V. Haar, C. Vorosmarty, S. Williams, and E. Yarosh, 2003: GCIP water and energy budget synthesis (WEBS). *J. Geophys. Res.*, **108** (D16), Art. No. 8609.
- Robock, A., and J. Mao, 1995: The volcanic signal in surface temperature observations. *J. Climate* **8**, 1086-1103.
- Robock, A., K. Y. Vinnikov, G. Srinivasan, J. K. Entin, S. E. Hollinger, N. A. Speranskaya, S. X. Liu, and A. Namkhai, 2000: The Global Soil Moisture

- Data Bank. *Bulletin of the American Meteorological Society*, **81**, 1281-1299.
- Robock, A., L. Luo, E. F. Wood, F. Wen, K. E. Mitchell, P. R. Houser, J. C. Schaake, D. Lohmann, B. Cosgrove, J. Sheffield, Q. Duan, R. W. Higgins, R. T. Pinker, J. D. Tarpley, J. B. Basara, and K. C. Crawford, 2003: Evaluation of the North American Land Data Assimilation System over the Southern Great Plains during the warm season.. *J. Geophys. Res.*, **108**(D22), 8846, doi:10.1029/2002JD003245.
- Rodell, M., P. R. Houser, U. Jambor, J. Gottschalck, K. Mitchell, C.-J. Meng, K. Arsenault, B. Cosgrove, J. Radakovich, M. Bosilovich, J. K. Entin, J. P. Walker, D. Lohmann, D. Toll, 2004: The Global Land Data Assimilation System, *Bull. Am. Met. Soc.*, **85**, 381-394.
- Rodo X., E. Baert, and F. A. Comin, 1997: Variations in seasonal rainfall in southern Europe during present century: Relationships with the North Atlantic Oscillation and the El Niño Southern Oscillation. *Climate Dyn.*, **13**, 275-284.
- Ropelewski, C. F., and M. S. Halpert, 1987: Global and regional scale precipitation patterns associated with the El Nino/ Southern Oscillation. *Mon. Wea. Rev.*, **115**, 1606-1626.
- Rossow, W.B., and R.A. Schiffer, 1991: ISCCP cloud data products. *Bull. Amer. Meteor. Soc.*, **72**, 2-20.
- Rouault, M., and Y. Richard, 2005: Intensity and spatial extent of droughts in southern Africa. *Geophysical Research Letters*, **32**(15), 4.
- Salby, M. L., and P. Callaghan, 1997: Sampling error in climate properties derived from satellite measurements: Consequences of undersampled diurnal variability, *J. Clim.*, **10**, 18-36.
- Scanlon, B. R., I. Jolly, M. Sophocleous, and L. Zhang, 2007: Global impacts of conversions from natural to agricultural ecosystems on water resources: Quantity versus quality. *Water Resources Research*, **43**, 18.
- Schlosser, C. A, A. G. Slater, A. Robock, A. Pitman, K. Y. Vinnikov, A. Henderson-Sellers, N. A. Speranskaya, and K. Mitchell, 2000: Simulations of a boreal grassland hydrology at Valdai, Russia: PILPS phase 2(d). *Mon. Wea. Rev.*, **128**, 301-321.
- Schubert, S. D., R. Rood, and J. Pfaendtnr, 1993: An assimilated data set for earth sciences applications. *Bull. Amer. Meteor. Soc.*, **74**, 2331-2342.
- Seneviratne, S. I., R. D. Koster, Z. C. Guo, P. A. Dirmeyer, E. Kowalczyk, D. Lawrence, P. Liu, C. H. Lu, D. Mocko, K. W. Oleson, and D. Verseghy, 2006: Soil moisture memory in AGCM simulations: Analysis of global land-atmosphere coupling experiment (GLACE) data. *Journal of Hydrometeorology*, **7**, 1090-1112.
- Serreze, M. C., and C. M. Hurst, 2000: Representation of mean Arctic precipitation from NCEP/NCAR and ERA reanalyses. *J. Climate*, **13**, 182-201.
- Serreze, M. C. et al., 2000: Observational evidence of recent change in the northern high-latitude environment. *Climatic Change* **46**, 159-207.
- Sheffield, J., A. D. Ziegler, E. F. Wood, and Y. Chen, 2004b: Correction of the high-latitude rain day anomaly in the NCEP/NCAR reanalysis for land

- surface hydrological modeling, *J. Climate*, **17**(19), 3814-3828.
- Sheffield, J., and E. F. Wood, 2007: Characteristics of global and regional drought, 1950-2000: Analysis of soil moisture data from off-line simulation of the terrestrial hydrologic cycle, *J. Geophys. Res.*, in press.
- Sheffield, J., G. Goteti, and E. F. Wood, 2006: Development of a 50-year high-resolution global dataset of meteorological forcings for land surface modeling. *J. Climate*, **19**(13), 3088-3111.
- Sheffield, J., G. Goteti, and E. F. Wood, 2006: Development of a 50-yr high-resolution global dataset of meteorological forcings for land surface modeling, *J. Climate*, **19** (13), 3088-3111.
- Sheffield, J., G. Goteti, F. Wen, and E. F. Wood, 2004: A simulated soil moisture based drought analysis for the United States, *J. Geophys. Res.*, **109**, D24108, doi:10.1029/2004JD005182.
- Shiklomanov, A. I., T. I. Yakovleva, R. B. Lammers, I. P. Karasev, C. J. Vorosmarty, and E. Linder, 2006: Cold region river discharge uncertainty - estimates from large Russian rivers. *J. Hydrology*, **326**(1-4), 231-256.
- Siebert, S., P. Doll, J. Hoogeveen, J. M. Faures, K. Frenken, and S. Feick, 2005: Development and validation of the global map of irrigation areas. *Hydrology and Earth System Sciences*, **9**, 535-547.
- Simmons, A. J., P. D. Jones, V. da Costa Bechtold, A. C. M. Beljaars, P. W. Källberg, S. Saarinen, S. M. Uppala, P. Viterbo, and N. Wedi, 2004: Comparison of trends and low-frequency variability in CRU, ERA-40, and NCEP/NCAR analyses of surface air temperature, *J. Geophys. Res.*, **109**, D24115, doi:10.1029/2004JD005306.
- Soman, V. V., J. B. Valdés, and G. R. North, 1995: Satellite sampling and the diurnal cycle statistics of Darwin rainfall data, *J. Appl. Meteorol.*, **34**, 2481-2490.
- Stackhouse, P. W., S. K. Gupta, S. J. Cox, J. C. Mikowitz, T. Zhang, and M. Chiacchio, 2004: 12-year surface radiation budget data set. *GEWEX News*, Twitchell, P., Ed., **14**(4), 10-12.
- Stedinger, J. R., R. M. Vogel, and E. Foufoula-Georgiou, 1993: Frequency analysis of extreme events, in *Handbook of Hydrology*, edited by D. R. Maidment, pp. 18.1- 18.66, McGraw-Hill, New York.
- Stine, S., 1994: Extreme and persistent drought in California and Patagonia during medieval time. *Nature*, **369**, 546-549.
- Sud, Y. C., D. M. Mocko, K.-M. Lau, and R. Atlas, 2003: Simulating the Midwestern U.S. drought of 1988 with a GCM, *J. Climate*, **16**, 3946-3965.
- Su, F., J. C. Adam, K. E. Trenberth, and D. P. Lettenmaier, 2006: Evaluation of surface water fluxes of the pan-Arctic land region with a land surface model and ERA-40 reanalysis, *J. Geophys. Res.*, **111**, D05110, doi:10.1029/2005JD006387.
- Susskind, J., P. Piraino, L. Rokke, L. Iredell and A. Mehta, 1997: Characteristics of the TOVS Pathfinder Path A Dataset. *Bull. Amer. Meteor. Soc.*, **78**, 1449-1472.

- Sutton, R. T. and L. R. Hodson, 2005: Atlantic forcing of North American and European summer climate. *Science*, **309**, 115-118.
- Swenson, S. C., and P. C. D. Milly, 2006: Climate model biases in seasonality of continental water storage revealed by satellite gravimetry. *Water Resour. Res.*, **42**, W03201, doi:10.1029/2005WR004628.
- Tarhule, A., and P. J. Lamb, 2003: Climate research and seasonal forecasting for West Africans: perceptions, dissemination, and use? *Bull. Amer. Met. Soc.*, **84**, 1741-1759.
- Wilhite, D. A., 2000: Drought as a natural hazard: Concepts and Definitions, in *Drought: A Global Assessment*, D. A. Wilhite, Ed., 3-18.
- Thornton, P. E., and S. W. Running, 1999: An improved algorithm for estimating incident daily solar radiation from measurements of temperature, humidity, and precipitation. *Agric. For. Meteorol.*, **93**, 211-228.
- Trenberth, K., and G. Branstator, 1992: Issues in establishing causes of the 1988 drought over N. America, *J. Climate*, **5**, 159- 172.
- Trenberth, K. E., 1999: Atmospheric moisture recycling: Role of advection and local evaporation. *J. Climate*, **12**, 1368-1381.
- Trenberth, K. E. and C. J. Guillemot, 1998: Evaluation of the atmospheric moisture and hydrological cycle in the NCEP/NCAR reanalysis. *Clim. Dynam.*, **14**, 213-231.
- Trenberth, K. E., and D. J. Shea, 2005: Relationships between precipitation and surface temperature. *Geophys. Res. Lett.*, **32**(14), 4.
- Trenberth, K. E., and J. W. Hurrell, 1994: Decadal atmosphere-ocean variations in the Pacific. *Climate Dynamics* **9**, 303.
- Uvo, C. B., 2003: Analysis and regionalization of Northern European winter precipitation based on its relationship with the North Atlantic oscillation. *International Journal of Climatology*, **23** (10), 1185-1194.
- van der Schrier, G., K. R. Briffa, P. D. Jones, and T. J. Osborn, 2006b: Summer moisture variability across Europe. *J. Climate*, **19** (12), 2818-2834.
- van der Schrier, G., K. R. Briffa, T. J. Osborn, and E. R. Cook, 2006a: Summer moisture availability across North America. *J. Geophys. Res.*, **111** (D11): Art. No. D11102.
- Verdon, D. C., S. W. Franks, 2006: Long-term behaviour of ENSO: Interactions with the PDO over the past 400 years inferred from paleoclimate records. *Geophys. Res. Lett.*, **33**(6), 5.
- Visbeck, M. H., J. W. Hurrell, L. Polvani, and H. M. Cullen, 2001: The North Atlantic Oscillation: Past, present, and future. *Proc. Nat. Acad. Science.*, **98**(23), 12876-12877.
- Wang, G. L., 2003: Reassessing the impact of North Atlantic Oscillation on the sub-Saharan vegetation productivity. *Global Change Biology*, **9**(4), 493-499.
- Wang, G. L., 2005: Agricultural drought in a future climate: results from 15 global climate models participating in the IPCC 4th assessment. *Climate Dynamics*, **25**, 739-753.
- WCRP, 1990: The Global Precipitation Climatology Project - Implementation and Data Management Plan. WMO/TD-No. 367, Geneva, June 1990, 47

- pp. and appendices.
- Wells, N., S. Goddard, and M. J. Hayes, 2004: A self-calibrating Palmer drought severity index, *J. Climate*, **17**, 2335-2351.
- Werth, D, and R. Avissar, 2002: The local and global effects of Amazon deforestation, *J. Geophys. Res.*, **107**(D20), 8087, DOI.10.1029/2001D000717.
- Western, A. W., R. B. Grayson, and G. Bloschl, 2002: Scaling of soil moisture: A hydrologic perspective, *Annual Review of Earth and Planetary Sciences*, **30**, 149-180.
- Wetherald, R. T., and S. Manabe, 1995: The mechanisms of summer dryness induced by greenhouse warming. *J. Clim.*, **8**, 3096-3108.
- Wetherald, R. T., and S. Manabe, 1999: Detectability of summer dryness caused by greenhouse warming. *Climatic Change*, **43**, 495-511.
- Wetherald R. T., and S. Manabe, 2002: Simulation of hydrologic changes associated with global warming. *J. Geophys Res.*, **107**, Art. No. 4379.
- Wigley, T. M. L., 2005: The climate change commitment. *Science* **307** (5716), 1766-1769.
- Wilby, R.L., Hay, L. E., Gutowski Jr., W. J., Arriitt, R. W., Takle, E. S., Pan, Z., Leavesley, G. H. and M. P. Clark, 2000: Hydrological responses to dynamically and statistically downscaled climate model output, *Geophys. Res. Lett.* **27**(8), 1199-1202.
- Wild, M., A. Ohmura, H. Gilgen, J-J. Morcrette, and A. Slingo, 2001: Evaluation of downward longwave radiation in general circulation models. *J. Climate*, **14**, 3227-3239.
- Wild, M., H. Gilgen, A. Roesch, A. Ohmura, C. N. Long, E. G. Dutton, B. Forgan, A. Kallis, V. Russak, and A. Tsvetkov, 2005: From dimming to brightening: Decadal changes in solar radiation at Earth's surface. *Science*, 6 May, 847-850.
- Wilhite, D. A., 2000: Drought as a natural hazard: Concepts and definitions, in *Drought: A Global Assessment*, edited by D. A. Wilhite, pp. 3-18, Routledge, London.
- Wilks, D. D., 1998: Multi-site generalizations of a daily stochastic weather generation model. *J. Hydrology*, **210**, 178-191.
- Wilks, D. S. and R. L. Wilby, 1999: The weather generation game: A review of stochastic weather models. *Progress in Physical Geography*, **23**, 329-357.
- Wood, E. F., D. P. Lettenmaier, X. Liang, B. Nijssen and S. W. Wetzel, 1997: Hydrological modeling of continental-scale basins. *Annu. Rev. Earth. Pl. Sc.*, **25**, 279-300.
- Wood, E. F., D. P. Lettenmaier, X. Liang, D. Lohmann, A. Boone, S. Chang, F. Chen, Y. J. Dai, R. E. Dickinson, Q. Y. Duan, M. Ek, Y. M. Gusev, F. Habets, P. Irannejad, R. Koster, K. E. Mitchell, O. N. Nasonova, J. Noilhan, J. Schaake, A. Schlosser, Y. P. Shao, A. B. Shmakin, D. Verseghy, K. War-rach, P. Wetzel, Y. K. Xue, Z. L. Yang, and Q. C. Zeng, 1998: The Project for Intercomparison of Land-surface Parameterization Schemes (PILPS) phase 2(c) Red-Arkansas River basin experiment: 1. Experiment description and summary intercomparisons. *Global and Planetary Change*, **19**, 115-135.

- Xin, X. G., R. C. Yu, T. J. Zhou, and B. Wang, 2006: Drought in late spring of South China in recent decades. *J. Climate*, **19**(13), 3197-3206.
- Yevjevich V., 1972: *Stochastic Processes in Hydrology*. Water Resources Publications: Fort Collins, CO.
- Zhang, R., and T. L. Delworth, 2006: Impact of Atlantic multidecadal oscillations on India/Sahel rainfall and Atlantic hurricanes, *Geophysical Research Letters*, **33**(17), 5.
- Zhang, X. B., L. A. Vincent, W. D. Hogg, and A. Niitsoo, 2000: Temperature and precipitation trends in Canada during the 20th century. *Atmosphere-Ocean*, **38**, 395-429.
- Zhang, Y. K. and K. E. Schilling, 2006: Increasing streamflow and baseflow in Mississippi River since the 1940 s: Effect of land use change. *Journal of Hydrology*, **324**, 412-422.
- Zhang, Y., W. B. Rossow, A. A. Lacis, V. Oinas, and M. I. Mishchenko, 2004: Calculation of radiative fluxes from the surface to top of atmosphere based on ISCCP and other global data sets: Refinements of the radiative transfer model and the input data, *J. Geophys. Res.*, **109**, D19105, doi:10.1029/2003JD004457.
- Zhao, M., and P. Dirmeyer, 2003: Production and analysis of GSWP-2 near-surface meteorology data sets. COLA Technical Report COLA Technical Report 159 [Available from the Center for Ocean-Land-Atmosphere Studies, 4041 Powder Mill Road, Suite 302, Calverton, MD 20705 USA], 22pp.
- Zhao, R. J., Y. L. Zhang, L. R. Fang, X. R. Liu, and Q. S. Zhang, 1980: The Xinanjiang model, in *Hydrological forecasting proceedings Oxford Symposium*, IASH 129, 351-356.
- Zheng, X., and R. E. Basher, 1999: Structural time series models and trend detection in global and regional temperature series. *J. Climate* **12**, 2347-2358.
- Ziegler, A. D., J. Sheffield, E. P. Maurer, B. Nijssen, E. F. Wood, and D. P. L. Lettenmaier, 2003: Detection of intensification in global- and continental-scale hydrological cycles: Temporal scale of evaluation. *Journal Of Climate*, **16**, 535-547.
- Zou, X. K., P. M. Zhai, and Q. Zhang, 2005: Variations in droughts over China: 1951-2003. *Geophys. Res. Lett.*, **32**(4), 4.

Samenvatting

Deze studie analyseert mondiale en regionale droogte gedurende de tweede helft van de 20^{ste} eeuw op basis van hydrologische model simulaties. Veranderingen in droogte karakteristieken in de 21^{ste} eeuw worden onderzocht met behulp van multi-scenario gegevens van verschillende klimaatmodellen. Een mondiale dataset van meteorologische gegevens voor de periode 1948-2000 is ontwikkeld voor deze simulaties door metingen te combineren met her-analyses. Systematische fouten en foutieve trends in neerslag, temperatuur en straling van deze her-analyses zijn gecorrigeerd omdat deze anders fouten in de waterbalans zouden veroorzaken. De simulaties zijn gebruikt om een maandelijks op bodemvocht gebaseerde droogteindex te ontwikkelen, die is gebruikt om het voorkomen, de variaties en de trends van droogte in de periode 1950-2000 te onderzoeken. Kortdurende droogtes (6 maanden of korter) komen het meest voor in vochtige gebieden. Droogtes van middellange duur (6 tot 12 maanden) komen vaker voor op gematigde breedtes, gedreven door persistente afwijkingen in bevroren bodemvocht. In de Sahel en delen van noordelijke hoge breedtegraden komen langdurige droogtes het vaakst voor. Ernstige droogtes worden systematisch geïdentificeerd op basis van de ruimtelijke dekking, zoals de droogtes in 1988 in de VS, in 1982/83 in Australië, in 1983/84 in de Sahel en in 1965/66 in India. Er is een door neerslag gedreven mondiale toenemende trend in bodemvocht, die vooral tot uiting komt in Noord Amerika. Desalniettemin zijn regionale verschillen duidelijk aanwezig, waarbij significante uitdroging in West Afrika met name opvalt. Trends in karakteristieken van droogte nemen over het algemeen af, maar statistisch significante veranderingen komen alleen voor op kleine schaal, en hebben betrekking op minder dan 10% van het continentale landoppervlak. De gelijktijdige afname van de ruimtelijke dekking van mondiale droogtes bedraagt 0.04% per jaar. Binnen de lange-termijn trends vinden we dat de jaarlijkse en tienjaarlijkse variaties in bodemvocht en droogtekarakteristieken die vooral worden veroorzaakt door ENSO variabiliteit, terwijl ook AMO in een aantal gebieden een belangrijke rol hierin kan spelen. Droogte wordt vooral veroorzaakt door variaties in neerslag, hoewel ook de temperatuur een effect heeft. Dit effect lijkt aan het einde van de 20^{ste} eeuw steeds belangrijker te worden, vooral op hoge noordelijke breedtes. Op mondiale schaal zijn de bodemvochtindex en de PDSI redelijk goed gecorreleerd, maar deze correlatie verdwijnt in koudere gebieden en seizoenen. Vooral recentelijk is dit goed te zien als de PDSI wijst op een sterke droogte-trend, mogelijk

door het gebruik van de temperatuur om verdamping te schatten. Om projecties van toekomstige droogtes te onderzoeken zijn bodemvochtgegevens van acht verschillende GCMs voor drie IPCC AR4 klimaatscenario's (B1, A1B, A2) gebruikt. Een afname in mondiaal bodemvocht in de 21^{ste} eeuw gaat gepaard met een verdubbeling van de ruimtelijke dekking en frequentie van kortdurende droogtes. Langdurige droogtes komen drie keer zo vaak voor. Op regionale schaal laten het Middellandse Zeegebied, West Afrika, Centraal Azië en Centraal Amerika grote toenames zien, net als het gematigde breedte gebied van Noord Amerika, maar dan met grotere verschillen tussen scenario's. Onder scenario B1 zijn de veranderingen het kleinst, terwijl de veranderingen voor A1B en A2 vergelijkbaar zijn. Hoewel de veranderingen over het algemeen monotoon stijgend zijn, zijn ze niet statistisch verschillend van natuurlijke variaties over meerdere decennia, anders dan voor de temperatuur, en deze hangt af van de droogtevariabele, de grootte van de verandering, de natuurlijke variabiliteit en de statistische betrouwbaarheid. In contrast hiermee staat het feit dat veranderingen in de gemiddelden van hydrologische variabelen, inclusief bodemvocht, bijna niet te detecteren zijn in de 21^{ste} eeuw, hetgeen impliceert dat veranderingen in extremen beter meetbaar zouden kunnen zijn dan veranderingen in gemiddelden.

Curriculum Vitae

Justin Sheffield was born in Basingstoke, UK, on 24th November 1968. He attended the Brighton Hill Secondary school and Queen Mary's College from 1982-88. He received his undergraduate degree (BSc, mathematics and oceanography) from the University of Southampton, UK. After spending a year working for Southampton council he moved to Newcastle upon Tyne where he gained a masters degree (MSc, engineering mathematics) from the University of Newcastle (UoN). His masters thesis was on the modeling of turbulent flow in open channels. Justin then took a research position at the Water Resource Systems Research Laboratory at the UoN where he stayed for the next 8 years, from 1992-99. During this time he worked with Prof. Enda O'Connell, head of the laboratory, James Bathurst and Chris Kilsby, carrying out research into a variety of hydrologic problems including flood forecasting, desertification, solute transport, and the hydrological impacts of land use and climate change. In 2000 he moved to the Center for Land Use and Water Resources Research at the UoN as a senior research associate, working under the supervision of Prof. Ian Calder on the impacts of land use change on the water cycle. He started his current position as a researcher in the Department of Civil Engineering at Princeton University in mid-2000, working with Prof. Eric F. Wood. He officially started work on his PhD thesis under the co-promotion of Eric and Peter Troch of Wageningen University, at the end of 2004.

Justin has worked on many projects over the past 7 years at Princeton related to the modeling and observation of the terrestrial water and energy budgets across a range of scales. His current interests center on the global land surface hydrological cycle and particularly the question of whether the hydrologic cycle is intensifying in response to climate change and global warming. He has worked on a number of multi-institutional projects funded by various agencies in the US, including the North American Land Data Assimilation System (NLDAS), the Land Information System (LIS) and the Northeast Climate Impacts Assessment (NECIA). He is a member of the scientific team for the recent NECIA and co-wrote the hydrologic impacts section. Justin is a reviewer for several journals that publish in the fields of hydrology, climate and remote sensing and has served as a reviewer for program proposals and as a member of review panels.

List of Peer-Reviewed Publications

First Author Publications

- Sheffield J.**, and E. F. Wood, Projected changes in drought occurrence under future global warming from multi-model, multi-scenario, IPCC AR4 simulations, submitted to Climate Dynamics.
- Sheffield, J.**, and E. F. Wood, Global trends and variability in soil moisture and drought characteristics, 1950-2000, from observation driven simulations of the terrestrial hydrologic cycle. *J. Climate*, in press.
- Sheffield, J.**, and E. F. Wood (2007), Characteristics of global and regional drought, 1950-2000: Analysis of soil moisture data from off-line simulation of the terrestrial hydrologic cycle, *J. Geophys. Res.*, 112, D17115, doi:10.1029/2006JD008288.
- Sheffield, J.**, G. Goteti, and E. F. Wood, 2006: Development of a 50-yr high-resolution global dataset of meteorological forcings for land surface modeling, *J. Climate*, 19 (13), 3088-3111.
- Sheffield, J.**, G. Goteti, F. Wen, and E. F. Wood, 2004: A simulated soil moisture based drought analysis for the United States, *J. Geophys. Res.*, 109, D24108, doi:10.1029/2004JD005182.
- Sheffield, J.**, A. D. Ziegler, E. F. Wood, and Y. Chen, 2004: Correction of the high-latitude rain day anomaly in the NCEP/NCAR reanalysis for land surface hydrological modeling, *J. Climate*, 17(19), 3814-3828.
- Sheffield, J.**, M. Pan, E. F. Wood, K. E. Mitchell, P. R. Houser, J. C. Schaake, A. Robock, D. Lohmann, B. Cosgrove, Q. Duan, L. Luo, R. W. Higgins, R. T. Pinker, J. D. Tarpley, and B. H. Ramsay, 2003: Snow process modeling in the North American Land Data Assimilation System (NLDAS): 1. Evaluation of model simulated snow cover extent. *J. Geophys. Res.*, 108 (D22), 8849, doi:10.1029/2003JD003274.

Co-Author Publications

- McCabe, M. F., Wood, E. F., Wójcik, R., Pan, M., **Sheffield, J.**, Su, H. and Gao, H. (2007). "Hydrological consistency using multi-sensor remote sensing data for water and energy cycle studies." *Remote. Sens. Environ.* (in press).
- Hayhoe, K., C. Wake, T. Huntington, L. Luo, M. D. Schwartz, **J. Sheffield**, E. F. Wood, B. Anderson, J. Bradbury, A. DeGaetano, T. J. Troy, and D. Wolfe. Past and future changes in climate and hydrological indicators in the U.S. Northeast. *Climate Dynamics*, 28 (4), 381-407, 10.1007/s00382-006-0187-8.
- Kumar, S. V., C. D. Peters-Lidard, Y. Tian, J. Geiger, P. R. Houser, S. Olden, L. Lighty, J. L. Eastman, P. Dirmeyer, B. Doty, J. Adams, E. Wood and **J. Sheffield** (2006), LIS - An Interoperable Framework for High Resolution Land Surface Modeling. In press, *Environmental Modeling and Software*, available online since 12 October 2005.

- Dery, S. J., **J. Sheffield**, and E. F. Wood, 2005: Connectivity between Eurasian snow cover extent and Canadian snow water equivalent and river discharge. *J. Geophys. Res.*, 110 (D23), , D23106.
- Ziegler, A. D., E. P. Maurer, **J. Sheffield**, B. Nijssen, E. F. Wood, and D. P. Lettenmaier, 2005: Detection time for plausible changes in annual precipitation, evapotranspiration, and streamflow in three Mississippi River sub-basins. *Climatic Change*, 72(1-2), 17-36.
- Mitchell, K. E., D. Lohmann, P. R. Houser, E. F. Wood, J. C. Schaake, A. Robock, B. A. Cosgrove, **J. Sheffield**, Q. Duan, L. Luo, R. W. Higgins, R. T. Pinker, J. D. Tarpley, D. P. Lettenmaier, C. H. Marshall, J. K. Entin, M. Pan, W. Shi, V. Koren, J. Meng, B. H. Ramsay, and A. A. Bailey, 2004: The Multi-institution North American Land Data Assimilation System (NLDAS): Utilizing multiple GCIP products and partners in a continental distributed hydrological modeling system. *J. Geophys. Res.*, 109, D07S90, doi: 10.1029/2003JD003823.
- Schaake, J. C., Q. Duan, V. Koren, K. E. Mitchell, P. R. Houser, E. F. Wood, A. Robock, D. P. Lettenmaier, D. Lohmann, B. Cosgrove, **J. Sheffield**, L. Luo, R. W. Higgins, R. T. Pinker, and J. D. Tarpley, 2004: An inter-comparison of soil moisture fields in the North American Land Data Assimilation System (NLDAS). *J. Geophys. Res.*, 109, D01S90, doi:10.1029/2002JD003309.
- Lohmann, D., K. E. Mitchell, P. R. Houser, E. F. Wood, J. C. Schaake, A. Robock, B. A. Cosgrove, **J. Sheffield**, Q. Duan, L. Luo, W. Higgins, R. T. Pinker, and J. D. Tarpley, 2004: Streamflow and water balance intercomparisons of four land-surface models in the North American Land Data Assimilation System project. *J. Geophys. Res.*, 109, D07S91, doi: 10.1029/2003JD003517.
- Ziegler, A. D., **J. Sheffield**, E. P. Maurer, B. Nijssen, E. F. Wood, D. P. Lettenmaier, 2003: Detection of Intensification in Global and Continental-Scale Hydrological Cycles: Temporal Scale of Evaluation, *J. Climate*, 16, 535-547.
- Bathurst, J. C., **J. Sheffield**, X. Leng, and G. Quaranta, 2003: Decision support system for desertification mitigation in the Agri basin, southern Italy. *Phys. Chem. Earth*, 28 (14-15), 579-587.
- Pan, M., **J. Sheffield**, E. F. Wood, K. E. Mitchell, P. R. Houser, J. C. Schaake, A. Robock, D. Lohmann, B. Cosgrove, Q. Duan, L. Luo, R. W. Higgins, R. T. Pinker, and J. D. Tarpley, 2003: Snow process modeling in the North American Land Data Assimilation System (NLDAS): 2. Evaluation of model simulated snow water equivalent. *J. Geophys. Res.*, 108 (D22), 8850, doi:10.1029/2003JD003994.
- Cosgrove, B. A., D. Lohmann, K. E. Mitchell, P. R. Houser, E. F. Wood, J. Schaake, A. Robock, C. Marshall, **J. Sheffield**, L. Luo, Q. Duan, R. T. Pinker, J. D. Tarpley, R. W. Higgins, and J. Meng, 2003: Real-time and retrospective forcing in the North American Land Data Assimilation Systems (NLDAS) project. *J. Geophys. Res.*, 108 (D22), 8842, doi:10.1029/2002JD003118.

- Cosgrove, B. A., D. Lohmann, K. E. Mitchell, P. R. Houser, E. F. Wood, J. C. Schaake, A. Robock, **J. Sheffield**, Q. Duan, L. Luo, R. W. Higgins, R. T. Pinker, and J. D. Tarpley, 2003: Land surface model spinup behavior in the North American Land Data Assimilation System (NLDAS). *J. Geophys. Res.*, 108 (D22), 8845, doi:10.1029/2002JD003119.
- Luo, L., A. Robock, K. E. Mitchell, P. R. Houser, E. F. Wood, J. C. Schaake, D. Lohmann, B. Cosgrove, F. Wen, **J. Sheffield**, Q. Duan, R. W. Higgins, R. T. Pinker, and J. D. Tarpley, 2003: Validation of the North American Land Data Assimilation System (NLDAS) retrospective forcing over the Southern Great Plains. *J. Geophys. Res.*, 108 (D22), 8843, doi:10.1029/2002JD003246.
- Robock, A., L. Luo, E. F. Wood, F. Wen, K. E. Mitchell, P. R. Houser, J. C. Schaake, D. Lohmann, B. Cosgrove, **J. Sheffield**, Q. Duan, R. W. Higgins, R. T. Pinker, J. D. Tarpley, J. B. Basara, and K. C. Crawford, 2003: Evaluation of the North American Land Data Assimilation System over the Southern Great Plains during the warm season. *J. Geophys. Res.*, 108 (D22), 8846, doi:10.1029/2002JD003245.
- Pinker, R. T., J. D. Tarpley, I. Laszlo, K. E. Mitchell, P. R. Houser, E. F. Wood, J. C. Schaake, A. Robock, D. Lohmann, B. A. Cosgrove, **J. Sheffield**, Q. Duan, L. Luo, and R. W. Higgins, 2003: Surface radiation budgets in support of the GEWEX Continental Scale International Project (GCIP) and the GEWEX Americas Prediction Project (GAPP), including the North American Land Data Assimilation System (NLDAS) project. *J. Geophys. Res.*, 108 (D22), 8844, doi:10.1029/2002JD003301.
- Mellor, D., **J. Sheffield**, P. E. O'Connell and A. V. Metcalfe. 2000. A stochastic space-time rainfall forecasting system for real time flow forecasting I: Development of MTB conditional rainfall scenario generator. *Hydrology and Earth System Sciences*, 4, 603-615.
- Mellor, D., **J. Sheffield**, P. E. O'Connell and A. V. Metcalfe. 2000. A stochastic space-time rainfall forecasting system for real time flow forecasting II: Application of SHETRAN and ARNO rainfall runoff models to the Brue catchment. *Hydrology and Earth System Sciences*, 4, 617-626.
- Lukey, B. T., **J. Sheffield**, J. C. Bathurst, R. A. Hiley, and M. Mathys, 2000. Test of the SHETRAN technology for modelling the impact of reforestation on badlands runoff and sediment yield at Draix, France. *J. Hydrol.*, 235, 44-62.
- Lukey, B.T., **J. Sheffield**, J. C. Bathurst, J. Lavabre, N. Mathys, & C. Martin, 1995. Simulating the effect of vegetation cover on the sediment yield of Mediterranean catchments using SHETRAN. *Physics & Chemistry of the Earth*. 20(3-4): 427-432